A multi-phenotypic GWA screen for renal function in *Drosophila*

Keqin Li

Supervisor: Prof Julian A. T. Dow

Submitted in fulfilment for the degree of Doctor of Philosophy in Molecular Genetics

School of Molecular Biosciences

College of Medical, Veterinary and Life Sciences

University of Glasgow

February 2025

Author’s Declaration

I declare that the content presented in this thesis is entirely my own work, except where otherwise stated, and has not been submitted for any other degree.

Keqin Li

This thesis is dedicated to my wife.

Abstract

Renal function plays a critical role in maintaining water-salt homeostasis and survival of most animal species. Impaired renal function has been associated with kidney stone disease, with evidence linking compromised tubular secretion to the progression of renal dysfunction in humans. Moreover, substantial genetic contributions have been identified in both kidney stone formation and tubular transport of endogenous solutes and xenobiotics. Therefore, understanding the genetic basis of nephrolithiasis and tubular transport may provide valuable insights into the mechanisms underlying nephrolithiasis, impaired tubular secretion, and their contributions to renal function decline. Genome-wide association studies in humans have reported several sequence variants associated with kidney function and kidney stone disease. Calcium-based urinary stones account for more than 80% of all kidney stones, and tubular transport represents another important renal functional parameter apart from glomerular filtration. Despite this, only a handful of genes implicated in calcium nephrolithiasis and tubular transport have been identified. The genetic basis of variation in susceptibility to kidney stones and renal tubular secretion remains largely unclear. While association studies are powerful and unbiased tools for identifying risk loci, several challenges persist in human studies.

The Malpighian tubules of *Drosophila*, functional analogues of human kidneys, have been demonstrated to be an excellent model for studying human renal function and disease. The *Drosophila melanogaster* genetic reference panel serves as a valuable genetic resource for investigating the genetic basis of complex traits. In this study, we utilized inbred, fully sequenced lines from the panel to identify genetic variants influencing kidney stone formation and the secretion capacity of renal tubules. Calcium crystals were quantified in the renal tubules of fly lines subjected to a lithogenic diet, and the fluid secretion capacity of the dissected tubules was measured. Furthermore, the genetic basis of neuroendocrine regulation of secretion was explored using two neuropeptides targeting distinct cell types. We found considerable and reproducible phenotypic variation in both crystal formation and fluid secretion ability. Interestingly, no

correlation was observed between the development of renal crystals and basal fluid secretion rates, despite low urine volume being a recognized risk factor for kidney stone disease.

Association studies were conducted to identify genetic variants associated with the observed phenotypic variation. A total of 68 polymorphisms corresponding to 41 genes were associated with crystal formation, while 155 polymorphisms corresponding to 92 genes were linked to basal secretion rate. Candidate genes harbouring these polymorphisms were functionally validated through RNAi-mediated knockdown. Interactions between candidate genes and their physically and genetically interacting genes were extracted from curated databases. Functional enrichment analysis of the clustered gene networks revealed that biological processes, including the Wnt signalling pathway and extracellular acidification, were associated with the gene networks identified in the analysis of stone formation. Additionally, processes such as the electron transport chain, aerobic respiration, and mitochondrial ATP synthesis were linked to variation in basal secretion rate.

In conclusion, this study presents the first genome-wide association analysis of renal crystal formation and tubular fluid secretion in *Drosophila*, identifies multiple candidate loci and pathways, and helps to prioritise human genes and pathways as potential therapeutic targets for kidney stone disease and impaired tubular transport. This study has thus demonstrated the utility of a systematic, unbiased screen in identifying genes of interest in renal function in both insects and humans.

Acknowledgements

Many thanks to my supervisors, Prof Julian A. T. Dow and Prof Shireen A. Davies, for providing me the opportunity to be a member of their group and for their support and guidance throughout my PhD. I thank them for the freedom they gave me in deciding the direction my research should take, for the patience in answering my questions, and for the encouragement that kept me motivated throughout this journey.

Many thanks to the CSC-Glasgow Joint Scholarship for funding the PhD, and BBSRC for funding the research.

Many thanks to Dr Sue Krause for her support, guidance, and tasty peanut butter cookies along the way, and to Dr Anthony Dornan for the induction on my first day in the group, help, and great scientific advice ever since. I would like to thank Dr Andrew Gillen for his exceptional bioinformatics expertise, Miss Shannon Keenan for her help and support, Dr Karen McLuskey for her advice, and Miss Xueying Bai and Dr Chandan Maurya for the enjoyable conversations.

I would like to thank Dr Rhoda Stefanatos and Mr Kevin Myers for their help and advice for qRT-PCR. I would also like to thank Dr Adam Dobson for his advice and support in conducting the association studies and Dr Nathan Woodling for his advice and support. Thanks to other members of fly groups, in past and present, and to kind ladies of the prep room for their help and support. Thanks to those kind people from Cordero's lab, past and present, for the time with pastries, wines, and joys.

Finally, I thank my mom and dad for their love and support. I thank my wife for her love and constant support and for all the late nights and early mornings.

I apologise to everyone that I've inevitably forgotten.

Table of Contents

List of Tables

List of Figures

List of Abbreviations

°C	Degree Celsius
AGT	Alanine-Glyoxylate Aminotransferase
AIP	Advanced Intercross Population
ANOVA	Analysis of Variance
BDSC	Bloomington *Drosophila* Stock Centre
cAMP	Cyclic 3',5'-Adenosine Monophosphate
CaOx	Calcium Oxalate
CaP	Calcium Phosphate
CapaR	Capability Receptor
CASR	Calcium-Sensing Receptor
cDNA	Complementary DNA
ClC-5	Cl^-/H^+ Exchange Transporter 5
CO_2	Carbon Dioxide
DAPI	4',6-Diamidino-2-Phenylindole
DF	Degrees of Freedom
DGRP	*Drosophila melanogaster* Genetic Reference Panel
DNA	Deoxyribonucleic Acid
dRTA	Distal Renal Tubular Acidosis
DSHB	Developmental Studies Hybridoma Bank
ECM	Extracellular Matrix
ESKD	End-Stage Kidney Disease
EtBr	Ethidium Bromide
Fas3	Fasciclin 3
FPKM	Fragments per Kilobase of Transcript per Million Mapped Reads
GCA	General Combining Ability
gDNA	Genomic DNA
GFP	Green Fluorescent Protein
GFR	Glomerular Filtration Rate
GWA	Genome-Wide Association
KD	Knockdown
KSD	Kidney Stone Disease
LD	Linkage Disequilibrium
M	Molar
MAF	Minor Allele Frequency
MT	Malpighian Tubule
mtROS	Mitochondrial Reactive Oxygen Species
NaOx	Sodium Oxalate
NHE3	Sodium/Proton Exchanger 3
NKCC2	Sodium-Potassium-Chloride Cotransporter
Ø	Diameter
OAT	Organic Anion Transporter
OCT	Organic Cation Transporter
OMIM	Online Mendelian Inheritance in Man
PBS	Phosphate Buffered Saline

PC	Principal Cell
PCA	Principal Component Analysis
PCR	Polymerase Chain Reaction
pH	Potential of Hydrogen
PLC/IP_3	Phospholipase C/Inositol 1,4,5-Trisphosphate
QQ	Quantile-Quantile
qRT-PCR	Quantitative Real-Time PCR
QTL	Quantitative Trait Loci
RNA	Ribonucleic Acid
RNAi	RNA Interference
RSC	Renal Stem Cell
RTA	Renal Tubular Acidosis
SC	Stellate Cell
SCA	Specific Combining Ability
SD	Standard Deviation
SEM	Standard Error of the Mean
shRNAs	Short Hairpin RNAs
SNP	Single Nucleotide Polymorphism
snRNA-seq	Single-Nucleus RNA Sequencing
T.U.R.D.	The Ultimate Reader of Dung
TAL	Thick Ascending Limb
TBE	Tris-Borate-EDTA
TRiP	Transgenic RNAi Project
UAS	Upstream Activating Sequence
V-ATPase	Vacuolar H^+-ATPase
VDRC	Vienna *Drosophila* Resource Centre

Chapter 1 Introduction

1.1 Renal function and water and ion homeostasis

The kidneys and their evolutionary precursor structures are essential for the survival of animals. In most organisms, death occurs within days after the complete cessation of renal function (Finco, 1997). These excretory structures play a central role in maintaining water and ion balance, with a variety of transport and neuroendocrine mechanisms involved in this regulation. In the human nephron, the regulation of water and sodium balance can be viewed as two distinct systems, primarily controlled by the vasopressin and renin-angiotensin-aldosterone systems (Schrier, 2006).

1.1.1 Regulation of water balance

Water, as the largest single constituent of the human body, accounts for approximately 60% of body weight (Verbalis, 2003). Total body water is divided into two compartments: intracellular fluid, comprises approximately two-thirds of the total, and extracellular fluid, which accounts for the remaining third. Water homeostasis is maintained by balancing water intake and loss. As terrestrial organisms, humans lose water through urine, faeces, respiration, and perspiration and gain it through food and drink (Delpire and Gagnon, 2018). Despite significant fluctuations in salt and water intake, terrestrial mammals maintain a relatively stable extracellular fluid osmolality (Darrow and Yannet, 1935). The regulation of water balance is largely controlled by thirst, which is governed by osmoreceptors, and antidiuresis, which is regulated by arginine vasopressin. When plasma osmolality changes, cell volume adjusts accordingly. These changes in cell volume are detected by osmoreceptors in the hypothalamus (Oliet and Bourque, 1993), leading to the release of arginine vasopressin into the bloodstream (Verney, 1947). The vasopressin receptor, V2, located in the renal collecting duct, is activated by circulating vasopressin. The activation of the receptor increases the renal water permeability of the collecting duct by inserting the water channel aquaporin-2 into the apical

membranes of principal cells (Knepper, 1997). The binding of vasopressin to its receptor activates the Gs adenylyl cyclase system, which elevates intracellular levels of cyclic 3',5'-adenosine monophosphate (cAMP). The activation of protein kinase A by cAMP phosphorylates preformed aquaporin-2 in intracellular vesicles. This phosphorylation facilitates the trafficking and insertion of aquaporin-2 into the apical membrane (Greenberg and Verbalis, 2006). In the basolateral membrane, two other water channels are constitutively present, making the insertion of aquaporin-2 the limiting step in regulating water permeability.

1.1.2 Regulation of sodium balance

Sodium is another major determinant of body fluid homeostasis, alongside water. The sodium–potassium pump (Na^+/K^+-ATPase), a ubiquitous enzyme responsible for establishing and maintaining the transmembrane electrochemical gradients of sodium and potassium, accounts for approximately one-third of the total energy expenditure in animal cells (Hodeify et al., 2024) and up to two-thirds of energy expenditure in neurons (Mohan et al., 2019). This high energy expenditure of sodium–potassium pump underscores the critical importance of maintaining sodium balance. Unlike water intake, which can be regulated by thirst, there is limited evidence supporting a significant role for regulated sodium intake in humans (Verbalis, 2003). In patients with various disorders that cause severe depletion of sodium and extracellular fluid, the absence of salt appetite has been observed. Consequently, the kidneys assume a more significant role in regulating sodium homeostasis through renal excretion.

Two classical mechanisms, glomerular filtration rate (GFR) and adrenal aldosterone secretion, play a role in regulating renal Na^+ excretion (Verbalis, 2003). The difference between the filtration rate and tubular reabsorption of Na^+ determines the amount of Na^+ excreted. GFR is influenced by several factors, such as glomerular plasma flow and capillary surface area (Verbalis, 2003). Under normal conditions, up to 99% of the filtered Na^+ (approximately 25 mol per day) is reabsorbed (Bie, 2018). When the amount of filtered sodium increases, Na^+ reabsorption by the proximal tubule also rises through

tubuloglomerular feedback (Verbalis, 2003). Sodium intake leads to changes in arterial blood pressure. High sodium consumption can result in water retention, as sodium is rapidly and actively absorbed by the gastrointestinal tract. This increased blood volume, resulting from water retention, raises blood pressure in the arterial vessels, leading to higher renal blood flow (Grillo et al., 2019), an increased glomerular filtration rate (GFR), and, consequently, more sodium being filtered.

With a reduced sodium load, its reabsorption becomes more efficient, and excretion decreases (Selkurt, 1954). The effective circulating volume is monitored by sensor and effector elements. In response to renal hypoperfusion and reduced tubular sodium content, the renin-angiotensin-aldosterone system is activated. Angiotensinogen, secreted by the liver, is cleaved by renin from juxtaglomerular cells and converted into angiotensin II (Paul et al., 2006). Angiotensin II enhances sodium reabsorption by increasing the activity of the Na^+-H^+ antiporter (Cano et al., 1994). Under the regulation of angiotensin II, aldosterone, synthesised in the adrenal cortex, is secreted. This increases the concentrations of epithelial sodium channels at the apical membrane, thereby enhancing sodium reabsorption in the collecting tubules (Paul et al., 2006).

1.1.3 Renal dysfunction

The glomerular filtration rate is the widely accepted indicator of overall kidney function, and its level is used to define chronic kidney disease (CKD) (Webster et al., 2017). The estimated global prevalence of CKD is 13.4% (Hill et al., 2016), and the annual healthcare expenditure for CKD in the United States alone was estimated at 10.7 billion dollars (Ozieh et al., 2017). Decreased kidney function is indicated by a GFR of less than 60 ml/min per 1.73 m^2 or the presence of kidney damage markers for at least three months. Patients with a GFR of less than 15 ml/min per 1.73 m^2 are classified as having end-stage kidney disease (ESKD), requiring either a kidney transplant or dialysis for survival. Various factors, including diabetes, hypertension, and inflammation, contribute to the decline in renal function (Lopez-Novoa et al., 2010, Webster et al., 2017).

Several studies have demonstrated that nephrolithiasis can also impair kidney function (Gillen et al., 2005, Haley et al., 2016, Chuang et al., 2020, Alexander et al., 2012, Rule et al., 2009). The presence of kidney stones is significantly associated with an increased risk of CKD or ESKD (Alexander et al., 2012, Chuang et al., 2020, Rule et al., 2009). Potential mechanisms linking kidney stones to adverse renal outcomes may involve renal damage caused by stone formation (Alexander et al., 2012, Coe et al., 2010). Additionally, renal tubular secretion is an important renal functional parameter, apart from glomerular filtration, as endogenous solutes and medications are rapidly cleared by the renal tubules (Wang and Kestenbaum, 2018). Associations between low clearance of secretory solutes and tubulointerstitial fibrosis, as well as the progression of renal function decline, have been observed (Garimella et al., 2022, Suchy-Dicey et al., 2016, Chen et al., 2020). Increased phosphaturia also accelerates the decline in renal function (Santamaria et al., 2018), and renal phosphate homeostasis involves both glomerular filtration and tubular reabsorption (Blaine et al., 2015).

1.2 Kidney stone disease

Kidney stone disease (KSD) is a condition characterised by the formation of crystal concretions within the kidneys. It affects approximately 10% of adults worldwide (Singh et al., 2022a), and the estimated annual economic cost associated with the diagnosis, treatment, and prevention of nephrolithiasis is projected to exceed 4 billion dollars by 2030 in the United States alone (Antonelli et al., 2014, Roberson et al., 2020). The prevalence and incidence of KSD have been reported to be increasing globally (Romero et al., 2010). The aetiology of kidney stones is complex and multifactorial, with both genetics and environmental factors contributing to the risk of developing KSD. Extrinsic factors, including geography, climate, diet, and water intake (Moe, 2006), also play a significant role in the formation of kidney stones, alongside genetic factors.

1.2.1 Types of kidney stones

The chemical composition of kidney stones varies depending on the chemical composition of the urine (Alelign and Petros, 2018). Based on differences in mineral composition and pathogenesis, there are four major types of kidney stones.

1.2.1.1 Calcium stones

The most common type of kidney stone is a calcium stone, which accounts for more than 80% of all urinary calculi (Coe et al., 2005). These stones can form as calcium oxalate (CaOx) or calcium phosphate (CaP) crystals, either alone or in combination. Among patients with first-time symptomatic kidney stones, up to 94% have calcium stones, with 76% of these being calcium oxalate (Singh et al., 2015). CaOx crystals exist in two forms: CaOx monohydrate (COM) and CaOx dihydrate (COD) (Bensatal and Ouahrani, 2008). Compared with COD stones, COM stones are more commonly observed clinically (Daudon et al., 2004) and are the most thermodynamically stable form of kidney stones (Alelign and Petros, 2018). The ten-year recurrence rate is higher for COD stones (38%) than for COM stones (26%) among CaOx stone formers. Several risk factors, including hypercalciuria, hyperoxaluria, and hypocitraturia, contribute to the development of CaOx stones (Dal Moro et al., 2005).

Calcium phosphate primarily exists in the form of basic CaP (apatite), calcium hydrogen phosphate dihydrate (brushite), or tricalcium phosphate (whitlockite) (Khan et al., 2016). Apatite often appears as a powdery mass filling spaces between other types of crystals, particularly CaOx stones. Major risk factors for the formation of CaP crystals include hypercalciuria, hypocitraturia, and a high urinary pH (Siener et al., 2013). CaOx crystals are more likely to form when urinary pH is between 5.0 to 6.5, while CaP stones typically form when pH exceeds 7.5 (Alelign and Petros, 2018). The 10-year symptomatic recurrence rate for calcium oxalate and hydroxyapatite stones is approximately 30% (Singh et al., 2015).

1.2.1.2 Uric acid stones

Uric acid crystals account for about 8-10% of kidney stones worldwide. Patients with obesity and insulin resistance are at higher risk of developing uric acid nephrolithiasis (Ekeruo et al., 2004, Daudon et al., 2006). Low urinary pH, particularly below 5.5, is considered the primary factor responsible for the formation of uric acid stones (Sakhaee et al., 2002). In addition to the insolubility of uric acid caused by low urinary pH and dehydration, excessive urinary excretion of uric acid, known as hyperuricosuria, also contributes to the formation of uric acid crystals. Excessive intake of purine-rich foods (Fellström et al., 1983) and conditions that lead to overproduction of uric acid, such as gout, can result in elevated levels of urinary uric acid. Furthermore, the use of uricosuric drugs increases the rate of stone formation in patients with gout (Shekarriz and Stoller, 2002). Increasing urine pH and promoting large urine volumes are effective strategies to prevent the recurrence of uric acid calculi (Becker, 2007).

1.2.1.3 Struvite stones

Struvite stones, which account for about 10% of kidney stones (Han et al., 2015), are also known as infection stones or triple phosphate stones (Griffith, 1978). These stones are a mixture of magnesium ammonium phosphate and carbonate apatite. Urease-producing bacteria are the primary culprits behind infection-induced struvite stones. Pathogens such as *Proteus mirabilis, Klebsiella pneumonia,* and *Pseudomonas aeruginosa* are commonly associated with their formation (Griffith, 1978). Urease produced by these pathogens hydrolyses urea into ammonia and carbon dioxide, increasing urinary pH, reducing the solubility of phosphate, and leading to the formation of large staghorn calculi (Griffith, 1978). Compared with sterile and acidic urine from healthy kidneys, urine from stone-containing kidneys is alkaline and contains higher levels of cellular debris and protein (BROWN, 1901). In adults, women are more likely to develop struvite stones than men, while the opposite is true in children (Rodman, 1998). With

surgical intervention and antibiotics, struvite stones, which were historically associated with high mortality, are now treatable.

1.2.1.4 Cystine stones

Apart from rare xanthine stones, which are typically associated with inborn metabolic disorders, cystine stones are the least common type of kidney stones, accounting for less than 2% of cases. They are primarily caused by an autosomal recessive disorder that results in defects in the renal transporter for the amino acid cystine (Biyani and Cartledge, 2006). The impaired reabsorption of cystine leads to elevated urinary cystine levels, which, due to its poor solubility, form crystals at normal urinary pH. Increasing fluid intake, administering oral potassium citrate, and limiting sodium and protein intake can help reduce cystine excretion (Fattah et al., 2014).

1.2.2 Mechanisms of the formation of kidney stones

The aetiology of kidney stones is complex and not fully understood (Aggarwal et al., 2013). The formation of stones involves physicochemical changes and the supersaturation of urine. In a supersaturated state, solutes precipitate, leading to nucleation and, ultimately, the formation of crystal concretions. The transition from a liquid to a solid phase is influenced by factors such as pH and the concentration of excess molecules. Stone-forming substances such as calcium, phosphorus, uric acid, and oxalate are key risk factors for crystallization. Although all kidney stones share common events in the mineral phase of formation, the specific sequence of events leading to stone formation varies depending on the type of stone and the composition of the urine (Alelign and Petros, 2018). A reduced level of inhibitors promotes calcification in supersaturated urine, while an increase in promoters fosters it. For example, the presence of uric acid reduces the solubility of CaOx and increases crystallization (Sikirić et al., 1997). Various cellular and extracellular events, including nucleation, crystal growth and aggregation, and crystal-cell interaction, are

involved in kidney stone formation (Figure 1.1) (Alelign and Petros, 2018). These processes also provide therapeutic targets for kidney stone disease.

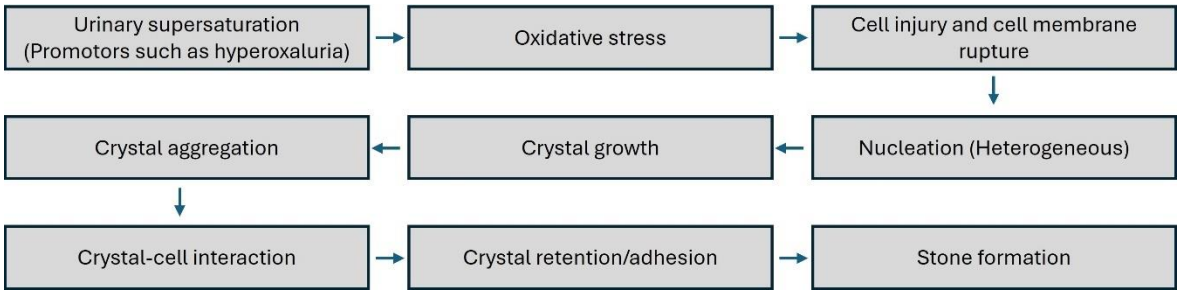

Figure 1.1 Various cellular and extracellular events during kidney stone formation. Taken from (Alelign and Petros, 2018).

1.2.2.1 Nucleation

In supersaturated urine, nucleation is the initial step in the transformation from a liquid to a solid phase. Free ions or molecules begin to form microscopic clusters that can precipitate. For example, when charged soluble calcium and oxalate combine, they form insoluble CaOx crystals. In supersaturated solutions, if promoters outweigh the inhibitors, nucleation occurs (Basavaraj et al., 2007). This process typically happens heterogeneously in urine, as a lower level of supersaturation is needed compared to homogeneous nucleation (Robertson, 1969). Heterogeneous nucleation can occur in the presence of proteins, other organic polymers, and crystals of another mineral. Epithelial cells, urinary casts, and red blood cells can act as nucleating centres (Aggarwal et al., 2013). Zinc (Barker et al., 2020) and albumin (Cerini et al., 1999) have also been found to play a role in nucleation. Once a nucleus is formed, a lower chemical pressure is required for further crystallization (Alelign and Petros, 2018). Additionally, the organic matrix, such as mucopolysaccharide, can serve as a binding agent, promoting nucleation and crystal aggregation (Ahmed et al., 2016).

1.2.2.2 Crystal-cell Interaction

The attachment of grown crystals to the renal tubule is referred to as crystal-cell interaction or crystal retention. This interaction is a crucial step in the

development of kidney stone disease (Khan et al., 1999). Under conditions of hyperoxaluria, renal tubular epithelial cells are damaged by high concentrations of oxalate or sharp COM crystals (Khan, 2006). Crystal-cell interaction leads to the movement of crystals from the basolateral side of the cells to the basement membrane (Courbebaisse et al., 2016). The crystals may then be internalized by the cells and anchored to the basement membrane of the kidney. Numerous membrane vesicles produced through cellular degradation after cell injury act as nucleators for calcium crystals. Additionally, injured cell membranes can become inverted and serve as sites for crystal adhesion (Alelign and Petros, 2018), as COM crystals have a stronger affinity for the inverted anionic membrane (Khan et al., 2002). Some urinary polyanionic molecules, such as glycoproteins and citrate, can prevent the binding of COM crystals to the cell membrane by coating the crystals. Adhesion of COM crystals to microvilli on the cell surface and their subsequent internalization have also been observed in tissue culture (Alelign and Petros, 2018).

1.2.2.3 Crystal growth and agglomeration

After a crystal nucleus is formed in the kidney, it grows through encrustation upon exposure to urine (Khan and Hackett, 1987). Two basic pathways are involved in the formation of a stone nucleus, and both can be active in any stone carrier (Linnes et al., 2013, Khan et al., 2016). The first pathway is the free-particle mechanism (Finlayson and Reid, 1978, Kok and Khan, 1994), which suggests that crystals nucleate, grow, and aggregate within the urine of the renal tubules. Once large particles or plugs are formed, they are retained inside the kidneys either by becoming large enough or by attaching to the tubular epithelium. The alternative mechanism is the fixed-particle mechanism, where stones form by attaching to Randall's plaques. The plagues begin with the formation and deposition of CaP crystals in the renal interstitium (Khan and Canales, 2015). These two mechanisms differ in the location of the initial nidus (Khan et al., 2016). Both plugs and plaques are coated with macromolecules produced by renal epithelial cells upon exposure to tubular crystal deposition, which further promotes crystallization and stone growth. Ultimately, the

formation and growth of CaOx crystals over plaques or plugs can lead to the development of a calcific stone attached to the renal papillary tip (Khan et al., 2016).

1.2.3 Genetics of kidney stone disease

Strongly heritable features have been linked to kidney stone disease and its associated risk factors (Singh et al., 2022a). Individuals with a family history of kidney stones are significantly more likely to develop stones compared with those without a family history. Studies have found that 16-37% of stone formers have a family history of the condition, compared with just 4-12% of healthy individuals (Resnick et al., 1968, McGeown, 1960). Furthermore, twin studies have estimated the heritability of nephrolithiasis to be 56% (Goldfarb et al., 2005, Goldfarb et al., 2019). Male twins show a higher estimated heritability of 56-57%, compared with 46% in females. These findings suggest that genetic factors play a significant role in the development of kidney stones, although much remains to be learned about the specific genetic contributions to the formation of stones.

1.2.3.1 Monogenic causes

Approximately 15% of kidney stone disease cases are attributed to monogenic mutations, as revealed by a high-throughput mutation analysis (Halbritter et al., 2015). More specifically, 11% of nephrolithiasis cases in adults have a single-gene cause, while 21% of cases with a single-gene cause are found in paediatric cohorts. Monogenic mutations were identified in 50 out of 79 families with paediatric CKD and suspected nephrolithiasis through whole-exome sequencing with homozygosity mapping (Braun et al., 2016). Key features, such as early onset of kidney stone disease, multiple recurrent stone episodes, and nephrocalcinosis, may suggest a monogenic cause (Singh et al., 2022a). Most known monogenic forms are associated with hypercalciuria.

Bartter syndrome. Bartter syndrome is a group of channelopathies that affect sodium chloride reabsorption in the thick ascending limb (TAL) of the loop of

Henle, typically inherited in an autosomal recessive pattern (Amirlak and Dawson, 2000). Disrupted sodium reabsorption leads to excessive urinary sodium loss, resulting in hypokalaemia, metabolic alkalosis, and hyperaldosteronism (Policastro et al., 2018). The TAL reabsorbs about 25% of filtered sodium primarily through the sodium-potassium-chloride cotransporter (NKCC2) (Seyberth, 2008). The lumen-positive transepithelial potential generated by active salt reabsorption drives passive paracellular reabsorption of divalent cations, including calcium and magnesium (Seyberth and Schlingmann, 2011). Impaired sodium reabsorption in Bartter syndrome results in reduced calcium reabsorption, leading to hypercalciuria. Mutations in six genes have been linked to the syndrome. Bartter syndrome type I is caused by mutations in the *NKCC2* gene (Simon et al., 1996a), while type II is caused by biallelic mutations in the *KCNJ1* gene, which encodes the renal outer medullary potassium channel (Simon et al., 1996b).

Dent disease and Lowe syndrome. Dent disease is caused by X-linked recessive mutations in either *CLCN5* or *OCRL*, corresponding to type I and type II Dent disease, respectively (Ehlayel and Copelovitch, 2019). Approximately 30-50% of patients with Dent disease type I develop kidney stones, typically composed of CaOx and/or CaP (Blanchard et al., 2016, Singh et al., 2022a). *CLCN5* encodes the electrogenic Cl^-/H^+ exchange transporter 5 (ClC-5), which is primarily expressed in the proximal tubule and collecting duct (Pusch and Zifarelli, 2015). Knockout of *Clcn5* in mice results in abnormal endosomal function (Wang et al., 2000). Mutations in *CLCN5* also lead to defects in the reabsorption and processing of low molecular weight proteins (Nielsen et al., 2016), which are typically reabsorbed through endocytic pathways involving megalin and cubilin. A portion of calcium reabsorption also occurs via megalin receptor-mediated endocytosis (Christensen et al., 1998). About 98% of filtered calcium is reabsorbed by the nephron, with 65% of this occurring paracellularly in the proximal tubule (Anglani et al., 2019), driven by the activity of the sodium/proton exchanger 3 (NHE3) (Anglani et al., 2019). ClC-5 is necessary for the exocytic trafficking of NHE3 (Lin et al., 2011), which may explain why 81 out of 88 (92%) patients with Dent disease type I develop hypercalciuria (Blanchard

et al., 2016). Mutations in *OCRL* also lead to Lowe syndrome, which shares features such as hypercalciuria and nephrocalcinosis, although kidney stones are found in fewer than 20% of affected patients (Bockenhauer et al., 2008).

Distal renal tubular acidosis. Primary distal renal tubular acidosis (dRTA) is caused by impaired urinary acidification in the collecting tubule. Biallelic mutations in genes encoding subunits of vacuolar H^+-ATPases (V-ATPases), such as *ATP6V0A4*, *ATP6V1B1,* and *ATP6V1C2*, as well as mutations in *SLC4A1*, which encodes the chloride-bicarbonate counter transporter, can result in primary dRTA (Wagner et al., 2023). A mutation in *WDR72*, which encodes WD repeat-containing protein 72, also leads to impaired trafficking of V-ATPases and causes primary dRTA. These proteins are primarily expressed in type A intercalated cells, and mutations in these genes account for more than 80% of diagnosed cases of primary dRTA (Singh et al., 2022a). Nephrolithiasis is a common complication of primary dRTA because CaP precipitates at a high pH level. Chronic metabolic acidosis, another feature of this disorder, leads to the loss of calcium from bone, contributing to stone formation (Watanabe, 2018).

Primary hyperoxaluria. Primary hyperoxaluria is a rare inborn disorder resulting from errors in glyoxylate metabolism, leading to excessive urinary excretion of oxalate (Cochat and Rumsby, 2013, Hoppe, 2012). When calcium is present in the urine, CaOx crystals can form easily, causing nephrocalcinosis and kidney stones (Lieske et al., 1992). Biallelic mutations in *AGXT* (Cochat et al., 2006), which encodes liver-specific alanine-glyoxylate aminotransferase (AGT), in *GRHPR* (Garrelfs et al., 2019), which encodes glyoxylate reductase/hydroxypyruvate reductase, or in *HOGA1* (Singh et al., 2022b), which encodes a liver-specific mitochondrial enzyme, cause primary hyperoxaluria type 1, 2, and 3, respectively. Mutations in *AGXT* account for approximately 80% of primary hyperoxaluria type 1. To reduce the risk of stone formation and renal injury caused by this disorder, increased fluid intake and inhibitors of CaOx crystallization, such as citrate, are commonly employed.

1.2.3.2 Polygenic factors

For the majority of patients with kidney stone disease, both genetic and environmental factors play a role, with the genetic contribution to the development of idiopathic stones remaining considerable (Howles and Thakker, 2020). Genome-wide association (GWA) studies have identified multiple loci with polygenic effects, revealing a group of genes and molecular pathways that contribute to the risk of the disease. Some of these genes, such as *CASR*, *SLC34A1*, and *CYP24A1*, are also linked to monogenic causes of stone disease or nephrocalcinosis.

In 2009, the first GWA study was conducted in Dutch and Icelandic populations (Thorleifsson et al., 2009), identifying two synonymous variants in *CLDN14* associated with kidney stones and bone mineral density. One of these variants, rs219780[C], was homozygous in approximately 60% of the Icelandic population in the study and was linked to a 1.6-fold increased risk of developing kidney stones. Increased expression of *CLDN14* was observed when an intronic single nucleotide polymorphism (SNP) was introduced in vitro, potentially due to the creation of a novel transcription factor binding site by the SNP (Ure et al., 2017). Additionally, a GWA study including 11,130 patients and 187,639 controls identified nine variants in the noncoding region of *CLDN2* associated with a higher risk of nephrolithiasis (Curry et al., 2020). *CLDN2* encodes Claudin-2, a paracellular cation channel protein involved in calcium reabsorption in the proximal tubule. Claudin-2 mutant mice exhibited impaired calcium transport in the renal tubule, coupled with increased net intestinal calcium absorption. Analysis of cis-acting expression quantitative trait loci was performed in *CLDN2,* and seven risk variants were strongly associated with decreased Claudin-2 expression.

A variant in *UMOD*, which encodes uromodulin, was found to be protective against kidney stones in the Icelandic population. However, the same variant, rs4293393[T], was also associated with an increased risk of CKD (Gudbjartsson et al., 2010). In another GWA study conducted in a Japanese population, variants of

SLC34A1, *AQP1*, and *DGKH* were found to be associated with the development of CaOx stones (Urabe et al., 2012). Additionally, a relationship between the variant of *SLC34A1* and reduced estimated GFR was also established. A variant in *ALPL*, rs1256328[T], was identified as a risk locus for kidney stones in a Han Chinese population (Li et al., 2018). The *ALPL* gene encodes tissue-nonspecific alkaline phosphatase, an enzyme involved in biomineralization, particularly during the growth and development of bones and teeth (McKee et al., 2013, Mornet et al., 2001). The variant rs1256328[T] has been found to be associated with kidney stones in another GWA study, and a missense variant in *ALPL*, rs34605986[A], which correlates with rs1256328[T], also showed a strong association with kidney stones (Oddsson et al., 2015).

Associations between common variants and urinary traits that serve as risk factors for kidney stones, including urinary calcium, magnesium, and uric acid excretion, as well as urine volume, were investigated in a large European cohort (Ware et al., 2019). Variants near *TRPM6* were found to be associated with urinary magnesium excretion, while the allele rs17216707[T] was significantly linked to increased daily calcium excretion. Although rs17216707[T] was not associated with gene expression in any tissue types, it is located upstream of *CYP24A1*, which encodes a catabolic enzyme for 1,25-dihydroxyvitamin D and 25-hydroxyvitamin D. This SNP has also been associated with concentrations of fibroblast growth factor 23, a bone-derived hormone that regulates phosphorus and vitamin D metabolism (Robinson-Cohen et al., 2018). In 2023, a larger meta-analysis of the GWA study of kidney stone disease was conducted in a European population, including 17,969 cases and 720,199 controls (Hao et al., 2023). The study identified 44 risk loci, including 28 of which were novel (Figure 1.2). Cells in the proximal tubule were found to be the most relevant cells where risk variants likely act in a tissue-specific manner. The study prioritised 233 genes involved in ion homeostasis, with a specific focus on calcium and magnesium. Additionally, a phenome-wide genetic correlation analysis between nephrolithiasis and 1,781 diseases (Hao et al., 2023) revealed strong genetic correlations between kidney stone disease and both genitourinary and digestive diseases.

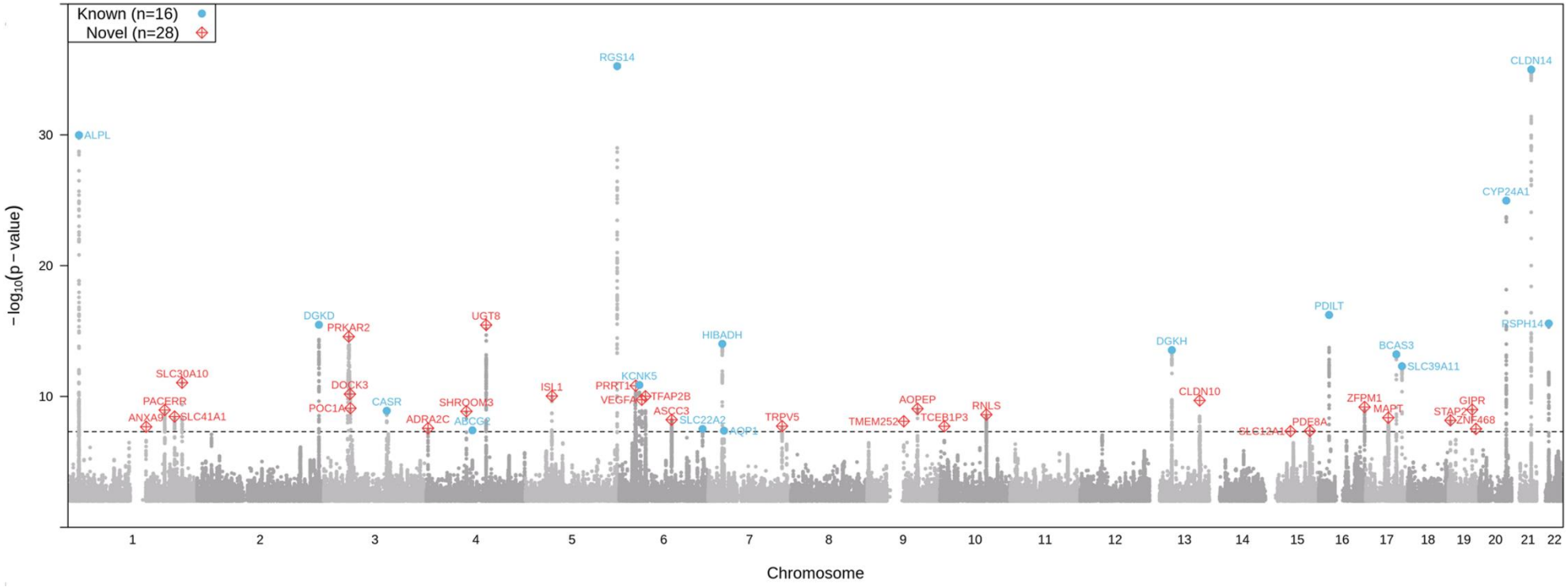

Figure 1.2 Manhattan plot of GWA study of kidney stone disease.
The top variants are labelled in blue for known and red for novel loci. The dashed line stands for a genome-wide significance threshold. Taken from (Hao et al., 2023).

1.3 Tubular transport

Nephrons are the basic functional units of the kidneys, with each kidney containing approximately 1.2 million of these units. Each nephron (Figure 1.3) is made of the Bowman's capsule, the proximal tubule, the loop of Henle, and the distal tubule (Wallace, 1998). In addition to glomerular filtration, the renal system helps maintain the volume and composition of the extracellular fluid through tubular reabsorption and secretion (Wallace, 1998). The renal tubule regulates three major types of substances: electrolytes, nonelectrolytes, and water. Electrolytes include sodium, calcium, potassium, phosphate, and chloride, while nonelectrolytes include glucose, amino acids, urea, and uric acid.

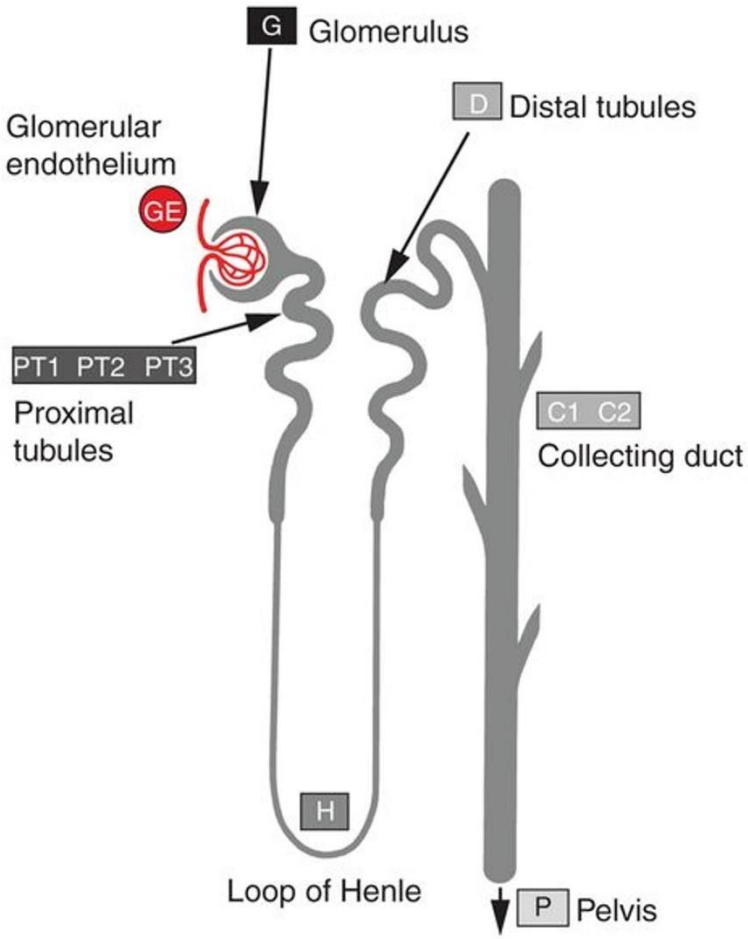

Figure 1.3 Nephron anatomy with cell clusters marked.
Epithelial cell types include convoluted (PT1), straight and convoluted (PT2 and PT3), ascending and descending (H), distal and principal (D), type A (C1), type B (C2), and pelvic epithelium (P) cells. Taken from (Young et al., 2018).

1.3.1 Tubular reabsorption

Both active and passive transport mechanisms contribute to tubular reabsorption. For example, most glomeruli-filtered calcium (approximately 98-99%) is reabsorbed along the nephron, with 60-70% of the reabsorption occurring in the proximal tubule, 20-25% in the TAL, and 10-15% in the distal tubule (Downie and Alexander, 2022). In the proximal tubule, more than 60% of calcium is reabsorbed paracellularly, with a small amount of transcellular calcium transport. This paracellular reabsorption of calcium is likely mediated by both diffusion and solvent drag (Edwards and Bonny, 2018). Sodium is transported into the cell by the apically localised NHE3 and subsequently into the bloodstream by Na^+/K^+-ATPase at the basolateral membrane. Claudins, specifically CLDN2 and

CLDN12, confer high calcium permeability in the proximal tubule. The osmotic gradient created by transepithelial sodium movement facilitates solvent drag-mediated paracellular calcium reabsorption (Alexander et al., 2013). Similarly, in the TAL, calcium reabsorption is highly dependent on sodium reabsorption (Downie et al., 2021) and is tightly regulated. A major regulator is the calcium-sensing receptor (CASR), located at the basolateral membrane, which upregulates the abundance of the paracellular calcium blocker, Claudin-14 (Toka et al., 2012). Furthermore, CASR regulates the activity of NKCC2 and ROMK, an apical potassium channel (Carmosino et al., 2015), which are involved in establishing the positive luminal membrane potential necessary for calcium reabsorption. In the distal tubule, calcium is reabsorbed transcellularly. This process involves the calcium channel TRPV5 at the apical membrane, calcium-binding proteins such as Calbindin-D_{28K} in the cytoplasm, and either Ca^{2+}-ATPase or the Na^{+}/Ca^{2+} exchanger at the basolateral membrane, all of which mediate transepithelial calcium movement (Boros et al., 2009). This process is regulated by hormones, such as PTH, $1,25(OH)_2$VitD, and calcitonin (Downie and Alexander, 2022).

1.3.2 Tubular secretion

About 20% of renal plasma flow is filtered by the glomeruli, while the remaining 80% flows through the peritubular capillaries, where it is regulated by the renal tubules (Wang and Kestenbaum, 2018). Substances like protein-bound molecules are minimally filtered due to their size and the properties of the glomerular basement membrane. These molecules are primarily cleared through tubular secretion. Many uremic toxins, which current dialysis modalities fail to remove, as well as commonly prescribed medications effectively, are known substrates of organic anion transporters (OATs) and organic cation transporters (OCTs) in the proximal tubule (Duranton et al., 2012, Wikoff et al., 2011, Ren et al., 2015). Significant intraindividual and interindividual variation in proximal tubular secretion of endogenous markers has been observed (Rivara et al., 2017), with a high genetic contribution to the variation in renal drug clearance (Yin et al., 2006, Leabman and Giacomini, 2003). The proximal tubules play a crucial role in

clearing of both endogenous solutes and xenobiotics, such as medications, from the circulation, although this function is often overlooked (Wang and Kestenbaum, 2018).

The lack of suitable exogenous markers for tubular secretion has limited in vivo studies of tubular function. Recently, resazurin, a cell viability dye, has been identified as an exogenous sensor of kidney tubular function and viable nephron mass (Martinez et al., 2025). When injected intravenously, resazurin exhibits a high plasma protein binding property and is primarily secreted by the renal tubules in mice. Upon injection, the blue-coloured resazurin, which exhibits weak fluorescence, is taken up by tubular cells via OATs. Within the cells, resazurin is converted to a highly fluorescent, pink-coloured resorufin by mitochondrial and cytosolic reductases and then to ß-D-glucuronide, an orange-coloured compound with weak fluorescence, by uridine diphosphate–glucuronosyltransferase. Under normal conditions, the ratio of resorufin to ß-D-glucuronide in urine is 1:20, allowing for a sensitive measure of renal tubular function. In mouse models of acute kidney injury, this resazurin-based method can detect the loss of tubular function much earlier than serum creatinine analysis. Furthermore, it enables the detection of loss of tubular mass and function despite normal GFR levels in mice with unilateral ischemia-reperfusion injury and kidney hypoplasia (Martinez et al., 2025).

1.4 Quantitative trait and genome-wide association study

1.4.1 Quantitative trait

Quantitative traits are those for which the observed variation results from the segregation of several to many naturally occurring polymorphic genes (Kearsey and Pooni, 2020). Compared to environmental factors, the impact of allelic differences on the phenotype is usually small, making it relatively difficult to determine the genotype based on the individual's phenotype. Understanding the genetic architecture of variation in quantitative traits presents a major challenge in biology (Mackay et al., 2009). Unravelling the relationship between

variation in DNA sequences and that in phenotypes will provide molecular markers essential for predicting disease risk, personalizing therapeutic treatments, and optimizing breeding programmes (Mackay et al., 2009).

When Mendel's laws of inheritance were rediscovered in the early 20th century, a significant debate arose between Mendelians and biometricians (Olby, 1989). The Mendelians sought for Mendelian patterns of inheritance in qualitative traits, while the biometricians focused on traits with normally distributed phenotypic values (Plomin et al., 2009). The Mendelians believed that Mendelian factors in the next generation were inherited from parents following Mendel's laws, and that complex traits also followed these simple inheritance patterns. In contrast, the biometricians argued that complex traits were distributed not qualitatively but quantitatively, and that Mendel's laws of inheritance were applicable only to peas. In 1918, the differences between Mendelians and biometricians were reconciled by Ronald A. Fisher (Fisher, 1918). He pointed out that a trait would be normally distributed if it is affected by several genes, even if each gene is inherited following Mendel's laws (Figure 1.4). Although Fisher's reconciliation helped bridge the gap, Mendelians and quantitative geneticists continued down different paths. Quantitative geneticists typically used animal strains and twin studies to explore the cumulative effects of genetics without focusing on the number of genes involved or their individual effects. Meanwhile, precursors of modern molecular geneticists focused on understanding how genes work. It was generally believed at the time that identifying specific genes for complex traits would not be possible.

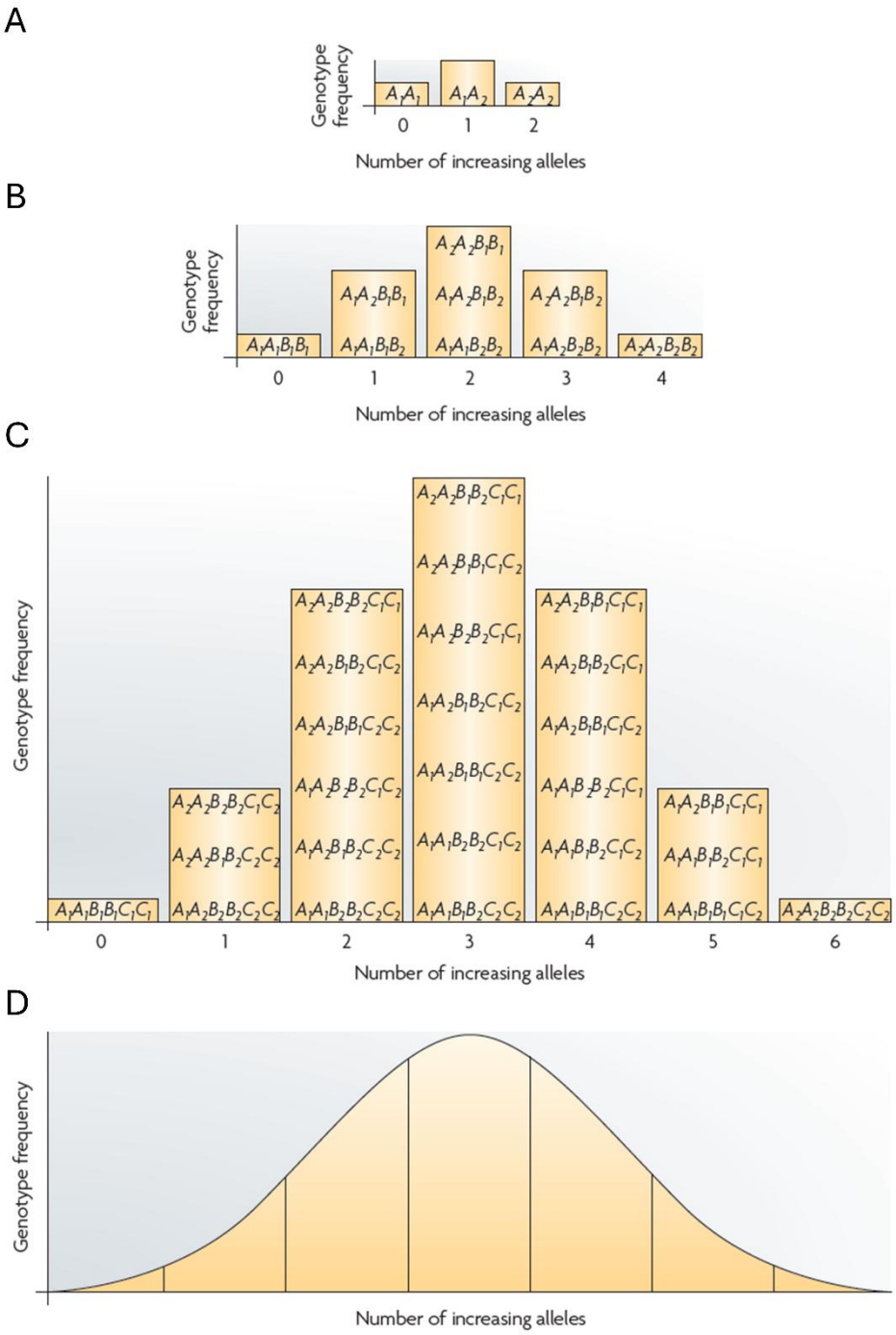

Figure 1.4 Quantitative traits or polygenic traits.
(A) Two alleles at a single locus produce three genotypes and three phenotypes if the allelic effects are additive. If the same equal and additive effects were assumed, 9 genotypes corresponding to 5 genotypes were observed by having 2 genes (B), and 27 genotypes with 7 phenotypes resulted from 3 genes were observed (C). (D) A normally distributed curve can be observed with unequal and non-additive allelic effects and some environmental influence. Taken from (Plomin et al., 2009).

1.4.2 Quantitative trait locus mapping and genome-wide association study

Quantitative trait loci (QTLs) are regions of the genome that contribute to the variation in complex or quantitative traits (Mackay, 2001). The basic concept of QTL mapping is to associate genotype and phenotype in a population with genetic variation (Broman and Sen, 2009). While such mapping studies in humans would be the most straightforward for biomedical research, several challenges exist. First, such studies in humans are expensive, especially when whole-genome sequencing is involved. Second, it is difficult to account for the effects of varying environments and individual life histories. Additionally, there is a high possibility of spurious associations due to population structure. More specifically, a significant difference in allele and genotype frequencies between cases and controls can result from difference in genetics and disease prevalence among subpopulations (Marchini et al., 2004). An excellent alternative is the use of animal models, which facilitates genotype-phenotype mapping for complex traits, including common diseases. Through experimental crosses, QTL mapping can be performed to identify regions in linkage disequilibrium (LD) with molecular markers for qualitative traits. QTL mapping was first described nearly a century ago when factors for size differences in *Phaseolus vulgaris* were found to be linked with factors associated with pigmentation (Sax, 1923). Breeding strategies, including backcross and intercross, have led to successful QTL mapping (Consortium, 2003). In a backcross, the simplest type of cross, two inbred lines are crossed to produce the first generation (F1). The F1 individuals are then crossed with one of the parental lines to generate backcross progeny. As a result of recombination during meiosis, chromosomes in the progeny are typically mosaic. The non-dominant effect of the allele on the chromosome provided by the parental line in the second cross can be detected. In addition to the backcross, intercross is also commonly used. In an intercross, F1 siblings are crossed to obtain F2 progeny. Recombinant chromosomes from either parent can be inherited in the F2 individuals, allowing the detection of dominant alleles on either the maternal or paternal chromosome. Moreover, the degree of dominance at a given QTL can be estimated (Broman and Sen, 2009). With

multiple generations of intercrossing, advanced intercross lines can be developed, enabling fine mapping due to the shorter span of LD resulting from multiple generations of recombination (Broman and Sen, 2009).

Although Fisher demonstrated that qualitative Mendelian inheritance can explain quantitative genetic traits, it became possible to identify genes with small effects on complex traits following the discovery of millions of DNA markers in the 1980s (Plomin et al., 2009). Qualitative disorders influenced by multiple genes can also be considered qualitative traits, as cases and controls can be interpreted simply as being the extremes of quantitative dimensions (Plomin et al., 2009). Unlike the recombinant genotypes generated by experimental crosses, historical recombination events in natural populations provide materials for high-resolution mapping (Figure 1.5). Similar to QTL mapping, marker loci are genotyped, and phenotypes are evaluated in the population of interest for association studies. Single nucleotide polymorphisms are commonly used markers in these studies. In the Human Genome Project, more than 2 million SNPs were characterised (Venter et al., 2001, Sachidanandam et al., 2001). With the large number of markers, higher genetic resolution can be achieved in genome-wide association studies. The resolution for linkage mapping is measured in centimorgans, whereas association studies are measured in kilobases (Mackay, 2001). The first genome-wide association study, performed in 2002, investigated susceptibility to myocardial infarction (Ozaki et al., 2002), followed by the landmark GWA study, conducted in 2005, on age-related macular degeneration (Klein et al., 2005). Many successful associations have been performed in humans and animal models since then.

The advantages of GWA studies include their success in identifying novel genotype-phenotype associations and discovering novel biological mechanisms (Tam et al., 2019). While GWA studies are powerful tools for examining the relationship between phenotypes and genotypes, they have been a subject of controversy. The relatively small increments in disease risk conferred by most identified variants suggest that only a small proportion of heritability is explained by these markers (Manolio et al., 2009). Additionally, GWA results may

be confounded by cryptic population stratification (McClellan and King, 2010). Population stratification arises when individuals from different ancestral backgrounds are included in a study, and these backgrounds have distinct allele frequencies for specific genetic variants. A variant associated with a trait is not always the causal locus, but a proxy to it because of linkage disequilibrium. If variants in all genes are implicated, the findings would be uninformative (Tam et al., 2019). A GWA study has identified 20 polymorphisms associated with the adult height (Weedon et al., 2008); however, these loci only explained less than 3% of the population variation in height (Goldstein, 2009). To explain 80% of the population variation in height, an estimated 93,000 SNPs would be required. Even if each remaining variant explained as much as 0.05% of the variation, approximately 1,500 variants would be needed to account for the missing heritability, which leads to an unmanageable number of common variants (Goldstein, 2009). Therefore, post-GWA study experiments, including functional studies, gene network analysis, and translational medicine, have been proposed to address these issues. For example, evidence suggests that the causal loci often function through regulatory effects on the expression of target genes (Gallagher and Chen-Plotkin, 2018). Candidate variants for follow-up studies can be prioritised by integrating GWAS findings with functional genomics data.

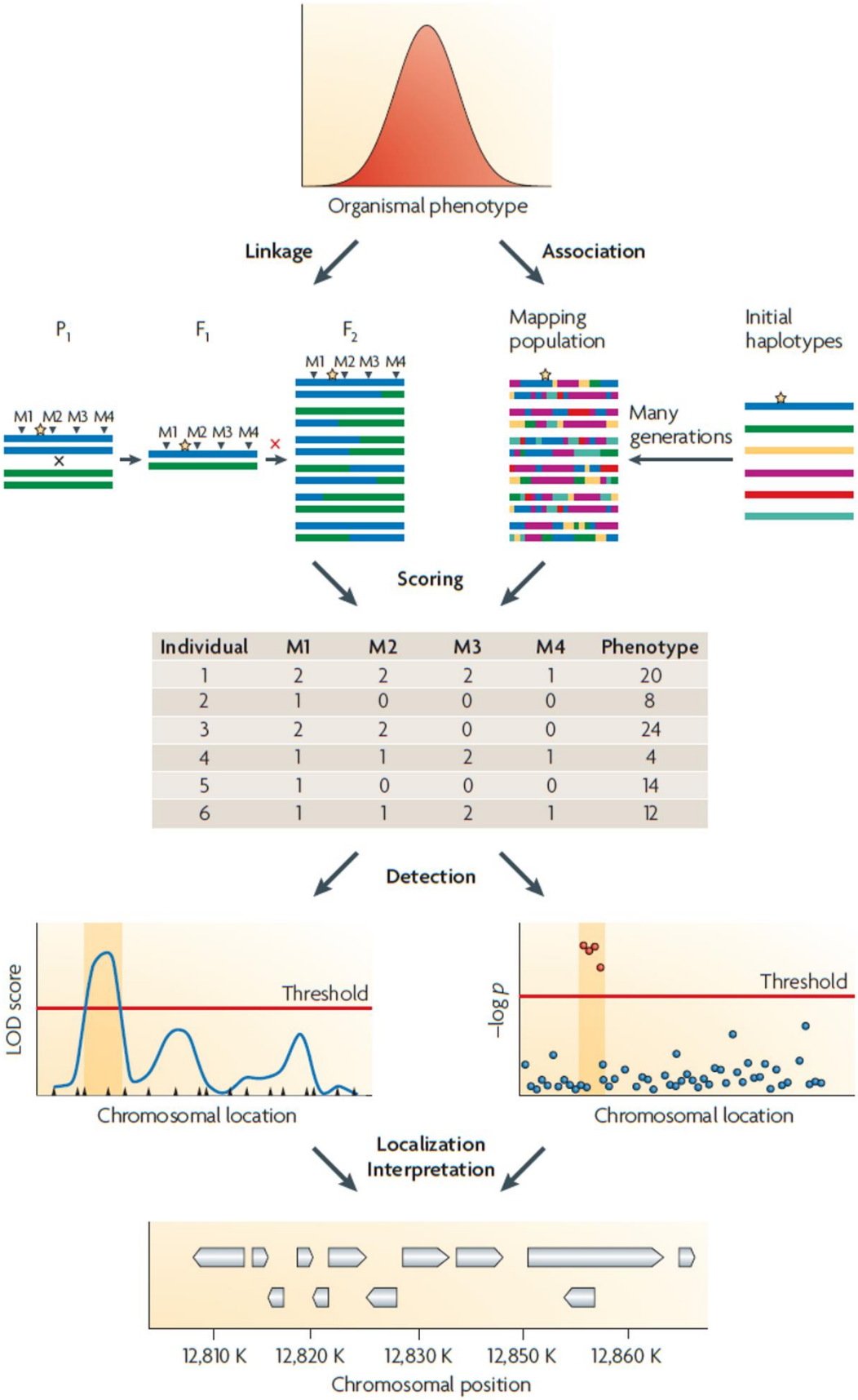

Individual	M1	M2	M3	M4	Phenotype
1	2	2	2	1	20
2	1	0	0	0	8
3	2	2	0	0	24
4	1	1	2	1	4
5	1	0	0	0	14
6	1	1	2	1	12

Figure 1.5 Quantitative trait locus mapping.
QTL mapping aims to identify the genetic basis of variation in quantitative traits. Both linkage-based analysis and association mapping utilize recombination events, but while linkage analysis uses recombinant markers from experimental crosses, association mapping relies on historical recombination events. Map positions are typically estimated through interval mapping, whereas association mapping tests markers individually. Taken from (Mackay et al., 2009).

1.5 *Drosophila melanogaster*

1.5.1 History of *Drosophila* as a genetic model

Drosophila melanogaster, the fruit fly, is one of the most extensively studied organisms in biology (Adams et al., 2000). Around 1900, Charles W. Woodworth, a graduate student in the laboratory of William E. Castle, was the first to demonstrate the availability of *Drosophila* for experimental purposes (Allen, 1975). Another member of the group, Frederic W. Carpenter, who studied behavioural responses in insects, also began working with *Drosophila* (Carpenter, 1905). In addition to Thomas H. Morgan, two other individuals were directly inspired by Castle's work (Allen, 1975). They were William J. Moenkhaus, who focused on heredity and sex determination, and Franke E. Lutz, who was interested in heredity and evolution. Since the first published work on heredity by Castle's laboratory in 1906 (Castle et al., 1906) and the identification of the *white* gene by Morgan in 1910 (Morgan, 1910), *Drosophila* has been widely used as a genetic model in biological research for over a century.

To date, five Nobel Prizes have been awarded to drosophilists. In 1933, Morgan received the Nobel Prize in Physiology or Medicine for his demonstrations concerning the role played by chromosomes in heredity. In 1927, Hermann J. Muller discovered that the mutations could be induced by X-ray irradiation (Muller, 1927). Nineteen years later, Muller was awarded the Nobel Prize in Physiology or Medicine for this discovery. Following 1910, the subsequent 50 years of research in *Drosophila* focused on dissecting the principles of inheritance, while studies on many other biological processes were developed between 1960 and 2010 (Bellen et al., 2010). In the research of developmental biology, the Nobel Prize in Physiology or Medicine 1995 was awarded jointly to

Drosophila researchers, Edward B. Lewis, Christiane Nüsslein-Volhard, and Eric F. Wieschaus, for their discoveries regarding the genetic regulation of early embryonic development. In 2011, the Nobel Prize in Physiology or Medicine was once again awarded to a *Drosophila* researcher, Jules A. Hoffmann, who shared the honour with two other scientists for their discoveries in innate immunity (Lemaitre et al., 1996). In the 1970s, mutations in a previously unknown gene, named *period*, were found to disrupt the circadian clock in flies (Konopka and Benzer, 1971). The Nobel Prize laureates in 2017, Jeffrey C. Hall, Michael Rosbash, and Michael W. Young, succeeded in isolating the *period* gene and identifying other clock genes involved in a self-regulating clockwork mechanism during the 1980s and 1990s (Bargiello et al., 1984, Zehring et al., 1984, Hardin et al., 1990, Vosshall et al., 1994). Altogether, *Drosophila* has been used to investigate numerous developmental and cellular processes.

1.5.2 Advantages of using *Drosophila* as a model organism

Drosophila was originally a forest-dwelling species confined to a limited region of equatorial Africa. However, today, it can be found in laboratories and kitchens all over the world (Keller, 2007). By 1900, just 25 years after its initial discovery on American soil, *Drosophila* had become the most common species across the country (Keller, 2007). Around the same time, it was being cultured in laboratories for experimental purposes. Similar to another widely used laboratory animal, *Mus musculus*, which started as a human commensal and spread globally due to human activity (Boursot et al., 1993), *Drosophila* shares the same factors contributing to its success as a commensal and its popularity as a laboratory animal. The flies have a short generation span, the ability to produce large numbers of offspring, and can be easily cultured on a wide variety of food sources.

1.5.2.1 Life cycle of *Drosophila*

Like beetles and moths, the fruit fly is holometabolous, undergoing complete metamorphosis with four stages: egg, larva, pupa, and adult (Markow, 2015).

Once the egg is fertilized and laid by the female, the embryo develops for about one day at 25°C before hatching into a larva. After passing through three distinct developmental stages (L1 to L3) with two moults, the first instar larva becomes the third instar larva, a process that takes about 48 h. The third larval stage lasts around 72 h, during which the animal grows substantially and becomes highly mobile before pupation. The immobile state of development marks the start of pupation, which occurs approximately 120 h after the beginning of embryonic development. During metamorphosis, most of the larval tissues are destroyed, except for the Malpighian tubules (MTs), which survive and are retained in the adult (Denholm, 2013). Some adult tissues, such as wings and eyes, develop from imaginal discs. Metamorphosis can be divided into two stages: a 12 h prepupal period followed by the pupal period, which lasts about 84 h. Eclosion occurs approximately 9 days after the egg is laid. A newly eclosed female will be virgin for 5-8 h at 25°C (Prokop and Root, 2013). After mating, the sex peptide from the male's seminal fluid triggers the onset of egg laying (Kubli, 1992). A single mated female fruit fly can produce up to 500 eggs over the course of her lifetime (Hyde, 1921), and the median lifespan of commonly used lab trains ranges from 50 to 70 days (Woodling, 2024). Similar to humans, sexual dimorphism in life expectancy is observed, with individuals of the homogametic sex living longer than those of the heterogametic sex (Seifarth et al., 2012).

1.5.2.2 Genetic similarities between *Drosophila* and human

With over 670 million years having passed since the divergence between protostomes and deuterostomes (Ayala et al., 1998), one might expect little genetic similarity between *Drosophila* and humans. However, the genetic control of body axis formation and segmentation has been conserved between flies and mammals (Simeone et al., 1992). This conservation extends to cellular mechanisms underlying diverse biological processes, including rhythmic functions (Young and Kay, 2001) and innate immunity (Lemaitre et al., 1996, Poltorak et al., 1998). Furthermore, cloning of the *maroon-like* gene in *Drosophila* led to the

identification of its human homologue, a gene responsible for classical xanthinuria type II (Ichida et al., 2001).

In 2000 and 2001, the 120-megabase euchromatic portion of the *Drosophila* genome (Adams et al., 2000) and the 2.91-billion base pair consensus sequence of the euchromatic portion of the human genome (Venter et al., 2001) were generated, respectively, using the whole-genome shotgun sequencing strategy. The genome annotations revealed 14,113 and 26,588 protein-encoding transcripts in *Drosophila* and humans, respectively. Although *Drosophila* contains a smaller number of genes, 48% of its genes have evolutionarily conserved human homologues (Yamamoto et al., 2014). A mosaic genetic screen of lethal mutations on the *Drosophila* X chromosome identified 165 genes, 93% of which have homologues in humans. Additionally, 714 out of 929 distinct OMIM human disease genes have highly similar cognates in *Drosophila* (Reiter et al., 2001). Taken together, these findings demonstrate that *Drosophila* serves as a powerful model for studying human disease genes.

1.5.2.3 Genetic tools and resources in *Drosophila*

With over a hundred years of use, *Drosophila* has become a cornerstone of genetic research, supported by an unparalleled wealth of tools, databases, and resource centres dedicated to this animal model. This has made *Drosophila* one of the most genetically tractable organisms, enabling milestone discoveries in biology. Key findings in *Drosophila* have also inspired and guided numerous research efforts in vertebrates (Bellen et al., 2010).

The P-element transposon (Cooley et al., 1988), along with P-element-based genetic tools such as the GAL4/UAS system (Brand and Perrimon, 1993), can be used to integrate exogenous DNA into the germline of *Drosophila*. These systems are designed for a variety of applications, including gene disruption, gene tagging, and inducible gene expression. Balancer chromosomes (Muller, 1927, Muller, 1918) enable the maintenance of heterozygous mutations, allowing the study of essential genes in heterozygotes, where homozygous mutations are lethal. *Drosophila* remains the only multicellular organism in which more than

95% of mutations in essential genes can be easily and effectively maintained (Bellen et al., 2010). Furthermore, the introduction of the CRISPR/Cas9 system in *Drosophila* has enhanced the ability to generate mutations, and high-resolution melt analysis enables highly sensitive detection of these mutations (Gratz et al., 2013, Bassett et al., 2013).

Drosophila stock centres, such as the Bloomington *Drosophila* Stock Centre (BDSC) and the Vienna *Drosophila* Resource Centre (VDRC), provide a wide range of genetic tools, including RNAi fly stocks for loss-of-function studies, TRiP-CRISPR overexpression lines for gene activation in gain-of-function experiments, and fly lines carrying human cDNA for cross-species studies. The Berkeley *Drosophila* Genome Project (BDGP) gene disruption project generated 7,140 lines predicted to disrupt 39% of annotated *Drosophila* genes (Bellen et al., 2004, Spradling et al., 1999). Additionally, the Transgenic RNAi Project (TRiP) at Harvard Medical School includes 11,491 lines, covering 71% of *Drosophila* genes (Perkins et al., 2015). FlyBase (Ashburner and Drysdale, 1994) is the primary database for integrated genetic and genomic data used by drosophilists. Furthermore, FlyAtlas provides a comprehensive view of gene expression across multiple tissues in *Drosophila* (Chintapalli et al., 2007, Leader et al., 2018), aiding in the identification of novel functions for genes that are predominantly expressed in unexpected tissues. In 2022, a comprehensive single-cell atlas of the adult *Drosophila* was released, profiling 580,000 individual cells and identifying more than 250 cell types across 15 tissues (Li et al., 2022). This atlas provides an invaluable resource for understanding genetic perturbations and diseases at single-cell resolution.

1.5.3 *Drosophila* genetics

One of the greatest advantages of using *Drosophila* as a model organism is the ability to easily manipulate its genome. In genetic studies, both the environment and the genetic background of flies can be well controlled. Both forward and reverse genetic approaches can be employed to understand the relationship between genes and phenotypes in *Drosophila*.

1.5.3.1 Balancer chromosomes

Balancer chromosomes, first described nearly a century ago by Muller in *Drosophila* (Muller, 1918), are chromosomes that are multiply inverted and rearranged. They are extensively used in stock maintenance and complex crosses (Miller et al., 2019). Inversions, or crossover suppressors, can be induced by radiation treatment (Roberts, 1970, Roderick and Hawes, 1970) or chemical mutagenesis (Auerbach, 1949). Additionally, homologous recombination can efficiently induce chromosomal rearrangements at a frequency of 1% to 4% (Egli et al., 2004). The multiple inversions and rearrangements constrain recombination and impede the recovery of recombinant products by preventing meiotic DNA double-strand breaks from being repaired as crossovers (Hentges and Justice, 2004). With two additional properties, the presence of dominant markers and lethality caused by recessive mutations, balancers enable the maintenance of stocks carrying single deleterious allele mutations. Recessive lethal or sterile mutations balanced with balancers can be maintained as heterozygous stocks while still producing viable offspring. Dominant markers other than *Curly* or *Stubble*, such as green fluorescent protein (GFP), have also been developed (Casso et al., 1999), enabling the selection of desired animals during the larval stage. It is important to note that not all balancers are equal, as different inversions suppress meiotic recombination in different chromosomal regions (Miller et al., 2019). In addition to maintaining stocks, balancer chromosomes can also facilitate the selection of new lethal mutations in mutagenesis screens (Hentges and Justice, 2004).

1.5.3.2 P-element

Mobile genetic elements were first described by Barbara McClintock in maize, where these mobile elements were referred to as “control elements” and were coordinated by a second genetic element, the “activator” (McClintock, 1956). These transposable genetic elements are DNA segments capable of moving along or between chromosomes in the presence of the regulator. P-elements are a type of mobile genetic element discovered in *Drosophila*, where they cause

hybrid dysgenesis (Kidwell et al., 1977, Sved, 1979). One characteristic of hybrid dysgenesis is nonreciprocality. When females of M strains, which lack P-elements, are mated to males of P strains, which contain P-elements, defects, such as sterility, mutation, and male recombination, are often observed in the offspring. However, no dysgenic traits are seen in the progeny from the reciprocal cross or self-crosses. Furthermore, due to alternative splicing, the transposition of P-elements is restricted to germ cells (Roche et al., 1995), so the F1 individuals are somatically normal. Transposition is suppressed in flies with the “P cytotype” but is permissible with the “M cytotype”, with the repressor being maternally expressed. When a P strain female, which expresses the repressor, is mated to a male from either M or P strains, transposition is suppressed in the progeny. With the introduction of desired DNA into the P transposable element, germline transformation allows the incorporation of new genetic material into the genome (Rubin and Spradling, 1982, Spradling and Rubin, 1982). This process facilitates the generation of transgenic organisms. The BDGP lines were generated using single P-element insertions (Spradling et al., 1999, Bellen et al., 2004). P-elements have also been used for enhancer trapping. A P-element carrying a reporter gene (e.g., *lacZ*, *GFP*) is linked to a weak promoter. When the P-element inserts near a gene's enhancer, the reporter gene is expressed under the control of that enhancer, revealing the tissue-specific expression pattern (O'Kane and Gehring, 1987).

1.5.3.3 GAL4/UAS system

As the second generation of enhancer trapping, the GAL4/UAS system (Brand and Perrimon, 1993) is probably the most popular and versatile genetic tool used in *Drosophila*. GAL4, a transcriptional activator protein found in yeast important for galactose metabolism, can bind to DNA and activate transcription (Ptashne, 1988). The activity of GAL4 is repressed by the GAL80 protein in the absence of galactose. When galactose is present, the repression is alleviated, and the upstream activation sequence (UAS) is specifically targeted by GAL4, leading to the transcription of genes involved in galactose metabolism. The DNA binding and transcriptional activation ability of GAL4 were also demonstrated in

Drosophila (Fischer et al., 1988) and mammalian cells (Kakidani and Ptashne, 1988, Webster et al., 1988), but only for promoters that contain GAL4 binding sites.

The introduction of the GAL4/UAS system to *Drosophila* was accomplished in 1993 by Andrea H. Brand and Norbert Perrimon (Brand and Perrimon, 1993). On the one hand, promoters could be subcloned upstream of GAL4 in the pGaTB vector, while the gene of interest was introduced into the pUAST vector. These two vectors were individually integrated into two transgenic lines by P-element transformation. In the F1 progeny resulting from a cross between these two fly lines, the transcription of the gene of interest would be activated by GAL4 from the other parental line. On the other hand, an enhancer detection screen could be performed. The mobilization of a single X-linked enhancer detection GAL4 cassette, pGawB, in a hemizygous lethal strain was induced by a defective P-element on the third chromosome of a “jumpstarter” strain. The random integration of GAL4 into the genome produced enhancer trap lines under the control of a diverse array of genomic enhancers. With this binary system, sequences behind GAL4 binding sites can be expressed with distinct temporal and spatial patterns. The downstream sequence can include a gene for overexpression or short hairpin RNAs (shRNAs) for knocking down the expression of a specific gene. Temporal control of the system is achieved by introducing temperature-sensitive GAL80 into the system or using RU486 in the GeneSwitch system. Modified GAL4 systems, such as split GAL4, have also been developed. In split GAL4, the DNA binding domain and activation domain are fused to separate heterodimerizing leucine zipper motifs. Functional GAL4 protein reconstitution, which activates UAS and downstream sequence, occurs only when these fusion proteins are expressed in the same cell (Luan et al., 2006). Additionally, the development of split-intein GAL4, which is repressible by GAL80, allows for temporal control of the system (Ewen-Campen et al., 2023). The development of other binary systems, such as LexA/LexAOP and QF/QUAS, also allows the separate control of genes of interest, distinct transgenic manipulations of different cell populations, and generation of intersectional expression patterns (Potter and Luo, 2011).

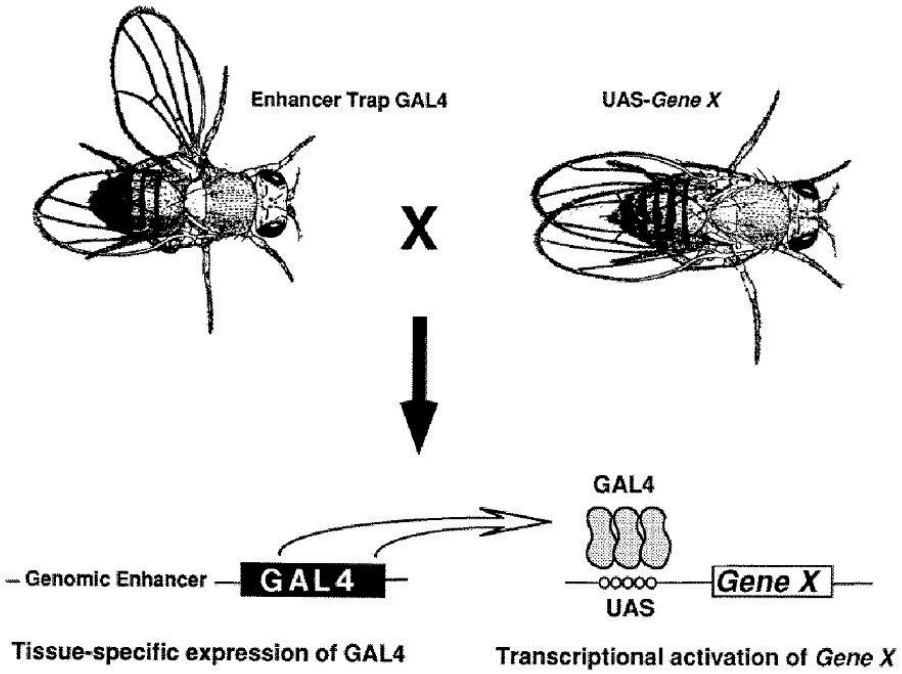

Figure 1.6 The *Drosophila* GAL4/UAS system.
To express gene X in a specific tissue, virgin females of the UAS line were crossed with males of the tissue specific GAL4 line. In the next generation, GAL4 was induced by the adjacent enhancer, leading to the expression of gene X in a tissue-specific manner. Taken from (Brand and Perrimon, 1993).

1.5.4 The *Drosophila melanogaster* genetic reference panel

Understanding the genetic basis of quantitative or complex traits is crucial for animal and plant breeding, as it helps uncover evolutionary forces shaping variation, predict phenotypes, and personalise medication for individuals. While the principle of genotype-phenotype mapping is relatively straightforward, it remains challenging in most species. The *Drosophila melanogaster* genetic reference panel (DGRP) is a collection of 205 fully inbred fly lines derived from a single outbred wild population (Huang et al., 2014, Mackay et al., 2012). After 20 generations of full-sibling inbreeding, only 16% of the lines exhibited more than 2% segregating autosomal variants, and 4% had more than 2% segregating X-linked variants (Huang et al., 2014), suggesting that most variants became homozygous after inbreeding. This approach resulted in minimal genetic variation within individual lines but maximised genetic variation across lines, reflecting the variation found in the natural population. The DGRP genome

contains approximately 4 million polymorphic markers, with most of them being single nucleotide polymorphisms (Mackay et al., 2012, Huang et al., 2014). Two key characteristics define the DGRP. First, the genomic relationships among DGRP lines are relatively low. Second, the pairwise linkage disequilibrium between polymorphic markers decays rapidly with increased distance. The low population structure among the DGRP lines minimizes the risk of spurious associations arising from stratified populations, and the low linkage between markers facilitates the identification of causal loci or loci in linkage with casual ones.

It is worth noting that highly deleterious alleles were purged from the panel during inbreeding, as approximately 1,500 isofemale lines were established, with about 200 lines remaining today (Mackay and Huang, 2018). Additionally, during inbreeding, selection for epistatic interactions between variants that increase fitness may have occurred. Adaptation to the laboratory environment, along with changes in allele frequency, would also be possible. Because GWA analyses were conducted on only about 200 DGRP lines with several million tests, it is reasonable to expect that only a few variants would reach the multiple-comparison-corrected threshold (Anholt and Mackay, 2018). In most association studies using the DGRP, a null uniform distribution of the quantile-quantile (QQ) plots was observed, suggesting enrichment of the true positive associations, typically at a nominal p value of 10^{-5}. Therefore, this threshold can be used as an empirical threshold to prioritise variants for downstream verification (Anholt and Mackay, 2018).

The DGRP has been widely used to investigate the genetic architecture of complex traits, including longevity (Ivanov et al., 2015), gut immunocompetence (Sleiman et al., 2015), and olfactory behaviour (Swarup et al., 2013). Considerable phenotypic and genetic variation has been observed for all quantitative traits. Furthermore, genotype-by-environment interactions have been observed in studies of lifespan under different temperatures (Huang et al., 2020) or dietary restrictions (Wilson et al., 2020), as well as in microbiota-related host nutritional indices (Dobson et al., 2015). In addition, the DGRP has

facilitated the study of epistasis or genetic modifiers of disease-causing genes. For example, a *Drosophila* model of NGLY1 deficiency was crossed with a panel of the DGRP lines (Talsness et al., 2020), revealing a phenotypic spectrum of lethality ranging from 0 to 100% in the resulting progeny and identifying *Ncc69* as the top association hit. NKCC1, the orthologue of *Drosophila* Ncc69, exhibited altered average molecular weight and decreased function in *Ngly1*$^{-/-}$ mouse cells. Additionally, a continuous and highly heritable distribution of eye degeneration caused by expressing human mutant preproinsulin (hINS^{C96Y}) was observed in F1 generations from crosses between the transgenic line carrying the mutant preproinsulin and a subset of the wild-derived strains (He et al., 2014). This study identified *sfl* as the genetic modifier of hINS^{C96Y}-induced eye degeneration.

In addition to GWA analyses, extreme QTL mapping can also be performed in the DGRP by constructing outbred advanced intercross populations (AIPs). This approach enables a larger sample size for mapping, as it allows the generation of many genotypically different individuals (Mackay and Huang, 2018). Unlike conventional association mapping, individuals with extreme phenotypic values can be collected, and the two pools can be sequenced after phenotyping, as the causal alleles are likely to be enriched in the extreme lines. Overall, the DGRP has proven to be a valuable genetic resource for studying the genetic basis of complex traits.

1.5.5 The *Drosophila* Malpighian tubule

Insects, which are characterised by their small size, have a large surface-to-volume ratio (O'Donnell, 2022, Dow, 2009), suggesting that they are constantly exposed to osmotic stresses in the terrestrial environment. The Malpighian tubule is a major excretory organ responsible for osmoregulation, transport, metabolism, and detoxification in most insects. It was first described by Marcello Malpighi in the seventeenth century, using the silkworm *Bombyx mori* (Davies et al., 2019). Significant progress in understanding the Malpighian tubule was made in the twentieth century. Vincent B. Wigglesworth established original functional assays of tubule function, which were later followed by his students James A.

Ramsay and Simon H.P. Maddrell (Dow and Davies, 2001). With the advancement of *Drosophila* genetics, the *Drosophila* Malpighian tubules have emerged as a rapid and effective model for studying renal development, function, and disease.

1.5.5.1 Structure and function

Drosophila has four blind-ended Malpighian tubules, which are joined by common ureters at the boundary of the midgut and hindgut (Figure 1.7). The anterior pair, located on the right, are oriented forward, reaching as far as the thorax of the adult, while the left pair is located posteriorly. The tubules can be divided into four domains based on their morphology and function: the enlarged initial segment, transitional segment, main segment, and lower tubule (Dow et al., 1994, Sozen et al., 1997). The initial segment in the anterior tubules is involved in calcium storage (Dube et al., 2000b, Browne and O'Donnell, 2016) and the elimination of excess dietary Ca^{2+}. Approximately 85% of the Ca^{2+} that enters the tubule is sequestered as granules (Dube et al., 2000a), and the anterior tubules contain much more calcium (25-30% of the total calcium content in the fly) compared with the posterior tubules (Dube et al., 2000b). The main segments of both the anterior and posterior tubules secrete K^+-rich fluid, with high secretion rates observed on a per-cell volume basis (Dow et al., 1994, O'Donnell and Maddrell, 1995). The lower tubule is responsible for reabsorbing water and K^+.

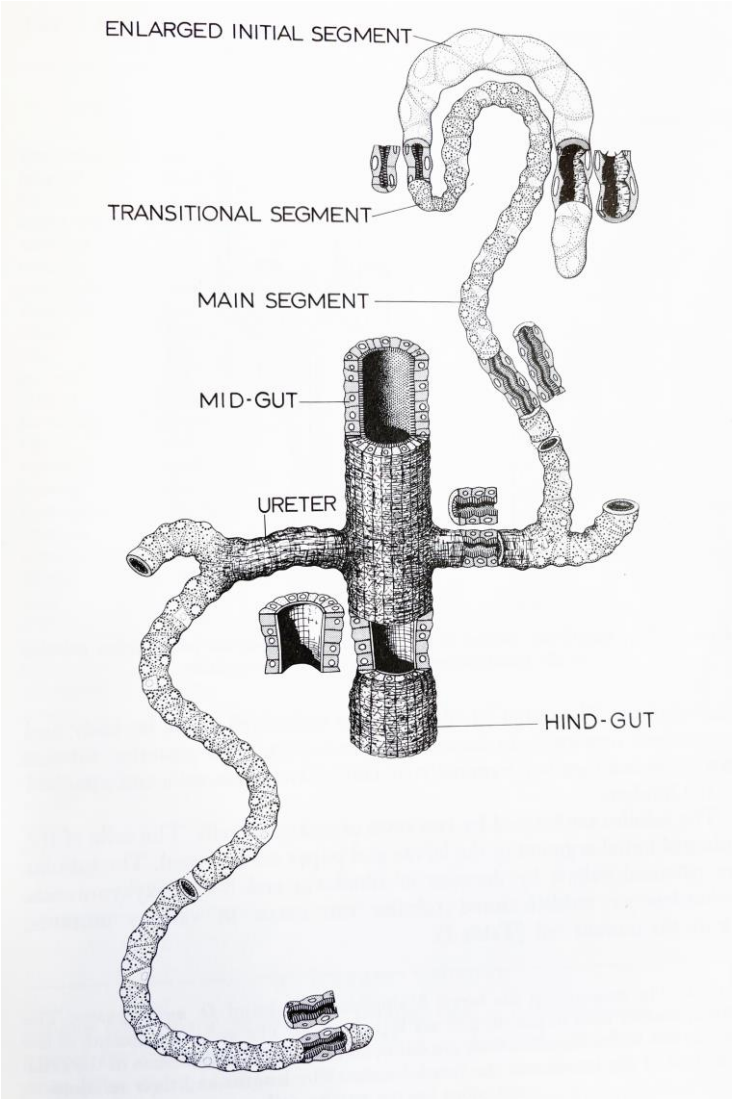

Figure 1.7 Morphology of the *Drosophila* MT.
There are four tubules in *Drosophila*, and each tubule has four distinct morphologic regions: initial, transitional, and main segments, and lower tubule. Each pair converge through common ureters at the midgut-hindgut junction. Taken from (Wessing and Eichelberg, 1978).

In the Malpighian tubules of *Drosophila*, there are three major cell types: primary principal cells (PCs), intercalated secondary stellate cells (SCs), and renal stem cells (RSCs). The number of PCs and SCs remains constant throughout the larval, pupal, and adult stages (Sozen et al., 1997). Interestingly, SCs are only present in the distal regions of the MTs and are absent from the proximal parts, such as the lower tubules. In contrast, RSCs are present only in the region of lower tubules and ureters in adult MTs (Singh et al., 2007). The PCs exhibit deep basal infoldings, long apical microvilli, and a highly elaborate

cytoarchitecture characterised by a large number of mitochondria. This configuration suggests that PCs are metabolically active and involved in significant ion transport. On the other hand, SCs have simpler structures and fewer mitochondria (Wessing and Eichelberg, 1978), indicating different functional roles between the two cell types. The metabolically active PCs express large ion transport complexes such as V-ATPases (Allan et al., 2005) and Na^+/K^+ exchangers (Torrie et al., 2004), which facilitate the transepithelial movement of cations. To complete a circuit of the current, transcellular chloride shunt controlled by chloride channels and water movement by aquaporins take place in SCs (Cabrero et al., 2014, Cabrero et al., 2020).

Enhancer trap lines have revealed the existence of at least two distinct subpopulations of PCs (Sozen et al., 1997). Additionally, secondary cells, distributed evenly throughout the distal parts of the posterior tubules, were also found in the initial and transitional segments of the anterior tubule but exhibited a bar-shaped morphology. RSCs, first described as “tiny cells” in lower tubules and posterior midgut, were proposed to monitor fluid secretion and secrete neurohormones (Sozen et al., 1997). They were found to be proliferating, as indicated by positive phospho-histone-H3 staining (Singh et al., 2007). Mosaic lineage labelling indicated that these cells, as pluripotent stem cells, can differentiate into *teashirt*-positive and *cut*-positive cells. However, it has been reported that renal stem cells are unipotent and only replenish PCs in the stem cell zone upon injury (Wang and Spradling, 2020, Wang and Spradling, 2022). Recently, single-nucleus RNA sequencing identified nine distinct clusters of cells in the adult fly MTs (Figure 1.8), with new markers validated by driving fluorescent reporters using the corresponding Gal4 lines (Xu et al., 2022). This work further enhanced our understanding of the complexity and diversity of the cell types in this important tissue. For example, the transcription factor *fruitless* was found to play a role in stem cell regeneration, whereas genes such as *Prip* and *CG1093* contribute to the regulation of SC morphology.

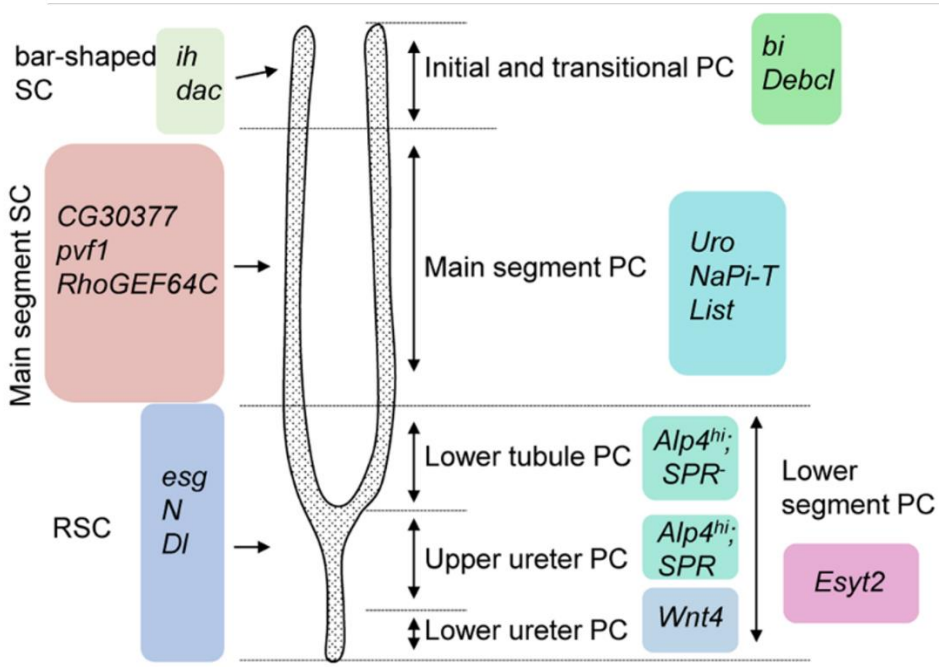

Figure 1.8 Cell types identified in the MTs based on differentially expressed marker genes.
There are nine distinct clusters representing regionally specific principal cells, stellate cells, and renal stem cells. Markers for renal stem cells are *escargot*, *Notch*, and *Delta*. Markers for bar-shaped SCs are I_h *channel* and *dachshund*. The main segment SCs are defined by the expression of *CG30377*, *pvf1*, and *RhoGEF64C*. Markers for lower tubule PCs, upper ureter PCs, lower ureter PCs, and lower segment PCs are: SPR^-, $Alp4^{hi}$; SPR^+, $Alp4^{hi}$; *Wnt4; and Esyt2*, respectively. The expression of *bifid*, *Debcl*, *Uro*, *NaPi-T*, and *List* defines principal cells in distal tubules. Taken from (Xu et al., 2022).

Like other species in the Order of Diptera, two secretory cell types in *Drosophila* MTs, PCs and SCs, along with neuropeptide signalling, coordinate tubular fluid secretion and regulate ion and water homeostasis (Dow et al., 2021, Dow et al., 2022). These signalling mechanisms involve receptors that are specifically expressed in either PCs or SCs (Figure 1.9). For example, receptors for the neuropeptide Kinin are confined to SCs (Radford et al., 2002), while receptors for Capa (Terhzaz et al., 2012) and DH_{31} (Coast et al., 2001) are exclusively expressed in PCs. Upon ligand recognition by these neuropeptide receptors, intracellular calcium levels are increased, triggering distinct responses in the two cell types. In mitochondria-enriched PCs, an increase in cytosolic calcium activates mitochondria at the apical brush border. This configuration leads to increased ATP synthesis, which drives cation secretion (Terhzaz et al., 2006, Beyenbach et al., 2010). In SCs, the level of intracellular calcium is regulated by

the phospholipase C/inositol 1,4,5-trisphosphate (PLC/IP_3) pathway, which triggers the release of calcium from intracellular stores upon activation. This calcium release activates secCl, a secretory Cl^- channel (Feingold et al., 2019). The secretion of cations and chloride ions into the tubule lumen is accompanied by the osmotic flow of water, facilitated by specialized water channels (Cabrero et al., 2020). This mechanism ensures the bulk flow of an approximately isotonic saline solution, helping maintain ion and water balance in the insect.

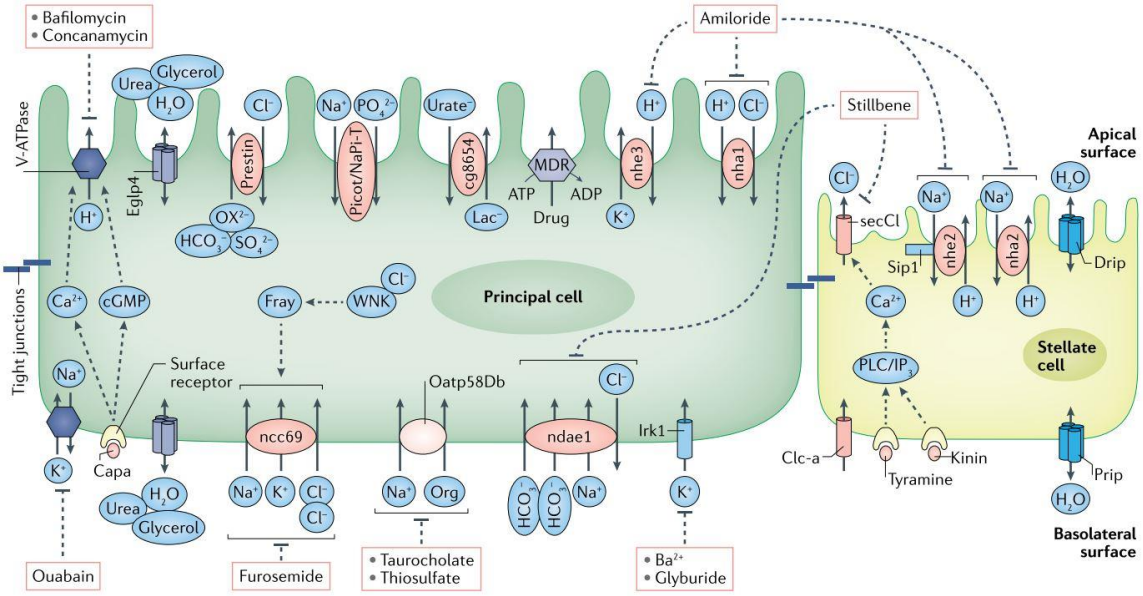

Figure 1.9 Cross-section diagram of the Malpighian tubule.
The V-ATPase expressed in the principal cell is used for electrogenic proton transport, while Cl^- shunt conductance and the osmotic movement of water occur through the stellate cell, which expresses high levels of Cl^- and water channels. Several protein pumps, transporters, and channels and their human homologues can be pharmacologically inhibited. Taken from (Dow et al., 2022).

1.5.5.2 Development

The development of *Drosophila* Malpighian tubules, serving as a model for tubulogenesis, has been studied extensively, revealing striking similarities with renal development in humans. These similarities are particularly evident in the coordinated intercalation of an embryonic cell lineage that undergoes a mesenchymal-to-epithelial transition (Denholm et al., 2003, Cho and Dressler, 2003). *Drosophila* Malpighian tubules arise from the shared hindgut primordium and develop through a series of well-defined steps: (i) cell specification of

tubule primordia, (ii) eversion of the tubule primordia, (iii) cell division, (iv) mesenchymal recruitment, (v) cell rearrangement, and (vi) functional maturation marked by the presence of uric acid crystals (Beyenbach et al., 2010, Dow and Romero, 2010, Denholm, 2013).

During *Drosophila* tubule development, the specification of the tubule primordia occurs approximately 7 hours after embryogenesis begins (stage 11). At this stage, four clusters of approximately 20 cells, characterised by the coexpression of transcription factors *cut* and *Kruppel*, are specified to adopt the tubule fate (Hatton-Ellis et al., 2007). The spatial restriction of this coexpression is regulated by Wnt signalling within the gut. Interestingly, while the ectopic coexpression of *Kruppel* and *cut* leads to cell differentiation and uric acid precipitation, it does not result in the formation of tubule branches (Hatton-Ellis et al., 2007). In response to TGF-*β* signalling, the expression of *Doc* and *brk* specifies the anterior and posterior tubules, respectively, and facilitates the eversion process (Hatton-Ellis et al., 2007). During this eversion, the primordial cells maintain their apicobasal polarity. Two groups of cells emerge ventrally, while the other two groups arise laterally. Cells projecting toward the caudal mesoderm become the posterior tubules, while the others become the anterior tubules, establishing left-right asymmetry. At stage 12, additional divisions, driven by an EGF-like ligand from the tip cells, generate all the primary cells found in adult tubules, thereby maintaining a constant cell number (Janning et al., 1986, Skaer and Arias, 1992). By mid-embryogenesis (stage 13), cell proliferation ceases, but the number of tubule cells is fortified by integrating cells from caudal visceral mesoderm (Denholm et al., 2003). These cells undergo a mesenchymal-to-epithelial transition and develop apicobasal polarity after migration. They are referred to as stellate cells and express the transcription factor *tsh*. Failure to integrate SCs results in premature death of the animal and impaired responses to the neuropeptide Kinin (Denholm et al., 2003). During stages 13 to 16, the tubules begin to elongate and develop their morphology mainly through cell rearrangements. Initially, the tubules consist of a single layer of epithelial cells, with 8-12 cells around the circumference. After rearrangements, the epithelium is reduced to approximately two cells in

circumference. At the same time, the tubules ramify into the body cavity following highly stereotypical routes. Mutation of *punt* or *schnurri* causes abnormalities in tubule localisation (Jack and Myette, 1999). Towards the end of embryogenesis (stage 17, 22 h after fertilization), the tip cell locates itself in its final position, the alary muscle for the anterior tubules and the hindgut visceral nerve for the other pair. The tubules also develop functional competence at this time point, as evidenced by the formation of white uric acid crystals in the lumen of posterior tubules.

After embryonic development is finished, the larval tubules undergo further growth by increasing both nuclear and cell size (Denholm, 2013). During pupal development, MTs survive the metamorphosis and are retained in the adult. However, the length of the tubules is reduced to half of their size at the larval stage. Changes in cell morphology are also observed. SCs, which are cuboidal in larval tubules, become bar-shaped in the initial segment and stellate-shaped in the main segment after eclosion.

1.5.5.3 Modelling renal function and disease

Dozens of *Drosophila* genes, corresponding to human kidney genetic diseases, have been identified in the renal tubules (Miller et al., 2013). Given the strong genetic similarities between humans and *Drosophila*, along with the versatile genetic tools available, *Drosophila*, with its simpler renal tubule structure, serves as an excellent model for studying renal function and disease.

Nephrolithiasis. More than 75% of human kidney stone cases are caused by the formation of calcium oxalate (Singh et al., 2015). The formation of calcium phosphate and uric acid crystals is a constitutive process, and the development of calcium oxalate stones can also be observed in *Drosophila*. Under polarized light microscopy, birefringent calcium oxalate and uric acid stones can be easily visualized and quantified in dissected MTs or living larvae through the transparent cuticle (Dow et al., 2022). In whole adult flies, CaOx crystals can also be detected using micro-computed tomography (Hirata et al., 2012). Dietary supplementation with oxalate (Hirata et al., 2012), hydroxy-L-proline (Khan et

al., 2006), or ethylene glycol (Chen et al., 2011) readily induces the formation of calcium oxalate crystals within the tubule lumen. Additionally, the ubiquitous knockdown of *CG3926* causes the formation of CaOx crystals, while dietary N-acetyl-L-hydroxyproline reduces the number of crystals in the tubule (Yang et al., 2018). Xanthinuria types I and II are rare inborn metabolic disorders resulting from defective purine metabolism, often manifesting as xanthine nephrolithiasis in humans (Miller et al., 2013). In *Drosophila*, mutants of *rosy* and *maroon-like* genes, which affect the function of xanthine dehydrogenase, show the accumulation of xanthine and the formation of tubular xanthine concretions (Mitchell and Glassman, 1959).

In a *Drosophila* model of nephrolithiasis induced by the inhibition of xanthine dehydrogenase, analysis of both fly and human calcified plaques revealed a high enrichment of zinc (Chi et al., 2015). Genetic, dietary, and pharmacologic modifications of zinc levels alter stone formation. In another model, where stone formation was induced by feeding flies with sodium oxalate (NaOx), anti-nephrolithiasis agents were screened by analysing the amount of calculi in excreta. Arbutin was found to be an effective anti-lithogenic agent (Ali et al., 2018). Additionally, oral potassium citrate has been shown to be protective against hyperuricosuric calcium oxalate and uric acid nephrolithiasis (Pak and Peterson, 1986, Pak et al., 1986), and it also alleviates crystals induced by ethylene glycol (Chen et al., 2011). The anion transporter dPrestin, a potent oxalate transporter, is strongly expressed in *Drosophila* renal tubule. RNAi-mediated knockdown of *dPrestin* reduced the formation of microliths upon dietary oxalate supplementation (Hirata et al., 2012).

Tubular disorders. Renal tubular acidosis (RTA) is characterised by insufficient acid clearance in the body. Type I RTA is associated with a deficiency in V-ATPases in the collecting duct of the nephron. The α-intercalated cells located in the distal nephron have high expression levels of V-ATPases (Alper et al., 1989). Mutation of subunits of V-ATPases causes distal RTA in humans, often with a potential loss of auditory function (DeFranco et al., 1995, Karet et al., 1999). In *Drosophila*, the entire V-ATPase gene family has been investigated for the

lethal phenotype, revealing a common defect in renal acidification. This defect is indicated by a reduced amount of uric acid crystals in the tubule lumen (Allan et al., 2005). Acidic urine pH levels are a major risk factor for uric acid stones. Furthermore, polycystic kidney disease, commonly characterised by the presence of multiple fluid-filled cysts in the kidneys, is a common cause of end-stage renal disease (Bergmann et al., 2018). Mutations in *PKD1* and *PKD2* are the major causes of this monogenic disorder (Rossetti et al., 2007, DJ, 1992). In *Bicc1* mutant mice, the antagonism between *Bicc1 and* repressive activity of the *miR*-17 microRNA family on the 3' UTR of *Pkd2* mRNA is mitigated, resulting in the reduced *Pkd2* mRNA levels (Tran et al., 2010). Mutation of *Drosophila* orthologue of *Bicc1*, *Bicaudal C*, also results in upregulation of the TOR pathway and polycystic kidney disease-like phenotypes in *Drosophila* (Gamberi et al., 2017). This cystic phenotype can be substantially ameliorated by rapamycin treatment.

1.6 The aim of the study

The DGRP lines have been proven to be an excellent tool for studying complex traits, and *Drosophila* Malpighian tubules provide an outstanding model for human renal function and disease. Given that 1) an increased risk of renal dysfunction has been associated with nephrolithiasis and impaired tubular secretion and 2) strong genetic components have been identified in the formation of kidney stones and tubular transport in humans, understanding the genetic basis of nephrolithiasis and tubular transport may offer new insights into the mechanisms underlying nephrolithiasis, impaired tubular secretion, and their contributions to renal function decline.

Thus, the major objectives of this study are:

(1) To measure the formation of kidney stones in 186 DGRP lines, perform GWA analysis on this quantitative trait, identify candidate loci and genes associated with the trait, conduct RNAi-mediated knockdown of the

shortlisted genes, and verify their functional roles in renal crystal formation under lithogenic conditions in Chapter 3.

(2) To measure the basal, Capa-stimulated, and both Capa and Kinin-stimulated fluid secretion rates in 183 DGRP lines, perform GWA analyses, identify candidate loci/genes associated with these traits, conduct functional verification of the candidates, and uncover novel genes involved in the tubular transport in Chapter 4.

(3) To investigate the function of a candidate gene *Fasciclin 3*, identified through a pilot GWA study of baseline fluid secretion, in primary and secondary cells of the Malpighian tubules in Chapter 5.

(4) To investigate the function of *Muc11A*, a gene highly and specifically enriched in Malpighian tubules, in the renal tubule and provide insights into the specialized function of this tissue in Chapter 6.

The data and findings of these objectives will constitute the rest of this thesis and, hopefully, provide novel insights into the genetic basis of renal function.

Chapter 2 Materials and Methods

2.1 *Drosophila melanogaster*

2.1.1 *Drosophila* culture

The fruit flies, *Drosophila*, were cultured in plastic fly vials containing approximately 7 ml of standard *Drosophila* medium (Table 2.1), plugged with BuzzPlugs (Scientific Laboratory Supplies, catalogue no. FLY1008). All fly stocks were maintained at 22°C with 45% relative humidity and a 12 h light: 12 h dark cycle in an insectary. To maintain the fly stocks, dozens of flies were transferred into new vials with fresh fly medium every other week. For experimental purposes, eggs laid by stock-derived flies were collected for three days and kept in an incubator at 25°C. Ten to twenty female progenies were used to collect F2 generations for performing experiments, avoiding the transgenerational effects of stock crowding on phenotypes. Fly lines ordered from stock centres were quarantined for at least three generations with mineral oil (Sigma, catalogue no. 330760), and the presence of mites was monitored regularly.

Table 2.1 The standard *Drosophila* medium.

Ingredients	Amounts per litre
Agar	10 g
Sucrose	15 g
Glucose	30 g
Yeast	35 g
Maize meal	15 g
Wheat germ	10 g
Treacle	30 g
Soya flour	1 tablespoon
Nipagen	10 ml
Propionic acid	5 ml

2.1.2 Fly stocks

The fly lines used in our study, apart from the DGRP lines, are listed in Table 2.2. The DGRP lines used in our study are listed in Appendix 1.

Table 2.2 List of fly lines used in the study.

Fly line	Description	Source
Canton S	Wild-type fly line	In-house line
Dahomey	Wild-type fly line	Woodling lab
Oregon R	Wild-type fly line	In-house line
w^{1118}	*white* mutant	In-house line
da-Gal4	*Gal4* under the control of *daughterless* promoter	Sanz lab
CapaR-Gal4	*Gal4* under the control of *CapaR* promoter	In-house line
ctB-Gal4	*Gal4* under the control of *cut* promoter	Denholm Lab
c724-Gal4	*Gal4* under the control of *tsh* promoter	In-house line
c724-Gal4; CapaR-Gal4	*Gal4* under the control of *tsh* and *CapaR* promoter	Constructed in the study
ctB-Gal4; Gal80^{TS}	Thermosensitive *ctB-Gal4*	Dr Jérôme Bohère
UAS-*mGFP; CapaR-Gal4*	Expresses membrane-bound GFP under the control of *CapaR-Gal4*	In-house line
UAS-*mGFP; ctB-Gal4*	Expresses membrane-bound GFP under the control of *ctB-Gal4*	Constructed in the study
c724-Gal4; UAS-mGFP	Expresses membrane-bound GFP under the control of *c724-Gal4*	In-house line
UAS-*mGFP*	Expresses membrane-bound GFP under the control of UAS	BDSC# 5137
w^{1118}; UAS-empty	Coisogenic control line for KK lines from VDRC	VDRC# 60100
y^{1} *v*^{1}; ; UAS-TRiP-empty	Coisogenic control line for BDSC lines with 3rd chromosome target sites	BDSC# 36303
y^{1} *v*^{1}; UAS-TRiP-empty	Coisogenic control line for BDSC lines with 2nd chromosome target sites	BDSC# 36304
UAS-*CG7289*-RNAi	Expresses dsRNA for RNAi of *CG7289* under UAS control	BDSC# 60460
UAS-*Dlg5*-RNAi	Expresses dsRNA for RNAi of *Dlg5* under UAS control	BDSC# 61334
UAS-*Shab*-RNAi	Expresses dsRNA for RNAi of *Shab* under UAS control	BDSC# 55682
UAS-*Eip71CD*-RNAi	Expresses dsRNA for RNAi of *Eip71CD* under UAS control	BDSC# 42877
UAS-*ATP8B*-RNAi	Expresses dsRNA for RNAi of *ATP8B* under UAS control	BDSC# 63037

UAS-*timeout*-RNAi	Expresses dsRNA for RNAi of *timeout* under UAS control	BDSC# 36863
UAS-*fz2*-RNAi	Expresses RNAi construct against *fz2* under UAS control	VDRC# 108998
UAS-*SPR*-RNAi	Expresses RNAi construct against *SPR* under UAS control	VDRC# 106804
UAS-*sdt*-RNAi	Expresses dsRNA for RNAi of *sdt* under UAS control	BDSC# 37510
UAS-*RunxA*-RNAi	Expresses dsRNA for RNAi of *RunxA* under UAS control	BDSC# 33353
UAS-*Pde1c*-RNAi	Expresses dsRNA for RNAi of *Pde1c* under UAS control	BDSC# 55925
UAS-*Ncc69*-RNAi	Expresses dsRNA for RNAi of *Ncc69* under UAS control	BDSC# 28682
UAS-*sowah*-RNAi	Expresses dsRNA for RNAi of *sowah* under UAS control	BDSC# 65930
UAS-*RhoGAP71E*-RNAi	Expresses dsRNA for RNAi of *RhoGAP71E* under UAS control	BDSC# 32417
UAS-*Baldspot*-RNAi	Expresses dsRNA for RNAi of *Baldspot* under UAS control	BDSC# 44101
UAS-*Gaf*-RNAi	Expresses dsRNA for RNAi of *Gaf* under UAS control	BDSC# 43201
UAS-*Glut4EF*-RNAi	Expresses dsRNA for RNAi of *Glut4EF* under UAS control	BDSC# 57461
UAS-*CG8027*-RNAi	Expresses RNAi construct against *CG8027* under UAS control	VDRC# 109400
UAS-*CG7656*-RNAi	Expresses RNAi construct against *CG7656* under UAS control	VDRC# 100791
UAS-*bi*-RNAi	Expresses dsRNA for RNAi of *bi* under UAS control	BDSC# 28341
UAS-*Sik3*-RNAi	Expresses dsRNA for RNAi of *Sik3* under UAS control	BDSC# 57302
UAS-*Pdp1*-RNAi	Expresses dsRNA for RNAi of *Pdp1* under UAS control	BDSC# 40863
UAS-*smp-30*-RNAi	Expresses RNAi construct against *smp-30* under UAS control	VDRC# 103377
UAS-*fs(1)h*-RNAi	Expresses dsRNA for RNAi of *fs(1)h* under UAS control	BDSC# 41693
UAS-*Pde8*-RNAi	Expresses dsRNA for RNAi of *Pde8* under UAS control	BDSC# 51892
UAS-*Pde6*-RNAi	Expresses dsRNA for RNAi of *Pde6* under UAS control	BDSC# 25828

UAS-*jvl*-RNAi	Expresses dsRNA for RNAi of *jvl* under UAS control	BDSC# 67897
UAS-*CG32206*-RNAi	Expresses dsRNA for RNAi of *CG32206* under UAS control	BDSC# 66946
UAS-*pip*-RNAi	Expresses dsRNA for RNAi of *pip* under UAS control	BDSC# 34613
UAS-*Eip74EF*-RNAi	Expresses dsRNA for RNAi of *Eip74EF* under UAS control	BDSC# 29353
UAS-*Ent3*-RNAi	Expresses RNAi construct against *Ent3* under UAS control	VDRC# 47537
UAS-*Indy*-RNAi	Expresses RNAi construct against *Indy* under UAS control	VDRC# 9981
UAS-*Muc11A*-RNAi-1	Expresses RNAi construct against *Muc11A* under UAS control	VDRC# 101320
UAS-*Muc11A*-RNAi-2	Expresses RNAi construct against *Muc11A* under UAS control	VDRC# 24993
UAS-*Fas3*-RNAi	Expresses RNAi construct against *Fas3* under UAS control	VDRC# 3091
UAS-*Cdc42 DN*-RNAi	Expresses dominant negative *Cdc42* under UAS control	BDSC# 6288
UAS-*Cdc42 CA*-RNAi	Expresses constitutively active *Cdc42* under the control of UAS	BDSC# 4854
Balancer line	Carries balancer chromosomes	BDSC# 3703

2.1.3 *Drosophila* mating schemes

To inhibit the expression of a particular gene, 10 to 20 virgin females from a *Gal4* line were collected and mated with 3 to 10 male flies from corresponding RNAi line. The cross was kept in an incubator at 25°C, and eggs were collected for three days before transferring the parental flies into a new vial. Another set of cross between the *Gal4* line and the coisogenic control line was made. The F1 generations from the crosses were used as experimental and control flies, respectively. For genes whose knockdowns during the development were lethal, a temperature-sensitive GAL80 system was employed. Eggs were collected and kept at 18°C until adulthood, during which the knockdown was suppressed. Once F1 adults emerged, the flies were transferred to the incubator at 29°C to induce the knockdown. Unless otherwise stated, 7- to 10-day-old female flies were used

in the experiments conducted in this study. The RNAi lines and their corresponding controls used for the functional verification of candidates identified through association analyses are listed in Appendix 9.

A stable fly line, containing the 2nd and 3rd chromosomes from two different fly lines, was constructed according to the cross scheme in Figure 2.1. As an expample, a new fly line expressing *Gal4* under the control of both *tsh* and *CapaR* promoters was constructed. This fly line was used to drive the knockdown of genes of interest in both primary and secondary cells in MTs.

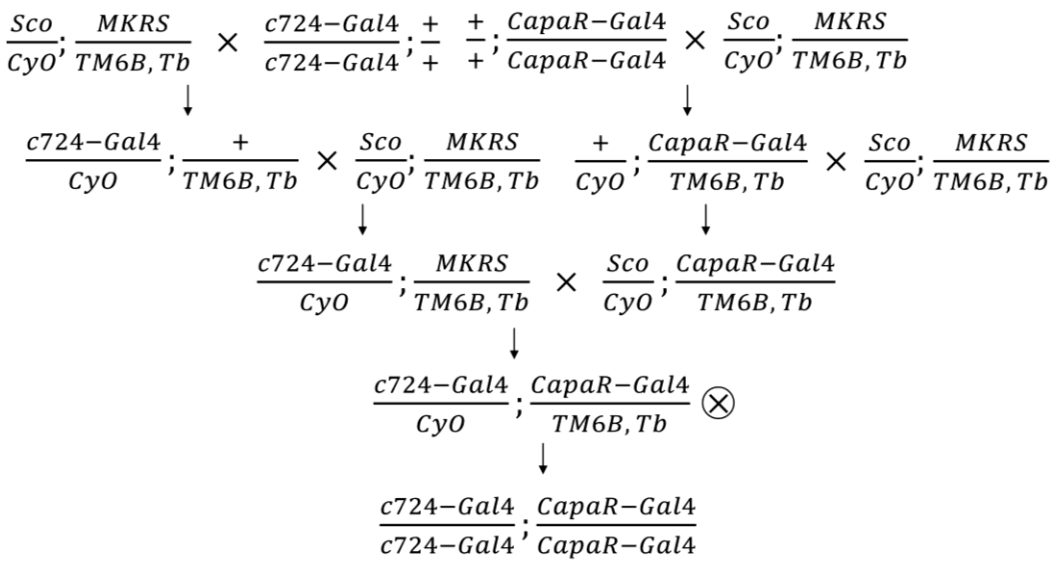

Figure 2.1 An example of cross scheme.
It is used to generate a stable fly line containing the 2nd and 3rd chromosomes from two different fly lines.

2.1.4 Dissection of *Drosophila* MTs

Anterior Malpighian tubules from female adults were used in the study, unless otherwise stated. Flies were anaesthetised on ice and dissected in Schneider's medium (Gibco, catalogue no. 21720024) or in 1× PBS (137 mM NaCl, 10 mM Na_2HPO_4, 2.7 mM KCl, 1.8 mM KH_2PO_4; pH 7.4). The flies were placed upside down in the solution. One pair of forceps was holding the thorax, while the other pair was holding the very end of the abdomen and tearing the body wall open. The anterior MTs were freed by cutting the common ureter and then collected.

For tubules used for RNA extraction, tissues were dissected on ice and transferred to the Pre-Filled Bead Mill Tubes (Fisher Scientific, catalogue no. 15545799) placed on dry ice. Collection tubes were filled with 1 ml QIAzol lysis reagent (QIAGEN, catalogue no. 79306) once enough tissues had been collected. Samples were then homogenised using a bead disruptor and stored at -70°C until RNA extraction.

2.2 Molecular biology

2.2.1 Total RNA extraction

Approximately one hundred pairs of tubules or ten whole flies were prepared for RNA extraction using the RNeasy Mini Kit (QIAGEN, catalogue no. 74104). MTs were collected as described in section 2.1.4. Whole files were collected in mill tubes with ceramic beads (Fisher Scientific, catalogue no. 15555799) and homogenised in 1 ml QIAzol lysis reagent. After homogenisation, the homogenates were incubated at room temperature for 5 min, mixed with 200 µl chloroform, and incubated for an additional 5 min. The samples were then centrifuged for 15 min at 12,000× g at 4°C. The upper aqueous phase (approximately 400 µl) was transferred to a new collection tube and mixed with 600 µl of absolute ethanol by pipetting. The mixed samples were transferred into columns provided by the kit and centrifuged at 8,000× g for 1 min at room temperature. Before washing with the washing buffer, samples were treated with RNAse-free DNase I (QIAGEN, catalogue no. 79254) to remove genomic DNA. After two washes, the columns containing RNA were centrifuged again to further dry the membrane. RNA was then eluted with 30 µl of RNAse-free water. The quantity and purity (A260/A280) of each sample were determined using a Nanodrop spectrophotometer. Purified RNA was stored at -70°C.

2.2.2 Genomic DNA extraction

Genomic DNA (gDNA) was extracted from whole flies using the Genomic DNA Mini Kit (Invitrogen, catalogue no. 10593245). Briefly, ten whole flies were

anesthetized with carbon dioxide (CO_2), transferred to Eppendorf tubes filled with 180 µl digestion buffer and 20 µl proteinase K, and homogenised with pellet pestles. After incubation at 55°C for 1 h with proteinase, particulate materials were removed by centrifugation at maximum speed for 3 min. The supernatant was transferred to a new microcentrifuge tube and mixed with RNase, lysis buffer, and absolute ethanol. The digested samples were then processed according to the instructions provided by the kit. gDNA was eluted from the columns using elution buffer and stored at -20°C.

2.2.3 cDNA synthesis

Complementary DNA (cDNA) was synthesised using SuperScript™ II Reverse Transcriptase (Invitrogen, catalogue no. 18064022). For samples used in quantitative real-time PCR (qRT-PCR), same amount of total RNA was used for each reverse transcription reaction to minimize the variation in cDNA amount among different biological replicates. In each reaction, up to 5 µg of total RNA was mixed with 1 µl Oligo$(dT)_{12-18}$ and 1 µl dNTP Mix and heated at 65°C for 5 min. Then, 4 µl First-Strand Buffer, 2 µl 0.1 M DTT, and 1 µl RNaseOut were added, and the mixture was incubated at 42°C for 2 min. After incubation, 1 µl reverse transcriptase was added to each reaction, and a further incubation was carried out at 42°C for 50 min. The reaction was inactivated by heating at 70°C for 15 min. The synthesised cDNA was stored at -20°C.

2.2.4 Polymerase chain reaction and agarose gel electrophoresis

DreamTaq DNA Polymerase (Thermo Scientific, catalogue no. EP0701) or Phusion High-Fidelity DNA Polymerase (Thermo Scientific, catalogue no. F530) was used for polymerase chain reaction (PCR). In each reaction, 1 µl cDNA or gDNA was used as the template, and gradient PCR was performed with annealing temperatures ranging from 55°C to 65°C to optimize primer efficiency. PCR reactions were carried out in 0.2 ml PCR tubes (Starlab) using a thermocycler (PEQLAB Biotechnologie GmbH), with the thermal cycling condition outlined in Table 2.3.

Table 2.3 A typical thermal cycling protocol.

Step	Temperature	Time	Number of cycles
Initial denaturation	95°C	2 min	1
Denaturation	95°C	15 s	30
Annealing	55-65°C	15 s	
Extension	72°C	1 min every 1 kb	
Final extension	72°C	5 min	1

PCR products were analysed by agarose gel electrophoresis. Agarose gels containing approximately 0.1 µg/ml ethidium bromide (EtBr) were prepared using 0.5× TBE buffer (Table 2.4), with agarose concentrations ranging from 1% to 2%, depending on the expected product size. The gel was run at a constant voltage of 110 V for 30 min, and the PCR products were visualized using an ultraviolet transilluminator.

Table 2.4 10× TBE buffer recipe.

Ingredients	Amounts per litre
Tris base	108 g
Boric acid	55 g
0.5 M EDTA solution (pH 8.0)	40 ml
Double-distilled H_2O	900 ml

2.2.5 qRT-PCR

qRT-PCR was performed using SYBR Green PCR Master Mix (QuantiNova, catalogue no. 208054). Primers spanning exon-exon junctions were designed using Primer-BLAST (Ye et al., 2012) and are listed in Appendix 2. The product length ranged from 70 to 200 bp. PCR tubes (Applied Biosystems, catalogue no. 4358293) or 96-well plates (Applied Biosystems, catalogue no. 4346907) were used for the reactions. Each 20 µl reaction contained 10 µl SYBR Green PCR Master Mix, 2 µl ROX Reference Dye, forward and reverse primers at final concentrations of 0.7 µM, and 1-2 µl template. A StepOnePlus Thermocycler (Applied Biosystems) was used to carry out qRT-PCR. A melting curve and a standard curve were generated for each primer pair to ensure specific amplification and acceptable efficiency (90-110%), respectively. In all cases, qRT-PCR reactions were run in technical triplicates, with three biological

replicates included for each condition. The qRT-PCR reaction was carried out according to the conditions in Table 2.5. *RpL32* was used as a reference gene. Relative expression levels of candidate genes were calculated using comparative Ct method, as described in Applied Biosystems User Bulletin No. 2 (P/N 4303859), and were plotted with lower and upper limits. Statistical analysis was performed using non-normalised (ΔCt) values from the three biological replicates.

Table 2.5 Real-time cycler protocol.

Step	Temperature	Time	Number of cycles
Initial denaturation	95°C	2 min	1
Denaturation	95°C	5 s	40
Combined annealing/extension	60°C	10 s	

2.3 Microscopy

2.3.1 Polarized light microscopy

To visualize CaOx crystals formed in MTs, a polarized light microscope was used, as oxalate and uric acid stones are birefringent under polarized light. Two polarizing filters were placed perpendicularly on the either side of the specimen. A high-contrast image could only be observed in the presence of a birefringent sample. After dissection, samples were immediately imaged under the polarizing microscope, specifically the Zeiss Stemi 508 stereo microscope (Carl Zeiss), equipped with two polarizing filters, a Zeiss Apo 1.5× FWD 53 mm objective, a 0.5× camera adapter, and a Axiocam 105 colour camera. All images were captured at 2.5× magnification.

2.3.2 Confocal microscopy and immunofluorescence

The LSM 880 confocal microscope system (Carl Zeiss) was used to visualize fluorophores-labelled proteins. The excitation wavelength were 405 nm, 488 nm, and 543 nm for DAPI (Sigma, catalogue no. D9542), Alexa Fluor 488-conjugated secondary antibodies, and Alexa Fluor 546-conjugated secondary antibodies,

respectively. Z-stack images were acquired with the confocal microscope and subsequently processed using Zen Blue software (Carl Zeiss).

To prepare specimens for immunofluorescence, anterior tubules, left attached to part of the gut, were dissected in Schneider's medium. The samples were then fixed in 4% paraformaldehyde in PBS on a nutator for 20 min. After fixation, the tubules were washed three times with PBT (0.15% Triton X-100 in 1× PBS) for 15 min each. Prior to incubation with appropriate primary antibodies at 4°C overnight, the samples were blocked with PTN (5% normal goat serum in PBT) for 1 to 2 hours at room temperature. Afterward, the samples were washed three times with PBT, 15 min each. Samples were then incubated with secondary antibodies in the dark for 2 to 3 hours at room temperature or overnight at 4°C. Following three 15 min washes with PBT, Phalloidin-TRITC (Sigma, catalogue no. P1951) was applied for 30 min, if needed, before staining with DAPI for 2 min. After two washes in 1× PBS, samples were mounted with either 1× PBS or antifade mounting medium (VectorLabs, catalogue no. H-1000-10) for imaging. The primary and secondary antibodies and their working concentrations are listed in Table 2.6. The working concentration for DAPI was 1 µg/ml.

Table 2.6 List of antibodies.

Antibody	Host species and dilution	Source
Anti-Dlg1	Mouse, 1/500	DSHB, 4F3
Anti-Arm	Mouse, 1/100	DSHB, N27A1
Anti-Hnt	Mouse, 1/20	DSHB, 1G9
Anti-PH3	Rabbit, 1/200	Cell Signalling Technology, 9701
Alexa Fluor 488-conjugated anti-mouse	Goat, 1/600	Life Technologies
Alexa Fluor 546-conjugated anti-mouse	Goat, 1/600	Life Technologies
Alexa Fluor 488-conjugated anti-rabbit	Goat, 1/600	Life Technologies

2.4 Assessment of physiological phenotypes

2.4.1 Development of renal stones

Calcium oxalate crystals were induced in renal tubules by feeding flies with a standard fly food supplemented with 0.1% (w/v) NaOx (Sigma, catalogue no. 379735) for 72 h. To avoid any changes in salt concentration due to evaporation, fly food was freshly prepared. After being fed with the lithogenic diet, flies were knocked down by immersion in 70% (v/v) ethanol, washed with distilled water, and kept on ice in 1× PBS solution until dissection. *Drosophila* anterior MTs, attached to the gut, were dissected in 1× PBS and mounted on microscope slides (Epredia, catalogue no. 12362098) coated with poly-L-lysine (Sigma, catalogue no. P8920). Tubules were then imaged using the Zeiss Stemi 508 stereo microscope. Crystals in tubule lumen were manually outlined, and stone areas and tubule sizes were quantified using Fiji (Schindelin et al., 2012).

2.4.2 Fluid secretion rates

Fluid secretion assays were performed as previously described (Dow et al., 1994, Davies et al., 2019). A Petri dish (Ø 90 mm) was prepared with a layer of paraffin wax (Sigma, catalogue no. 327212), and wells were drilled using a drill bit. Metal pins (Fine Science Tools, catalogue no. 26002-10) were inserted beside each well. During the measurement, the wax layer was covered with mineral oil, and a 9 µl mixture of 1:1 of Schneider's medium and *Drosophila* saline (Table 2.7) was added to each well. Trace amounts of amaranth (Sigma, catalogue no. A1016) were added to the mixture, with a final concentration of approximately 0.042 µg/µl, for contrast purposes. Anterior tubules were dissected in Schneider's medium and transferred to the 9 µl mixture. One end of each tubule was placed in the mixture, while the other end was wrapped around the metal pin. Fluids secreted by tubules were collected at the common ureter and placed on the surface of the wax layer using a fine glass rod. The secreted droplets became spherical, and their diameters were measured with an ocular micrometre or from images taken with an Axiocam 105 colour camera. The

volume of secreted fluid was calculated using the formula $\frac{4}{3}\pi r^3$. Baseline (basal) secretion rates were measured for 30 min. Two diuretic neuropeptides, Capa-1 and Kinin, were added sequentially to the mixture at a stock concentration of 10^{-6} M to study neuroendocrine control of fluid transport. Stimulated secretion rates were measured for another 30 min for each neuropeptide. Secretion-related traits used in association analyses are explained in Figure 2.2. This protocol allows the measurement of 3 separate physiological parameters in a single experiment.

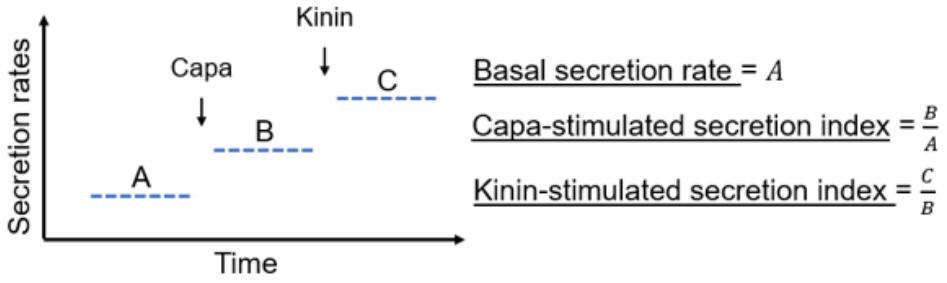

Figure 2.2 Phenotypic values used in association analyses.

Table 2.7 The recipe for 1 litre *Drosophila* saline.

Component	Amount	Final concentration
H_2O	About 800 ml	-
2.5 M NaCl	47 ml	117.5 mM
1 M KCl	20 ml	20 mM
1 M $CaCl_2$	2 ml	2 mM
1 M $MgCl_2$	8.5 ml	8.5 mM
1 M $NaHCO_3$	10.2 ml	10.2 mM
1 M HEPES	15 ml	15 mM
1 M NaH_2PO_4	4.3 ml	4.3 mM
Glucose	3.6 g	20 mM
Adjust pH to 7.0		
Top up to 1 litre with H_2O, and filter sterilize		

Extracted from (Schellinger and Rodan, 2015).

2.4.3 Food intake

Measurements of food intake were performed as described previously (Wu et al., 2020). Briefly, five 7-day-old females were transferred into a Falcon tube (CELLSTAR, catalogue no. 210261), with a 5.5 mm food container fixed at the

top of the tube. Standard fly food, supplemented with a blue dye (1% w/v, erioglaucine disodium salt, Sigma, catalogue no. 861146), was prepared. The flies were fed with the dye-containing food for 72 h, and the food was replaced daily to account for potential effects of egg-laying and evaporation on food accessibility. After the feeding period, the dye-containing food was replaced with non-dyed food, and the flies were given another 3 h to ensure all dye-containing food was excreted. To quantify food intake, excreta were recovered from the tube walls and cap with distilled water, and the absorbance at 630 nm was measured using a Nanodrop spectrophotometer. Food consumption was calculated using a standard curve. All tubes were laid on their sides and kept in incubators during the assay.

2.4.4 Stone formation in vitro

Mixtures of Schneider's medium and *Drosophila* saline (1:1) were prepared, with or without 1 mM NaOx. Bafilomycin A1 (Cell Signalling Technology, catalogue no. 54645S), with a working concentration of 50 μM, was diluted in dimethyl sulfoxide and added to the mixture to inhibit the activity of V-ATPases. Anterior tubules from Canton S flies were dissected in Schneider's medium, transferred into the prepared mixtures, and incubated for 1 h. The renal tubular accumulation of CaOx microliths was captured using a Zeiss Stemi 508 stereo microscope and subsequently quantified using Fiji.

2.4.5 Lifespan

Freshly eclosed flies were collected within 2 days and allowed to mate for 48 h. After mating, flies were anesthetized using a CO_2-dispensing porous pad. Approximately a hundred female flies per condition were collected and housed in groups of 10 flies per vial. Flies were transferred to fresh food every 2–3 days, and during each transfer, the number of deaths and censored flies were recorded until all flies had died.

2.4.6 Desiccation and starvation tolerance

Protocols for phenotyping desiccation and starvation tolerance were adapted from previous work in the lab (Terhzaz et al., 2015). Briefly, 7- to 10-day-old female flies were anesthetized on ice and placed in groups of 10 in either empty vials for the desiccation assay or vials containing 1% agar for the starvation assay. The open end of the vials for the desiccation assay was sealed with parafilm (Fisher Scientific, catalogue no. 10018130). Vials were checked hourly for dead flies during the desiccation assay and twice a day during the starvation assay until all flies were dead.

2.4.7 Chill-coma recovery time

Female flies were transferred to empty vials and subjected to a cold shock in a mixture of ice and water for 4 h. Following the cold shock, flies were transferred to a filter paper at 22°C, and the recovery time for each individual fly was recorded. A fly was considered to have recovered when it was able to right itself with all six legs.

2.4.8 Wet and dry weight

Groups of 5 to 20 adult flies were anesthetized with CO_2, transferred to Eppendorf tubes, and weighted using a precision balance. The flies were then killed by freezing at -70° for 1h and dried at 60° for 24 h. After the fly samples reached room temperature, their dry weight was weighted.

2.4.9 Abdominal size

To measure the abdominal size of flies, a Petri dish with a layer of paraffin wax was filled with mineral oil. Female adults were killed by immersion in the mineral oil, and side-profile images were captured using a Zeiss Stemi 508 stereo microscope. The width of the abdomen was measured at A3 segment, and the area of the abdomen was outlined and measured using ZEN Blue software.

2.4.10 Morphology of excreta

T.U.R.D. software (Wayland et al., 2014) was used to quantify faecal output. Briefly, flies were fed with a standard fly food containing 2.5% (w/v) erioglaucine disodium salt for 48 h. The open side of the fly vial was then capped with a Petri dish (Ø 35 mm) instead of a buzz plug, and the vial was kept on its side. Excreta were collected for 1 h, and images of the Petri dish were analysed using T.U.R.D. software to quantify the size and number of the faeces.

2.5 Bioinformatics

2.5.1 Quantitative genetics

All data were analysed in R Studio using the R statistical language version 4.3.2 (R Core Team, 2013). The linear mixed-effects model (*lmer*) from the *lme4* R package (Bates et al., 2015) was used to test the effects of potential covariates on phenotypes with the formula $Y = \mu + W + I + L + B + \epsilon$, where W denotes the *Wolbachia* infection status (fixed effect), I is the 5 major inversions present in the DGRP panel (fixed effect), L is the DGRP line (random effect), B is the effect of block (random effect), and ϵ is the error variance. The information on *Wolbachia* infection and major genomic inversion was retrieved from DGRP freeze 2 (http://dgrp2.gnets.ncsu.edu). The random effect of the line was not nested within the block because each line was included in more than one block. For the stone area, tubule size was included as a random effect in the mixed model, and the phenotype was normalized due to the non-normal distribution. The *anova()* and *rand()* functions in the *lmerTest* package (Kuznetsova et al., 2017) were used to assess the significance of the fixed and random effects in the dataset, respectively. The models were simplified through stepwise removal of non-significant factors, and the minimal models were performed. The residuals ϵ from the regressions, in which the line effect was omitted, were used as adjusted phenotypes for genome-wide association analyses.

Broad-sense heritability (H^2) for each trait was estimated as $H^2 = {\sigma^2}_L/({\sigma^2}_L + {\sigma^2}_E)$ where ${\sigma^2}_L$ is the variance component among lines, ${\sigma^2}_E$ is the sum of all other sources of variation. Variance components were extracted using *VarCorr()* function.

2.5.2 GWA analysis

To identify genetic variants associated with phenotypic traits, quality control and association analyses were performed using PLINK version 1.9 (Purcell et al., 2007) and GEMMA (Zhou and Stephens, 2012), respectively. Genotypes were downloaded from the DGRP freeze 2. Markers called at least 4 times in the pool of tested lines were included in association analyses (with a minimum minor allele frequency of approximately 2%). Markers and individuals with missingness greater than 10% and 20%, respectively, were excluded. After filtering, a different subset of genetic variants remained for each trait tested (2,315,319 markers for the stone area and 2,288,271 for the fluid secretion rate). To control for confounding cryptic relatedness in the DGRP, estimated relatedness matrices were calculated in GEMMA using pruned variants ($r^2 < 0.2$). The association for each trait was examined by the likelihood ratio test (Xing et al., 2012), fitting a linear mixed model using GEMMA. An empirical threshold of 10^{-5} (Anholt and Mackay, 2018) was used in GWA analyses and candidate variants were annotated based on Flybase release 5.57 (http://flybase.org). The LD heatmaps were generated in R using the package *ggplot2*, and the package *qqman* was used to make QQ and Manhattan plots.

2.5.3 Interaction network analysis

The genetic and physical interaction networks curated by FlyBase were downloaded. The genes and their products served as nodes in the networks, while interactions between them were represented as edges. Candidate genes identified by GWA analysis, along with their interacting genes, were extracted and mapped onto a graphical representation of the interaction network using the *igraph* package (Csardi and Nepusz, 2006) in R. Additionally, genes within the

interaction network were clustered, functional enrichment analyses for these clusters were conducted. The clusters were visualized using Cytoscape (Doncheva et al., 2019). The full STRING network of the genes was imported with a cutoff score of 0.4. The granularity parameter used to cluster the networks was set to 4, as the default. Subnetworks were selected, and the not clustered network, rather than the 'genome', was selected as background. Categories with false discovery rates less than 0.05 were considered statistically enriched for the selected subnetworks.

2.5.4 Human orthologues of *Drosophila* genes

Human orthologues of the candidate fly genes were obtained using the DRSC Integrative Orthologue Prediction Tool (Hu et al., 2011, Hu et al., 2021). Orthologues with low ranked scores are excluded.

2.6 Statistics

Statistical analyses were conducted using either R Studio or GraphPad Prism 10 (GraphPad Software). The specific tests and statistical significance are described in each figure legend.

2.6.1 ANOVA

To assess the strain effect on stone formation and food intake in wild-type flies, as well as the effect of bafilomycin treatment on stone formation in vitro, a type III analysis of variance (ANOVA) was conducted using the *Car* library. The *AICcmodavg* R package was employed to compare the fit of the models, with the model exhibiting the lowest Akaike Information Criterion values being selected (Mazerolle, 2020). If the best-fit model included the strain effect, Tukey's post-hoc test was performed using the *emmeans* library. Interval plots were generated to visualize groupwise statistical significance. Additionally, ANOVA and post-hoc tests were applied to compare the means of three or more groups in GraphPad Prism 10, as demonstrated in the wet and dry weight assays.

2.6.2 Mixed model ANOVA

To validate the function of candidate genes identified by GWA analyses, linear mixed models (using the *lme4* package) were employed, accounting for genotype (RNAi versus background) as a fixed effect and replicate as a random effect. The full model was defined as $Y = \mu + G + R + \epsilon$, where Y represents the phenotype, G is the fixed effect of genotype, and R is the random effect of replicate. The reduced model was $Y = \mu + R + \epsilon$. Full model and reduced model were compared using the *anova()* function to assess the significance of the genotype (p value).

2.6.3 Analysis of diallel cross

To assess the significance of GCA (additive effects and their interactions) and SCA (non-additive effects and their interactions) in crystal formation within the DGRP, a diallel cross analysis according to Griffing (Griffing, 1956) was performed in R Studio using the *DiallelAnalysisR* package. A complete diallel cross (Figure 2.3) was conducted, and as the parents were selected from a wider population, Method I and Model II were employed for the analysis. In this model $Griffing(Pheno, Environment, Male, Female, diallelcross, 1{,}2)$, the ANOVA table and genetic components were extracted to assess the significance of GCA and SCA, as well as the ratio of GCA to SCA.

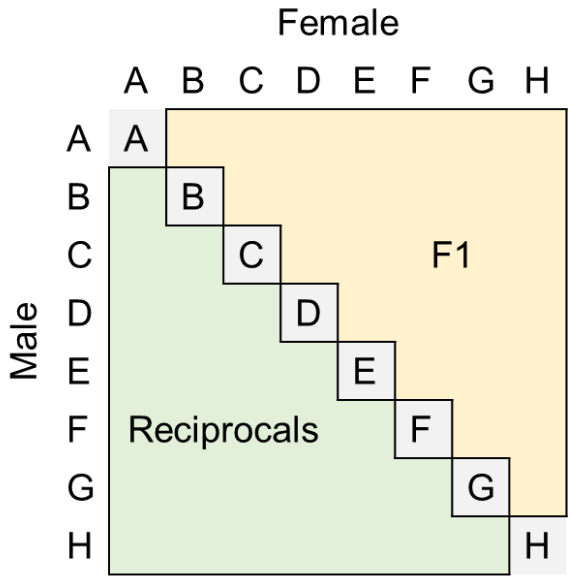

Figure 2.3 An example of full diallel cross.
All parental lines were crossed with each other, each cross was done in both directions, and self-crosses were also included.

2.6.4 The log-rank test

The log-rank test was used to analyse the statistical significance of survival curves, including lifespan, desiccation and starvation tolerance, and chill-coma recovery time, using GraphPad Prism 10.

2.6.5 Two-tailed *t*-test

To compare the means of two independent groups, a Student's *t*-test was conducted using GraphPad Prism 10 or Excel. Non-normalised (ΔCt) values from three biological replicates of the control group were compared with those of the knockdown group to assess the significance of knockdown efficiency by RNAi. Difference in traits, such as abdominal size and number of faecal spots, between control and knockdown flies were also analysed using the two-tailed *t*-test.

Chapter 3 The Genetic Basis of Variation in Nephrolithiasis in *Drosophila*

3.1 Summary

Kidney stone disease, also known as nephrolithiasis, is a common yet complex disorder with high a heritability, resulting in a significant economic burden. Genome-wide association studies in humans have reported several genetic variants associated with kidney stone disease. However, only a handful of genes implicated in calcium nephrolithiasis have been identified. The genetic basis underlying the variation in susceptibility to kidney stone formation remains poorly understood. Here, we employed inbred, fully sequenced lines of the *Drosophila melanogaster* genetic reference panel to investigate genetic variants that influence the formation of kidney stones. Calcium crystals were induced and quantified in the anterior renal tubules of fly lines fed with a lithogenic diet. Considerable phenotypic variation in crystal formation was observed in the renal tubules. To identify genetic variants associated with the phenotypic variation, association studies were conducted, followed by the validation of candidate genes harbouring polymorphisms through loss-of-function mutations.

3.2 Results

3.2.1 Variation in stone formation in wild-type strains

To characterise natural variation in crystal formation in *Drosophila*, the areas of the renal tubule occupied by crystals, hereafter referred to as “stone areas”, were quantified in adults of three commonly used wild-type strains: Canton S, Dahomey, and Oregon R. Relatively few naturally occurring crystals were observed in the renal tubules; however, significant amounts of CaOx stones could be readily induced with a dietary supplement of NaOx (Figure 3.1A and Figure 3.3A). Furthermore, a significant genotype-by-environment interaction was observed for stone areas (Figure 3.1B and Table 3.1), suggesting an

environmentally plastic genetic architecture in the development of kidney stones. For NaOx-induced stone formation, the estimated board-sense heritability is 0.69 (Table 3.2), indicating that genetic variance accounts for a substantial portion of the phenotypic variation.

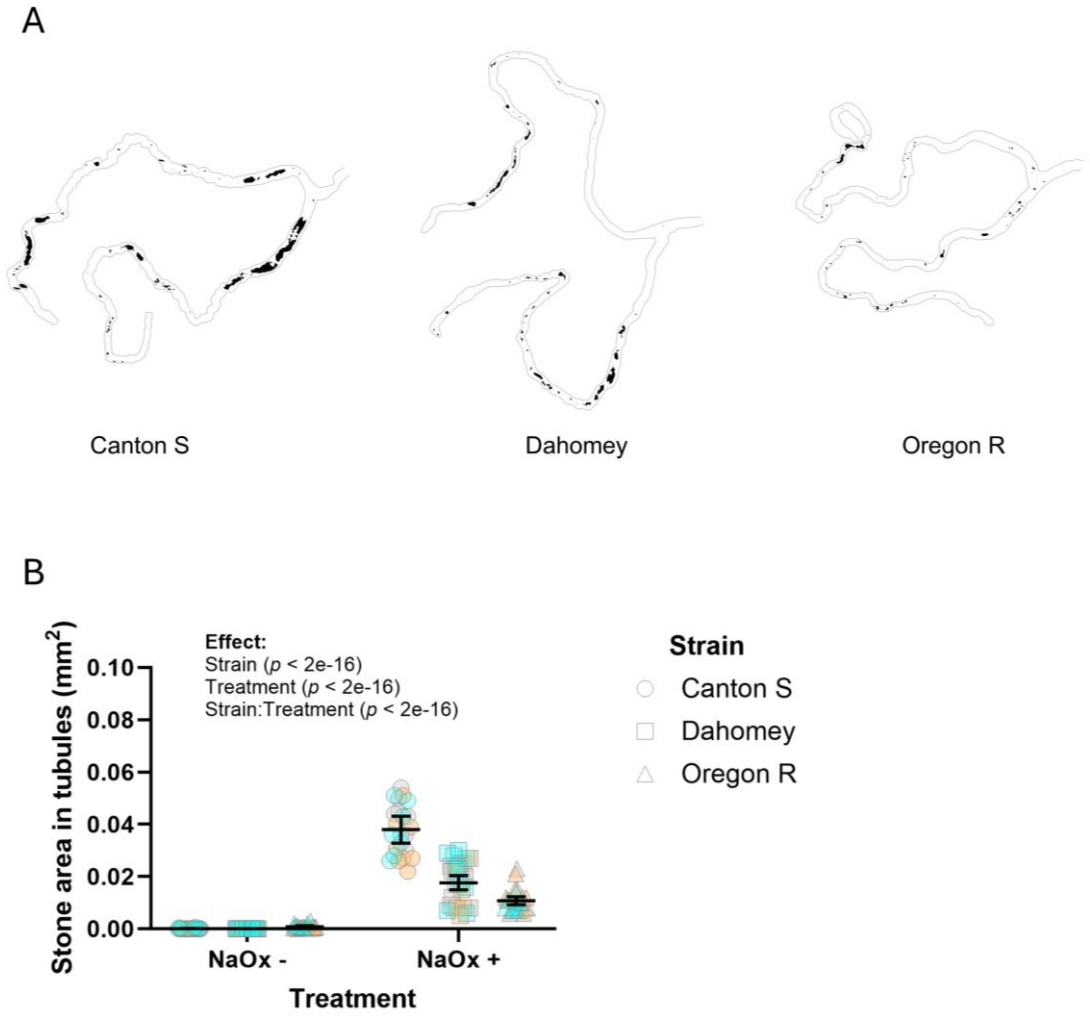

Figure 3.1 Variation in stone formation across three commonly used wild-type strains.
(A) An example of different amounts of crystals formed in the renal tubules of flies fed with NaOx. Crystals are depicted in black, and tubules are outlined in grey. (B) Stone areas in wild-type flies fed with or without NaOx. The mean of the means of each biological replicates and standard deviation (SD) are plotted in SuperPlots (Lord et al., 2020), where each colour corresponds to a different replicate (n=6-10 females per line and replicate, three biological replicates).

Table 3.1 Analyses of variance for line and treatment effects on stone formation (type III tests).

Term	Sum Sq	DF	F value	Pr (>F)
(Intercept)	0.0185282	1	627.246	< 2.2e-16*
Strain	0.0045928	2	77.742	< 2.2e-16*
Treatment	0.0176580	1	597.786	< 2.2e-16*
Strain:Treatment	0.0049642	2	84.028	< 2.2e-16*
Residuals	0.0042241	143		

Table 3.2 Variance components of NaOx-induced stone formation.

Groups	Variance	SD	H^2
Strain	0.000128	0.01132	0.69
Residual	0.000059	0.00765	

It is possible that the variation in crystal formation in the renal tubules could be attributed to differences in food consumption by the flies, as NaOx supplementation might affect food palatability. Additionally, wild-derived inbred lines exhibit variation in taste sensitivity (Uchizono and Tanimura, 2017). To investigate this possibility, the food intake of flies fed with or without NaOx was measured. The results indicated that the differences in crystal formation were not due to different food consumption. Although NaOx treatment increased food intake, supplementation with 0.1% NaOx did not result in significant differences in food intake across the strains (Figure 3.2 and Figure 3.3B). The three fly strains used, Canton S (Stern and Schaeffer, 1943), Dahomey (Puijk and De Jong, 1972), and Oregon R (Clayton and Paietta, 1972), were collected from Ohio, Dahomey (now Benin), and Oregon, respectively. These strains have distinct origins and histories, as well as different levels of mitochondrial reactive oxygen species (mtROS) production and lifespan (Sanz et al., 2010), in addition to distinct transcriptomic and metabolomic profiles (Gubina et al., 2019). Collectively, these findings suggest that renal crystal formation varies significantly among wild-type strains on a lithogenic diet, likely due to differences in their genetic backgrounds.

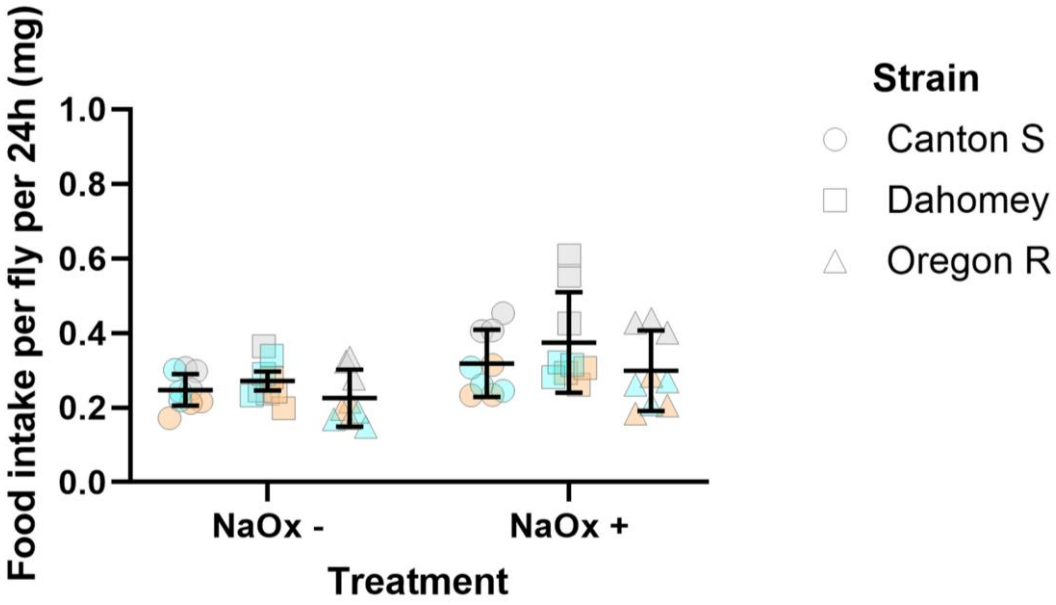

Figure 3.2 Food intakes in flies treated with or without NaOx.
The means of three biological replicates and SDs are plotted, with each colour representing a different replicate (n=5 females per tube, three tubes per line per replicate, three biological replicates).

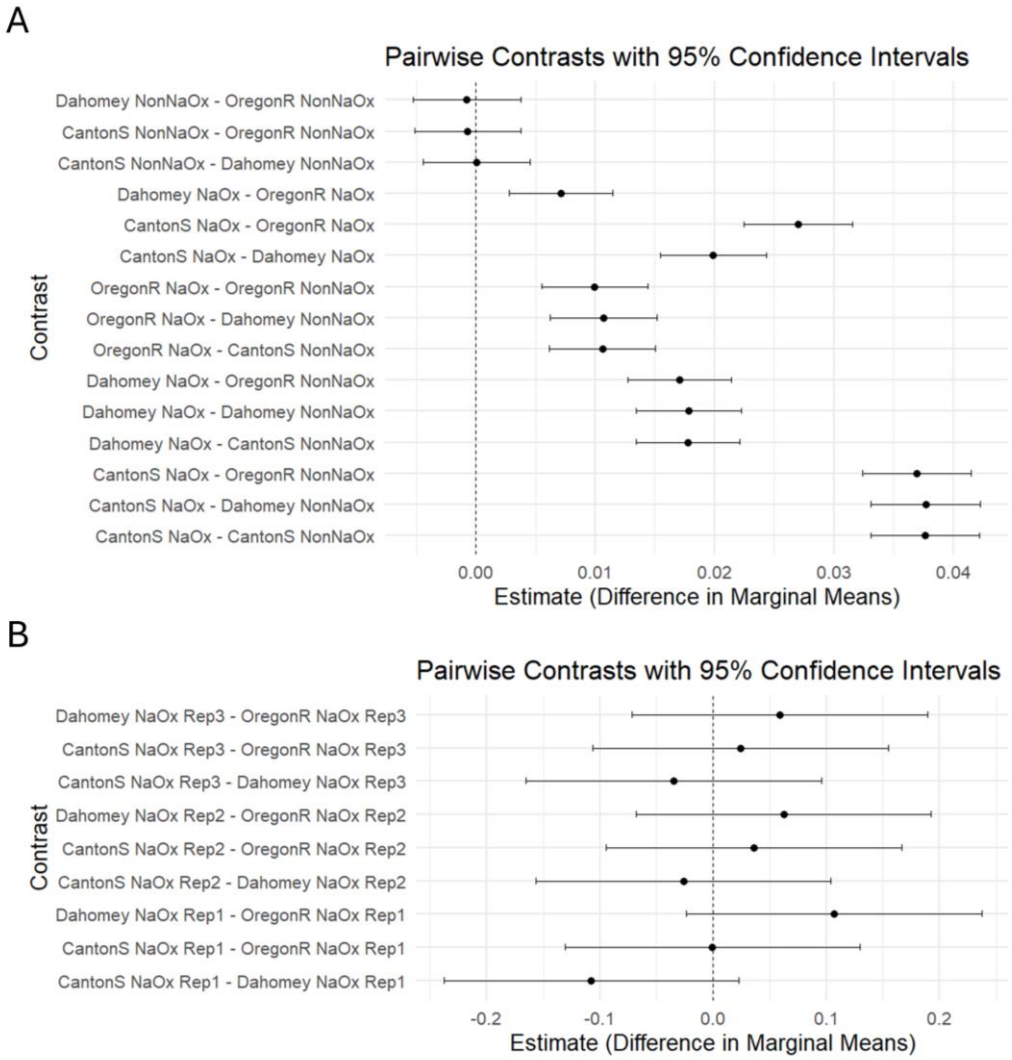

Figure 3.3 Post-hoc Tukey test assessing significance among wild-type strains. (A) Stone area. (B) Food intake. Following the type III ANOVA, a post-hoc Tukey test was conducted to determine significant differences between groups.

3.2.2 Quantitative genetics of stone formation in the DGRP

To assess the extent of variation in stone formation among genetically distinct individuals and to collect phenotypic data for association analysis, stone areas were measured in 186 DGRP lines. It was not possible to quantify the stone areas in all 186 DGRP lines in a single day. The stone areas (Figure 3.4A) and tubule sizes (Figure 3.4D) were measured across nine blocks, with Canton S used as a positive control during the measurements (Figure 3.4C). One biological replicate was recorded for 14 lines, two biological replicates for 158 other lines, and three biological replicates for 14 other lines. On average, 23 flies were dissected per

DGRP line. Substantial and reproducible phenotypic variation in stone formation was observed, with a broad-sense heritability (H^2) of 0.57 (Table 3.3). In some DGRP lines, only a small number of crystals were observed in the dissected tubules, while in others, the tubule lumens were filled with crystals (Figure 3.4A). For the 172 DGRP lines measured at least twice for stone formation, correlation analysis between the first two measurements revealed a strong positive correlation, with a Pearson's r of 0.7126 (Figure 3.4B). As a result, line means were used in subsequent GWA analysis.

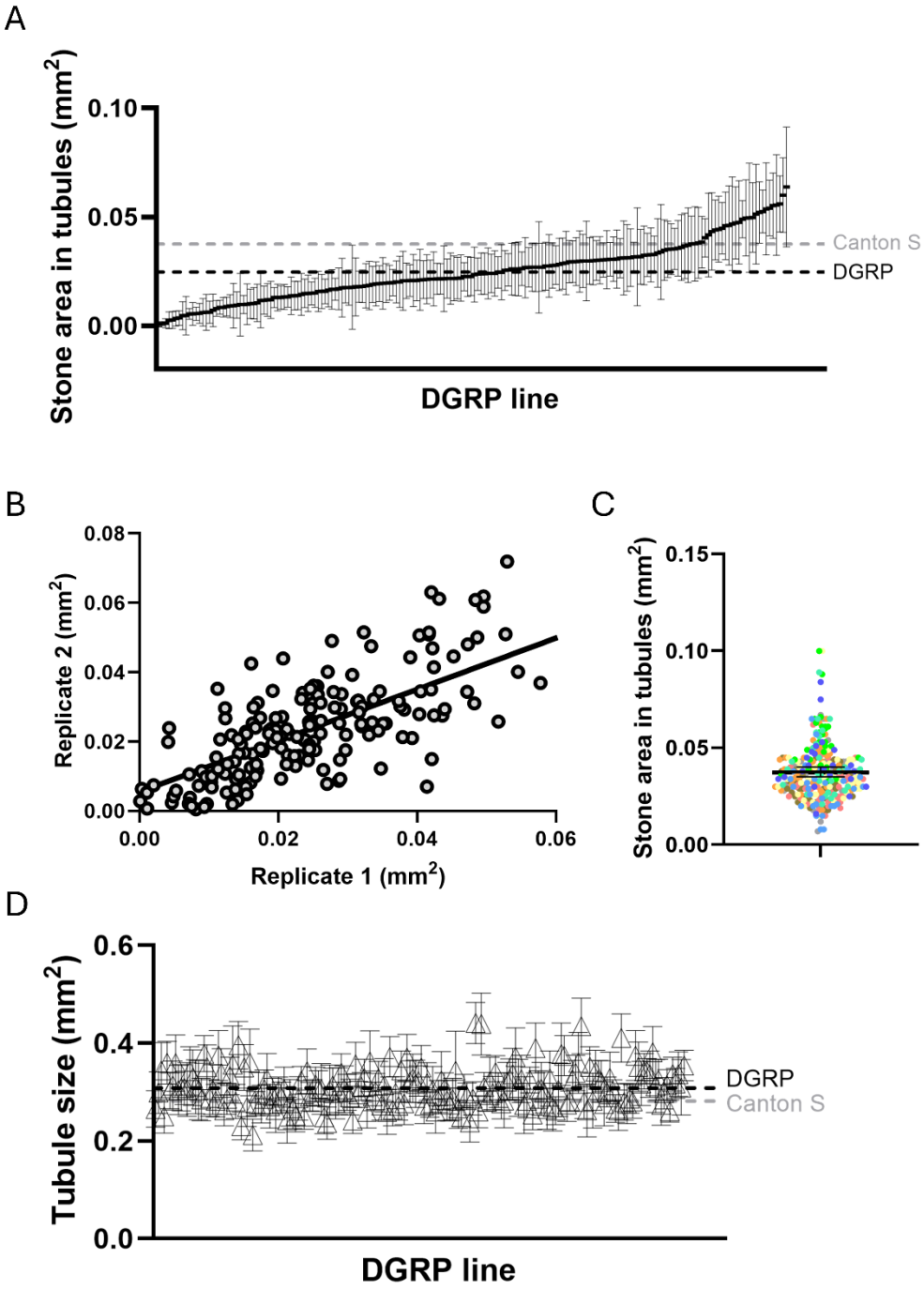

Figure 3.4 Variation in stone formation across the DGRP lines.
(A) Line means for crystal areas in 186 DGRP lines (**Appendix 3**) under a lithogenic diet. Error bars are SDs. (B) Correlation of stone areas across biological replicates of 172 DGRP lines (Pearson's $\boldsymbol{r = 0.7126, p < 0.0001}$). (C) Canton S was used as a positive control during the measurement of the DGRP lines. Each colour stands for a different block. (D) Tubule sizes were measured concurrently with the assessment of stone areas. The order of the X-axis is the same as in panel (A).

Table 3.3 Variance components of stone formation in the DGRP.

Groups	Variance	SD	H^2
Line	0.001997	0.04468	
Block	0.000153	0.01238	0.57
Residual	0.001352	0.03677	

Although most DGRP lines are genetically unrelated, as indicated by the genetic relationship matrix (Huang et al., 2014), it remains unclear whether lines with extreme phenotypic values in our study exhibit high genetic relatedness. To address this, eight lines with extreme stone areas were selected for further investigation. Pairwise relatedness was determined according to molecular markers in the DGRP, and no clustering among phenotypic classes was observed (Figure 3.5A). To gain insights into the genetic architecture of crystal formation, a full diallel cross of the eight lines was performed, and stone formation within the renal tubules of the F1 generation was quantified. The broad-sense heritability for the stone area was estimated to be 0.66 (Table 3.4).

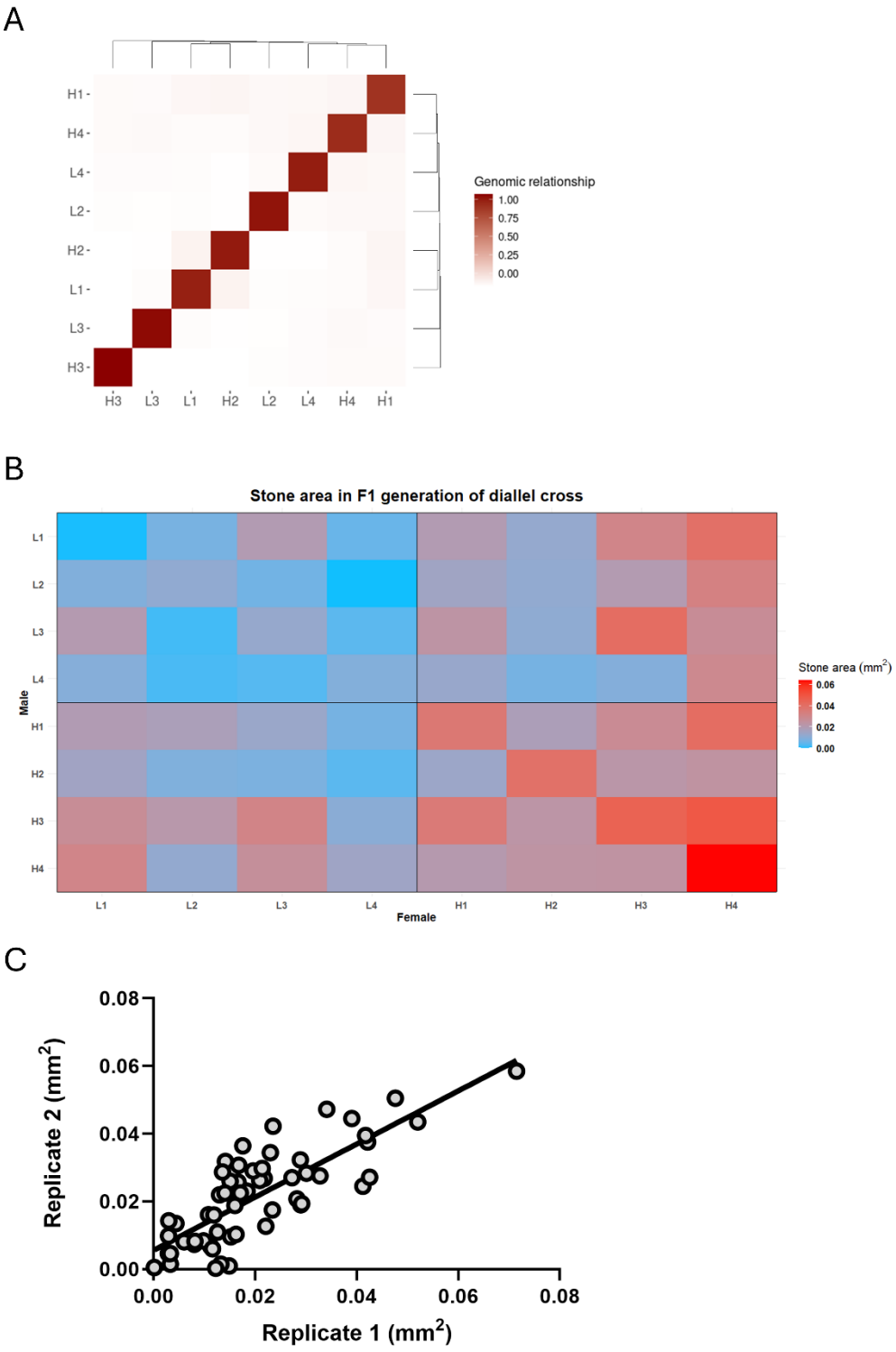

Figure 3.5 Full diallel cross between extreme lines.
(A) Heatmap of the genomic relationship matrix between 8 DGRP lines with extreme phenotypic values. (B) Heatmap of stone areas in the tubules of F1 progenies from an eight-parent diallel cross, consisting of four DGRP lines with fewer crystals in their tubules and four with more. The four DGRP lines with fewer crystals (DGRP -59, -149, -176, and -153, corresponding to L1, L2, L3, and L4) and four DGRP lines with more crystals (DGRP -738, -239, -730, and -360, corresponding to H1, H2, H3, and H4) were

used. (C) Correlation of stone areas across biological replicates in the diallel cross (Pearson's $\boldsymbol{r = 0.7954, p < 0.0001}$).

Table 3.4 Variance components of stone formation in diallel cross.

Groups	Variance	SD	H^2
Geno	0.000148	0.01217	
Block	0.000004	0.00199	0.66
Residual	0.000073	0.00855	

The F1 progenies from crosses between lines with smaller amounts of crystals tended to exhibit fewer crystals. In contrast, larger crystal areas were observed in the F1 flies from crosses between lines with more crystals (Figure 3.5B). An intermediate phenotype was seen in flies from crosses between the two groups, suggesting the presence of additive effects. Analyses of the diallel cross revealed significant general combining ability (GCA), reflecting additive effects (ANOVA $p < 0.0001$), and specific combining ability (SCA), reflecting non-additive effects (ANOVA $p < 0.0001$) (Table 3.5). A GCA/SCA ratio greater than 1 indicated a stronger contribution of additive genes to stone formation (Table 3.6). These results suggest that crystal formation in the renal tubule is largely a complex and additive trait.

Table 3.5 ANOVA for combining ability - method 1 and model 2.

	Df	Sum Sq	Mean Sq	F value	Pr(>F)
GCA	7	0.0075671	1.081e-03	11.6130	7.841e-07*
SCA	28	0.0026064	9.309e-05	11.3116	6.339e-14*
Reciprocal	28	0.0011332	4.047e-05	4.9178	3.378e-05*
Error	53	0.0004362	8.230e-06		

Table 3.6 Components of GCA and SCA.

Terms	Components
GCA	6.183862e-05
SCA	4.763916e-05
Reciprocal	1.612051e-05
Error	8.229280e-06
Additive	1.236772e-04
Dominant	4.763916e-05
GCA/SCA	1.298063e+00

3.2.3 GWA analysis of variation in stone areas

To identify genetic loci associated with variation in the development of renal crystals, a single-marker GWA analysis was conducted. The genome of the DGRP lines contained approximately 4 million polymorphisms (Mackay et al., 2012, Huang et al., 2014), and variants present in at least four individual lines were included in the association analysis, resulting in a minimum minor allele frequency of approximately 0.02. Markers and individuals with missingness more than 10% and 20%, respectively, were excluded. After filtering, 2,315,319 markers remained. Approximately 53% of the DGRP lines were infected with *Wolbachia*, and five major chromosomal inversions were present in the genome. Both factors could contribute to cryptic structures that might lead to false-positive associations (Huang et al., 2014). To address this, a mixed linear model was employed to estimate and account for the effects of *Wolbachia* and inversions. Additionally, if significant, the effects of block and tubule size were incorporated into the model to adjust for potential confounders. The results showed that neither *Wolbachia* infection nor chromosomal inversions were associated with variation in stone areas (Table 3.7), while block, as a random effect, was significantly correlated with the phenotypic variation (Table 3.8).

Table 3.7 Fixed effects of *Wolbachia* and major inversions on stone areas (Type III ANOVA table with Satterthwaite's method).

Terms	NumDF	DenDF	F value	Pr(>F)
Wolbachia	1	173.84	1.3891	0.2402
In(2L)t	2	174.36	0.0353	0.9654
In(2R)NS	2	174.95	0.0017	0.9983
In(3R)P	2	173.65	0.3787	0.6853
In(3R)K	2	174.00	1.5161	0.2224
In(3R)Mo	2	173.12	1.8651	0.1580

Table 3.8 Random effects of tubule size and block on stone areas (ANOVA-like table for random-effects: single term deletions).

Terms	AIC	LRT	Pr(>Chisq)
<none>	-15447		
Tubule size	-15446	3.3	0.06928
Line	-12224	3225.1	< 2e-16*
Block	-15365	84.7	< 2e-16*

To investigate whether any population structure is present in the DGRP lines, markers with r^2 less than 0.2 were pruned, and top principal components were identified. Principal component analysis showed that the top five principal components explained approximately 30% of the variance, with PC1 and PC2 accounting for 8.38% and 7.46% of the variance, respectively (Figure 3.6). The result suggested relatively low levels of population structure.

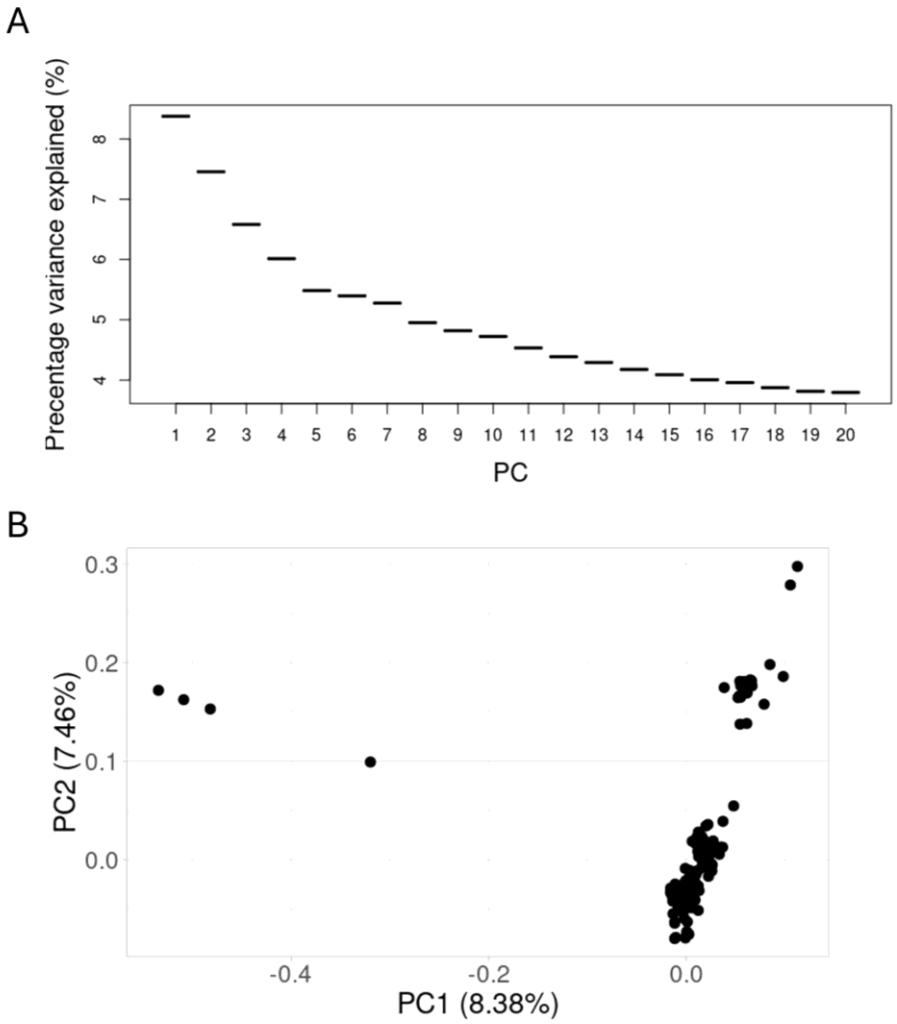

Figure 3.6 Principal component analysis (PCA) of polymorphisms with r^2 less than 0.2 in the DGRP.
(A) The percentage of variance explained by the first 20 principal components. (B) PC1 and PC2 captured 8.38% and 7.46% of the variance, respectively.

Although little population structure was expected in the DGRP, and most lines exhibited nearly zero relatedness with each other (Mackay and Huang, 2018), association analyses can be confounded by population structure and cryptic

polygenic relatedness (Price et al., 2010). To correct for population stratification, the centred relatedness matrix was estimated using the "-gk 1" option and incorporated into the association analysis with univariate linear mixed models in GEMMA (Zhou and Stephens, 2012). After accounting for block effects and confounding population structure, the association analysis identified 68 top polymorphisms (Appendix 5) in or near 41 genes (Table 3.9) at an empirical p value of 10^{-5} (Figure 3.7B). Although none of the variants reached the genome-wide significance threshold where the p value is 5×10^{-8}, deviations from expectations were observed at the empirical p value (Figure 3.7A), suggesting an enrichment of true positive associations. Since the GWA analyses were confined to approximately 200 DGRP lines with several million tests, few variants would be expected to show associations with p values that met the multiple-comparison-corrected threshold (Anholt and Mackay, 2018). Previous GWA studies of quantitative traits using the DGRP identified multiple trait-related polymorphisms at a nominal p value of 10^{-5} (Shorter et al., 2015, Huang et al., 2014, Spierer et al., 2021), with high validation rates for implicated genes. Consequently, the significance threshold with a p value of 10^{-5} was used in our study.

Table 3.9 List of candidate genes associated with stone areas.

Gene						
AstA-R1	*CG3625*	*CG6509*	*CheA46a*	*Shab*	*fz2*[*]	*sra*
rg	*Pino*	*spz4*	*Hil*	*Lkr*[†]	*mub*	*iab-8*
CG15465	*erm*	*CG33679*	*babos*	*Mp*	*CG14741*	*CR44258*
SPR[†]	*CG7289*[*]	*TfIIS*	*CG43795*	*SMSr*	*2mit*	*CG14322*
OdsH	*CG15362*	*CR41443*	*CG7991*	*CG8563*	*timeout*	*CR45650*
RunxB	*CR44912*	*CG13954*	*alpha-Spec*	*Eip71CD*[*]	*CR45109*	

Note: [*] indicates detailed discussion later; [†] denotes prior description in fly tubules.

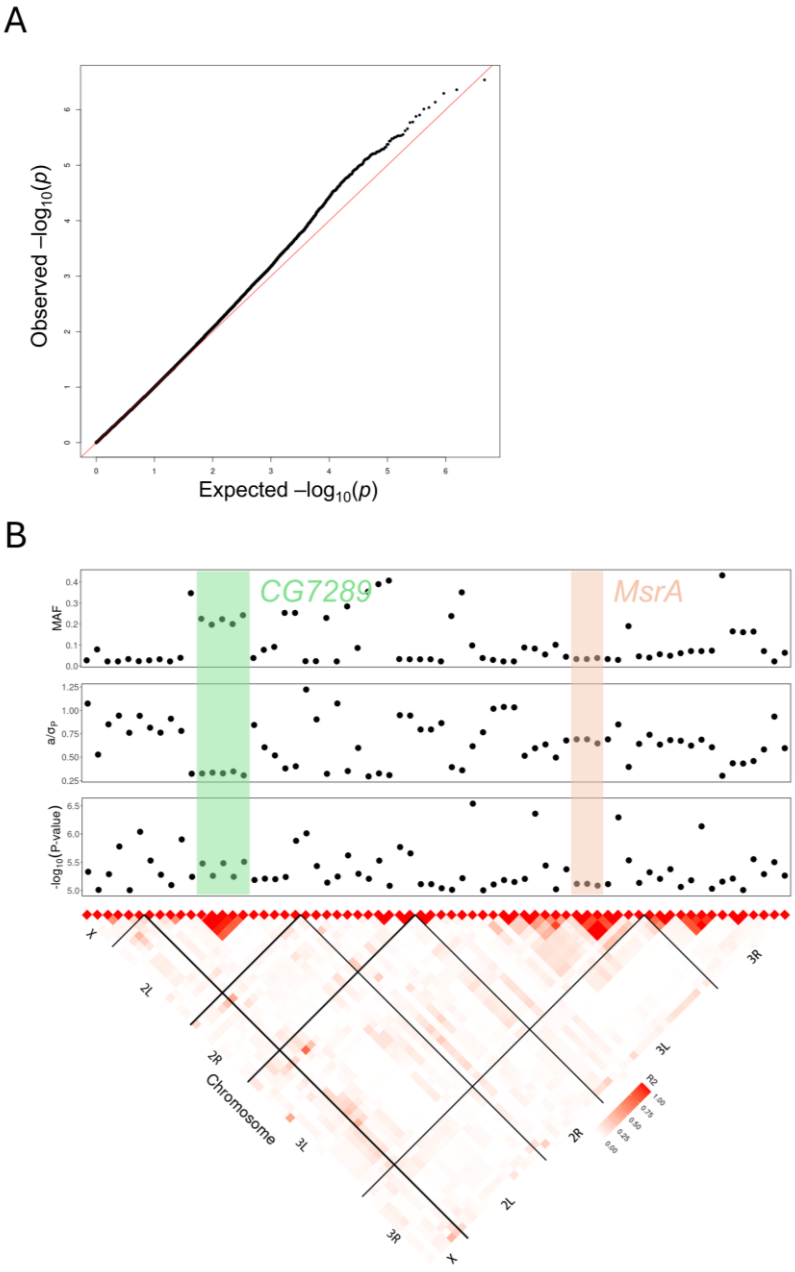

Figure 3.7 Genome-wide association between polymorphisms in the DGRP and variation in crystal formation.
(A) QQ plot of genome-wide $\boldsymbol{p}$ values ($-\boldsymbol{log10p}$) for stone areas. (B) All polymorphisms from single-marker analysis with $\boldsymbol{p < 10^{-5}}$ are shown. Top: the minor allele frequency (MAF), the effect size in phenotypic SD units ($\mathbf{a/\sigma P}$), and the significance of each polymorphism ($-\boldsymbol{log10p}$). Bottom: pairwise linkage disequilibrium among significant polymorphisms as measured by $\boldsymbol{r^2}$, with the five major chromosome arms demarcated by black lines.

Most of the polymorphisms were not in linkage disequilibrium, as indicated by the heatmap (Figure 3.7B, lower panel). Additionally, consistent with other GWA

studies using the DGRP, alleles with lower frequency exhibited larger effect sizes, and the majority of polymorphisms were intronic or intergenic (Figure 3.8).

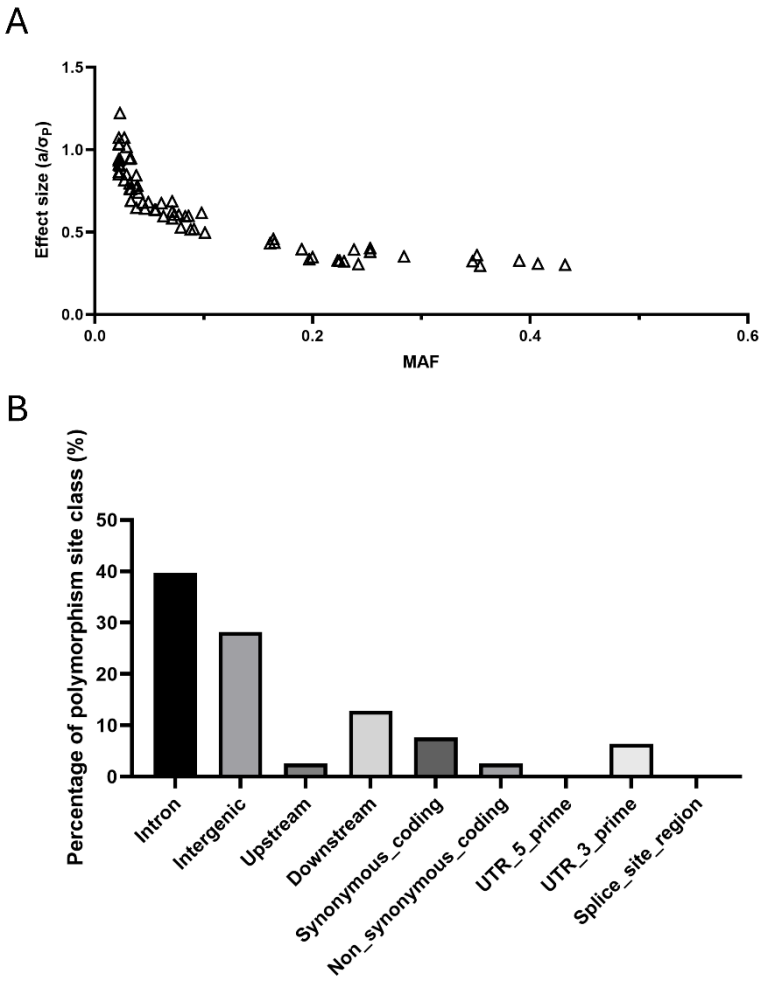

Figure 3.8 Top candidate polymorphisms for stone areas.
(A) Relationships between effect sizes and MAF. (B) Percentage of polymorphisms per site class.

In *Drosophila*, allele-level genetic interactions and physical interactions between two gene products have been curated by FlyBase (https://flybase.org/). Alleles include loss-of-function and gain-of-function mutations, and interaction molecule types are protein-protein, protein-RNA or RNA-RNA. We extracted the interacting genes of the 41 candidates identified by the GWA analysis on stone formation (Figure 3.9). Functional enrichment analysis of the clustered networks, where both interacting genes and identified candidate genes were

included, was conducted using STRING Enrichment in Cytoscape (Doncheva et al., 2019), with the original unclustered network used as the background. The analysis revealed associations between the two largest networks containing candidates and the Wnt signalling pathway and extracellular acidification, respectively (Figure 3.10, the first and third clusters).

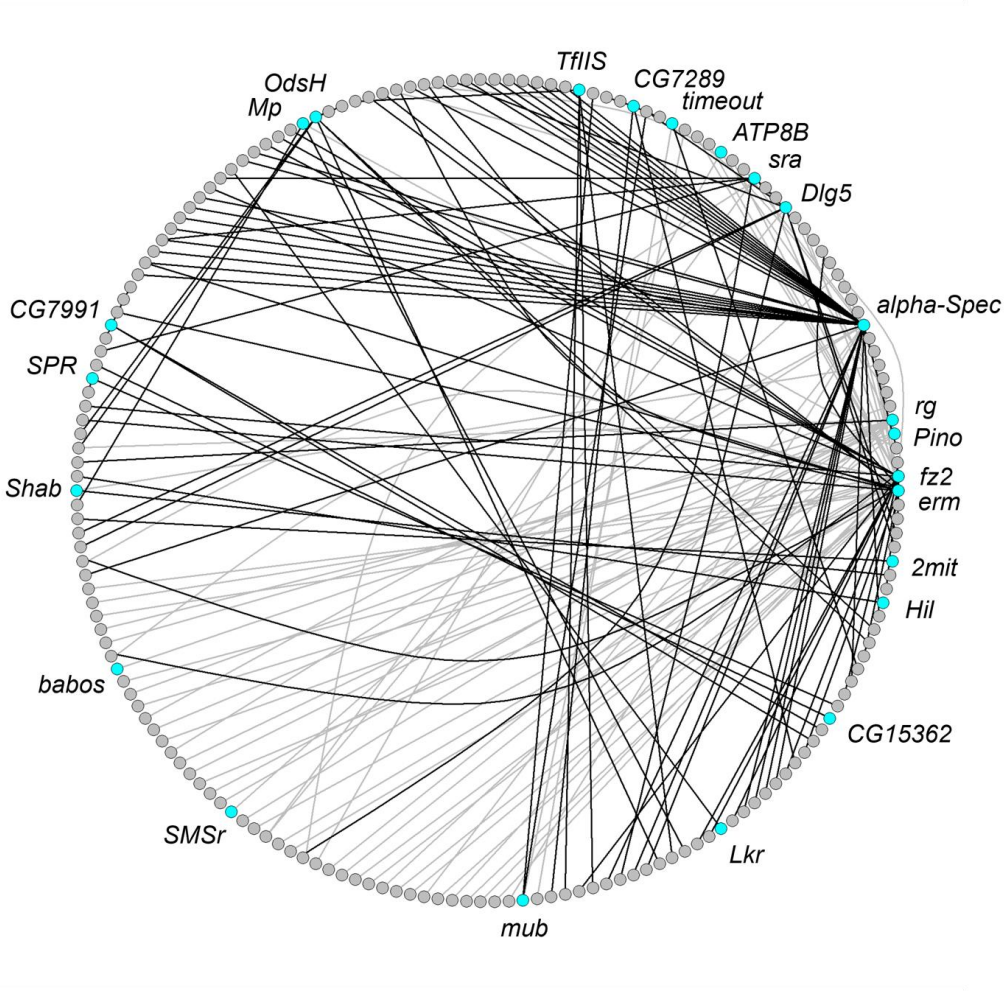

Figure 3.9 Interactions between candidates their interacting genes.
Candidates from the GWA analysis of stone areas are marked with cyan dots, while their genetically (grey line) and physically (black line) interacting genes are represented by grey dots.

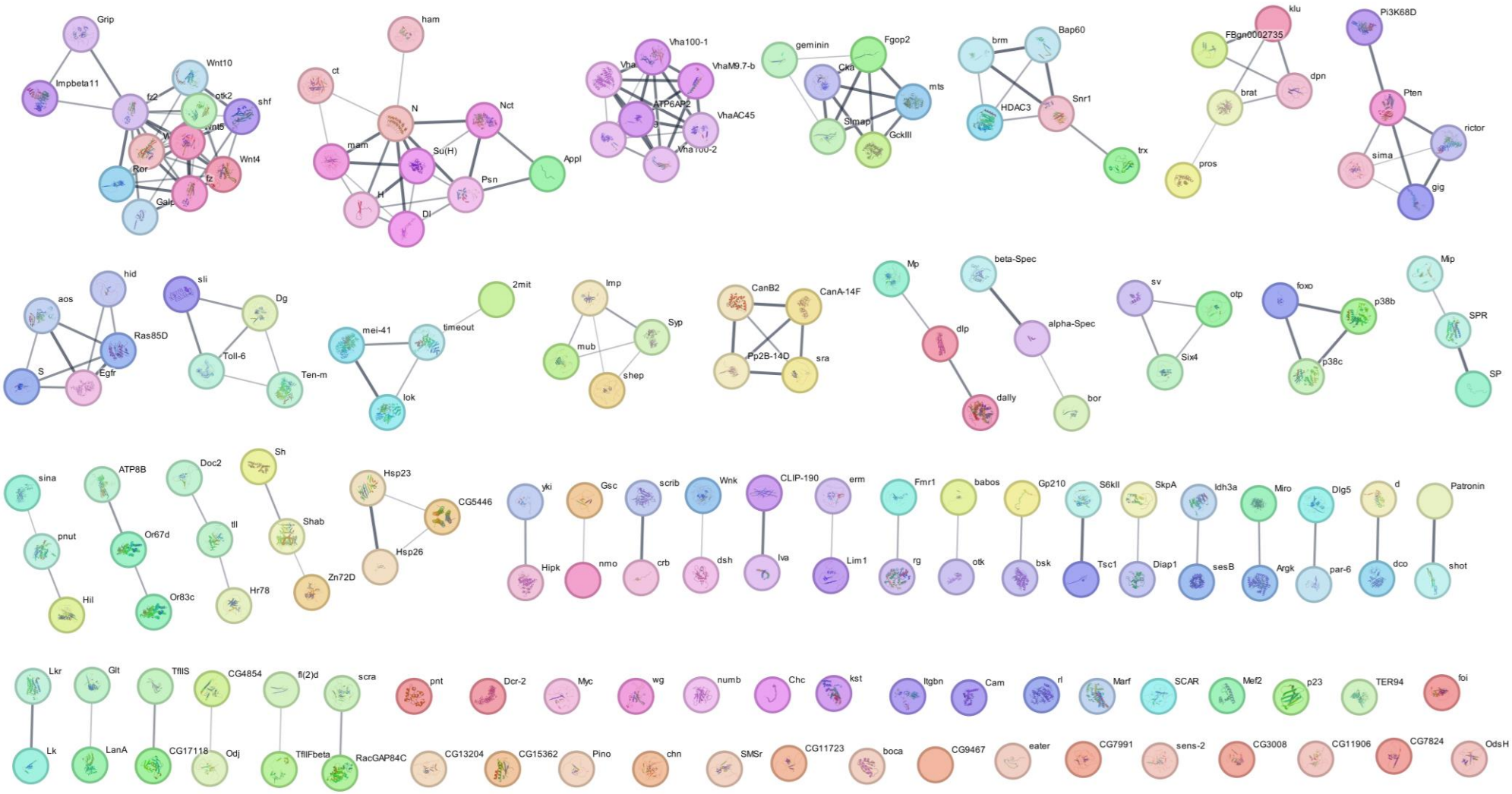
Grip
Impbeta11
Wnt10
fz2
otk2
shf
Wnt5
Wnt4
Ror
fz
ham
ct
N
Nct
mam
Su(H)
Psn
Appl
H
Dl
Vha100-1
VhaM9.7-b
ATP6AP2
VhaAC45
Vha100-2
geminin
Fgop2
Cka
mts
Slmap
GckIII
brm
Bap60
HDAC3
Snr1
trx
klu
FBgn0002735
dpn
brat
pros
PI3K68D
Pten
rictor
sima
gig
hid
aos
Ras85D
S
Egfr
sli
Dg
Toll-6
Ten-m
2mit
mei-41
timeout
lok
lmp
Syp
mub
shep
CanB2
CanA-14F
Pp2B-14D
sra
Mp
dlp
beta-Spec
alpha-Spec
dally
bor
sv
otp
Six4
foxo
p38b
p38c
Mip
SPR
SP
sina
pnut
Hil
ATP8B
Or67d
Or83c
Doc2
tll
Hr78
Sh
Shab
Zn72D
Hsp23
CG5446
Hsp26
yki
Hipk
Gsc
nmo
scrib
crb
Wnk
dsh
CLIP-190
lva
erm
Lim1
Fmr1
rg
babos
otk
Gp210
bsk
S6kII
Tsc1
SkpA
Diap1
Idh3a
sesB
Miro
Argk
Dlg5
par-6
d
dco
Patronin
shot
Lkr
Lk
Glt
LanA
TfIIS
CG17118
CG4854
Odj
fl(2)d
TfIIFbeta
scra
RacGAP84C
pnt
Dcr-2
Myc
wg
numb
Chc
kst
Itgbn
Cam
rl
Marf
SCAR
Mef2
p23
TER94
foi
CG13204
CG15362
Pino
chn
SMSr
CG11723
boca
CG9467
eater
CG7991
sens-2
CG3008
CG11906
CG7824
OdsH

Figure 3.10 Clustered networks of interactions.
This clustered version of the network, comprising both candidates and their interacting genes, was constructed from 176 nodes and 184 edges. Each node represents a protein, and each edge represents a functional interaction based on STRING. The darker the edge is, the higher the combined confidence of the functional interaction. Some of these networks are discussed in detail later in the chapter.

3.2.4 Functional validation of candidate genes

Eight candidates were selected from the association analysis of stone area for functional validation. RNAi was used to functionally test whether knockdown of candidate genes implicated by the GWA analysis affects crystal formation in renal tubules. *CG7289* and *fz2* were part of the clustered networks (Figure 3.10). Other candidates were selected based on the site class of polymorphisms and the presence of human orthologues. Tubule-specific or ubiquitous *Gal4* drivers were used to drive knockdowns according to the expression patterns of candidates, as shown by FlyAtlas (Leader et al., 2018) and FlyCellAtlas (Li et al., 2022, Xu et al., 2022). Stone areas induced by NaOx in Malpighian tubules of RNAi flies were compared with those of their coisogenic controls. A linear mixed model accounting for genotype and replicate was used to assess the significance of candidates in crystal formation. We confirmed that five out of eight candidates were implicated in the development of tubulolithiasis. Loss of *Discs large 5* (*Dlg5)* and *Shab* resulted in elevated crystal areas in the tubules, while knockdowns of *fz2*, *CG7289*, and *SPR* reduced the amount of tubuloliths (Figure 3.11A). Additionally, qRT-PCR was performed to assess the knockdown efficiency of RNAi against these five genes, and effective knockdown was confirmed (Figure 3.11B).

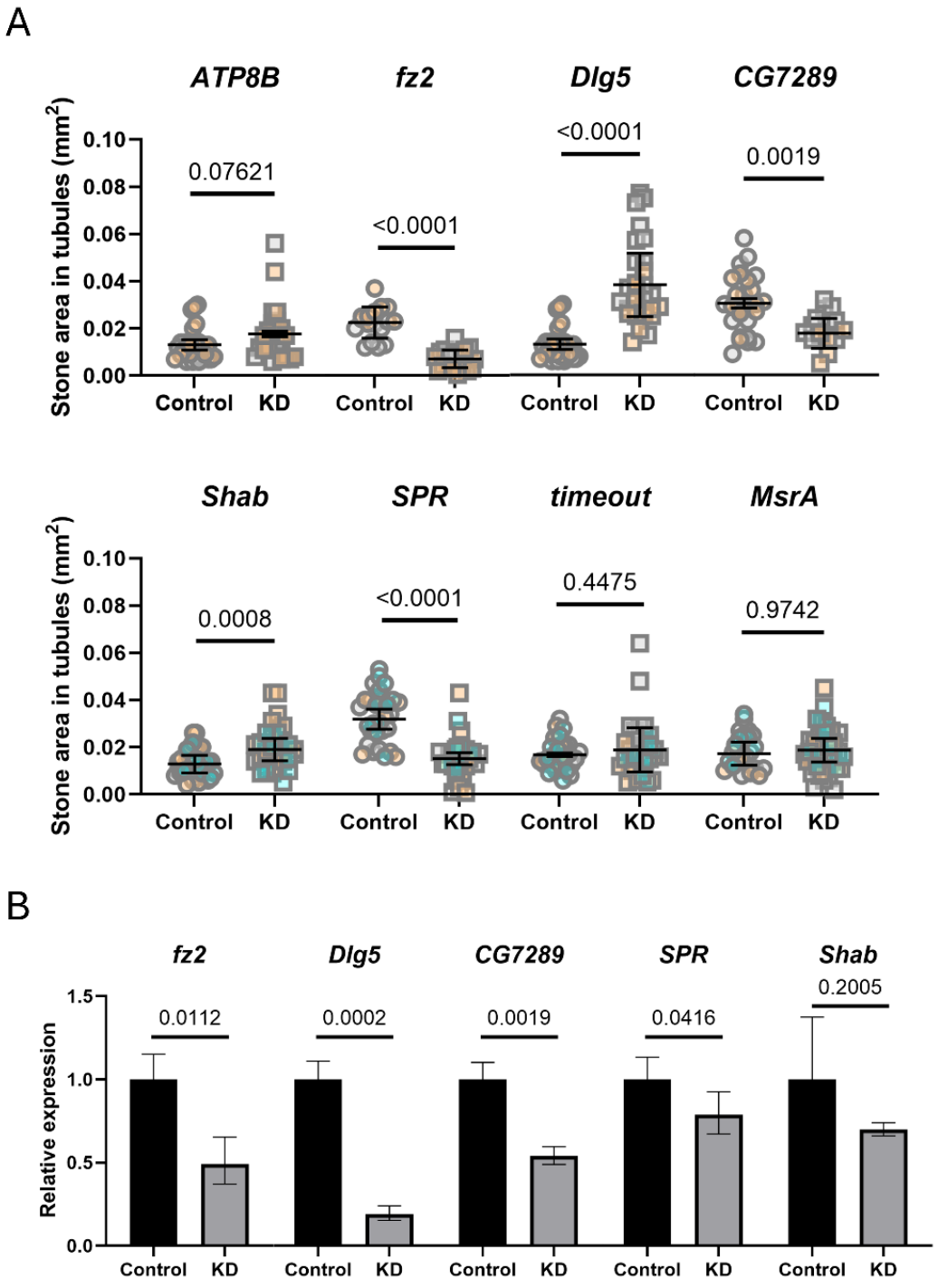

Figure 3.11 Validation of candidate genes using RNAi.
(A) Eight candidate genes identified from the GWA analysis of stone area were tested for their effects on stone formation in RNAi flies (KD), compared to their corresponding controls. Means of biological replicates and SDs are plotted, with each colour representing a different replicate (n=5-15 females per line and replicate, two to three biological replicates). Linear mixed models were used to determine the effect of genotype. (B) Validation of knockdown efficiency by qRT-PCR. Relative expressions with

lower and upper limits are plotted (three biological replicates, two-tailed Student's *t*-test).

As shown by BioGRID, a database of protein, chemical, and genetic interactions (Stark et al., 2006), the uncharacterised protein KIAA2013, the human orthologue of CG7289, interacts with V-ATPase assembly factors, which is consistent with the interactions observed in its fly counterpart. Given that bafilomycin is a known inhibitor of V-ATPases, and both CG7289 and its human orthologue KIAA2013 interact with V-ATPase subunits, the impact of bafilomycin treatment on crystal formation was investigated in dissected fly tubules. The results demonstrated that NaOx supplementation significantly induced crystal formation in the renal tubules, and this crystallization was effectively blocked by bafilomycin A1 treatment (Figure 3.12).

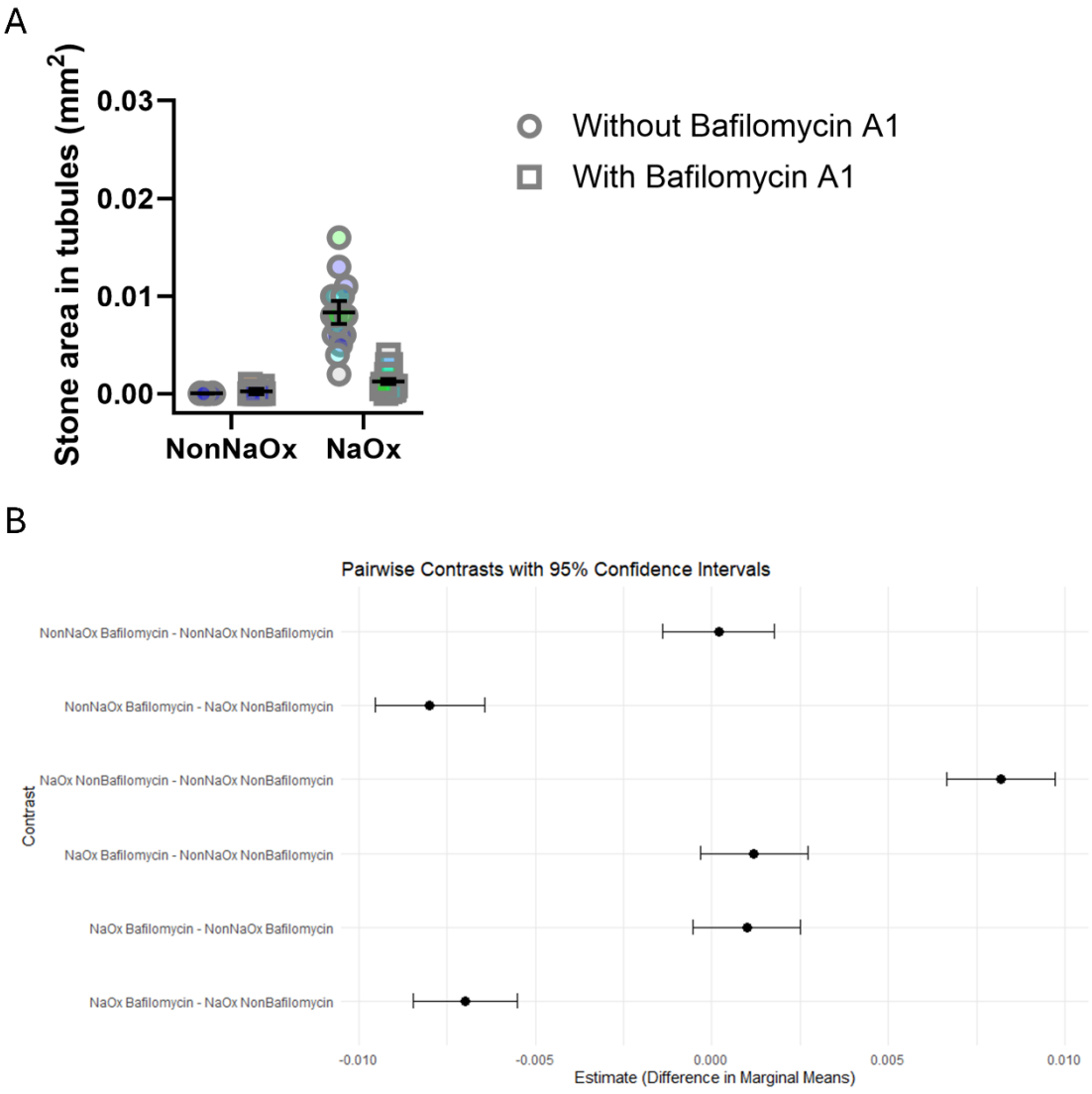

Figure 3.12 The effect of the V-ATPase inhibitor, Bafilomycin A1, on crystal formation was analysed in vitro.
(A) The means of biological replicates and SDs are plotted, with each colour representing a different replicate (n=4-6 pairs of tubules per sample and replicate, five biological replicates). (B) Following type III ANOVA, a post-hoc Tukey test conducted to determine significant groupwise differences.

3.3 Discussion

3.3.1 Quantitative genetics of the renal crystal formation

Exploring genetic differences among people could unfortunately, reinforce stereotypical features of populations, but it could also be beneficial to human health in the context of common health-related traits (Bamshad et al., 2004).

According to Soucie et al. (Soucie et al., 1994), the prevalence of kidney stones among Black individuals is approximately 44% that of White individuals, with rates among Hispanics and Asians falling between the two. These differences in prevalence can be partially explained by socioeconomic, lifestyle, and medical factors; however, additional investigation of genetic risk factors is necessary (Hsi et al., 2018). A family history of kidney stone disease increases an individual's likelihood of developing the condition (Resnick et al., 1968, McGeown, 1960), with a high degree of heritability observed in twin studies (Goldfarb et al., 2005, Goldfarb et al., 2019), suggesting that genetics plays an important role in the development of kidney stones or the susceptibility to kidney stones. Dozens of genome-wide association studies have been conducted to identify novel risk loci and molecular mechanisms associated with kidney stone disease in humans (Thorleifsson et al., 2009, Curry et al., 2020, Gudbjartsson et al., 2010, Urabe et al., 2012, Li et al., 2018, Ware et al., 2019, Hao et al., 2023). For example, a genetic locus, which is homozygous in approximately 62% of the studied population, confers a 1.6-fold increased risk of developing kidney stones (Thorleifsson et al., 2009). The aetiology of stone formation is multifactorial, and challenges remain in human studies. Using *Drosophila* as a simplified model for analysing kidney stone disease may offer valuable insights into genetic risk factors, as it allows for easier control of environmental variables and population stratification.

We first investigated whether natural variation presents in the tendency to develop renal stones under a lithogenic diet in *Drosophila*. Three commonly used laboratory strains, each with distinct origins and histories, exhibited varying amounts of crystals in their renal tubules. This variation in crystal development was not attributable to differences in food consumption, suggesting that differences in genetic background likely contribute to this phenotypic variation. Next, we assessed the tendency to develop renal stones in 186 DGRP lines and conducted a genome-wide association study examining polymorphic genetic markers resulting from historical recombination events. Substantial variation in crystal formation was observed across these lines. The highly reproducible phenotypic variation observed suggests that environmental sources of variation

have been minimized. To control for environmental factors, the DGRP lines were randomly allocated to different blocks, ensuring the randomization of environmental variables across lines and replicates. Increasing the number of DGRP lines phenotyped would enhance the statistical power for detecting true associations. However, the number of DGRP lines in our study was limited to approximately 180 due to the poor viability or unavailability of 20 other lines.

Diallel crosses are often employed in genetic studies to determine the mode of inheritance of the trait of interest, such as whether the trait is inherited in a dominant, additive, or non-additive manner. A diallel cross involves all possible matings between homozygous lines, including self- and reciprocal crosses (Hayman, 1954). However, due to practical limitations, this approach is not feasible for testing a large number of lines. In our study, four DGRP lines with the minimal tendency to develop renal crystals and four lines with the maximal tendency were selected to perform a complete diallel cross. The analysis of diallel crosses between the DGRP lines with extreme phenotypic values indicated that the majority of the genetic variance could be attributed to additive effects. The observation resembles the contribution of additive genetic factors observed in human nephrolithiasis, where narrow-sense heritability is larger than 50% (Goldfarb et al., 2019, Goldfarb et al., 2005).

To partition the total phenotypic variation in 186 DGRP lines, a linear mixed model that accounts for both line and block effects was employed. The block factor had a statistically significant effect on crystal formation, but it explained only approximately 4.4% of the total phenotypic variance (Table 3.3). This finding is consistent with the good mix of stone areas observed in Canton S, a positive control used during the measurements, across different blocks (Figure 3.4C). In contrast, the strain effect accounted for approximately 57% of the total variance, suggesting that a substantial portion of the variation in crystal formation can be attributed to inherited genetic factors.

3.3.2 Candidate genes

To identify candidate genes associated with the development of kidney stones, an association study was conducted. In this analysis, none of the polymorphisms reached the Bonferroni-corrected threshold. However, a nominal p value of 10^{-5}, commonly used in other GWA studies involving the DGRP, revealed deviations from expectations in the QQ plot, suggesting an enrichment of true positive associations. Using this nominal threshold, we identified 68 top polymorphisms corresponding to 41 genes associated with crystal formation. Of these, 28 genes have predicted human orthologues and 33 orthologues exhibit kidney expression with FPKM (fragments per kilobase of transcript per million mapped reads) levels larger than 10 (Figure 3.13 and Table 3.10). Some of the orthologues are involved in the transmission of extracellular signals (*GPR158*, *GPR83*, *KCNB1*, *DLG5*, *FZD5*) and DNA-binding and transcriptional activity (*HOXA10*, *TCEA1*, *FEZF2*, *UNCX*). MSRA, the orthologue of fly MsrA, was identified as a human kidney stone matrix protein with promising activity against crystallization (Narula et al., 2020). RNA-sequencing data revealed that *MSRA* expression was downregulated in the kidneys of rats with renal calculi (Zhu et al., 2023). However, knockdown of *MsrA* in our study did not exhibit a lithogenic effect, likely due to saturation of crystal formation in the tubules, tissue-specific effects, or a false positive association. Additionally, a polymorphism in *CPB2*, the *CG8563* in *Drosophila*, has been associated with the prevalence of chronic kidney disease (Yoshida et al., 2009), with its protein level upregulated in the kidneys of rats with calculi (Zhu et al., 2023). Twelve genes, *SPTAN1*, *AIG1*, *DLG5*, *TCEA1*, *SAMD8*, *RCAN2*, *RCAN1*, *MSRA*, *NBEA*, *ZNF106*, *SDK1*, and *NTM*, were found to be differentially expressed in the human papilla in response to stone disease (Canela et al., 2023). These suggest that several genes potentially linked to kidney stone disease have been identified in this study, although further functional verification is needed.

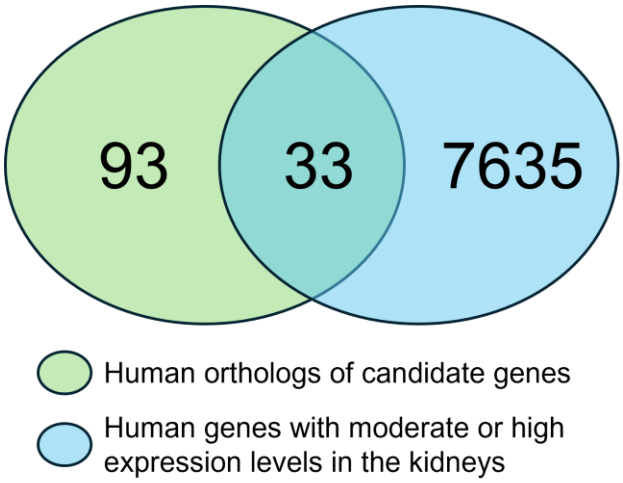

Figure 3.13 Thirty-three human orthologues of candidate genes exhibit moderate or high expression in the kidneys.

Table 3.10 Expression levels of human orthologues in the kidneys.

Gene symbol	FPKM value	Gene symbol	FPKM value	Gene symbol	FPKM value
AIG1	104.77	*HOXA9*	26.89	*PDZD11*	22.66
ATP10D	15.04	*HOXC10*	38.71	*RCAN1*	54.55
ATP11A	16.02	*HOXD10*	18.09	*RCAN2*	33.00
ATP11B	18.84	*HOXD9*	11.23	*SGMS1*	16.35
ATP11C	13.42	*KIAA2013*	22.59	*SGMS2*	14.98
ATP8B1	10.17	*LIMA1*	37.84	*SPTAN1*	39.65
COL12A1	11.97	*LRBA*	25.91	*SYNJ2BP*	25.00
COL18A1	71.34	*MSRA*	102.01	*TCEA1*	30.47
CPN2	13.55	*PCBP1*	156.52	*TCEA2*	29.10
FRZB	12.43	*PCBP2*	312.39	*TCEA3*	54.43
HOXA10	13.54	*PCBP4*	12.17	*ZNF106*	18.33

Data were obtained from (Fagerberg et al., 2014), with FPKM levels larger than 10.

Functional enrichment analysis of the clustered interaction networks containing candidate genes identified associations between two networks, each incorporating a candidate gene and biological processes such as the Wnt signalling pathway (Figure 3.14A) and extracellular acidification (Figure 3.14B). Previous studies have demonstrated that inhibiting the Wnt/ß-catenin signalling pathway can protect renal epithelial cells from the formation of CaOx crystals (Xu et al., 2021), while activating the Wnt/ß-catenin pathway promotes the osteogenic differentiation of human renal interstitial fibroblasts (Zhu et al., 2020). Conversely, DKK1, an inhibitor of the Wnt signalling pathway, has been

positively associated with the formation of calcium-containing upper urinary tract stones (Jou et al., 2014). Additionally, renal V-ATPases play a crucial role in luminal acidification (Breton and Brown, 2013, Wagner et al., 2004), and inappropriate urinary acidification may contribute to the development of calcium-based kidney stones (Dhayat et al., 2016, Wagner, 2008).

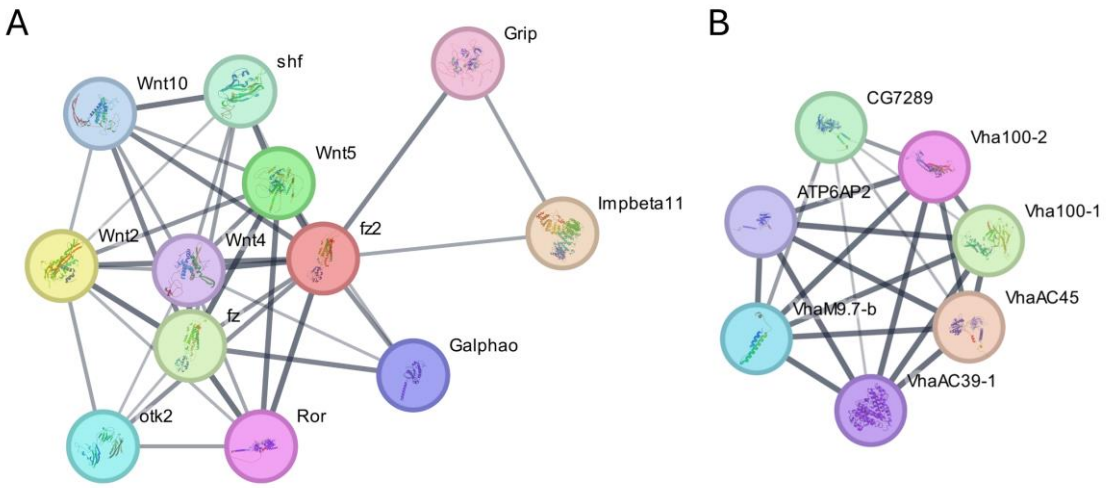

Figure 3.14 Two clustered interaction networks containing *fz2* or *CG7289*.
(A) The largest network and (B) the third-largest network from **Figure 3.10**.

RNAi-mediated knockdown of gene expression allows for the determination of whether candidate genes harbouring polymorphisms are implicated in the development of renal crystals. Five out of eight candidates have been confirmed to play a role in crystal formation. The discrepancies between functional validation and GWA analysis may arise from false positives in the associations, off-target effects of RNAi lines, or tissue-specific effects of the polymorphisms or genes. Furthermore, mutation- or RNAi-mediated disruptions of gene expression are likely to produce different effects compared with naturally occurring variants, which may exert more subtle influences on gene expression (Mackay and Huang, 2018). Additionally, many natural variants associated with the trait of interest are located in intergenic regions.

Human orthologues of *CG7289* and *fz2* are enriched in the proximal tubule of the healthy nephron, as shown in the Kidney Tissue Atlas (Hansen et al., 2022). In disease conditions such as CKD and acute kidney injury, this proximal tubule-

enriched expression is lost, implying their involvement in normal kidney function. A locus in *KIAA2013*, the human orthologue of *CG7289*, has been associated with the gradual loss of kidney function (Sugawara et al., 2023). According to BioGRID (Stark et al., 2006), the uncharacterised protein KIAA2013 interacts with V-ATPase assembly factors. This observation is consistent with its fly counterpart, which also has protein interactions with several V-ATPase subunits, as revealed by co-affinity purification coupled with mass spectrometry analysis (Guruharsha et al., 2011). Mutations in V-ATPase subunit genes, *ATP6V1B1* and *ATP6V0A4*, in humans have been associated with dRTA (Karet et al., 1999, Stover et al., 2002), and recurrent stone formers carrying a SNP in *ATP6V1B1* (c.481G>A; p.E161K) are more likely to contain calcium phosphate than stones from patients with the wild-type locus, due to the elevated urinary pH (Dhayat et al., 2016). Loss of *Drosophila* homologues of *ATP6V1B1* and *ATP6V0A4* in renal tubule also increases calcium oxalate crystal formation under lithogenic conditions (Fan et al., 2020). However, in our study, knockdown of *CG7289* resulted in a reduction in renal crystal formation. This finding suggests that inhibition of *CG7289* may not have the same effect on V-ATPase activity as RNAi-mediated knockdown of V-ATPase genes. Additionally, in the study by Fan et al., flies were treated with 0.3% NaOx once hatched, and both the anterior and posterior tubules were examined for the stone area. Asymmetry between the anterior and posterior tubules has been observed, not only in renal tubule function, supported by the anterior-specific storage of calcium as phosphate-rich mineral granules (Dube et al., 2000a), but also in the transcriptome (Chintapalli et al., 2012), highlighting the necessity to exclude one pair of tubules from the other in the experiment. Furthermore, prolonged NaOx feeding time did not lead to increased renal stone accumulation in the posterior tubules (Ghimire, 2019). In contrast, our study focused on the anterior tubules of 7-day-old adult female flies subjected to a diet containing 0.1% NaOx. This methodological difference may also contribute to the observed discrepancy. Additionally, in vitro renal stone formation was inhibited by Bafilomycin A1, a known V-ATPase inhibitor, supporting the notion that the lithogenic effects of V-ATPase gene knockdown differ from those caused by V-ATPase activity inhibition.

The Wnt signalling has been implicated in various human kidney disorders. Our study suggests that it also plays a role in the development of tubulolithiasis. Inhibition of the Wnt receptor Fz2 ameliorated tubular calcification in flies. A similar protective effect has been observed for SFRP5, an inhibitor of the Wnt pathway, in the context of vascular calcification of CKD patients (Deng et al., 2021). In contrast to *CG7289*, which is expressed in a limited number of cells at low expression levels in MTs, *fz2* is expressed in many principal cells and stellate cells with relatively high expression levels, as shown by FlyCellAtlas (Li et al., 2022, Xu et al., 2022). Given its broad expression pattern, knockdown of *fz2* was conducted in both PCs and SCs, raising the question of which cell type is primarily responsible for the protective effects observed following *fz2* knockdown.

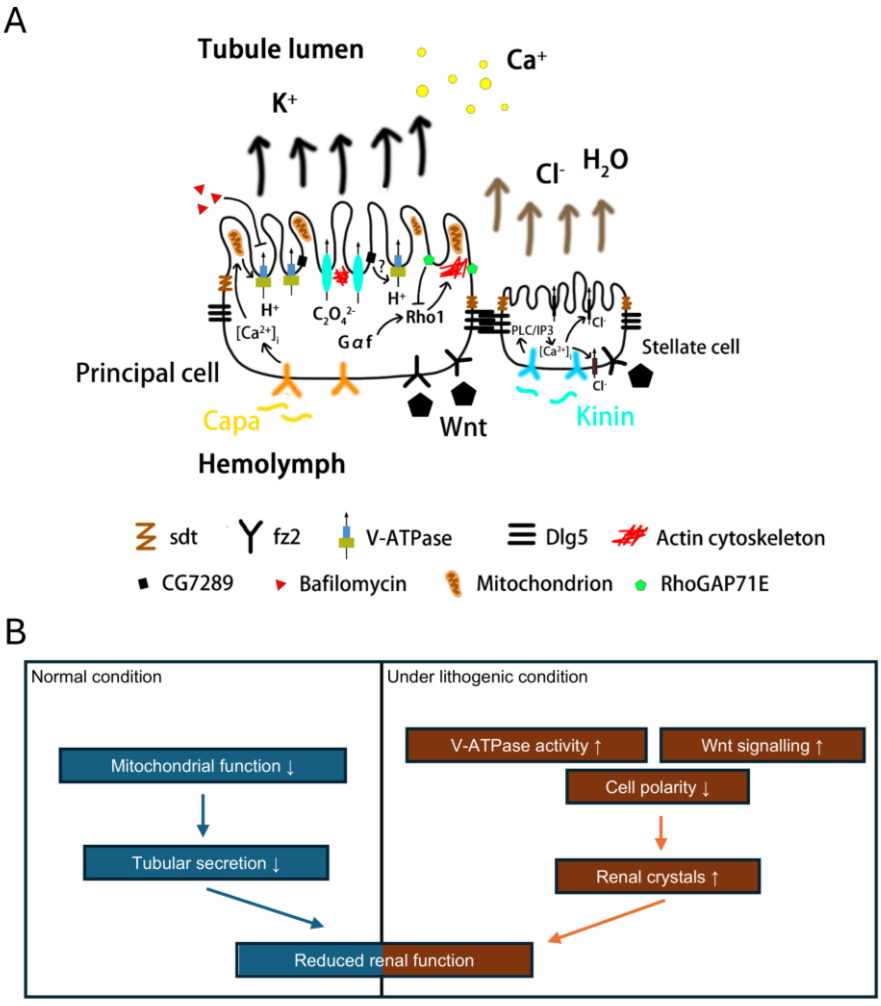

Figure 3.15 Graphical summary of risk factors contributing to renal dysfunction. (A) This panel illustrates a two-cell model for insect tubule fluid secretion, highlighting some candidates identified in the study. (B) This panel summarises risk factors associated with the candidate genes identified in this chapter and Chapter 4. Under lithogenic conditions, increased V-ATPase activity, activation of Wnt signalling, and disrupted cell polarity promote renal crystal formation, which disrupts renal function. Under normal conditions, reduced mitochondrial activity leads to decreased fluid secretion rates, impairing renal function.

Here, we present a successful GWA study on renal crystal formation in *Drosophila*, identifying multiple loci/pathways and validating candidate genes through RNAi-mediated silencing (Figure 3.15). The functions of these candidate loci, such as *fz2* and *CG7289,* correspond to that of their known human counterparts, which increases confidence in the identification of novel loci impacting stone formation.

Chapter 4 The Genetic Basis of Variation in Tubular Transport in *Drosophila*

4.1 Summary

Renal tubular transport is a key functional parameter of the kidneys in humans, regulating the reabsorption and secretion of various endogenous solutes and xenobiotics. Significant interindividual variation in proximal tubular secretion of endogenous markers (Rivara et al., 2017) and a strong genetic contribution to variation in renal drug clearance (Yin et al., 2006, Leabman and Giacomini, 2003) have been observed, although the genetic basis of this variation remains poorly understood. The Malpighian tubule, a major excretory organ in *Drosophila,* is known for its high secretion rates on a per-cell volume basis and provides an excellent model for studying the genetic basis of tubular transport. Using the *Drosophila melanogaster* genetic reference panel, basal secretion rates, Capa-stimulated secretion rates, and both Capa- and Kinin-stimulated secretion rates were measured in dissected renal tubules. Considerable phenotypic variation was also observed in these traits, which enables the identification of candidate loci or genes implicated not only in tubular transport under normal conditions but also in the neuroendocrine regulation of secretion. Candidate genes associated with the observed phenotypic variation were further functionally validated through RNAi-mediated knockdown.

4.2 Results

4.2.1 Variation in renal tubular transport in the DGRP

To characterise the natural variation in tubular transport, the basal fluid secretion rates of dissected tubules were quantified in 183 DGRP lines. Fluid secretion rates were measured in 28 experimental blocks, with Canton S used as a control. Additionally, the neuroendocrine regulation of tubular secretions was investigated using two diuretic neuropeptides, Capa-1 and Kinin, which target

different cell types within the tubules. Treatment with Capa-1 resulted in increased secretion rates, and the secretion reached its maximum when both Capa and Kinin were present (Figure 4.1).

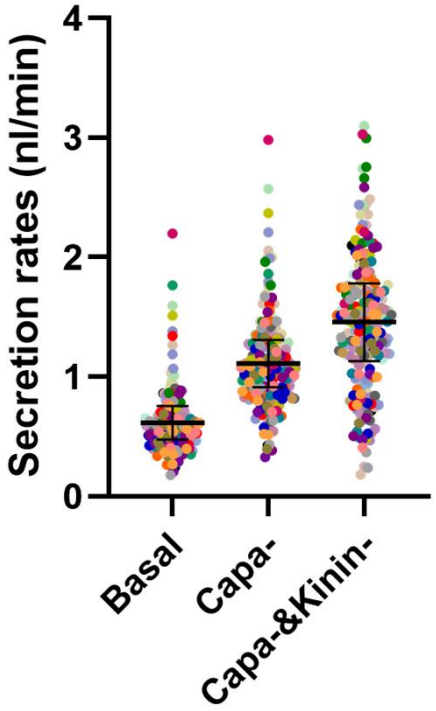

Figure 4.1 Fluid secretion rates of Canton S.
Canton S was used as a control during the measurement of the DGRP lines across different blocks. Labels on X-axis represent secretion rates under basal conditions (without stimulation) and following stimulation with the neuropeptides Capa and Kinin. Each colour stands for a different block. The means of block averages and SDs are plotted.

In the DGRP lines, considerable variation was observed, with the difference in basal secretion rates between the extreme lines exceeding seven-fold (Figure 4.2C). The average basal, Capa-stimulated, and both Capa- and Kinin-stimulated secretion rates for the DGRP lines were 1.19, 1.73, and 2.37 nl/min, respectively (Figure 4.2A to C and Appendix 4). To ensure the reliability and reproducibility of the results, basal secretion rates were measured twice in 29 DGRP lines, revealing a positive correlation between the two measurements, with a Pearson's r of 0.4525 (Figure 4.2D). Additionally, positive correlations were observed between basal secretion rates and neuropeptide-stimulated secretion rates (Figure 4.3A). There was also significant variation in the fold changes of

secretion rates stimulated by neuropeptides, referred to as the neuropeptide-stimulated secretion index (Figure 4.3B). Although lower urine volume is associated with a higher risk of kidney stone disease in humans (Moe, 2006), no correlation was found between the basal secretion rates and stone areas in flies (Pearson's $r = 0.0214, p = 0.7760$) (Figure 4.3C). This difference is likely due to that the basal secretion rates were measured using flies reared on standard fly food and the stone areas were quantified in animals fed with the lithogenic diet. The broad-sense heritability for tubular secretion-related traits was relatively low (Table 4.1), suggesting that genetic variance accounts for a greater proportion of phenotypic variance in the development of renal crystals than in the variation of tubular secretion.

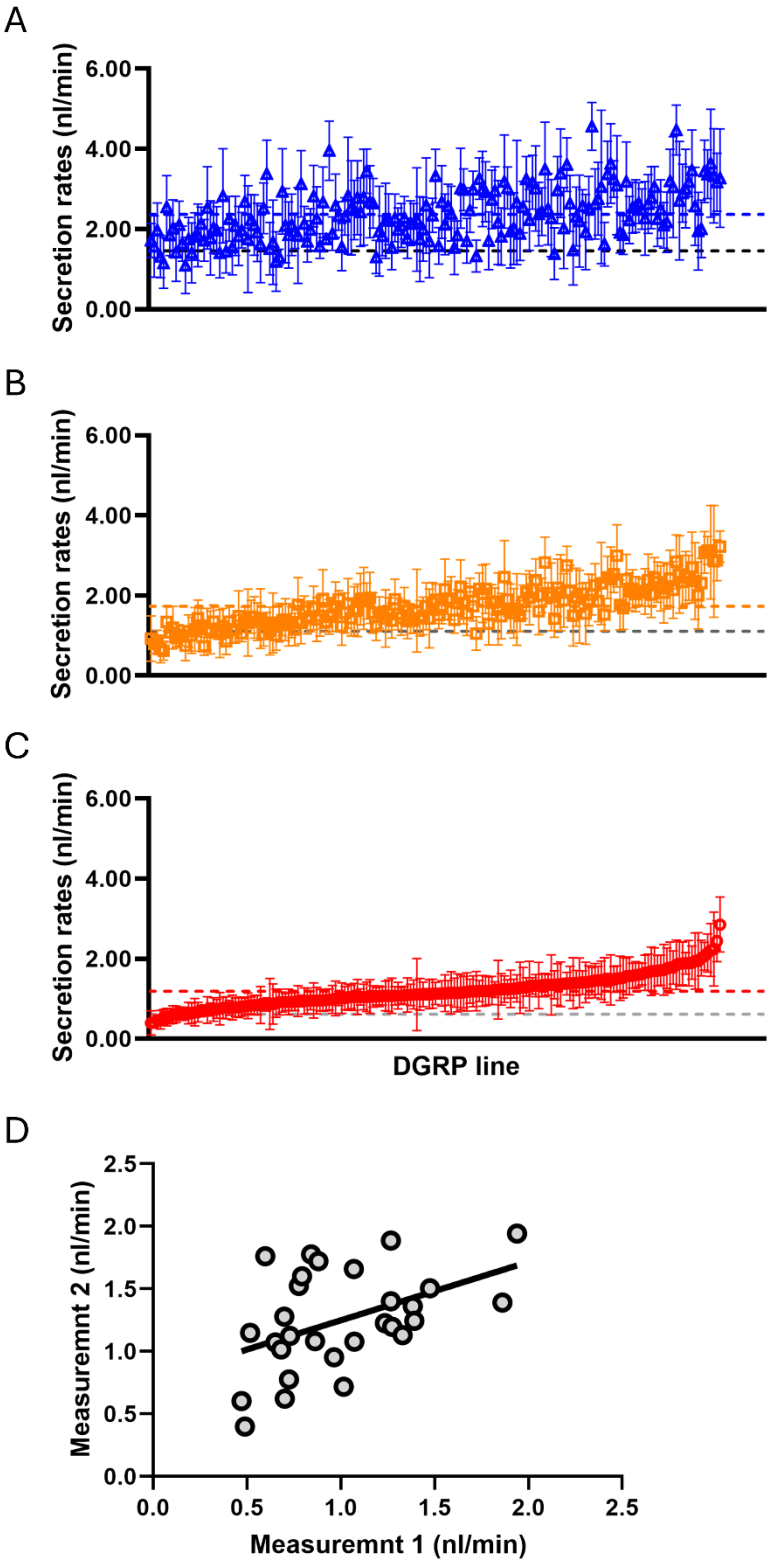

Figure 4.2 Mean fluid secretion rates for 183 DGRP lines.
(A) Both Capa- and Kinin-stimulated secretion rates. (B) Capa-stimulated secretion rates. (C) Basal secretion rate. Red, orange, and blue dashed lines stand for the mean

values across all DGRP lines for the corresponding secretion rates. Grey, dark grey, and black dashed lines indicate the secretion rates for Canton S. Error bars are SDs. (D) Correlation of basal secretion rates across two measurements of 29 DGRP lines (Pearson's $r = 0.4525, p = 0.0137$).

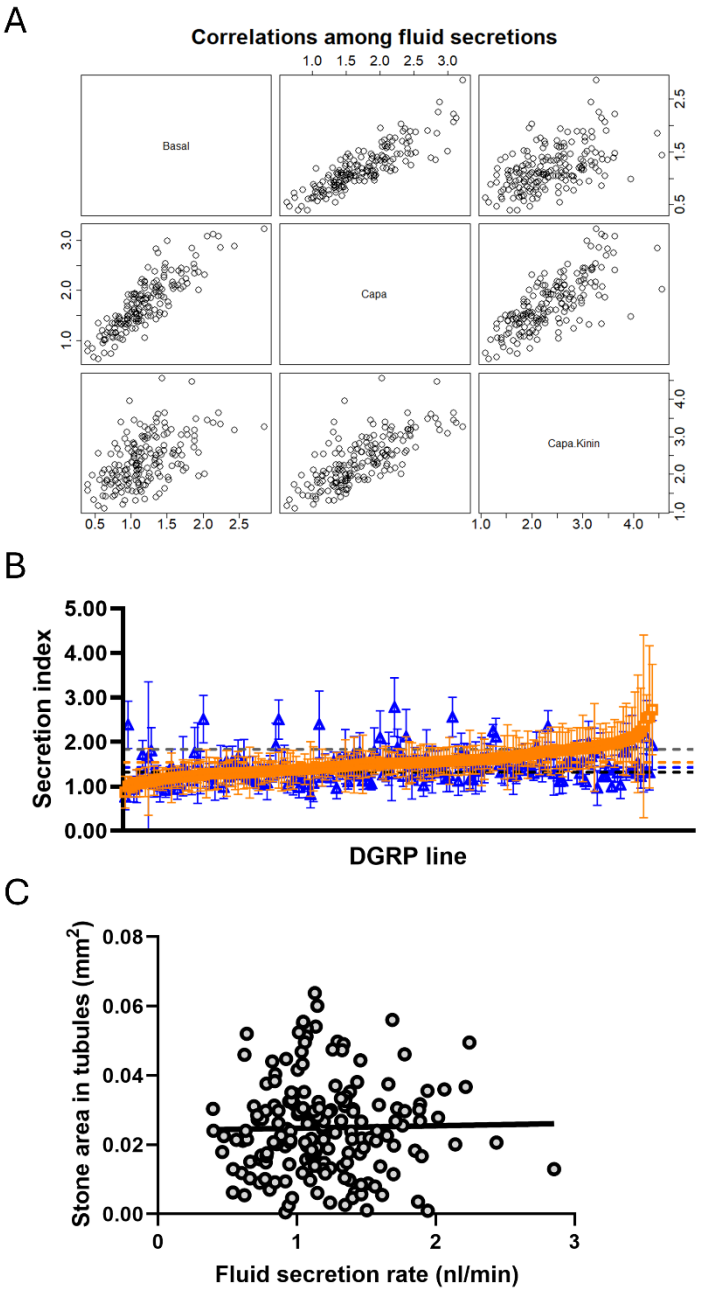

Figure 4.3 Natural variation in secretion rates.
(A) Correlation between basal, Capa- stimulated, and both Capa- and Kinin-stimulated secretion rates. (B) Capa- and Kinin-stimulated secretion indices in 183 DGRP lines. Error bars are SDs. (C) Correlation between the formation of crystals in renal tubule and the basal secretion rate in 180 DGRP lines (Pearson's $r = 0.0214, p = 0.7760$).

Table 4.1 Variance components of tubular secretion in the DGRP.

Traits	Groups	Variance	SD	H^2
Basal fluid secretion	Line	0.117686	0.34305	0.38
	Block	0.033146	0.18206	
	Residual	0.159271	0.39909	
Capa-stimulated secretion index	Line	0.057514	0.23982	0.22
	Residual	0.206716	0.45466	
Kinin-stimulated secretion index	Line	0.102521	0.32019	0.43
	Residual	0.137158	0.37035	

4.2.2 GWA analysis of variation in secretion rates

Single-markers association analyses were conducted to identify genetic loci associated with tubular transport in the DGRP genome, focusing on three quantitative traits: basal secretion rate, Capa-stimulated secretion index, and Kinin-stimulated secretion index. A major chromosomal inversion, In(2L)t, was found to covary with the basal fluid secretion rate (Table 4.2). No significant correlations were observed between *Wolbachia* infection or major chromosomal inversions and the neuropeptide-stimulated secretion indices. The block effect was found to be significantly related to the basal secretion rate and was thus included as a random effect in the linear mixed model to adjust the phenotype (Table 4.3). Given that the same dissected tubules were measured for all three secretion rates sequentially, the block effect did not show a significant covariation with the neuropeptide-stimulated secretion indices.

Table 4.2 Fixed effects of *Wolbachia* and major inversions on secretion-related traits (Type III ANOVA table with Satterthwaite's method).

Traits	Terms	NumDF	DenDF	F value	Pr(>F)
Basal secretion rate	*Wolbachia*	1	176.11	0.5698	0.4514
	In(2L)t	2	173.62	6.8987	0.0013*
	In(2R)NS	2	192.03	0.6086	0.5452
	In(3R)P	2	169.38	1.2942	0.2768
	In(3R)K	2	173.99	0.7757	0.4620
	In(3R)Mo	2	180.81	0.3093	0.7343
Capa-stimulated secretion index	*Wolbachia*	1	180.84	0.2491	0.6184
	In(2L)t	2	176.39	2.4685	0.0876
	In(2R)NS	2	215.06	1.5424	0.2162
	In(3R)P	2	167.89	1.1909	0.3065
	In(3R)K	2	175.14	0.4446	0.6418
	In(3R)Mo	2	165.21	0.4814	0.6188
Kinin-stimulated	*Wolbachia*	1	178.07	0.0946	0.7588

secretion index	In(2L)t	2	175.26	1.8537	0.1597
	In(2R)NS	2	196.28	1.5959	0.2053
	In(3R)P	2	170.97	1.6060	0.2037
	In(3R)K	2	175.94	1.2768	0.2815
	In(3R)Mo	2	174.95	0.0374	0.9633

Table 4.3 Random effects of block on secretion-related traits (ANOVA-like table for random-effects: single term deletions).

Traits	Terms	AIC	LRT	Pr(>Chisq)
Basal secretion rate	<none>	1940.6		
	Line	2364.3	425.67	< 2e-16*
	Block	1965.2	26.57	2.54e-07*
Capa-stimulated secretion index	<none>	2139.7		
	Line	2272.8	135.08	< 2e-16*
	Block	2137.8	0.02	0.8881
Kinin-stimulated secretion index	<none>	1641.0		
	Line	2034.2	395.19	< 2e-16*
	Block	1639.6	0.57	0.4496

Although few variants reached the Bonferroni-corrected significance threshold, a nominal p value of 10^{-5} was used to prioritise top polymorphisms. A total of 155 polymorphisms (Appendix 6), corresponding to 92 genes (Table 4.4), were identified in association with basal secretion (Figure 4.4A and Figure 4.5A). Additionally, 59 polymorphisms (Appendix 7) linked to 44 genes (Table 4.5) were associated with the Capa-stimulated secretion index, and 197 polymorphisms (Appendix 8) corresponding to 109 genes (Table 4.6) were associated with the Kinin-stimulated secretion index (Figure 4.4B and C and Figure 4.5B and C). A similar negative relationship between MAF and effect size was observed (Figure 4.6A), and most of the polymorphisms were found to be located within introns (Figure 4.6B).

Table 4.4 List of candidate genes associated with basal secretion rates.

Gene						
*kirre**	*CR44654*	*Spn28Da*	*pds5*	*trh*†	*dysc*	*Ace*
CR44833	*CG11178*	*Snoo*	*CG8321*	*MsR1*	*CG7656*	*jvl*
Ptp4E	*RpL37a*	*Sps2*	*Drep-1*	*shep*	*RhoGAP71E*	*Tm2*
l_1_G0148	*drd*	*CG5022*	*hts*	*corn*	*Pka-C3*	*Mur89F*
CG4095	*vap*	*CG17124*	*CR43430*	*CG43078*	*Abl*	*beat-IIb*
l_1_G0255	*chas*	*Pde1c*	*CG3216*	*CG34356*	*Baldspot*	*Dscam3*
*sdt**	*RunxA*	*CR44732*	*Sdc*	*ect*	*Galphaf*	*cpo*
CG1632	*Rbp9*	*dl*	*CG6758*	*CR44327*	*zetaCOP*	*fru*†
CG12125	*Mad*	*Dhc36C*	*CR45151*	*CG44837*	*CG33052*	*Tomosyn*

CG32712	*CG12400*	*unpg*	*CG3045*	*byn*†	*CG33051*	*Spn28Db*
org-1	*Hsp60C*	*CG8027*	*inaD*	*CG5883*	*CG7630*	*Prip*†
CG42339	*Wnt10*	*CR45309*	*PIP5K59B*	*CrzR*	*Indy*	*CG13579*
CG2540	*ninaC*	*brp*	*CG5549*	*Ncc69**†	*Teh1*	*sowah*
Glut4EF						

Note: * indicates detailed discussion later; † denotes prior description in fly tubules.

Table 4.5 List of candidate genes associated with Capa-stimulated secretion index.

Gene						
bi	*Dyrk2*	*lola*	*CG32333*	*CG32085*	*trn*	*CG9451*
CR32773	*CadN*	*fas*†	*CG43292*	*CG11652*	*CG32206*	*CR44932*
CG17646	*CR44916*	*GEFmeso*	*Pdp1*	*CG6053*	*pncr009:3L*	*jvl*
Elp3	*jing*	*Sik3*	*CG34356*	*CG17154*	*brv1*	*smp-30*
morgue	*CR43724*	*Fili*	*dpr6*	*CG4300*	*CG32212*	*Vha100-2*†
CG14275	*CR45309*	*nahoda*	*rt*	*Pbgs*	*CG9449*	*CG44009*
Mekk1	*CG42613*					

Note: † denotes prior description in fly tubules.

Table 4.6 List of candidate genes associated with Kinin-stimulated secretion index.

Gene						
CG4586	*CG33671*	*Spn*	*CG7275*	*Task6*	*Su_z_12*	*jvl*
CG3040	*Iswi*	*sif*	*CG13455*	*hdc*	*CG7433*	*CG7362*
hdm	*hts*	*Vap-33B*	*CG7272*	*Abi*	*Clc*	*nsl1*
Ykt6	*CR43430*	*Rcc1*	*CG7857*	*Kif19A*	*CG6951*	*Ubx*
snz	*bl*	*CG33993*	*CG7841*	*Pde6**†	*CR43888*	*CR44256*
fs_1_h	*CG15653*	*LanA*	*Z600*	*Rbp6*	*CG14567*	*CG5873*
Tomosyn	*mRpL54*	*ltl*	*gdl-ORF39*	*Eip74EF*	*CG12163*	*Dscam3*
CR45059	*cpa*	*CG8177*	*gdl*	*Indy*	*CG33293*	*Vha13*
CR44113	*Cht8*	*CR44543*	*fwe*	*CG32204*	*alpha-Est3*	*subdued*†
CG15431	*CG4554*	*CG32085*	*SsRbeta*	*pip*	*alpha-Est4*	*RASSF8*
CG9109	*px*	*rols*	*Pgm*	*CG32206*	*pyd*	*Lgr3*
eya	*CG44252*	*CG6793*	*CG30355*	*CG3376*	*Glut4EF*	*CG1646*
CG5604	*Pde8*	*tRNA:S2b:88A*	*Cpr47Ed*	*CG12091*	*CG34242*	*stops*
dac	*CG9850*	*snoRNA:291*	*CG33672*	*CG12090*	*Ent3*	*Doa*
CG12780	*cN-IIIB*	*Gycbeta100B*	*sima*	*dlp*	*RecQ5*	*CG7276*
Acsl	*ocm*	*Tsf2*	*CG43638*			

Note: * indicates detailed discussion later; † denotes prior description in fly tubules.

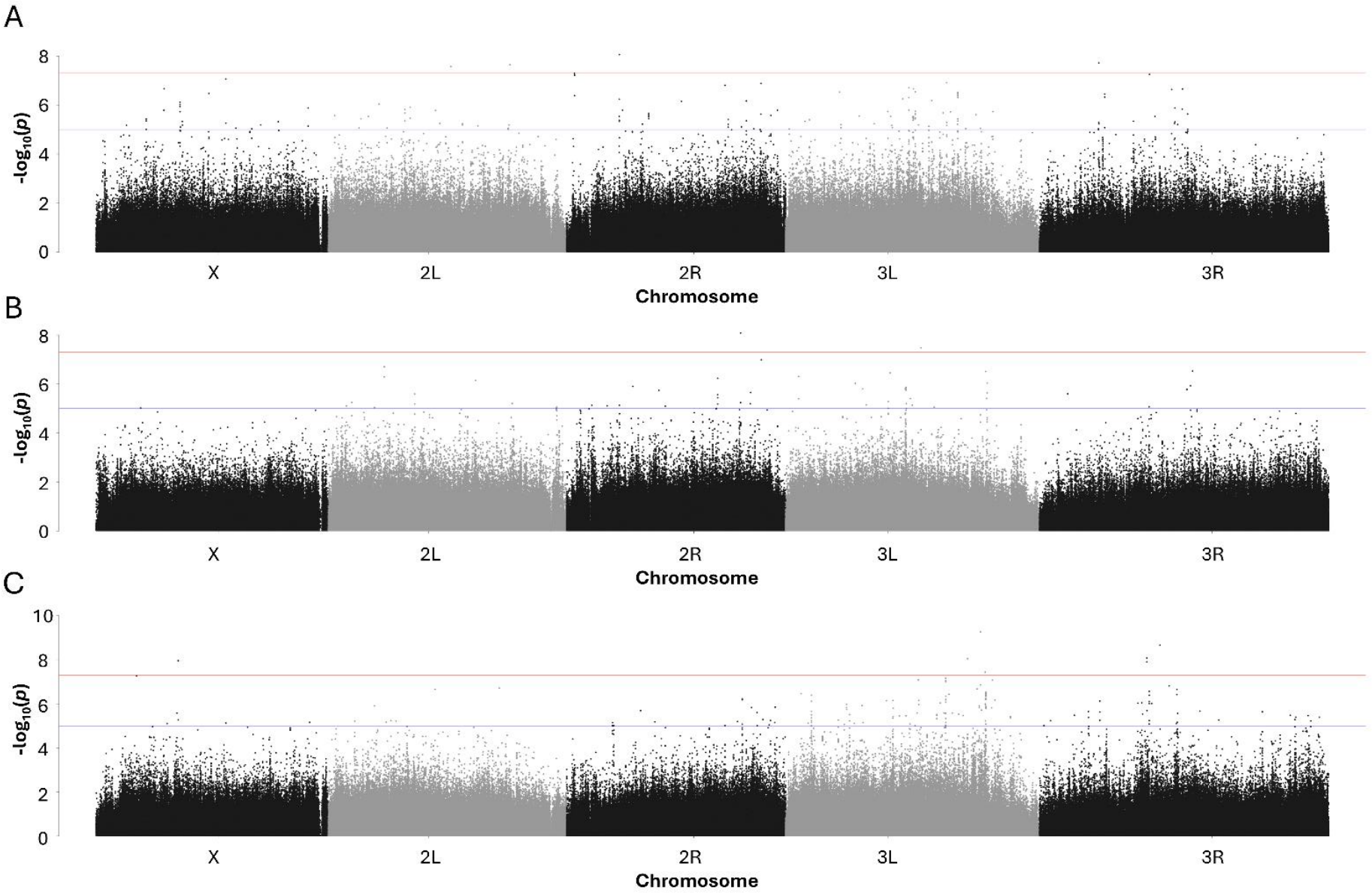
A
B
C
-log10(p)
0
2
4
6
8
10
X
2L
2R
3L
3R
Chromosome

Figure 4.4 Manhattan plots for the three GWA analyses.
(A) Basal secretion rate. (B) Capa-stimulated secretion index. (C) Kinin-stimulated secretion index. The blue line represents the suggestive association threshold where $\boldsymbol{p}$ value is $\mathbf{10^{-5}}$, while the red line indicates the Bonferroni-adjusted threshold where $\boldsymbol{p}$ value is $\mathbf{5 \times 10^{-8}}$.

To assess the biological processes that may contribute to the variation in basal secretion, genes interacting with the identified candidate genes were extracted (Figure 4.7A). Functional enrichment analysis of the clustered interaction networks revealed that the second-largest cluster was associated with biological processes, including the electron transport chain, aerobic respiration, and mitochondrial ATP synthesis (Figure 4.7B). Mitochondria, located in microvilli, generate ATP to fuel V-ATPases (Beyenbach, 2003). The presence of bafilomycin, an inhibitor of V-ATPases, abolishes *Drosophila* tubular secretion (Dow et al., 1994). In the mammalian nephron, the proximal tubule is particularly vulnerable to mitochondrial toxicity (Hall et al., 2009).

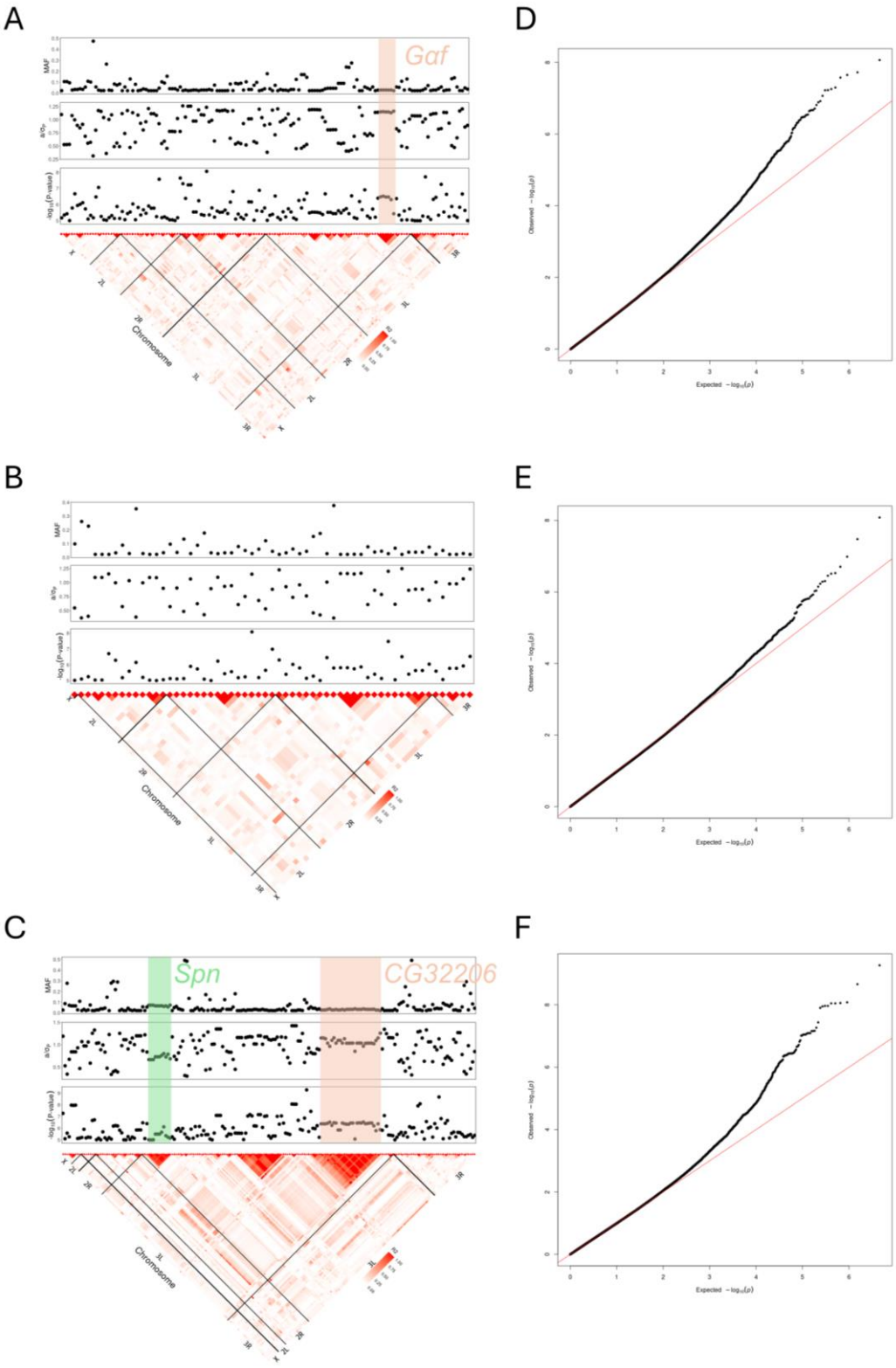

Figure 4.5 Genome-wide association between polymorphisms in the DGRP and variation in tubular secretion.
All polymorphisms from single-marker analyses with $p < 10^{-5}$ are shown for basal secretion rate (A), Capa-stimulated secretion index (B), and Kinin-stimulated secretion index (C). Top: the MAF, the effect size in phenotypic SD units ($\mathbf{a}/\boldsymbol{\sigma}\mathbf{P}$), and the

significance of each polymorphism ($-\boldsymbol{log10p}$). Bottom: pairwise linkage disequilibrium among significant polymorphisms, measured by $\boldsymbol{r^2}$, with the five major chromosome arms demarcated by black lines. (D), (E), and (F) QQ plots of genome-wide $\boldsymbol{p}$ values ($-\boldsymbol{log10p}$) for basal secretion rate, Capa-stimulated secretion index, and Kinin-stimulated secretion index, respectively.

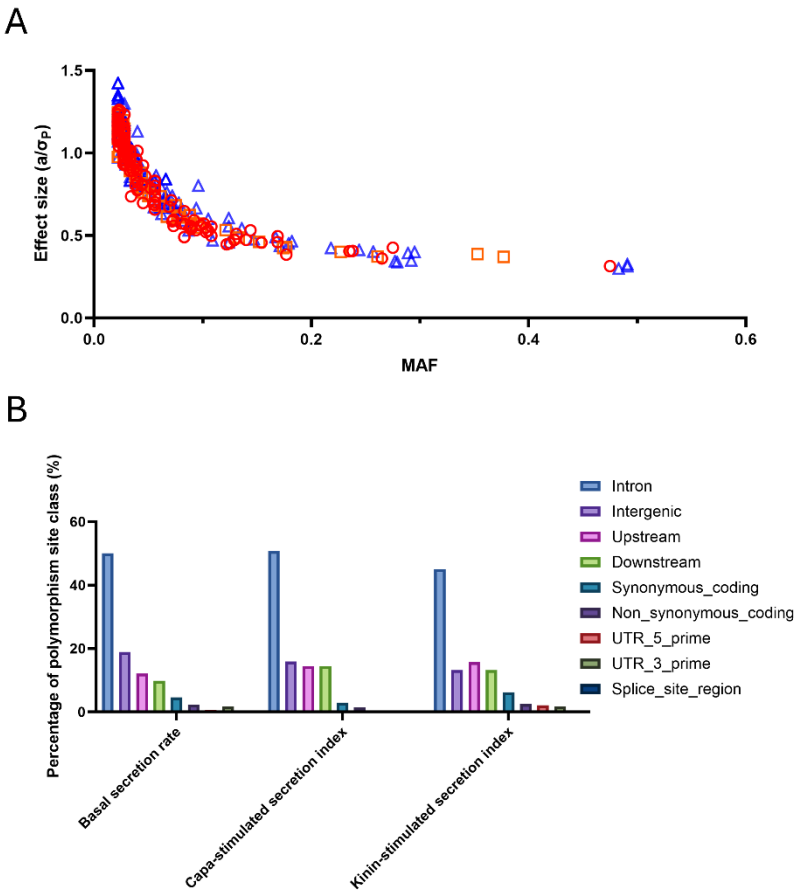

Figure 4.6 Top candidate polymorphisms for tubular secretion.
(A) The relationships between effect size and MAF, with red, orange, and blue representing polymorphisms identified in the analysis of basal secretion rate, Capa-stimulated secretion index, and Kinin-stimulated secretion index, respectively. (B) The percentage of polymorphisms categorized by site class.

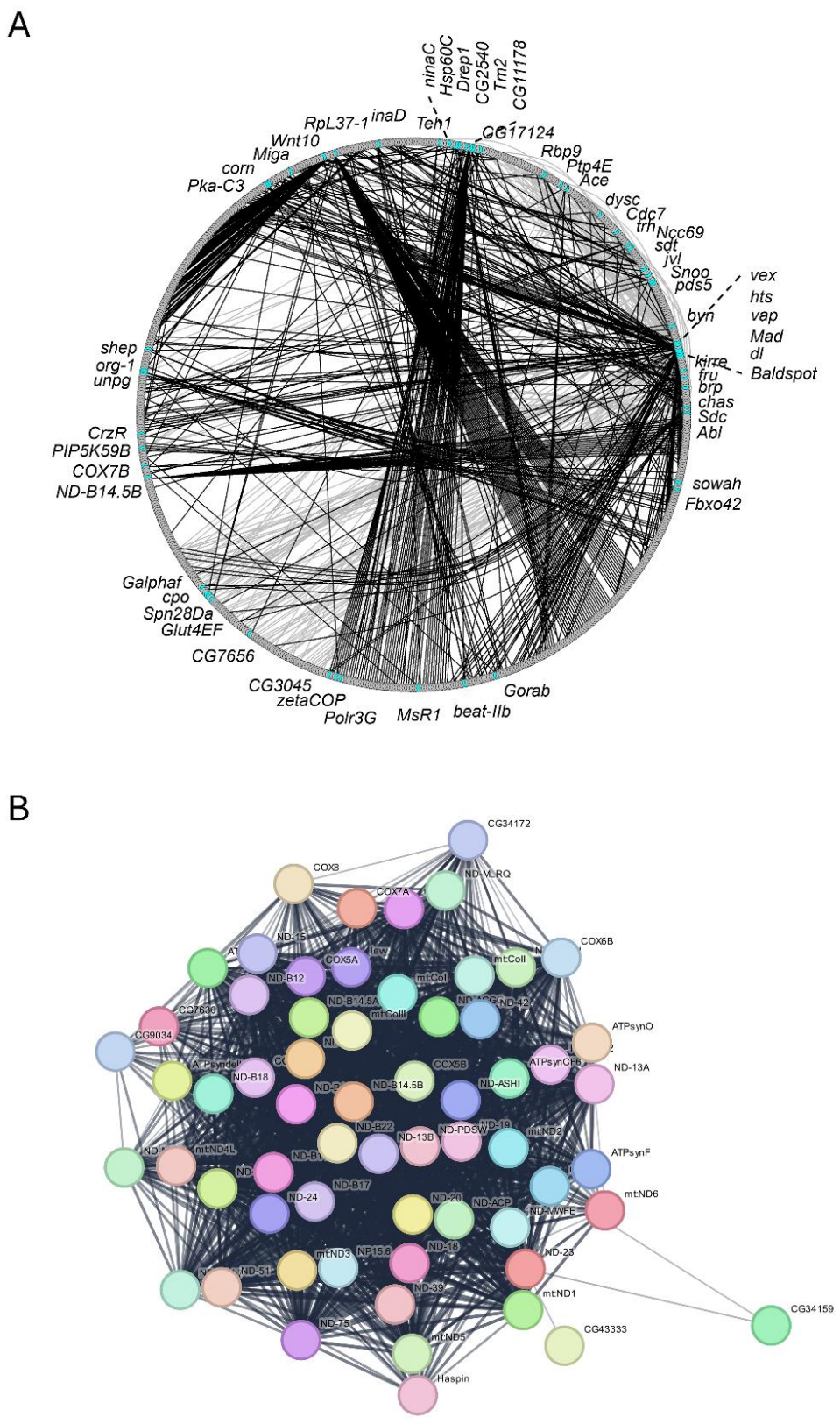

Figure 4.7 Gene interaction network including candidate genes.
(A) Interactions between candidates identified in the basal secretion analysis (cyan dots) and their genetically (grey line) and physically (black line) interacting genes (grey dots). (B) The second largest clustered network of these interactions.

4.2.3 Functional verification of candidate genes

4.2.3.1 Candidates revealed by analysis of basal secretion rate

Thirteen candidates identified in the association study of basal secretion rate were selected based on their expression level in tubules and the availability of RNAi lines for functional verification. According to their expression patterns as shown by FlyAtlas (Leader et al., 2018) and FlyCellAtlas (Li et al., 2022, Xu et al., 2022), the corresponding *Gal4* drivers were used (Appendix 9). Six of these candidates significantly affected baseline secretion rates (Figure 4.8). Inhibition of *Gaf*, *Glut4EF*, *sdt*, and *sowah* resulted in impaired basal secretion, whereas loss of *CG7656* and *RhoGAP71E* led to elevated secretion rates.

Although no correlation was found between basal secretion rate and the development of renal crystals in the DGRP (Figure 4.3C), the formation of crystals was assessed in RNAi flies targeting candidates identified from the secretion analysis. Inhibition of *sowah*, *CG8027*, and *Gaf* significantly altered the amount of crystal in the renal tubules (Figure 4.9). Interestingly, loss of *Gaf* or *sowah* resulted in reduced basal secretion, and more crystals were formed in the knockdown tubules under lithogenic conditions, suggesting a potential link between reduced tubular secretion and increased susceptibility to tubulolithiasis.

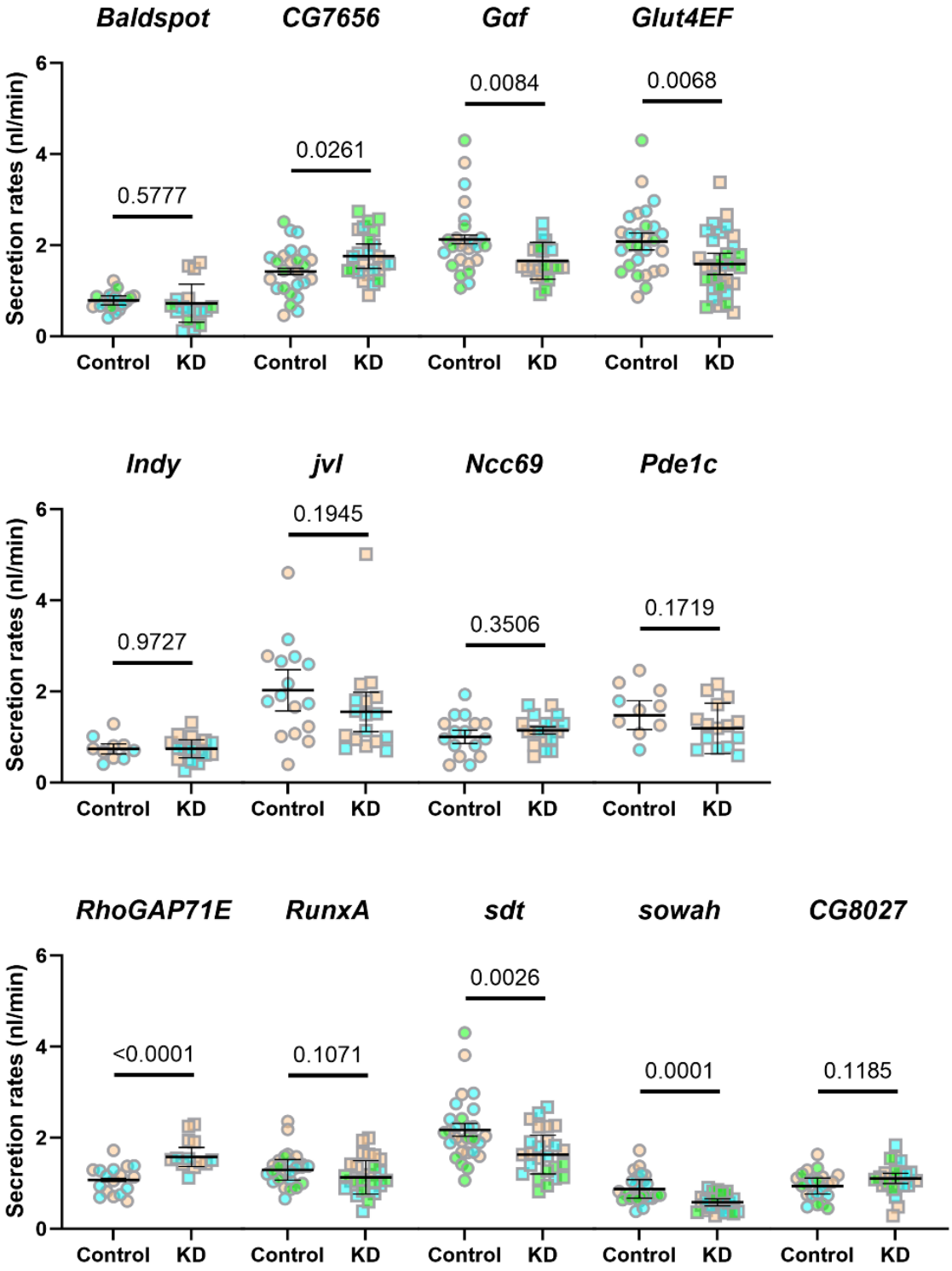

Figure 4.8 Validation of candidate genes identified from the analysis of basal secretion rate.
Candidate genes were investigated by using RNAi-mediated knockdown. Thirteen RNAi lines were tested for basal secretion rate along with their corresponding controls. The means of biological replicates and SDs are plotted, with each colour representing a

different replicate (two to three biological replicates). Linear mixed models were used to assess the effect of genotype on the secretion rate.

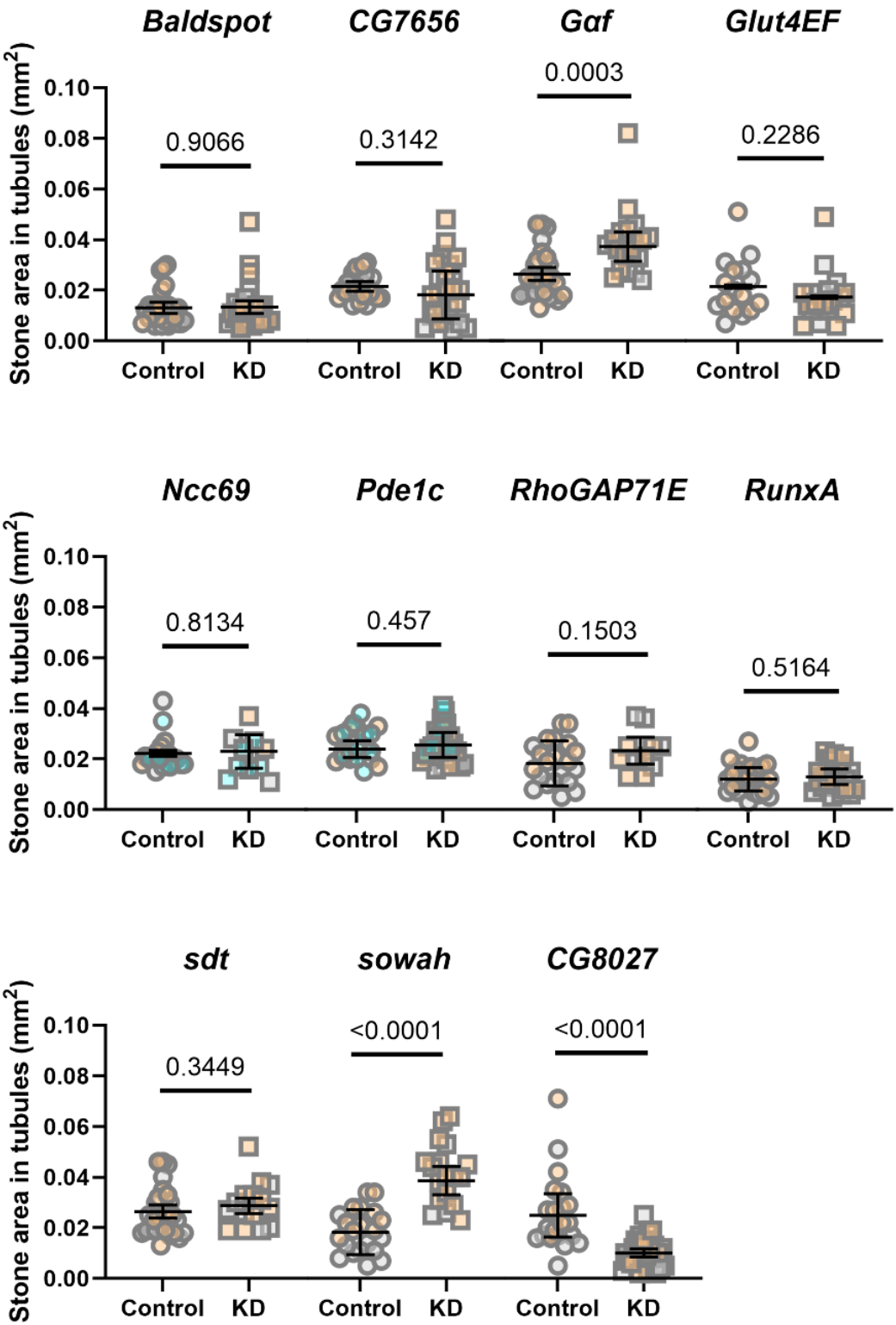

Figure 4.9 Development of renal crystals in flies.
Stone formation was quantified in RNAi flies targeting candidate genes. The means of biological replicates and SDs are plotted, and each colour stands for a different

replicate (two to three biological replicates). Linear mixed models were used to determine the effect of genotype on crystal formation.

4.2.3.2 Candidates revealed by analysis of neuropeptides-stimulated secretion indices

Neuropeptide-stimulated secretion was also investigated in RNAi lines targeting the corresponding candidates, providing insights into the neuroendocrine regulation of tubular secretion. There were five candidate genes selected from the list revealed by the association analysis of the Capa-stimulated secretion index and nine genes from that of the Kinin-stimulated secretion index for functional verification. For candidates associated with the Capa-stimulated secretion index, silencing any of these genes did not affect the fold change in secretion rates upon Capa treatment (Figure 4.10A). In contrast, inhibition of two of the nine genes significantly altered the Kinin-response index (Figure 4.10B). *Pde6* is expressed in both PCs and SCs, as shown by FlyCellAtlas. It has been shown to localise to the apical membrane and modulate tubule cGMP levels in PCs (Day et al., 2006). Overexpression of *Pde6* inhibits cGMP transport across the tubule, whereas inhibition of *Pde6* improves the transport. This modulation acts through cGMP-dependent protein kinase, contributing to epithelial fluid transport (Ruka et al., 2013). Interestingly, inhibition of *Pde6* in PCs resulted in an increased Kinin-stimulated secretion index. However, this non-cell-autonomous mechanism requires further investigation. Knockdown of *CG32206*, a gene with an uncharacterised function, impaired the Kinin-dependent response.

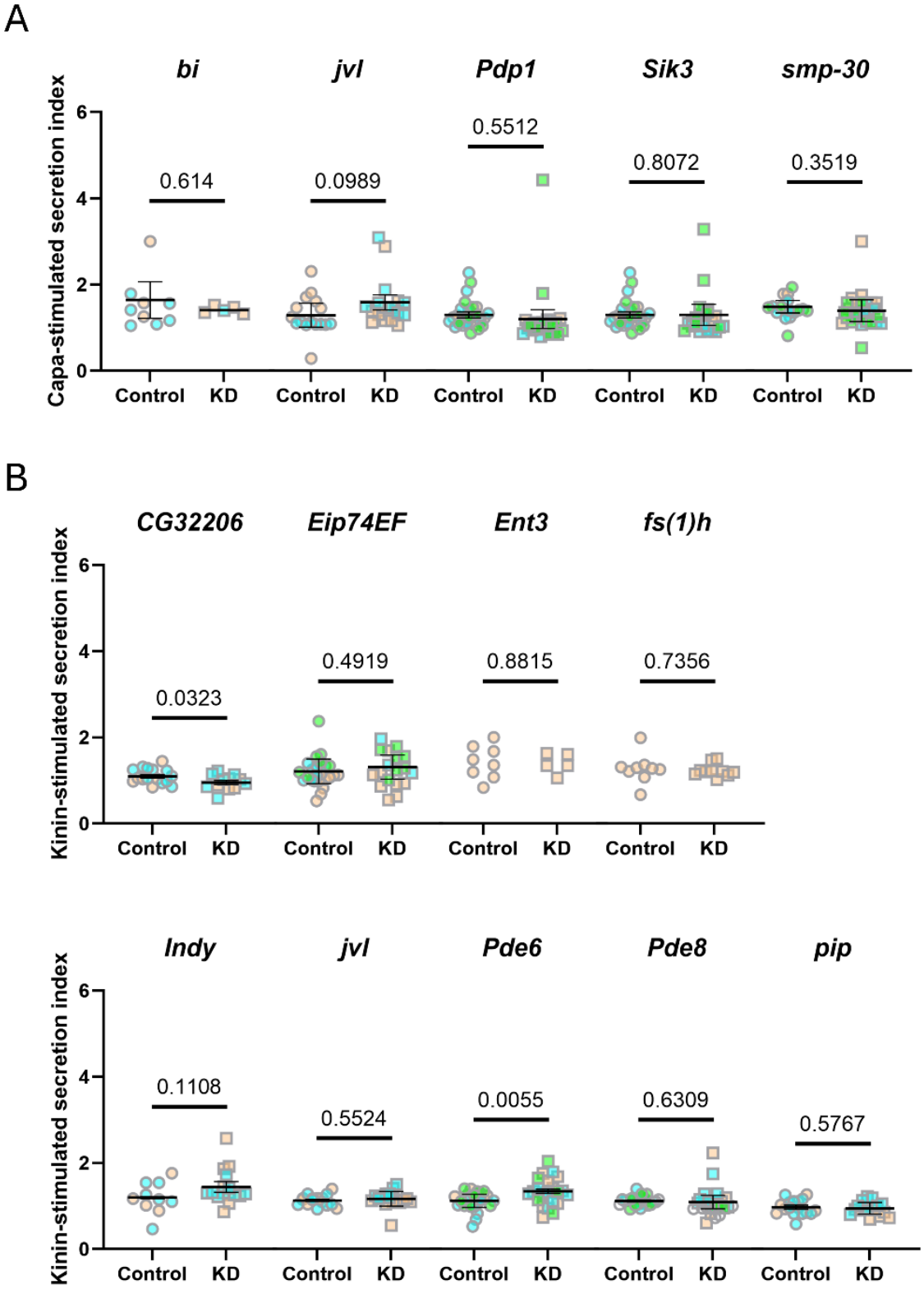

Figure 4.10 Validation of candidate genes identified by analysis of neuropeptide-stimulated secretion indices.
Fourteen RNAi lines were tested for neuropeptide-stimulated secretion rates along with their corresponding controls. (A) Candidates revealed by analysis of Capa-stimulated secretion index. (B) Candidates revealed by analysis of Kinin-stimulated secretion index.

The means and SDs of each biological replicate and are plotted, and each colour stands for a different replicate (up to three biological replicates).

4.3 Discussion

4.3.1 Tubular transport in *Drosophila* and humans

The kidneys play a crucial in excreting metabolic waste products and xenobiotics from the bloodstream (George et al., 2017). The primary mechanisms involved in this elimination process include glomerular filtration and tubular secretion. Molecules smaller than 65 kDa are often filtered through the glomerulus, while large or charged chemicals are usually cleared from the circulation by transporter-mediated renal secretion (George et al., 2017). Members of the solute carrier drug transporter family, such as the OATs and OCTs (Duranton et al., 2012, Wikoff et al., 2011, Ren et al., 2015) in the proximal tubule, are responsible for transporting these large or charged substrates. Renal clearance of endogenous markers and medications in the proximal tubules has been shown to exhibit significant intraindividual and interindividual variation (Rivara et al., 2017, Yin et al., 2006, Leabman and Giacomini, 2003). More than two-thirds of urate, a potent antioxidant in serum, is excreted by the kidneys (Bobulescu and Moe, 2012). GWA studies have identified eight transporter-coding genes implicated in the serum urate level (Anzai et al., 2012). Among them, a rare allele of rs6855911 in *GLUT9* has been linked to a reduced serum uric acid level in a Sardinian population (Li et al., 2007). *GLUT9* was first identified as a glucose transporter (Augustin et al., 2004) and later found to exhibit a substrate preference for urate over glucose (Shen et al., 2024), and it is involved in the efflux of urate towards the bloodstream (Anzai et al., 2008).

Additionally, uromodulin, the most abundant urinary protein under physiological conditions, is primarily produced by epithelial cells in the TAL of the loop of Henle and secreted into the lumen through a conserved proteolytic cleavage (Devuyst et al., 2017, Brunati et al., 2015). A meta-analysis of GWA studies for urinary levels of uromodulin indexed to creatinine has identified two genome-wide significant signals, *UMOD-PDILT* and *WDR72* (Joseph et al., 2022).

Associations between low clearance of secretory solutes due to tubulointerstitial fibrosis and the progression of renal function (Garimella et al., 2022, Suchy-Dicey et al., 2016, Chen et al., 2020) suggest that understanding molecular mechanisms of tubular transport may offer potential therapeutic candidates for renal dysfunction.

Due to the large surface-to-volume ratio (O'Donnell, 2022, Dow, 2009), terrestrial insects face consistent osmotic stress. Notably, *Drosophila* (Dow et al., 1994) and *Rhodnius* (Maddrell, 1991) exhibit the fastest secretion rates on a per-cell volume basis of any epithelia ever tested. Additionally, the abundance of solute transporters in the Malpighian tubules, highlighted by microarray (Wang et al., 2004) and RNA-sequencing datasets (Chintapalli et al., 2007, Leader et al., 2018), suggests that the tubule has important excretory functions in addition to osmoregulation. Many ion or solute transporters and channels, as well as surface receptors, described in *Drosophila* MTs, are functionally equivalent to proteins in mammalian nephrons (Dow et al., 2022). These highlight that *Drosophila* MTs provide an excellent model for studying epithelial transport.

4.3.2 Quantitative genetics

During the measurement of fluid secretion rates, Canton S was used as a positive control, with 183 DGRP lines randomly allocated to different blocks to monitor environmental fluctuations. A similar and moderate coefficient of variation was observed for stone formation (20%) and basal secretion rate (23%) in the Canton S strain, signifying low relative variability, or less fluctuation. Basal fluid secretion rates were measured across the 183 DGRP lines, yielding an average secretion rate of 1.19 nl/min, approximately twice that of Canton S. In addition to baseline secretion, the secretion rates stimulated by neuropeptides were also quantified. Significant phenotypic variation was observed across all three phenotypes, corresponding to two key traits: baseline secretion and neuroendocrine-stimulated secretion. Positive associations were observed between each pair of secretion rates, which may be attributed to the stimulating effects of the two neuropeptides and the fact that the same tubule

pair was continuously quantified for all three phenotypes. The difference between extreme lines for baseline secretion was greater than 6-fold, with a maximum secretion rate of 2.85 nl/min. Although low urine volume is a known risk factor for kidney stone disease, no correlation was observed between renal crystal formation and basal fluid secretion rates, likely due to the distinct diets in the assays.

The total phenotypic variation was partitioned using a linear mixed model, accounting for both line and block effects. Both were significantly associated with basal secretion rates, while only line effects were significantly associated with the secretion indices. This may be attributed to the use of the same tubule pair for the measurement of all three secretion phenotypes. Although block effects may contribute to the variation in secretion rates, they are accounted for and neutralized when calculating the secretion index. A large variance explained by residuals may imply high micro-environmental plasticity, i.e., individuals with the same genotype reared under common macro-environmental conditions do not have the same phenotype for quantitative traits (Morgante et al., 2015). Both stochastic or technical sources of variance and genetic components may produce such phenotypic differences (Lin et al., 2016). The Malpighian tubules serve as a major excretory organ, important for *Drosophila* to adapt to diverse environments. Alternatively, other factors, such as room temperature fluctuations or potential damage caused during dissections, that could not be accounted for might also contribute to this large residual variance. Relatively low heritability in the secretion traits indicated that factors other than genetics explain a large portion of the phenotypic variance. Additionally, one of the major chromosomal inversions, In(2L)t, was significantly associated with basal secretion rate. A particularly high level of chromosome differentiation, including chromosomal inversions, has been recorded in *Anopheles gambiae* (Coluzzi et al., 1985). The frequency of inversion 2Lα increases with the degree of aridity (Fouet et al., 2012), and this inversion has been linked to enhanced desiccation resistance in *Anopheles* (Gray et al., 2009). A similar frequency cline has been observed for the *Drosophila* inversion In(2L)t, with less than 10% in temperate climates and 40-60% in tropical populations

(Andolfatto et al., 1999), suggesting that the inversion In(2L)t could be an adaptive polymorphism.

4.3.3 Candidate genes

Association analyses identified 92, 44, and 109 candidate genes for basal secretion rate, Capa response index, and Kinin response index, respectively. Several mammalian orthologues of candidate genes have been implicated in renal function or kidney diseases. NEPH2, the orthologue of *Drosophila* kirre, functions to maintain the glomerular slit diaphragm (Gerke et al., 2005), and the loss of *zNeph2* results in leakiness of the glomerular filtration barrier (Neumann-Haefelin et al., 2010). Additionally, reduced urinary volume has been observed in *Nkcc1*-null mice (Wall et al., 2006), consistent with the study of its *Drosophila* orthologue (Rodan et al., 2012). A polymorphism in *PDE1A*, which is the human orthologue of *Drosophila Pde1c*, has been implicated in the development of nephrolithiasis and renal cystic disease (Yang et al., 2017), and apical NaDC1 immunolabeling in the proximal tubule suggests its essential role in tubular transport (Lee et al., 2017). Besides, the human orthologues of five candidate genes for basal fluid secretion (*Prip*, *GlyT*, *trh*, *Ncc69*, and *Indy*) are enriched in the kidney compared to 26 other tissues.

A subset of the candidate genes was selected for testing their function in renal secretion. Inhibition of *Gaf*, *Glut4EF*, *sdt*, and *sowah* showed impaired basal secretion, while loss of *CG7656* and *RhoGAP71E* resulted in elevated secretion rates. Stardust proteins, encoded by the *sdt* gene, colocalise with Crumbs to maintain cell polarity (Bachmann et al., 2001). This gene is predominantly expressed in PCs and SCs in renal tubules but not in RSCs. Its human orthologue, *PALS1*, is also highly expressed in all nephron segments composed of polarized cells (Berghaus et al., 2022). Mice lacking one copy of *Pals1* in nephrons developed a fully penetrant phenotype (Weide et al., 2017), and this can partially be explained by a reduction in mRNA/protein expression of nephron-specific transporters from the solute carrier gene family. The human orthologue of *sowah*, *SOWAHB*, is enriched in the distal convoluted tubule, while its

function is largely unknown. Moreover, a study has shown that *Ncc69* mutant tubules have decreased rates of fluid secretion and K^+ flux, and these defects can be rescued by the expression of wild-type *Ncc69* in PCs (Rodan et al., 2012). However, knocking down *Ncc69* in SCs, a gene specifically expressed in SCs according to FlyCellAtlas, did not affect fluid secretion rates in our study. This lack of effect may be due to insufficient RNAi knockdown efficiency compared to the complete loss of function resulting from a mutation or potential off-target effects (Ma et al., 2006), as gene expression was not quantified by qRT-PCR. Additionally, the discrepancy may arise from differences in experimental protocols, as fluid secretion rates were monitored over a longer period (2 h) in the study, in contrast to the short duration (30 min) in our study. This finding is supported by the observation that Capa-1 exhibits an antidiuretic effect in one study (Rodan et al., 2012), whereas it shows diuretic effects in others (Kean et al., 2002, Pollock et al., 2004).

Although no correlation was found between stone areas after NaOx feeding and basal secretion rates in the DGRP, loss of *Gaf* or *sowah* led to reduced basal secretion, and more crystals were formed in the knockdown tubules, suggesting potential links between reduced tubular secretion and the susceptibility to tubulolithiasis. Neuropeptide-stimulated secretion was also examined in RNAi lines targeting candidates. For example, inhibition of *Pde6* increased the Kinin-stimulated secretion index. Pde6 has been shown to modulate the tubule content of cGMP (Day et al., 2006), and cGMP, acting through cGMP-dependent protein kinase, contributes to epithelial fluid transport (Ruka et al., 2013). Additionally, biological processes, such as electron transport chain, aerobic respiration, and mitochondrial ATP synthesis, were associated with the clustered interaction networks by functional enrichment analysis.

This chapter highlights considerable natural variation in fluid secretion rates among wild-type DGRP lines under both resting and stimulated conditions. Notably, some of the significant genes have orthologues that impact human renal function or are enriched in the kidney, suggesting that some of the other hits may also be useful leads in understanding mammalian renal function.

Chapter 5 The Cell Adhesion Molecule *Fasciclin 3* is Required for the Epithelial Function of Malpighian Tubules in *Drosophila*

5.1 Summary

A pilot GWA study identified *Fasciclin 3* (*Fas3*), a candidate gene encoding a neural cell adhesion molecule, which is associated with variation in basal secretion rate. The function of this gene in renal tubules was studied. Since there are two major cell types in the tubule, primary cells and secondary cells, *Fas3* was knocked down in each of these cell types. Knockdown of *Fas3* in principal cells resulted in enlarged abdomens, lower fluid secretion rates, and increased body water content, all of which are consistent with prolonged desiccation survival. Furthermore, the absence of *Fas3* resulted in the formation of kidney stones and the proliferation of renal stem cells. In *Fas3* RNAi flies, staining for the septate junction protein Discs large was also compromised. Due to the loss of cytoarchitectural organisation, *Fas3* inhibition in stellate cells altered both the number and morphology of stellate cells in an age-related manner. Tubules with impaired stellate cells failed to secrete at a high rate in response to stimulation by the neuropeptide Kinin. These findings suggest that *Fas3* is necessary for normal renal epithelial function.

5.2 Results

5.2.1 Identification of *Fas3*

A pilot GWA study was conducted to identify candidate genes associated with tubular transport. Secretion rates were measured in Canton S and 30 DGRP lines. Although the fluid secretion rates of Canton S differed across the blocks, a larger variation was observed among the DGRP lines (Figure 5.1). This observation suggested that the genetic backgrounds might also contribute to the variation in

fluid secretion rates. After adjusting for the block effect, the basal secretion rates from the 30 DGRP lines were submitted to the DGRP analysis pipeline (http://dgrp.gnets.ncsu.edu/) for the pilot GWA analysis.

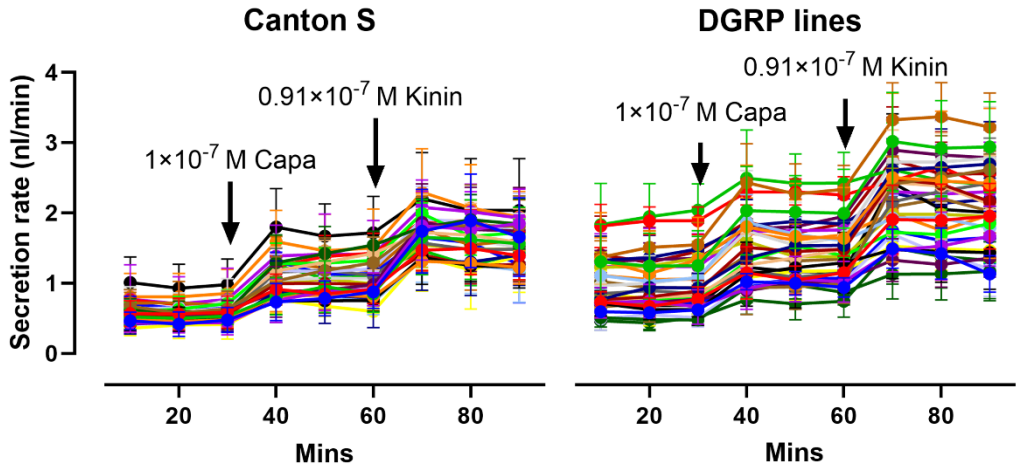

Figure 5.1 Fluid secretion rates among 30 DGRP lines.
Fluid secretion rates were measured in 30 DGRP lines across different blocks along with Canton S, which was used as a control. Each colour represents one individual block/day. Fluid secretion rates of the DGRP lines were shown on the right and that of Canton S on the left. Baseline secretion rates were measured for 30 min, followed by the measurement of neuropeptide-stimulated secretion rates. Data are presented as means with SDs.

Markers on the left arm of the second chromosome, along with their p values, were plotted on a Manhattan plot (Figure 5.2A). Six polymorphisms were significantly associated with the variation in basal secretion, as indicated by the pilot GWA study, with one reaching the Bonferroni-corrected threshold. According to the UCSC Genome Browser (version BDGP R5/dm3), the marker 2L_18381757_SNP is in the first intron of the *Fas3* gene (Figure 5.2B). Intronic SNPs can affect RNA processing, stability, and translation (Jacobsson et al., 2012) or maybe in linkage disequilibrium with causal loci. Since this SNP is in the *Fas3* gene region, the function of *Fas3* was further investigated. *Fas3* is widely expressed across different fly tissues, as indicated by FlyAtlas. In neurons, *Fas3* knockdown results in the death of olfactory circuit neurons, characterised by activated apoptotic cell death (Vaikakkara Chithran et al., 2024).

Based on the availability of RNAi lines against *Fas3* and previously verified on-target effects, the loss-of-function approach was employed to study its function in MTs. According to FlyCellAtlas (Xu et al., 2022, Li et al., 2022), *Fas3* is highly expressed in both PCs and SCs (Figure 5.3). We used *c724-Gal4; CapaR-Gal4* to inhibit *Fas3* expression in both PCs and SCs. Although the knockdown efficiency of *Fas3* was not quantified by qRT-PCR, the RNAi line targeting *Fas3* has been previously validated in another study, which reported a significant reduction in *Fas3* expression (Zhang et al., 2018). Knockdown flies exhibited enlarged abdomens in both males and females (Figure 5.4A), particularly in older flies or those reared at a higher temperature (data not shown). Interestingly, previous studies from our group have shown that flies with impaired tubular function, specifically those with dysfunctional fluid secretion in MTs, develop edema (Cabrero et al., 2014). To investigate whether this might be due to water accumulation in the body, we measured the wet and dry weights of the flies. The results showed that the wet weight of *Fas3* RNAi flies was higher than that of the controls. Still, this difference was not due to variations in the amount of organic and inorganic material, as no difference in dry weight was observed (Figure 5.4B). These findings suggest that *Fas3* knockdown flies contain more water, indicating that tubular transport may be impaired in these flies.

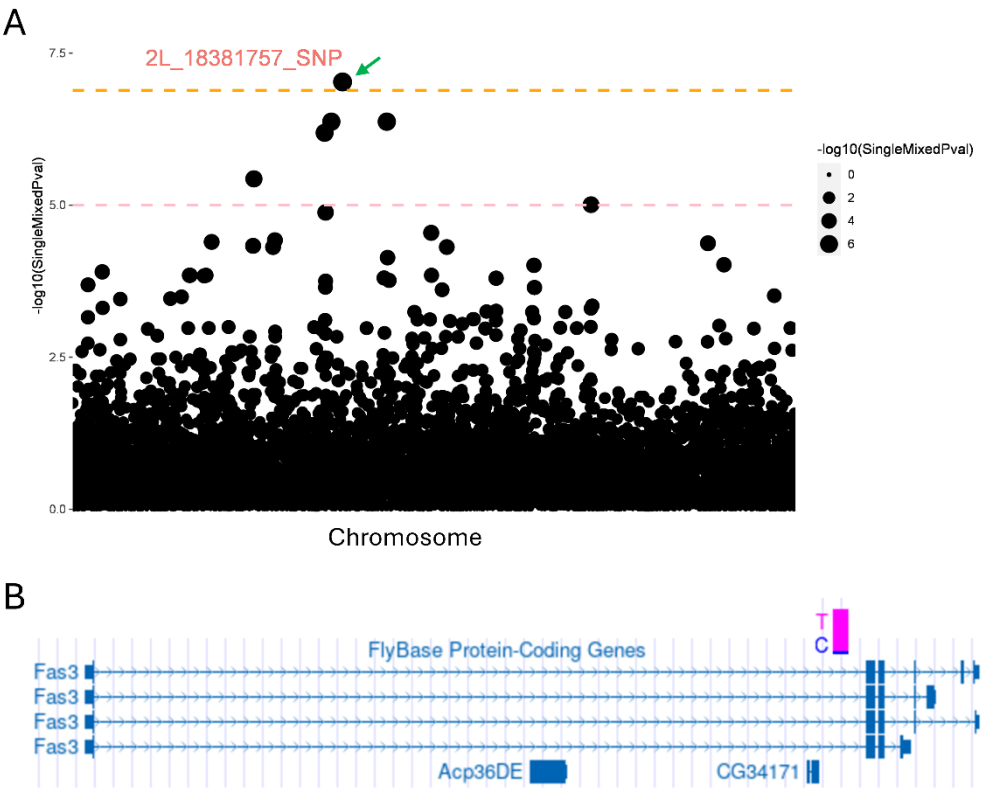

Figure 5.2 Association analysis results for markers on the second chromosome. (A) The Manhattan plot shows that the marker 2L_18381757_SNP is the most significant, with the pink dashed line representing the suggestive threshold and the orange dashed line indicating the Bonferroni-corrected threshold. X-axis represents the genomic location of SNPs on the chromosome 2L. Y-axis represents the significance of the association ($-\boldsymbol{log10p}$). (B) UCSC Genome Browser track of the marker 2L_18381757_SNP, which is in the first intron of the *Fas3* gene (genome.ucsc.edu). Four

Fas3 transcript variants is presented with dark boxes representing exons. The major allele T is in magenta, and the minor allele C in blue.

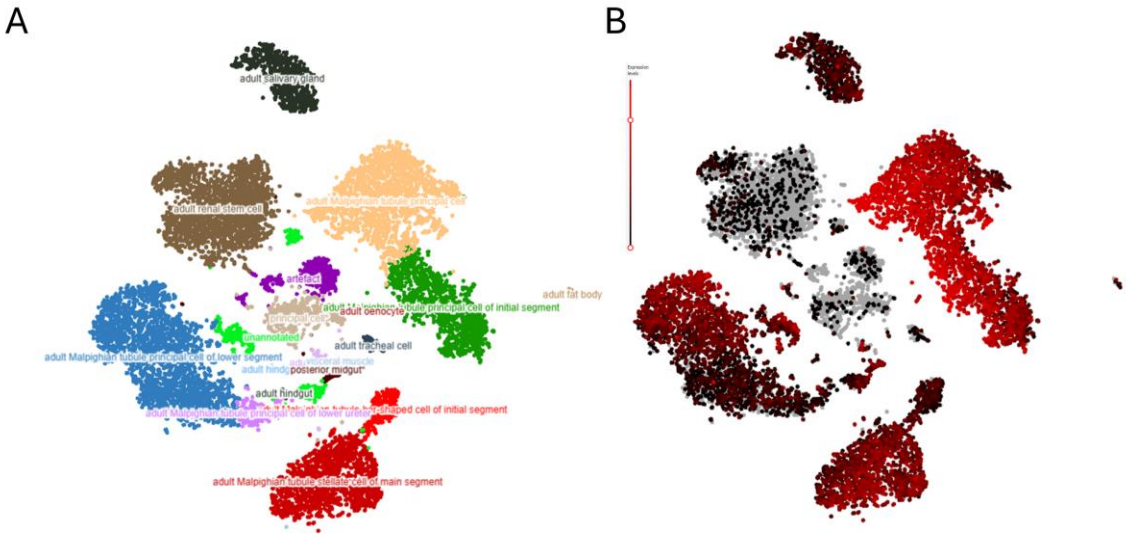

Figure 5.3 Expression pattern of *Fas3* in the Malpighian tubule.
(A) Cell type annotation in the adult fly kidney with 13,774 cells, as shown by t-SNE plot from the *Stringent* 10x dateset (scope.aertslab.org). (B) SCope representation of the

single cell data for *Fas3*. The intensity is proportional to the log-normalised expression levels. Each dot represents a single nucleus or cell.

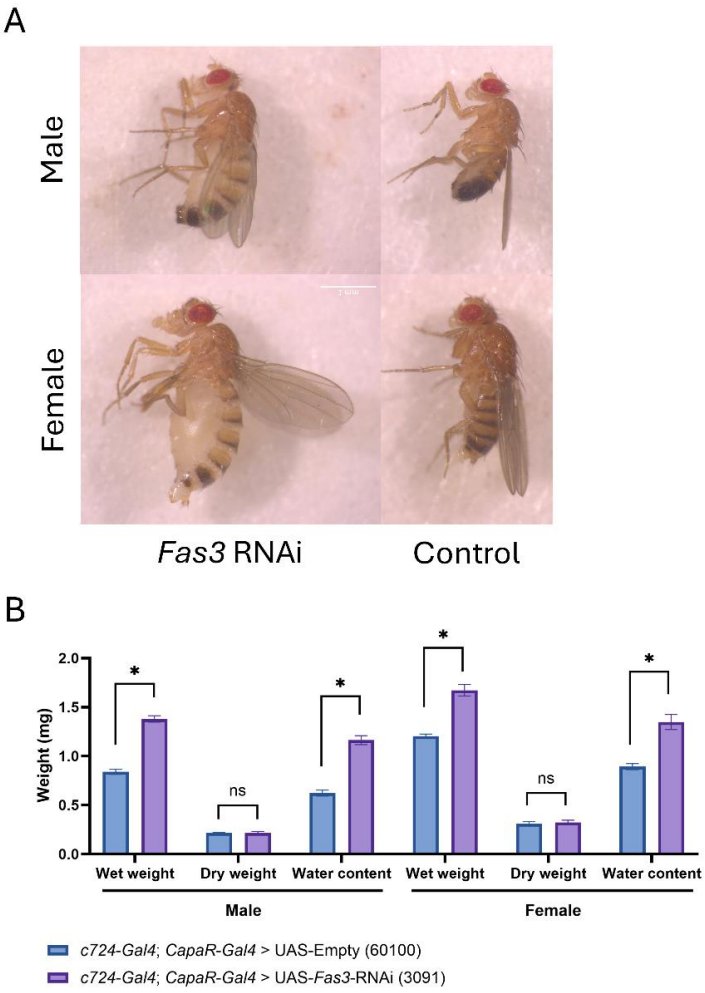

Figure 5.4 Knockdown of *Fas3* in both PCs and SCs.
(A) *Fas3* RNAi flies displayed inflated abdomens. Genotype of control: *c724-Gal4; CapaR-Gal4* > VDRC#60100; RNAi: *c724-Gal4; CapaR-Gal4* > VDRC#3091. Scale bar = 1 mm. (B) Measurement of wet and dry weights of control and *Fas3* KD flies. Data are presented as means with SDs (n=3, with each sample containing 6-10 flies). The asterisk indicates an adjusted $\boldsymbol{p}$ value less than 0.05, and ns denotes non-significant (two-way ANOVA followed by Sidak multiple comparisons test).

5.2.2 Analysis of *Fas3* in principal cells of the MTs

To investigate whether knockdown of *Fas3* in principal cells or stellar cells alone would recapitulate the edema observed when *Fas3* is knocked down in both cell types, PC- or SC-specific *Gal4* drivers were used to drive the knockdown. Using either the MT-specific Gal4 driver *ctB-Gal4* (Sudarsan et al., 2002) or *CapaR-Gal4* (Terhzaz et al., 2012), *Fas3* was inhibited in PCs, and a similar phenotype was observed (Figure 5.5A). Flies with *Fas3* knockdown exhibited a wider width and

larger abdomen size (Figure 5.5B). Although inflated abdomens were not present in every knockdown fly, older flies were more likely to develop inflated abdomens (Figure 5.5C), suggesting an age-dependent phenotype. This finding indicates that flies with inhibited *Fas3* expression are more susceptible to declines in renal function during aging. Measurement of fly body water content further confirmed that the abnormal abdominal swelling was caused by disrupted water homeostasis and the accumulation of body water (Figure 5.5D).

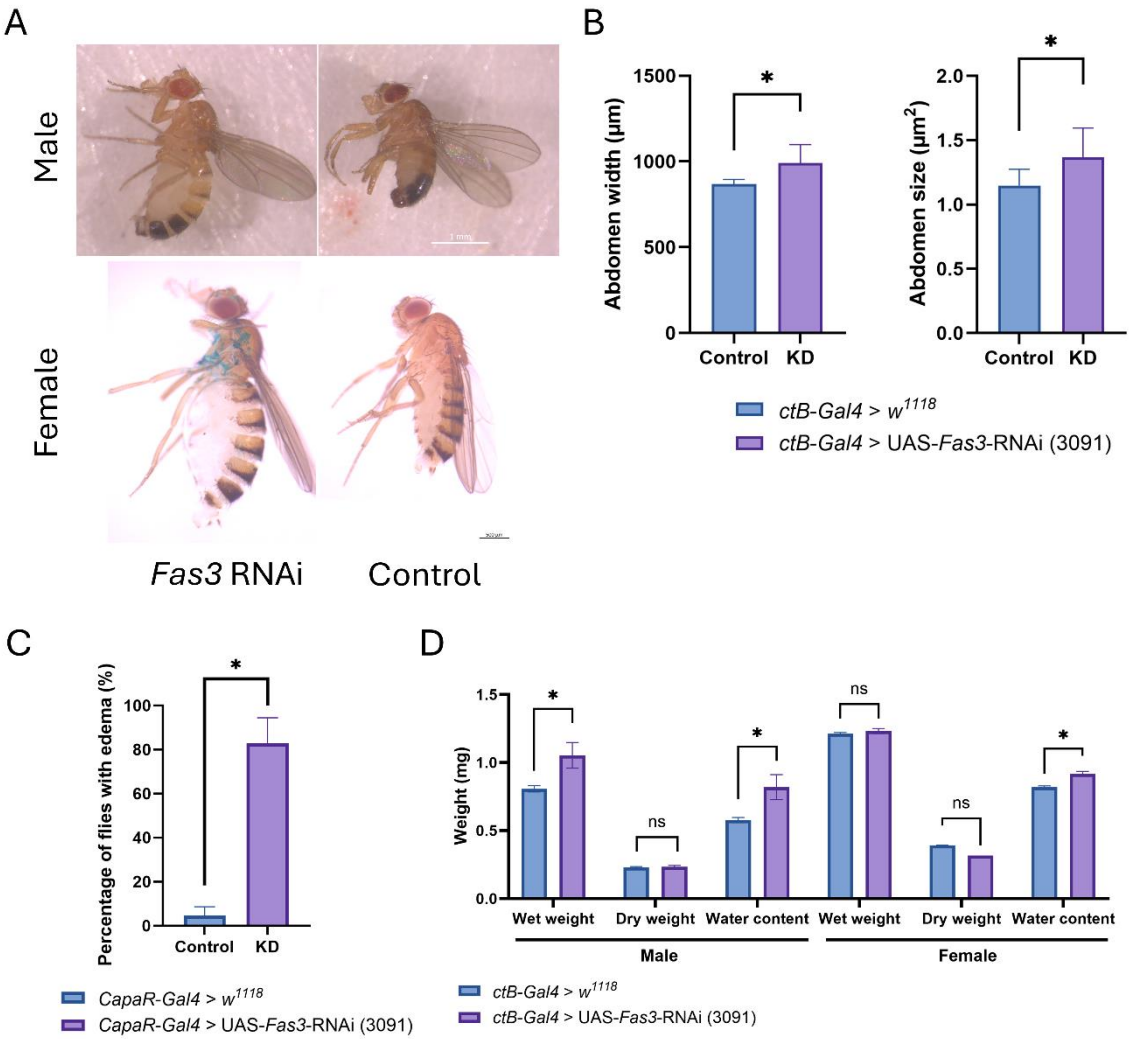

Figure 5.5 Knockdown of *Fas3* in PCs alone recapitulates the inflated abdomen phenotype.
(A) Compared with control flies, RNAi flies with inflated abdomen were observed. Genotype: male control, *ctB-Gal4* > VDRC#60100; male RNAi, *ctB-Gal4* > VDRC#3091; female control, *CapaR-Gal4* > w^{1118}; female RNAi, *CapaR-Gal4* > VDRC#3091. Scale bars: 1 mm for the upper two panels, 0.5 mm for the bottom two. (B) Abdominal width and size of control and RNAi flies (control, n=17; RNAi, n=20). (C) Percentage of 8-week-old flies with abdominal inflation, with or without *Fas3* knockdown (n=3, each sample contains 10-20 flies). (D) Measurement of wet and dry weights of control and *Fas3* KD flies (n=3, each sample contains 5-20 flies). Data are presented as means with SDs. The

asterisk indicates a $\boldsymbol{p}$ value less than 0.05 (two tailed Student's t-test used for tests in B and C, two-way ANOVA followed by Sidak multiple comparisons test for D).

The maintenance of water homeostasis in insects is largely performed by the MTs, in conjunction with the hindgut (Dow et al., 2021). To investigate the physiological function of MTs when *Fas3* is inhibited, fluid secretion rates were measured in *Fas3* RNAi tubules and their coisogenic control counterparts. As expected, tubules from the control group secreted fluid at much higher rates than those from the knockdown group under unstimulated conditions (Figure 5.6A). Stimulating the tubules with two commonly used diuretic peptides was unable to restore the secretion rates of the knockdown tubules to the baseline levels observed in the control tubules. Consistent with the reduced renal tubular transport and increased body water content, *Fas3* RNAi flies exhibited reduced sensitivity to desiccation stress (Figure 5.6C).

When flies are exposed to low temperatures, they often experience chill coma due to a loss of extracellular ion and water homeostasis (MacMillan et al., 2015, Macmillan and Sinclair, 2011). To recover from this paralysis, it is crucial to re-establish ion and water balance. Since *Fas3* KD tubules secrete much more slowly than their control equivalents and *Fas3* RNAi flies fail to maintain water homeostasis, we hypothesized that these flies would take longer to recover from paralysis induced by cold stress. Indeed, the measurement of chill coma recovery time showed that the median recovery time for *Fas3* RNAi flies was approximately twice that of control flies (Figure 5.6B). Additionally, knockdown of *Fas3* in PCs resulted in a shortened lifespan under normal conditions (Figure 5.6D), indicating that the dysfunction of MTs caused by the loss of *Fas3* also negatively impacted the overall fitness of the flies.

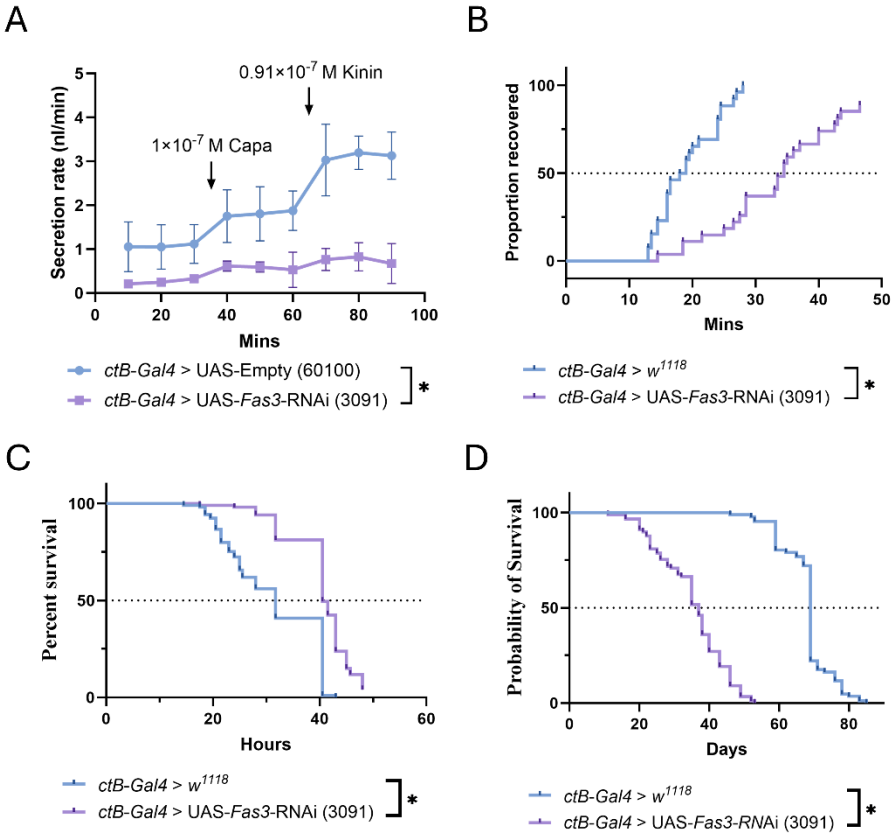

Figure 5.6 Loss of *Fas3* in PCs results in reduced tubular transport, altered stress tolerance, and impaired overall survival.
(A) Fluid secretion rates of control and *Fas3* knockdown renal tubules (control, n=10; RNAi, n=3). Data are plotted as means with SDs (two tailed Student's *t*-test). (B) Chill coma recovery time for control and knockdown flies (control, n=26, median recovery time = 18.5; RNAi, n=27, median recovery time = 34.5). (C) Survival curves for flies under desiccation stress (control, n=105, median survival = 31.75; RNAi, n= 101, median survival = 40.5). (D) Survival curves for flies under normal conditions (control, n=86, median survival = 69; RNAi, n= 89, median survival = 37). The log-rank test was used for survival curves. The asterisk indicates a $\boldsymbol{p}$ value less than 0.05.

As MTs are blind-ended tubes that open into the gut lumen at the junction of the midgut and hindgut, impaired tubule function may also affect faecal output. Quantification of the number and size of faecal deposits showed that *Fas3* RNAi flies had smaller faecal deposits, likely due to impaired tubular secretion (Figure 5.7). We speculate that the knockdown flies may increase the number of deposits as an alternative strategy to excrete as much waste as possible.

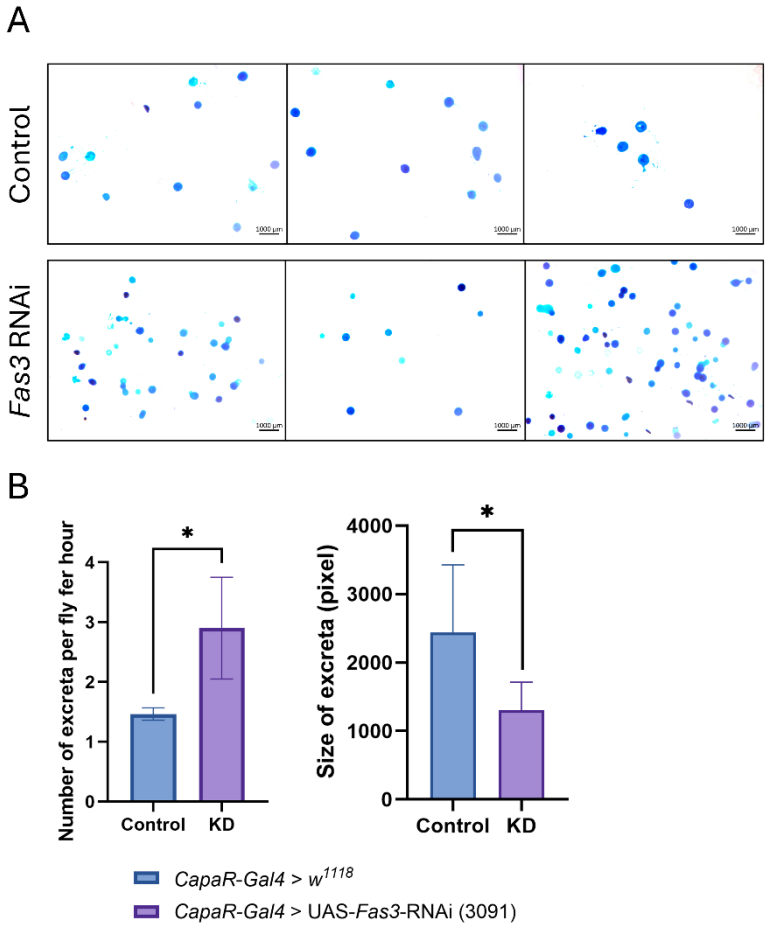

Figure 5.7 Faecal number and size in control and *Fas3* RNAi flies.
(A) Faeces excreted by control (upper panel) and RNAi (lower panel) flies when fed with erioglaucine disodium salt. (B) Number and size of faecal deposits (n=3, each sample contains 10-20 flies). Data are plotted as means with SDs (two tailed Student's *t*-test). * indicates a p value less than 0.05.

Interestingly, we also observed the formation of non-birefringent renal crystals in *Fas3* knockdown tubules. Few crystals were observed in young flies, but as the flies aged, the likelihood of crystal formation increased (data not shown), with more crystals present in the tubules (Figure 5.8). This observation could be due to disrupted epithelial integrity, as Fas3 is known to function as an adhesion molecule in *Drosophila* (Snow et al., 1989). Renal crystal formation is linked to epithelial transporters (Rose et al., 2019, Hirata et al., 2012), and the disruption of epithelial integrity may alter the subcellular localisation of these proteins. In control tubules, Fas3 localised to cellular junctions, but this localisation was lost upon *Fas3* knockdown (Figure 5.9A). To assess the impact on epithelial integrity, we performed immunostaining against the junctional protein Dlg1. The results showed that the distribution of Dlg1, and thus septate junction integrity, was

disrupted (Figure 5.9C). In control tubules, Dlg1 labelling was continuous and evenly distributed along the septate junction, while in the knockdown group, the labelling was less uniform and more fragmented. Mislocalised cytoplasmic Dlg1 was also observed in the main segment of RNAi tubules. Furthermore, in the lower tubules of knockdown flies, there was an increased number of small nuclei, indicative of renal stem cell proliferation, as marked by Hnt (Figure 5.9B). Renal stem cells are known to replenish lost differentiated cells, such as PCs (Singh et al., 2007, Wang and Spradling, 2022).

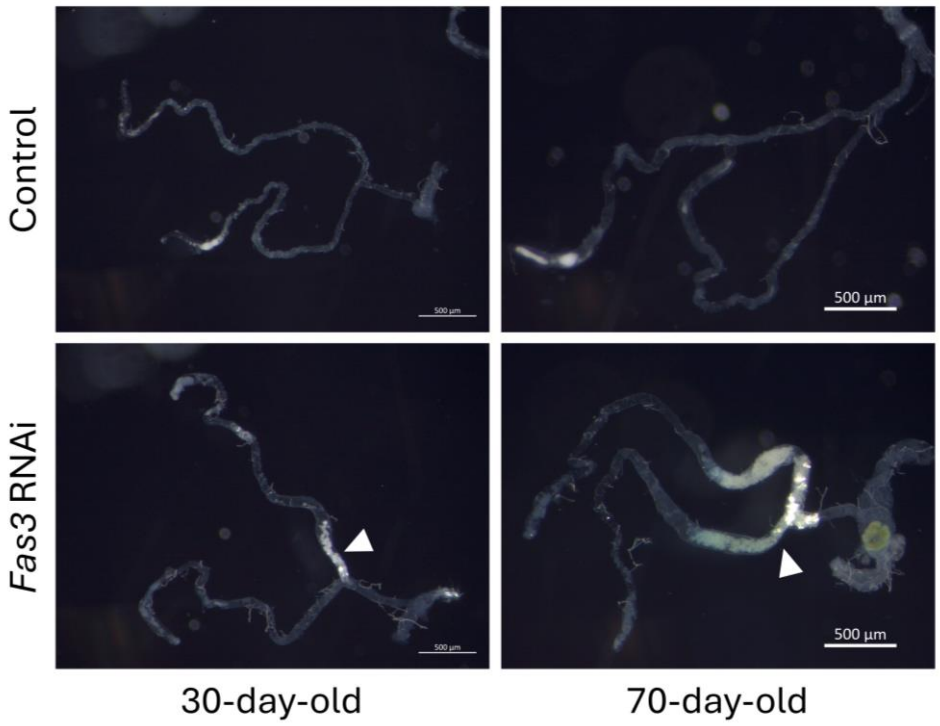

Figure 5.8 Development of renal crystals in *Fas3* knockdown flies.
Crystals can be observed in the tubules following the loss of *Fas3*. As the flies age, more crystals form. Genotype: control, *CapaR-Gal4* > w^{1118}; RNAi, *CapaR-Gal4* > VDRC#3091. Scale bar = 0.5 mm.

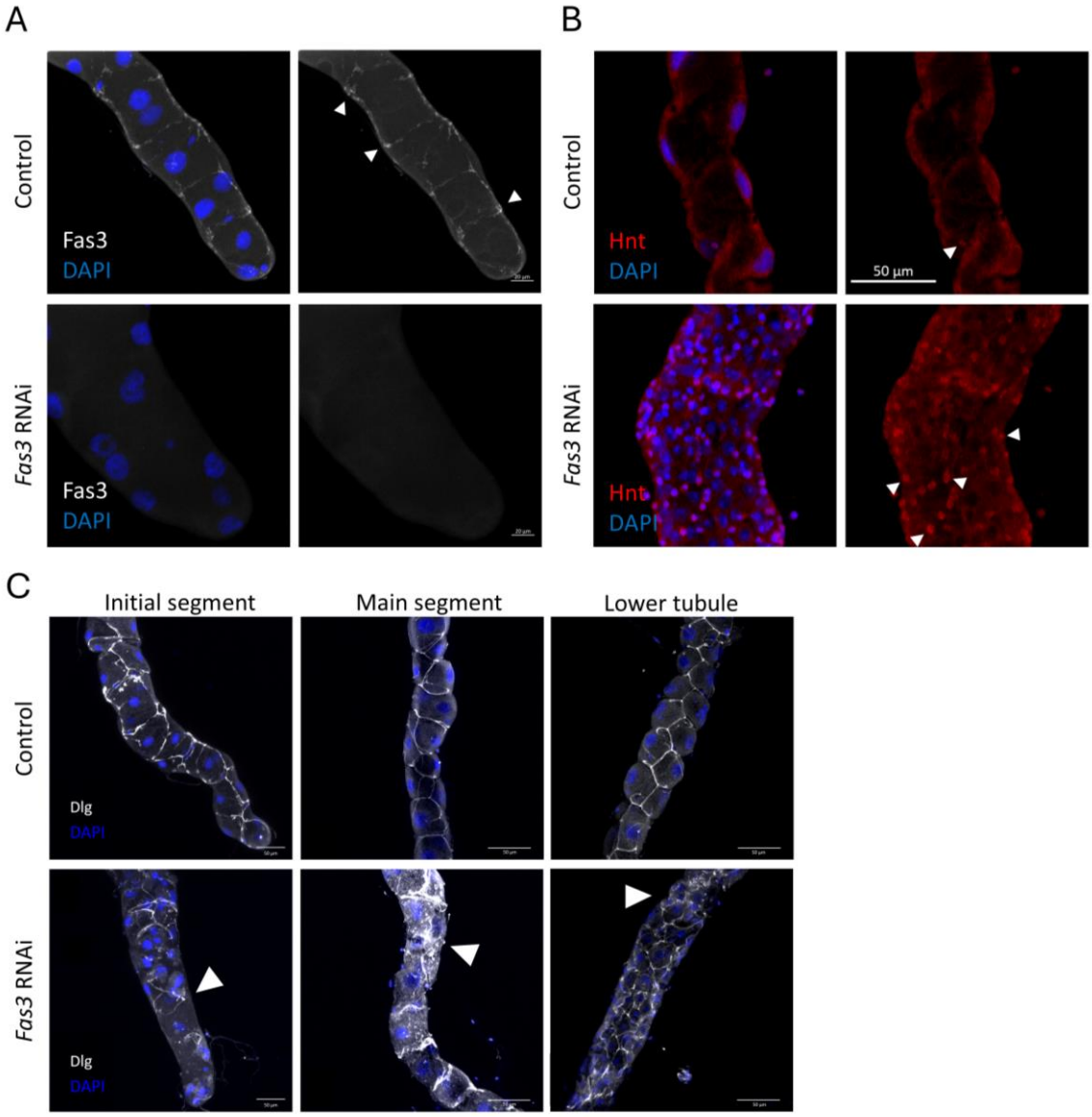

Figure 5.9 Loss of Fas3 disrupts the distribution of Dlg1 and induces the proliferation of renal stem cells.
(A) Immunostaining of Fas3 in the initial segment of the renal tubule in control and knockdown flies. Scale bars = 20 µm. (B) Immunostaining of Hnt, a marker of renal stem cells, in the lower tubule. (C) Immunostaining of Dlg1 in the three segments of the tubules. Scale bars = 50 µm in panels B and C. Genotype: control, *CapaR-Gal4* > w^{1118}; RNAi, *CapaR-Gal4* > VDRC#3091.

5.2.3 Analysis of *Fas3* in stellate cells of the MTs

Gal4 driver lines, *c724-Gal4* or *c724-Gal4*; UAS-*mCD8::GFP*, were used to drive the knockdown of *Fas3* in stellate cells. Unlike the knockdown of *Fas3* in PCs, the loss of *Fas3* in SCs did not result in abdominal inflation. However, a degeneration of SC morphology was observed in *Fas3* KD flies. This morphological change did not occur in newly eclosed flies. On day 0, SCs displayed normal

morphology; more specifically, SCs were bar-shaped in the initial segment and stellate in the main segment (Figure 5.10). By day 7, SCs in both regions had lost their typical morphology and had become spherical or cuboidal. Surprisingly, some GFP-labelled SCs appeared to be extruded from the epithelium into the tubule lumen in *Fas3* KD flies. (Figure 5.10, dashed box). The number of SCs was counted during ageing, with an example of control and knockdown tubules shown in Figure 5.11. SCs were labelled with GFP, and quantification of SC number is shown in Figure 5.12A. The results indicated that while the SC population in control flies decreased with age, this decline was significantly more pronounced in *Fas3* RNAi tubules (Figure 5.12A), suggesting that *Fas3* played an important role in maintaining SC numbers. However, despite the loss of SCs, no proliferation of renal stem cells was observed (Figure 5.11), likely because renal stem cells do not replenish principal cells or stellate cells in the upper tubules (Wang and Spradling, 2020).

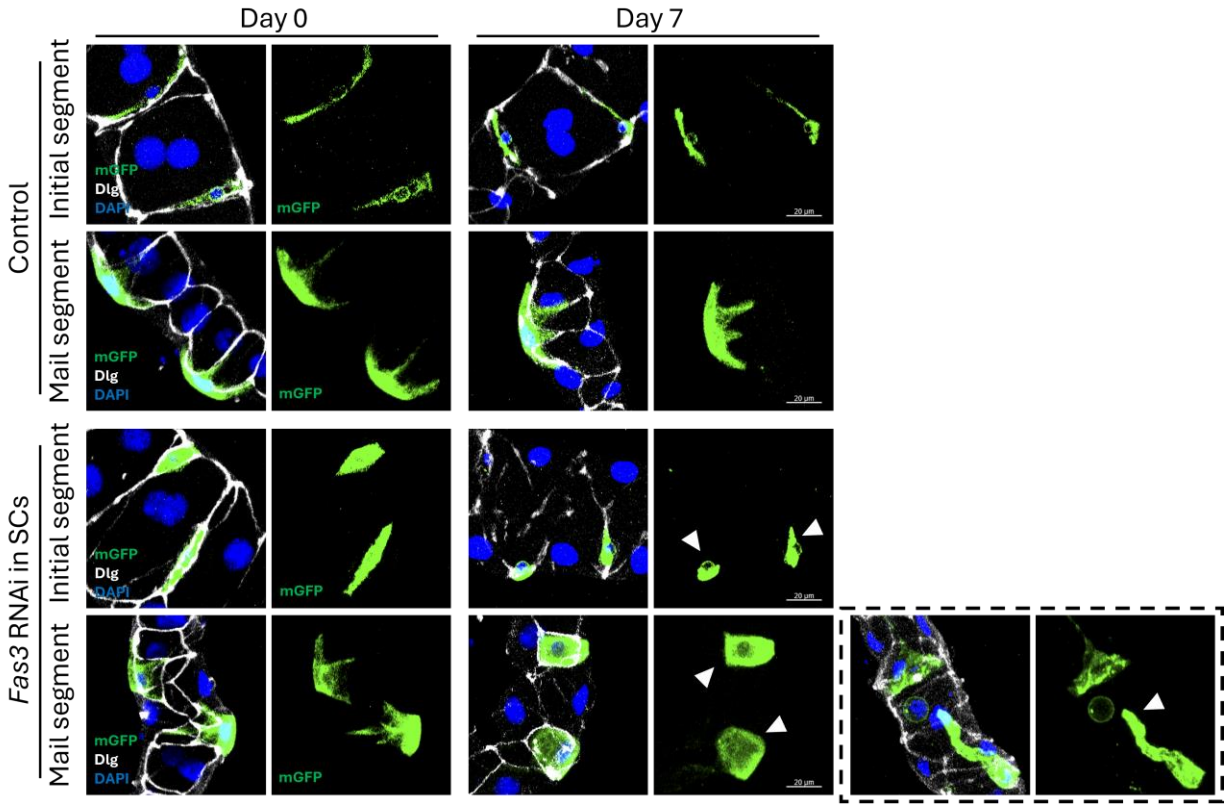

Figure 5.10 Loss of *Fas3* in SCs resulted in age-related changes in SC morphology.
In *Fas3* RNAi flies, stellate cells lose their typical star- and bar-shaped morphologies in the main and initial segments, respectively. Scale bars = 20 µm. Genotype: control, *c724-Gal4;* UAS-*mCD8::GFP* > w^{1118}; RNAi, *c724-Gal4;* UAS-*mCD8::GFP* > VDRC#3091.

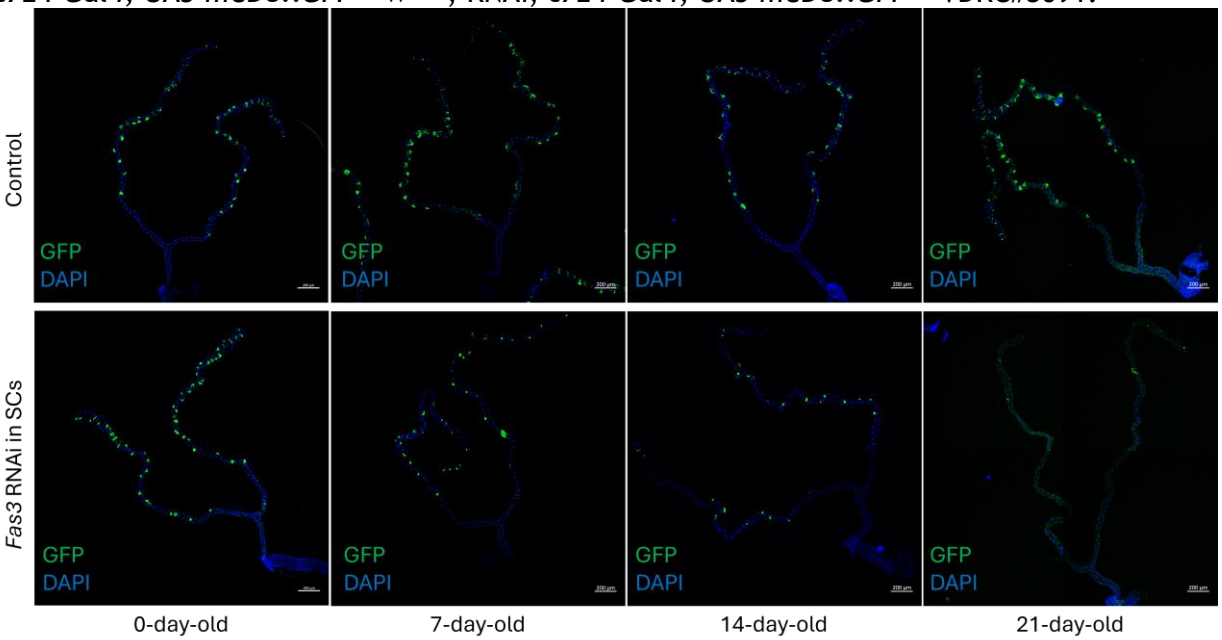

Figure 5.11 Number of SCs in tubules during ageing.
Z-stack of dissected anterior tubules from cross between *c724-Gal4;* UAS-*mCD8::GFP* and control or UAS-*Fas3*-RNAi flies. Scale bars = 200 µm.

The receptor of the neuropeptide Kinin is localised to the basement membrane of SCs and responds to peptide stimulation (Halberg et al., 2015). Based on the

observed positive correlation between SC number and stimulated secretion rates in individual MTs (Denholm et al., 2003), we hypothesized that the impaired morphology and decreased SC number in *Fas3* RNAi flies would result in diminished Kinin-stimulated secretion rates. Indeed, loss of *Fas3* resulted in significantly reduced secretion upon Kinin treatment (Figure 5.12B). However, baseline secretion rates remained unaffected by *Fas3* knockdown, suggesting that PCs are likely the primary contributors to fluid secretion under normal conditions. This finding is supported by the fact that mitochondria-enriched PCs generate a lumen-positive transepithelial potential through active cation secretion, followed by chloride and water shunts provided by SCs, which together achieve net fluid secretion (Dow et al., 2021). Furthermore, survival curves for control and knockdown flies showed no significant differences, which is consistent with the absence of edema and the unchanged baseline secretion rates following *Fas3* knockdown (Figure 5.12C).

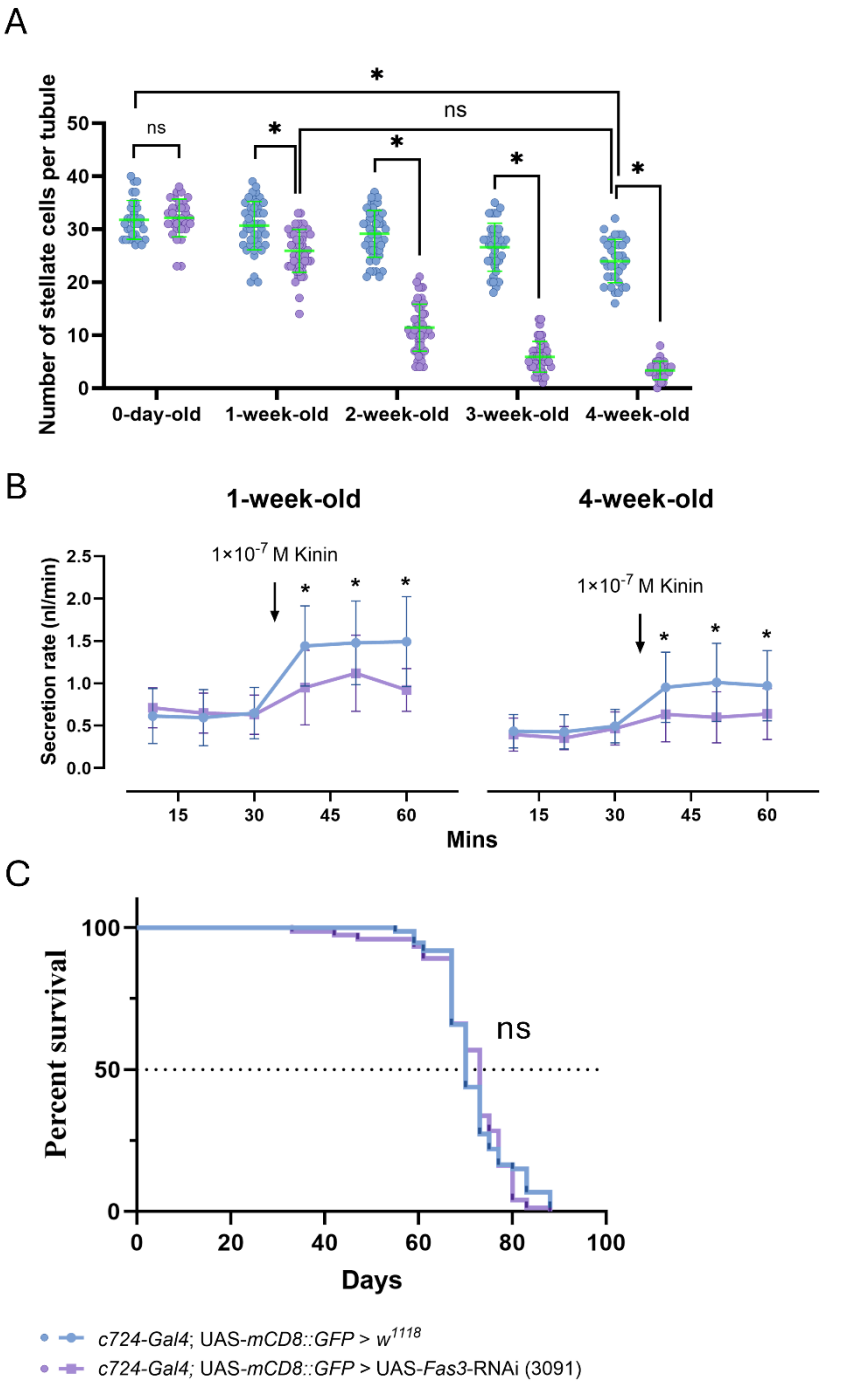

Figure 5.12 Depletion of *Fas3* in SCs results in the loss of the SC population and reduced stimulated secretion during aging.
(A) Quantification of SC number in tubules during aging (n>25, two-way ANOVA followed by Sidak multiple comparisons test). (B) Fluid secretion rates of control and *Fas3* knockdown renal tubules. Data are plotted as means with SDs (more than 7 pairs of tubules used for each group, two tailed Student's *t*-test). (C) Survival curves for flies under normal condition (control, n=73, median survival = 70; RNAi, n=74, median

survival = 73). The log-rank test was used for survival curves. The asterisk indicates that $\boldsymbol{p}$ value is less than 0.05, and ns means not significant.

The actin cytoskeleton, a dynamic network of filaments, plays a crucial role in cell and tissue morphogenesis (Pruyne and Bretscher, 2000). To examine the impact of *Fas3* knockdown on the actin cytoskeleton, immunostaining against F-actin was performed. The results showed that the distribution of F-actin in SCs was disrupted in *Fas3* RNAi tubules (Figure 5.13). In humans, nectins and cadherins work together to form adherens junctions by activating CDC42 and RAC (Sakisaka and Takai, 2004), with NECTIN3 being the predicted human orthologue of the *Drosophila* Fas3. An atlas of the human kidney has revealed that NECTIN3 is enriched in the proximal tubule epithelial cells of the nephron (Lake et al., 2023). To rescue the number and morphology of SCs in *Fas3* RNAi tubules, dominant negative and constitutively active mutants of *Cdc42* were introduced. Notably, SCs in tubules expressing the dominant negative *Cdc42* were cuboid (data not shown), suggesting that inhibition of *Cdc42* alone can mimic the morphological changes of SCs seen with *Fas3* loss but does not affect SC number (Figure 5.14). When the dominant negative form of *Cdc42* was introduced, the reduction in SC number was further exacerbated in *Fas3* RNAi tubules. Surprisingly, expressing a constitutively active form of *Cdc42* did not rescue the reduced SC number.

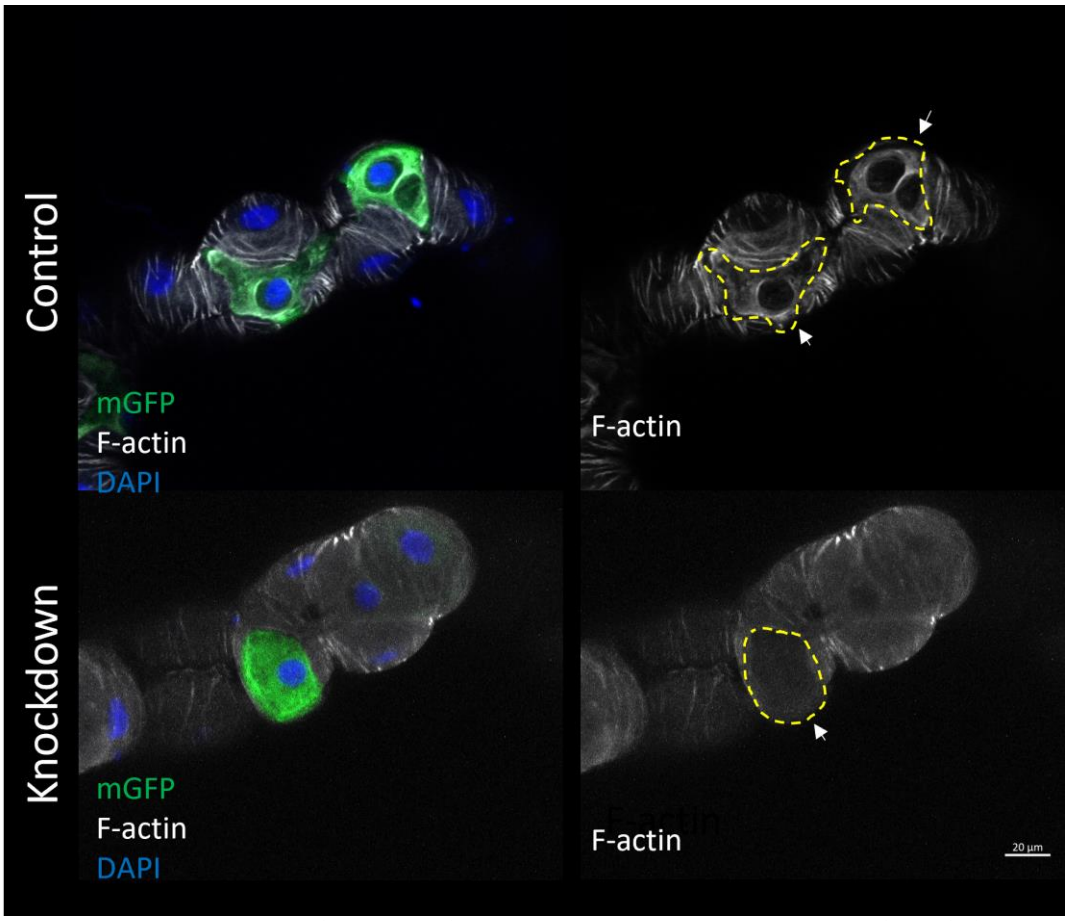

Figure 5.13 Loss of cytoarchitectural organisation in SCs upon *Fas3* knockdown. F-actin was labelled using Phalloidin to visualize the actin cytoskeleton. SCs are outlined with yellow dashed line. The white arrows indicate F-actin staining in SCs. In control flies, there are organized F-actin structures, whereas this staining is lost in *Fas3*

RNAi flies. Scale bars represent 20 μm. Genotype: control, *c724-Gal4;* UAS-*mCD8::GFP* > w^{1118}; RNAi, *c724-Gal4;* UAS-*mCD8::GFP* > VDRC#3091.

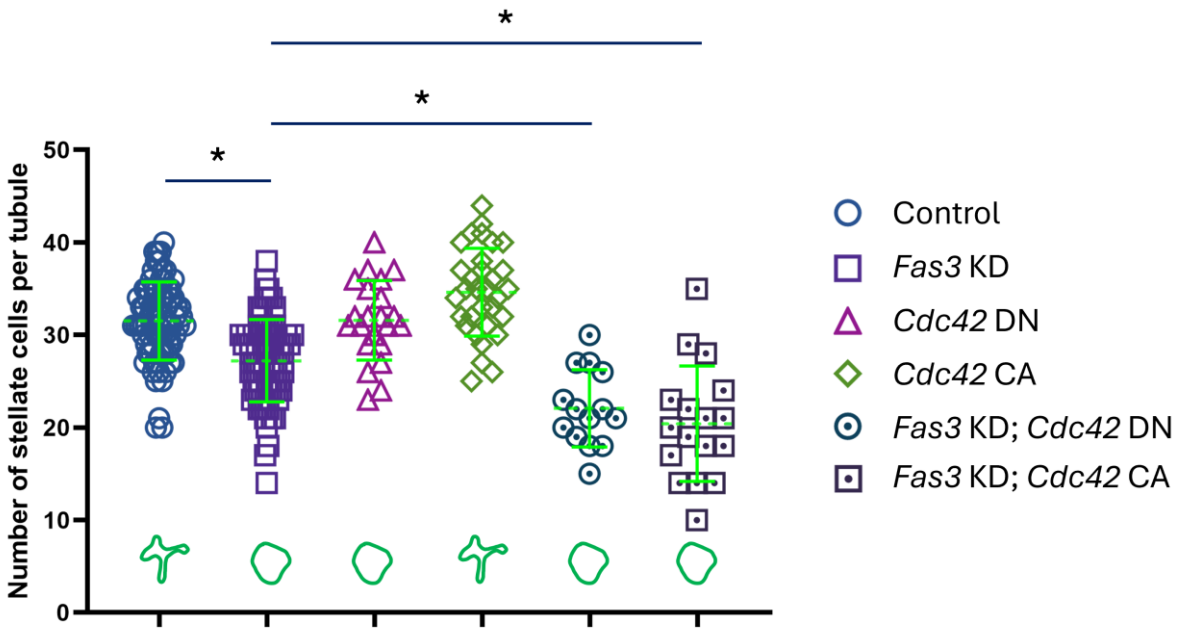

Figure 5.14 Expression of the constitutively active mutant of *Cdc42* failed to rescue the number of SCs in *Fas3* RNAi tubules.
Green symbols at the bottom represent the morphology of SCs in tubules. Genotype: +/*c724-Gal4*; +/UAS-*mCD8::GFP* (Control), +/*c724-Gal4*; UAS-*Fas3*-RNAi/UAS-*mCD8::GFP* (*Fas3* KD), UAS-*Cdc42*-DN/*c724-Gal4*; +/UAS-*mCD8::GFP* (*Cdc42* DN), UAS-*Cdc42*-CA/*c724-Gal4*; +/UAS-*mCD8::GFP* (*Cdc42* CA), UAS-*Cdc42*-DN/*c724-Gal4*; UAS-*Fas3*-RNAi/UAS-*mCD8::GFP* (*Fas3* KD; *Cdc42* DN), UAS-*Cdc42*-CA/*c724-Gal4*; UAS-*Fas3*-RNAi/UAS-*mCD8::GFP* (*Fas3* KD; *Cdc42* CA). Data are plotted as mean with SD. One-way ANOVA followed by Sidak multiple comparisons test was used. * indicates that the adjusted $\boldsymbol{p}$ value is less than 0.05, and ns indicates no significant difference.

5.3 Discussion

Cells within tissues are connected through cell-cell junctions, which regulate tissue homeostasis through critical cell processes such as tissue barrier function, cell proliferation, and migration (Garcia et al., 2018). The plasma membrane of epithelial cells is subdivided into two main regions, the apical and basolateral domains, which are segregated by a semipermeable barrier composed of a circumferential junctional complex (Tepass et al., 2001). This membrane asymmetry, along with the differentiation of membrane domains and cellular junctions, is maintained by protein complexes associated with key proteins such as Crumbs and DE-cadherin. Disruption of cellular polarity or epithelial integrity

can lead to physiological dysfunction, the onset of various diseases, and, ultimately, death.

Fas3 was identified as a candidate in a pilot GWA study involving 30 DGRP lines; however, it did not appear in the candidate gene list in the full screen. The discrepancy may be due to batch effects, as the two measurements were conducted more than a year apart, or the inflation of effect sizes caused by the small sample size (Marigorta et al., 2018, Ioannidis, 2008). The ectopic expression of *Fas3* has resulted in the aggregation of non-adhesive *Drosophila* S2 cells, demonstrating its capability to mediate adhesion in a homophilic, Ca^{2+}-independent manner (Snow et al., 1989). During *Drosophila* cardiogenesis, differential expression of *Fas3* regulates filopodia binding affinity and cell matching (Zhang et al., 2018). It is also required for the maintenance of adult olfactory interneurons (Vaikakkara Chithran et al., 2024). Fas3 is highly enriched at the septate junctions, with lower amounts in the lateral cell membranes and excluded expression at the adherens junctions (Woods et al., 1996). Its normal distribution is affected by the loss of Dlg. In the salivary gland of dlg^{m52} mutant larvae where septate junctions are largely eliminated, the amount of Fas3 is reduced and the protein is found unrestricted along the cell membrane (Woods et al., 1996). The tight junctional proteins Snakeskin and Tetraspanin 2a and the cell adhesion protein Mesh have been found to be necessary for the appropriate localisation of associated junctional proteins such as Dlg, Coracle, and Fas3 (Dornan et al., 2023).

However, the role of *Fas3* in the epithelium, MTs, remains elusive. In this study, the cell-specific involvement of *Fas3* in maintaining epithelial integrity within the MTs was investigated and elucidated, which confirmed its essential role in preserving epithelial integrity.

5.3.1 Edema in *Fas3* RNAi flies

Both PCs and SCs exhibit high levels of *Fas3* mRNA expression, suggesting a potential role for *Fas3* in their normal function. Knockdown of *Fas3* in PCs

recapitulated the edema observed upon inhibition of *Fas3* in both PCs and SCs, while knockdown in SCs alone did not result in the same phenotype. This finding highlights that PCs are the primary cells responsible for water homeostasis in the context of *Fas3* loss. This importance of PCs in tubules is supported by the fact that the number of PCs in the anterior tubules is approximately four times greater than that of SCs (Sozen et al., 1997), and PCs contain much more mitochondria, acting as major drivers of lumen-positive transepithelial potentials (Dow et al., 2021). The accumulated body water could be attributed to the impaired baseline secretion following *Fas3* knockdown.

Loss of the protein Dlg1, which is required for septate junction structure and cell polarity, results in a disrupted distribution of Fas3 (Woods et al., 1996). In contrast, we observed that the continuous and even distribution of Dlg1 along cellular junctions was lost upon *Fas3* inhibition, suggesting that epithelial integrity was compromised in *Fas3* RNAi tubules. This disruption may lead to the altered subcellular localisation of transporters, resulting in impaired fluid secretion by renal tubules and subsequent water retention. The normal basolateral distribution of Na^+/K^+-ATPase becomes apical in the proximal tubule under ischemic conditions, likely due to the breakdown of the tight junctional barrier (Brown and Stow, 1996). Additionally, the targeting and delivery of various membrane proteins depend on an intact microtubular network. Cadherins initiate a signalling pathway, in which cadherins connect adjacent cells at adherens junctions, altering microtubule organization by stabilizing microtubule ends (Chausovsky et al., 2000).

Chill coma recovery time and desiccation tolerance are closely linked to water homeostasis. In chill-susceptible *Drosophila* species, the selectivity of Na^+ and K^+ of the MTs is compromised, contributing to an increased level of extracellular K^+ and a loss of Na^+ and water balance (MacMillan et al., 2015, Macmillan and Sinclair, 2011, Andersen et al., 2017). In contrast, chill-tolerant species preserve ion selectivity in their tubules, allowing faster recovery from chill coma. Additionally, compared with *Drosophila melanogaster*, *D. suzukii* loses approximately 5% more body water after 18 h of desiccation and exhibits

significantly lower desiccation resistance (Terhzaz et al., 2018). In *Fas3* RNAi flies, an increased survival rate under desiccation conditions was observed, accompanied by a prolonged recovery time after cold shock. This finding is consistent with the impaired water homeostasis in these flies, mainly maintained by the MTs.

Interestingly, we also observed the development of renal crystals in tubules upon *Fas3* inhibition, accompanied by an induced proliferation of renal stem cells. Genetic disorders of renal tight junction, including mutations and polymorphisms of Claudin genes (e.g., *CLDN2* (Curry et al., 2020), *CLDN14* (Thorleifsson et al., 2009, Oddsson et al., 2015), and *CLDN16* (Weber et al., 2001)), also affect kidney stone disease, as revealed by association studies. Thus, crystal formation may result from disrupted epithelial integrity, which could lead to altered tubular secretion of substrates that readily form crystals. Like many other tissues containing adult stem cells, the MTs also harbour proliferating cells. Renal stem cells remain quiescent under normal conditions but are activated to remodel adult MTs upon injury by replenishing principal cells in the stem cell zone (Wang and Spradling, 2020). This replenishment of PCs also happens when xanthine stones form in the lower tubule (Wang and Spradling, 2022). Additionally, knockdown of *Snakeskin* in renal tubules causes compromised junctional integrity and an increased number of nuclei associated with RSCs (Dornan et al., 2023). We hypothesize that the increased population of RSCs is driven by the presence of renal crystals and the impaired cellular junction.

5.3.2 Population of SCs

After undergoing metamorphosis and eclosion, SCs become bar-shaped and stellate-shaped in the initial and main segments, respectively (Denholm, 2013). In SC-specific *Fas3* knockdown, SCs failed to attain mature stellar or bar shapes and became cubical in both tubule regions, with some extruded SCs from the plane of the MTs being observed. While the number of the two major cell types in the tubules is generally invariant (Sozen et al., 1997), we observed a subtle

yet significant decrease in the number of SCs during ageing under physiological conditions. This age-related decline in the SC population was exacerbated in *Fas3* knockdown tubules, together with impaired cellular morphology.

The actin cortex, which lies immediately beneath the plasma membrane of animal cells, along with myosin motors generating contractile forces, plays a crucial role in controlling cell shape and numerous physical cellular processes, including cell adhesion (Pruyne and Bretscher, 2000, Salbreux et al., 2012, Stricker et al., 2010). Disruption of the cytoskeleton can induce apoptosis via activation of the death receptor, CD95 (Kulms et al., 2002). Although the MTs evade destruction despite the expression of apoptotic proteins during metamorphosis, overexpression of these proteins results in malformed tubules with disrupted number and regular organization of PCs and SCs (Shukla and Tapadia, 2011, Tapadia and Gautam, 2011). Besides, the localisation of F-actin and Dlg is disrupted (Tapadia and Gautam, 2011). *Fas3* knockdown in SCs similarly resulted in a loss of cytoarchitecture. Additionally, impaired expression of the apoptotic marker Dcp-1 has been observed in MTs with disrupted SC organization (Dornan et al., 2023). Thus, the decrease in the SC population in *Fas3* RNAi tubules is likely due to the SC loss through apoptosis. Furthermore, the reduced SC population did not trigger the proliferation of renal stem cells, likely because renal stem cells are unipotent and only replenish principal cells in the stem cell zones (Wang and Spradling, 2020).

In humans, nectins and cadherins work together to form adherens junctions via the activation of CDC42 and RAC (Sakisaka and Takai, 2004). Nectins recruit and activate c-SRC, which in turn recruits both FRG and RAP1. The activation of FRG by RAP1 subsequently triggers the activation of CDC42. On the other hand, E-cadherin induces the activation of RAC. The activations of both CDC42 and RAC leads to the formation of filopodia through the reorganization of the actin cytoskeleton, which enhances the formation of adherens junctions. *Fas3* is the predicted *Drosophila* orthologue of human NECTIN3. To rescue the disrupted number and morphology of SCs, dominant negative and constitutively active mutants of *Cdc42* were introduced. While expression of the dominant negative

Cdc42 recapitulated the cuboidal morphology of SCs in *Fas3* RNAi flies (data not shown), the SC number was unaffected. Inhibition of *Cdc42* further reduced the number of SCs in the *Fas3* RNAi background, whereas activation of *Cdc42* did not restore the SC number to normal levels. These findings suggest that *Fas3* is necessary for maintaining the SC population.

Cuboidal SCs have been linked to the loss of apicobasal polarity and the ClC-a channel (Dornan et al., 2023). Additionally, disruption of cell polarity, accompanied by the relocation of the normally basolateral Na^+/K^+-ATPase, has been observed in some cystic epithelial cells in polycystic kidney disease (Brown and Stow, 1996). Thus, the fluid secretion of dissected MTs was investigated, and a compromised Kinin-stimulated response was found in *Fas3* RNAi flies. The unaffected basal fluid secretion of the MTs might be because the remaining SCs can functionally compensate for the loss of the majority of the SC population. In summary, although *Fas3* is expressed in both cell types, knockdown in each cell type exhibits distinct phenotypes (Figure 5.15), likely due to the different properties of these cell types. Although *Fas3* did not emerge from the main screen, it nonetheless significantly impacted tubule structure and function.

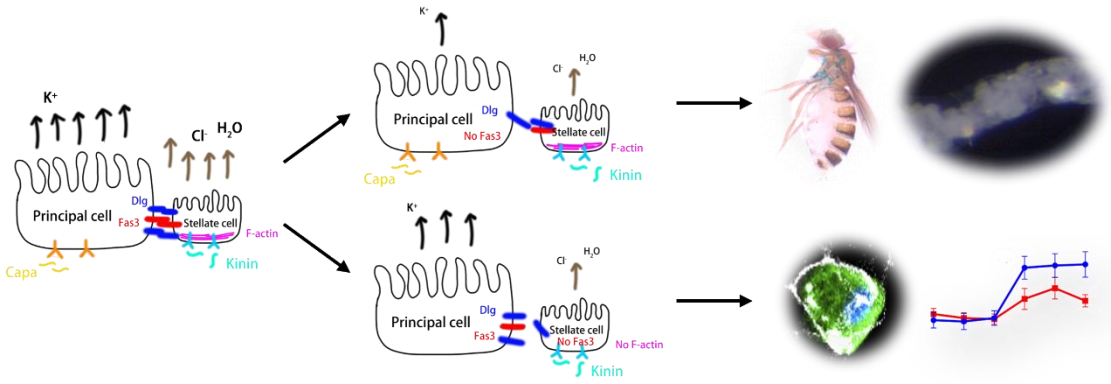

Figure 5.15 Diagram illustrating the role of Fas3 in maintaining tubule function. In PC-specific *Fas3* knockdown, flies exhibited an enlarged abdomen, filled with excessive water, and the development of renal crystals. While SC-specific knockdown only led to phenotypes specific to SCs, such as changes in stellate cell number and morphology and Kinin-stimulated secretion rate.

Chapter 6 Role of Tubule-Specific *Muc11A* in *Drosophila*

6.1 Summary

Cells exhibit remarkable efficiency in managing energy usage; for example, the spatial localisation and copy number of molecules are often constrained to minimize energy expenditure in neurons (Bergmann et al., 2025). Furthermore, a large portion of the genome is expressed with high tissue specificity in organisms such as *Drosophila* and humans (Chintapalli et al., 2007, Fagerberg et al., 2014). Functional analyses of tissue-specific proteins align closely with the function of the corresponding tissues or organs (Fagerberg et al., 2014). These observations suggest that studying tissue-enriched genes could provide valuable insights into the specialized functions of tissues and contribute to the development of therapeutic strategies for diseases involving tissue-specific processes. Although not a hit in the GWA study, *Muc11A* is highly enriched in the MTs of *Drosophila*, as shown by both microarray (Wang et al., 2004) and RNA sequencing data (Chintapalli et al., 2007, Leader et al., 2018). Therefore, it was selected for study. To investigate its role in this epithelium, PC-specific *Gal4* drivers were used to induce its knockdown. RNAi-mediated silencing of *Muc11A* resulted in impaired morphology of the initial segment of the renal tubule, with the formation of non-birefringent crystals, suggesting that *Muc11A* may play a critical role in maintaining a proper luminal environment that inhibits crystal formation. Additionally, the epithelial integrity of the tubules was compromised in the RNAi flies, consistent with the observed proliferation of renal stem cells.

6.2 Results

6.2.1 Expression pattern of *Muc11A*

Data from FlyAtlas.org showed that *Muc11A* is highly expressed in both larval and adult renal tubules (Figure 6.1A). This tissue-specific expression suggests that

Muc11A may be involved in the function of the MTs. Prior to investigating its role in MTs, we confirmed this tubule-specific expression in adults. qRT-PCR was performed using whole flies and dissected tubules. The results were consistent with the microarray data, showing that *Muc11A* expression was enriched approximately 3- to 6-fold in adult renal tubules (Figure 6.1B). To study the function of *Muc11A* in renal tubules, *ctB-Gal4* and *CapaR-Gal4* drivers were interchangeably used to induce tubule-specific knockdown, as FlyCellAtlas indicates high expression of *Muc11A* in PCs (Figure 6.1C). The knockdown efficiency was first assessed in RNAi flies, revealing a knockdown of about 70% in male and 85% in female (Figure 6.1D). Additionally, we observed that *Muc11A* expression was higher in females than in males.

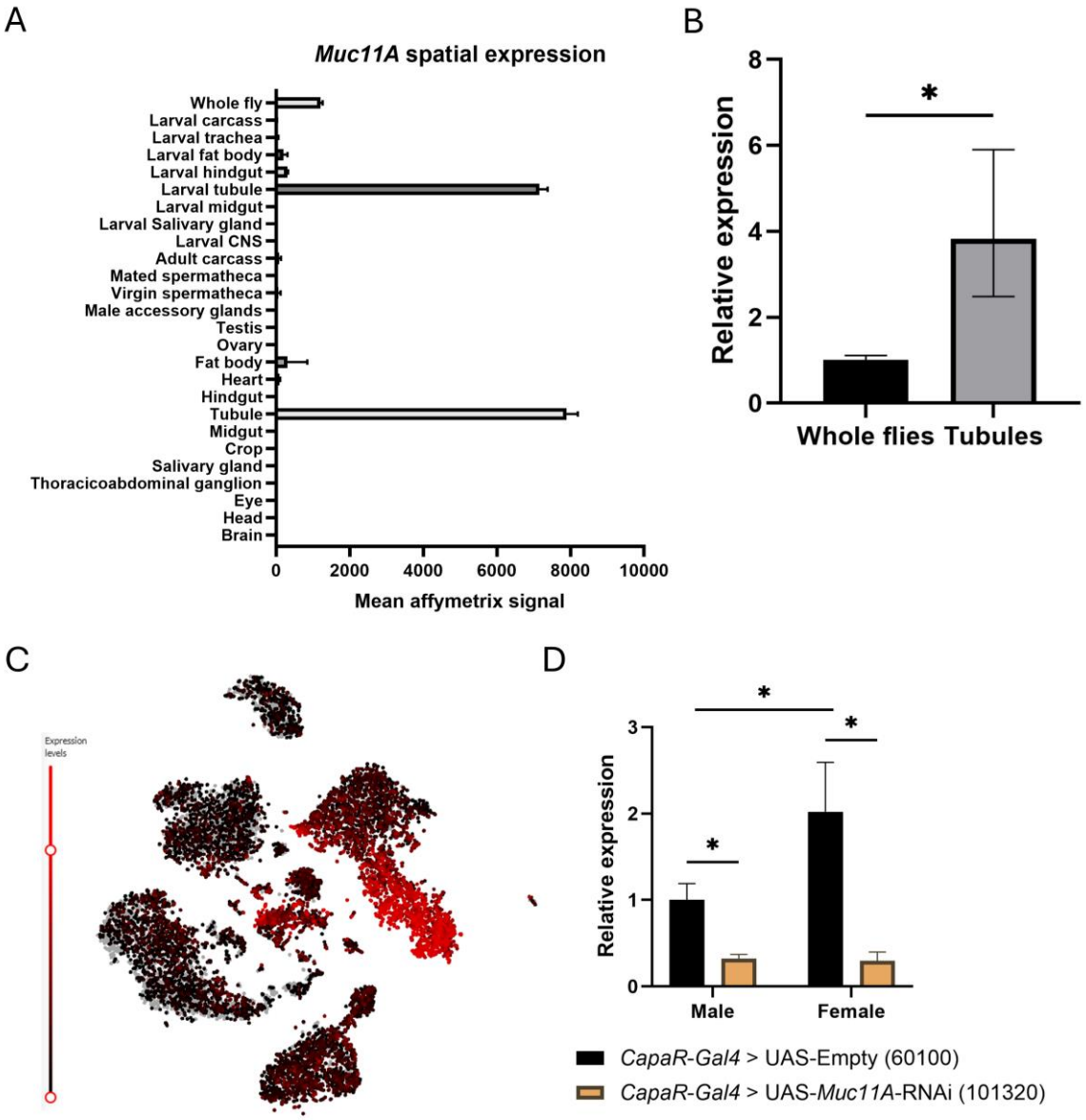

Figure 6.1 Expression pattern and knockdown efficiency of *Muc11A*.
(A) Spatial expression pattern of *Muc11A* across different tissues, as shown by data from flyatlas.org (Chintapalli et al., 2007). The mean normalized Affymetrix signal, which represents the normalized gene expression from microarray data, with standard error of the mean (SEM) is presented. (B) The gene expression of *Muc11A* in tubules was compared to that in whole flies. Whole flies and dissected tubules of Canton S were used for RNA extraction, and synthesised cDNA for qRT-PCR. qRT-PCR results confirm the tubule-enriched expression of *Muc11A* in wild-type flies (Student's *t*-test was used). (C) The t-SNE of *Muc11A* gene expression across the renal tubule. The expression is shown in red; the intensity is proportional to the log-normalised expression levels. (D) Knockdown efficiency in *Muc11A* KD tubules, as shown by qRT-PCR. Relative expression values with their lower and upper limits are plotted. * means a p value of less than 0.05.

6.2.2 Tubular morphological change and mineralization caused by loss of *Muc11A* in the MTs

Mucin11A is a potentially highly O-glycosylated protein, as indicated by its protein sequence, which is rich in threonines and serines (Syed et al., 2008). This glycoprotein is one of the components of the extracellular matrix, where it contributes to tissue morphogenesis and tubulogenesis (Kleinman et al., 2003, Loganathan et al., 2020). To investigate the role of *Muc11A*, the morphology of its knockdown tubules was examined. Enlarged initial segments, but not the lower tubules, were observed in *Muc11A* KD tubules (Figure 6.2). The overall length of the tubules was unaffected by knockdown. The initial segment of the renal tubules typically contains an abundance of small spherical granules, which are composed of concentric layers of calcium and magnesium, along with carbonate, phosphate, chloride, and an organic matrix of glycosaminoglycans or proteoglycans (Wessing and Zierold, 1992). In *Muc11A* KD tubule, however, solid and condensed crystals, rather than diffused luminal granules, were present in the tubule lumen (Figure 6.3A), suggesting that *Muc11A* plays a critical role in maintaining luminal granules. Alizarin red staining for calcium deposition was used to confirm the mineral composition of these deposits and assess their size. The results showed that calcium is one of the components of the deposits, which were absent in control tubules (Figure 6.3B and C).

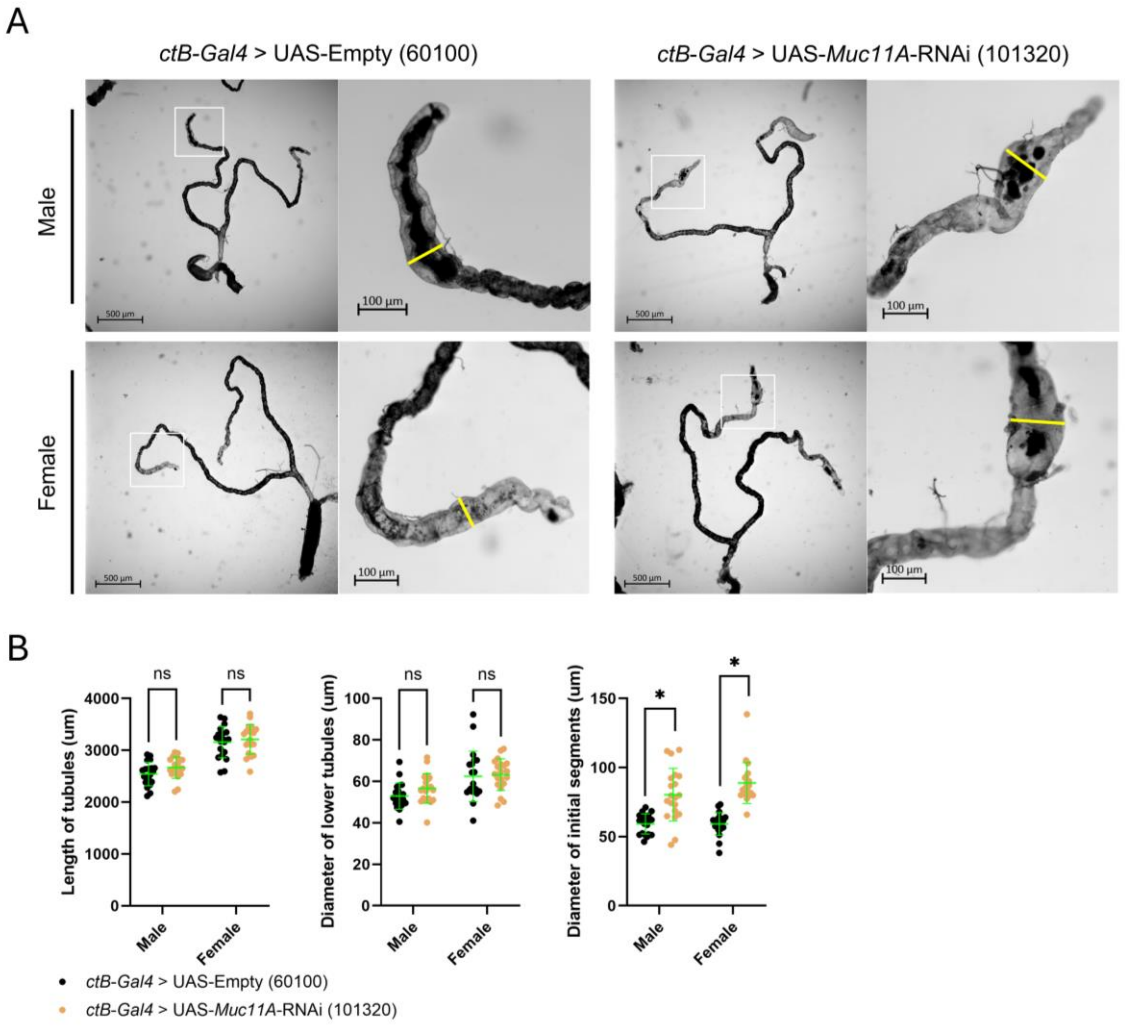

Figure 6.2 Abnormal morphology of the initial segment in *Muc11A* KD tubules. (A) Bright field images of control and *Muc11A* KD tubules. Scale bars represent 500 µm in unzoomed images and 100 µm in the zoomed-in images. (B) Quantification of tubule length and diameters. The diameter of the initial segment was measured at its widest point, as indicated by the yellow line. Individual tubules are represented as dots, with the mean and SD indicated. Two-way ANOVA followed by Sidak multiple comparisons test was performed. * means a p value less than 0.05.

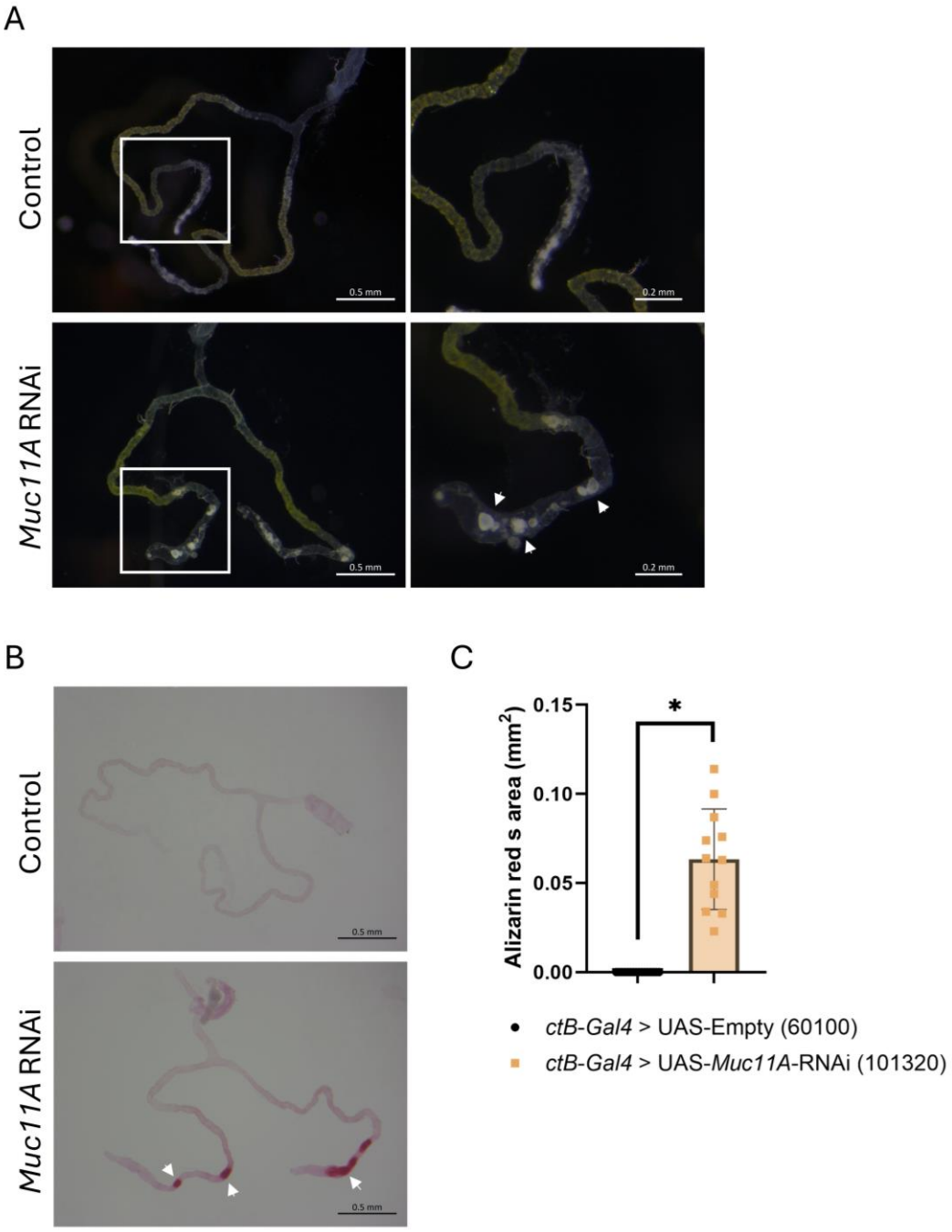

Figure 6.3 Development of kidney stones in *Muc11A* KD flies.
(A) Solid crystals indicated by white arrows, rather than diffused luminal granules, are present in the tubule lumen of RNAi flies. (B) Alizarin red staining of crystal-bearing *Muc11A* KD tubules (crystals stained in red are indicated by white arrows) and non-crystal bearing control tubules. (C) Quantification of the Alizarin red-stained area. Data are plotted as the mean with SD. A two tailed Student's *t*-test was used, and * for $\boldsymbol{p}$ value less than 0.05. Scale bars represent 500 µm in unzoomed images and 200 µm in zoomed-in images.

6.2.3 Proliferation of renal stem cells and impaired junction integrity in *Muc11A* KD tubules

In MTs containing xanthine stones, the loss of polyploid PCs is often observed due to their detachment from the tubule epithelium (Wang and Spradling, 2020, Wang and Spradling, 2022). Following injury, renal stem cells respond by proliferating and remodelling the damaged region. We suspected that renal stem cells in *Muc11A* KD flies would similarly react to mineralization by proliferating. As anticipated, an expanded population of renal stem cells was observed in the RNAi flies (Figure 6.4A and B). PH3 staining was used to mark mitotic cells in the MTs (Micchelli and Perrimon, 2006). No mitotic cells were observed in tubules with intact *Muc11A* expression (Figure 6.4C and D), as renal stem cells remain quiescent under normal conditions (Wang and Spradling, 2020). However, in *Muc11A* knockdown tubules, there was an increase in the number of PH3-positive cells, although not statistically significant. In addition to the proliferation of renal stem cells and their subsequent replenishment of PCs, a loss of the septate junction protein Dlg1 was also observed (Figure 6.5).

The physiological consequences of *Muc11A* knockdown were then assessed. No reduction in fluid secretion was observed, and chill coma recovery time remained unaffected (Figure 6.6A and B). To determine whether *Muc11A* knockdown affected fitness phenotypes, we examined egg-laying numbers and survival rates under a high salt diet. The results revealed that the loss of *Muc11A* in tubule principal cells reduced fecundity and increased the tolerance to high salt stress (Figure 6.6C and D).

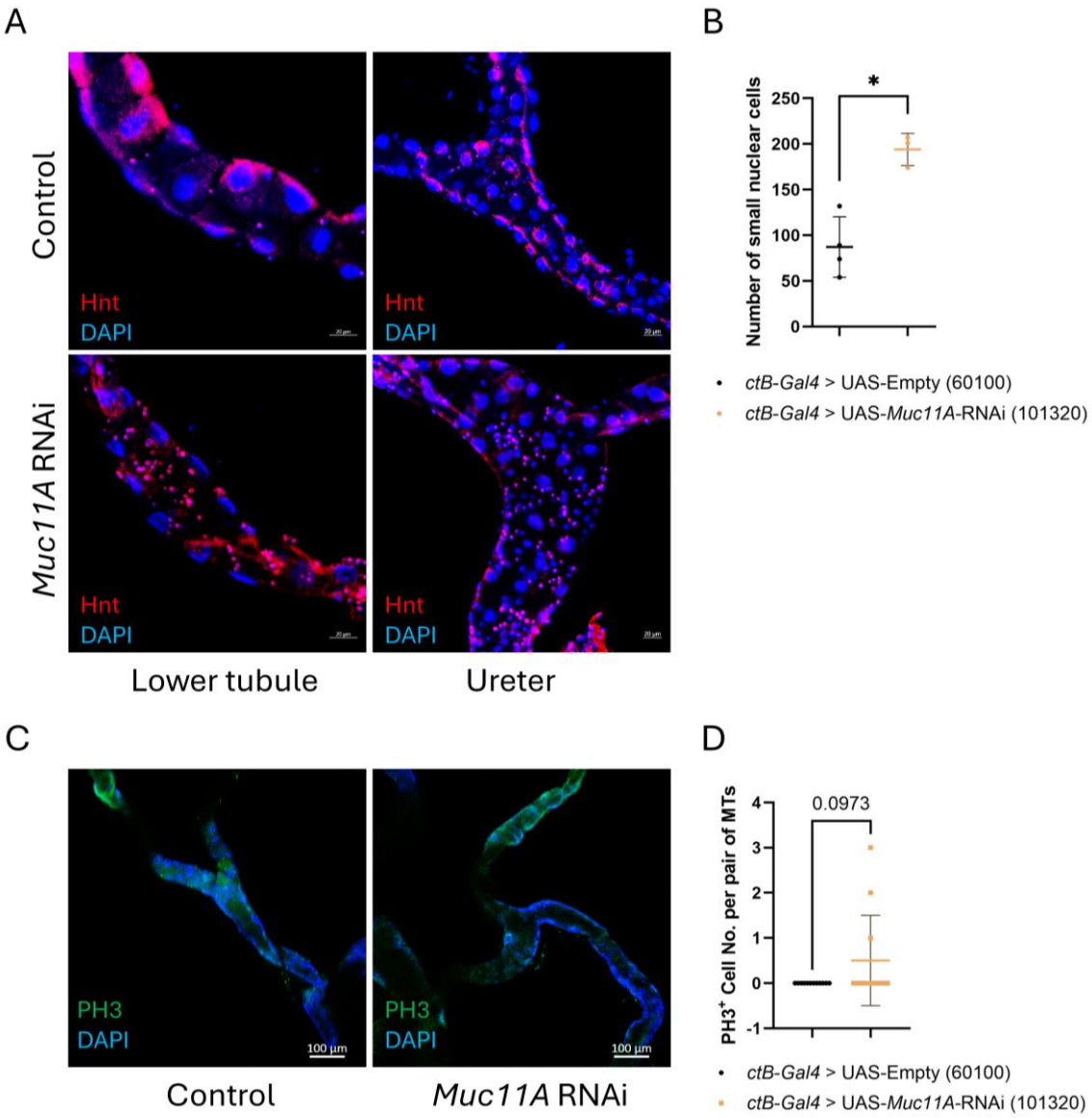

Figure 6.4 Proliferation of renal stem cells in *Muc11A* RNAi tubules.
(A) Immunostaining of Hnt in the lower tubule and ureter. Scale bars = 20 µm. (B) Quantification of the number of small nuclei in the tubules. (C) Immunostaining of PH3 (scale bars = 100 µm) and its quantification in (D). Data are presented as the mean with SD. Two tailed Student's *t*-test was used and * is labelled when p value less than 0.05.

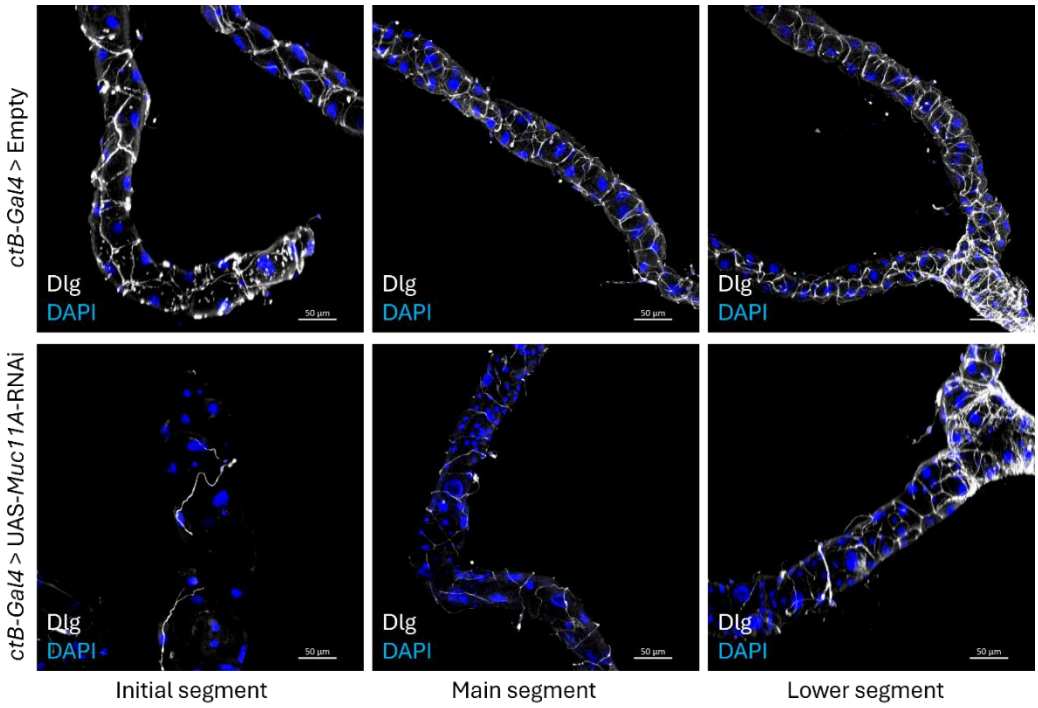

Figure 6.5 Loss of junction integrity of tubules with *Muc11A* inhibition.
Images of the initial segment, main segment, and lower tubules are shown. Scale bars = 50 µm.

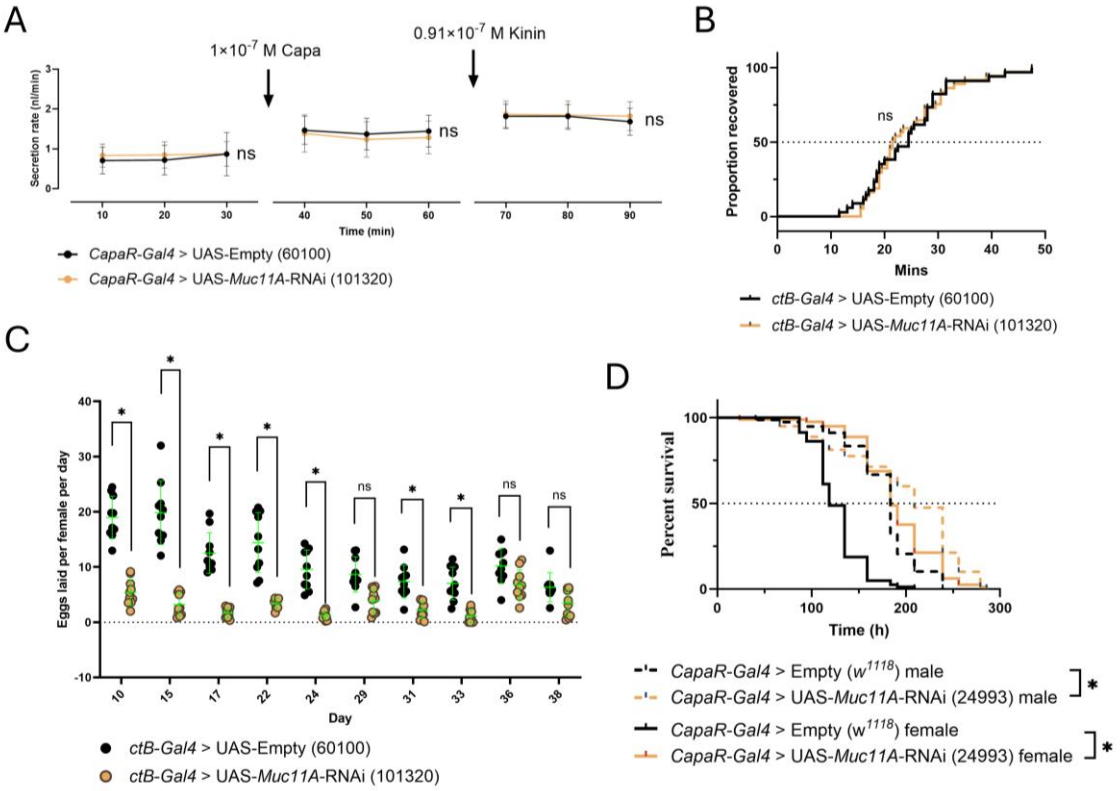

Figure 6.6 Physiological changes resulting from *Muc11A* knockdown.
(A) Fluid secretion rates in control and *Muc11A* KD tubules. Data are presented as mean with SD. (B) Chill coma recovery time for control and RNAi flies (control, n=34, median recovery time = 24.5; RNAi, n=37, median recovery time = 21.5). (C) Number of eggs laid by control and RNAi flies. Each dot represents an individual fly vial, with mean and SD plotted. Two-way ANOVA was performed for statistics. (D) Survival curves of control and RNAi flies under high salt conditions (3% NaCl) (control male, n=78, median survival = 183.5; control female, n=80, median survival = 118.5; RNAi male, n=80, median survival = 209; RNAi female, n=80, median survival = 183.5). Log-rank test was applied for survival analysis. The asterisk indicates that $\boldsymbol{p}$ value is less than 0.05, and ns means no significant difference.

6.3 Discussion

6.3.1 Tissue-enriched expression

Genes are expressed when they are required. Increases in gene expression incur energy costs (Wagner, 2005). How cells, tissues, and organs exhibit different gene and protein expression and what impact the global expression pattern has on the phenotype of different cells with distinct functions are central questions in human biology (Fagerberg et al., 2014). A human transcriptomics analysis,

which includes 20,050 protein-coding genes, has identified approximately 12% (3,499) tissue- or group-enriched genes (Fagerberg et al., 2014). Among these, 65 kidney-enriched genes have been defined, and immunohistochemistry analysis of 62 corresponding proteins has shown a strong bias for membrane-bound localisation. Additionally, 18 out of 20 highly tissue-enriched proteins are predicted to be transmembrane proteins, with 12 annotated as members of different solute carrier proteins. These findings suggest that the function of tissue-specific proteins is well in line with the function of the respective tissue or organ. For example, In *Drosophila*, the gene *rosy*, which encodes xanthine dehydrogenase, is enriched in the MTs, and its mutants develop xanthine-rich stones, mimicking the role of its human orthologue in causing classical xanthinuria (Mitchell and Glassman, 1959). Thus, studying tissue-enriched genes may offer valuable insights into the specialized functions of the tissue.

Mucins are large, extracellular glycoproteins comprised of many tandem repeats rich in serine, threonine, and proline (Bansil and Turner, 2006). In *Drosophila*, 17 mucin genes and 19 mucin-related genes have been identified (Syed et al., 2008). *Muc11A*, along with *Mur18B*, a mucin-related gene, is highly and specifically enriched in the MTs, as shown by FlyAtlas. Additionally, reverse transcription-PCR has shown that *Muc11A* is expressed throughout the development, with detectable expression also in fat body and proventriculus (Syed et al., 2008).

6.3.2 Function of *Muc11A* in MTs

We conducted a knockdown of *Muc11A* using PC-specific *Gal4* drivers and confirmed a high knockdown efficiency. Given its involvement in the formation of the extracellular matrix (ECM) and its chitin-binding domains (Syed et al., 2008), as well as ECM providing important biochemical and biomechanical cues for tissue morphogenesis, differentiation, and homeostasis (Frantz et al., 2010), we assessed the morphological changes in *Muc11A* RNAi tubules. In RNAi flies, we observed an enlarged initial segment of the renal tubules, with solid and condensed crystals instead of small spherical granules typically found in the

lumen. Additionally, the non-birefringent crystals formed in the tubules were found to contain calcium, as indicated by Alizarin red staining, suggesting that *Muc11A* knockdown impairs the maintenance of luminal granules. Consistent with observations in other fly lines harbouring renal crystals, the proliferation of renal stem cells was activated, as shown by positive labelling of Hnt and PH3. *Fst*, which shares homologous features with *Muc11A* and *Mur18B*, has been found to be essential for cold tolerance in *Drosophila* (Colinet et al., 2010). However, our study observed no changes in fluid secretion and chill coma recovery time. We further investigated whether other side-effects arise with *Muc11A* knockdown. Notably, a reduction in egg-laying and an increase in survival rate were observed in knockdown flies. However, in flies with remodelled MTs, trade-offs, such as reduced female fecundity and compromised salt tolerance, have been observed, along with thickened ECM and upregulated expression of several ECM and transmembrane transport genes in the tubules (Wang and Spradling, 2022). These elevated transport gene levels may explain the enhanced susceptibility to high salt stress in those flies. However, the reduced susceptibility to salt stress observed in our study needs further investigation.

During the embryogenesis, *Drosophila* Muc11A is expressed in the salivary glands from the stage 13. Its human orthologue, MUC1, is widely expressed on the surface of almost all epithelial cells (Bose and Mukherjee, 2020). In the mouse gastrointestinal tract, Muc1 acts as a critical element of the mucosal barrier to infection (McAuley et al., 2007). Following the oral infection, the bacterial pathogen *Campylobacter jejuni* is commonly detected in systemic organs of $Muc1^{-/-}$ mice within the first week, whereas wild-type mice are largely protected due to the presence of epithelial Muc1. Mucins, including MUC1, are highly glycosylated proteins. On the one hand, changes in host glycosylation cause inflammation; on the other hand, infection-induced inflammatory signalling can lead to changes in host glycosylation (Bose and Mukherjee, 2020). Moreover, the highly conserved cytoplasmic domain of MUC1 contains multiple protein binding motifs and phosphorylation sites, suggesting its important role in intracellular signalling. In humans, MUC1 exhibits immunofluorescence signals in the TAL, distal convoluted tubule, and collecting duct (Nie et al., 2016). Patients with

hypercalciuric nephrolithiasis have significantly decreased levels of urinary MUC1 compared with controls. The physical interaction between MUC1 and TRPV5, as well as with galectin-3, impairs the endocytosis of TRPV5, leading to increased urinary calcium reabsorption. These interactions suggest that enhancing MUC1 activity may be a potential strategy for treating calcium kidney stones. However, MUC1 is overexpressed and aberrantly glycosylated in epithelial cancers, where it interacts with galectin-3 to promote renal cancer progression and metastasis by clustering on the tumour cell surface (Yu et al., 2007). Moreover, the predominant expression of MUC1 mRNA and protein in the distal nephron and the urinary system may indicate segment-specific roles, such as distal nephron defence against ascending bacteria (Manrique-Caballero et al., 2025).

Chapter 7 Summary and Future Work

7.1 Summary

Given that *Drosophila* serves as an excellent model for studying human diseases, a multi-phenotypic genome-wide association screen for nephrolithiasis and secretion rates was conducted in the Malpighian tubules using the *Drosophila melanogaster* genetic reference panel. Numerous genetic polymorphisms were associated with the variation in quantitative traits in the study. The candidate genes harbouring these polymorphisms were functionally validated through RNAi-mediated knockdown. Several genes have been identified as being implicated in the development of renal crystals or in regulating fluid secretion rates. Biological processes such as the Wnt signalling pathway and extracellular acidification were linked to the development of renal stones, while categories including the electron transport chain, aerobic respiration, and mitochondrial ATP synthesis were found to contribute to baseline fluid secretion. Overall, this first global genotype-phenotype mapping study of renal function in *Drosophila* identified a group of novel loci and associated molecular pathways and validated candidate genes through RNAi-mediated silencing. These findings may increase our understanding of insect renal function and help to prioritise candidate human genes and pathways that serve as potential therapeutic targets for kidney stone disease and impaired tubular transport.

The second focus of this thesis is to investigate the role of *Fas3*, a candidate identified in a pilot GWA study, in the MTs. *Fas3* encodes an adhesion molecule that localises to the septate junction. Knockdown of *Fas3* in PCs and SCs exhibited distinct phenotypes in flies. In PCs, *Fas3* knockdown led to enlarged abdomens, with reduced fluid secretion rates and increased body water content, which were consistent with enhanced desiccation survival. Moreover, the presence of crystals in the tubular lumen was observed, accompanied by the proliferation of RSCs. However, in SCs, *Fas3* is required for the maintenance of its population and normal morphology, likely due to a loss of cytoarchitecture. Consequently, neuropeptide Kinin was unable to stimulate secretion rates in

Fas3 knockdown tubules, in contrast to controls. Additionally, inhibiting *Cdc42*, a small GTPase involved in polarity establishment, alone recapitulated the morphological defects in SCs observed with *Fas3* inhibition, and this defect was exacerbated by inhibition of both *Cdc42* and *Fas3*. Interestingly, while an increased number of SCs was observed upon activation of *Cdc42*, activating *Cdc42* in tubules with *Fas3* knockdown further reduced the SC population, compared with tubules where only *Fas3* was inhibited. Altogether, *Fas3* is necessary for the maintenance of the SC population and their mature morphology, as well as for the proper functioning of PCs.

A third focus of our study is the investigation of the role of the tubule-specific gene, *Muc11A*, in the MTs. Loss of *Muc11A* in PCs resulted in the formation of calcium renal stones, a phenomenon that parallels the function of its human orthologue, which is involved in the trans-epithelial uptake of calcium (Nie et al., 2016). In *Muc11A* RNAi tubules, impaired cellular junction integrity was observed, along with the proliferation of RSCs. However, these flies with *Muc11A* knockdown did not exhibit any changes in fluid secretion rates or cold tolerance. Notably, *Muc11A* RNAi flies displayed alterations in two other fitness traits: adult female fecundity and salt tolerance.

7.2 Limitations and future work

7.2.1 Genotype-phenotype mapping

The Bonferroni-adjusted threshold for multiple testing is considered the gold standard for genome-wide statistical significance in human GWA studies (Anholt and Mackay, 2018). With about 2.5 million common variants used in the association in the DGRP, the corresponding Bonferroni-corrected $\boldsymbol{p}$ value is approximately 2×10^{-8}. Although several polymorphisms have reached this threshold, the majority of variants fall below the significance threshold. Thus, the association analysis conducted using the DGRP is sufficiently powered to detect common variants with moderately large to large effects but is less effective for identifying variants with smaller effects (Mackay and Huang, 2018).

To enhance the power of GWA studies in detecting risk loci, several strategies can be employed. The first approach is to increase the sample size. The DGRP line have been expanded tenfold, from an initial 205 lines to the current 2,000 lines, which also entails a significant increase in workload. Therefore, without access to high-throughput phenotyping, collecting large-scale phenotypic data would be beyond the scope of a single researcher. Consequently, the adoption of high-throughput methods becomes essential. Alternatively, advanced intercross populations can be generated to facilitate fine mapping. A small number of lines with extreme phenotypes (Swarup et al., 2013), randomly selected lines (Huang et al., 2012), or genetically unrelated lines (Garlapow et al., 2017) can be crossed to create a base population. After many generations of intercrossing in large population sizes, a large number of animals with unique genotypes can be constructed. Bulk DNA sequencing of pooled individuals with extreme phenotypes can then be used to identify alleles that differentially segregate among these phenotypic extremes (Anholt and Mackay, 2018). This AIP-based strategy enables the detection of variants with low frequencies. However, it is worth noting that constructing an AIP may result in the loss of specific polymorphisms.

Most current GWA studies rely on single-marker approaches, testing the association between each individual polymorphism and the trait of interest. Although this approach can be effective when a single variant is responsible for the trait, it can be hard to estimate the joint effects of multiple genetic factors (Cho et al., 2010). Additionally, the need for multiple testing correction can make it too conservative to identify causal loci. Multicollinearity issues may arise, often due to LD, when attempting to incorporate information from multiple genetic variants. These issues become particularly problematic when the number of predictor variables far exceeds the sample sizes (Cho et al., 2010). This imbalance may increase the risk of overfitting, leading to associations that may not be replicable in new datasets.

Most polymorphisms associated with quantitative traits are usually intronic or intergenic loci, suggesting that they may exert a regulatory function. The

molecular functions of regulatory variants and the mechanisms causing alterations in gene expression are worth investigating in flies. One of the advantages of using *Drosophila* model is the availability of RNAi-mediated knockdown of candidate genes in a common isogenic background, which is frequently employed in DGRP GWA analyses (Mackay and Huang, 2018). However, disrupted gene expression due to mutations and RNAi are likely to have distinct effects than subtle naturally occurring polymorphisms (Mackay and Huang, 2018). Moreover, DNA polymorphisms do not directly affect variation in quantitative traits; intermediate phenotypes, such as transcript, protein, and metabolite abundance, might be attributed to the ultimate phenotypic variation, which facilitates the development of systems genetics approaches.

7.2.2 Functional verification

Functional studies of candidate genes in humans would be the most directly relevant for biomedical research; however, animal models have played a critical role in the exploration and characterization of disease pathophysiology, target identification, and the in vivo evaluation of novel therapeutic agents and treatments (McGonigle and Ruggeri, 2014). Given that more than 75% of human disease-causing genes are reported to have *Drosophila* orthologues (Reiter et al., 2001), and numerous fly lines have been constructed to express the human cDNA, it is relatively easy to build “humanized” fly models in which specific human genes are introduced to replace or supplement their fly counterparts. Human homologues of verified candidate genes, such as *FZD5* and *KIAA2013*, will be selected, along with those that exhibit kidney-enriched expression or altered expression under disease conditions. Two-pronged functional assays, based on rescue and overexpression experiments, can be employed to assess the function of variants or genes (Harnish et al., 2019). Specifically, endogenous fly genes are replaced with reference or variant human transgenes in the rescue experiments, whereas the reference and variant human protein are exogenously driven in a variety of tissues in the overexpression branch. Differences observed between the animal expressing reference and variant alleles would suggest a variant-specific effect (Harnish et al., 2019).

With the employment of human organoids, which are either stem cell-derived 3D culture systems or directly generated from patient biopsy samples, researchers can address questions that are difficult to investigate using animal models (Kim et al., 2020). The *SLC2A9* variant rs16890979 has been shown to affect serum uric acid levels (McArdle et al., 2008). To study the impact of this SNP on uric acid metabolism, kidney organoids derived from human embryonic stem cells with rs16890979 mutants have been constructed (Wu et al., 2024). The result shows that the introduction of this missense mutation reduces the uric acid absorption, together with increased absorption observed in *SLC2A9*-overexpressing organoids and decreased absorption in those with *SLC2A9* knockdown. Moreover, multi-lineage kidney assembloids enable controlled integration between nephrons and a single collecting duct, effectively mimicking functional kidney architecture (Wilson et al., 2025). A 3D bioprinted multiorgan hyperoxaluria model has been developed to recapitulate calcium oxalate crystallization and crystal-induced injuries in proximal tubules (Yoon et al., 2022). Therefore, shortlisted human genes relating to the crystal formation can be directed validated with the use of human kidney organoids or assembloids and CRISPR/Cas9.

This thesis has thus demonstrated the utility of a systematic, unbiased screen in identifying genes of interest in renal function in insects and prioritising candidate human orthologues.

Appendices

Appendix 1 List of the DGRP lines

DGRP line	BDRC number	DGRP line	BDRC number	DGRP line	BDRC number
DGRP-208	25174	DGRP-176	28149	DGRP-804	28236
DGRP-301	25175	DGRP-177	28150	DGRP-805	28237
DGRP-303	25176	DGRP-181	28151	DGRP-808	28238
DGRP-304	25177	DGRP-189	28152	DGRP-810	28239
DGRP-307	25179	DGRP-195	28153	DGRP-812	28240
DGRP-313	25180	DGRP-217	28154	DGRP-818	28241
DGRP-315	25181	DGRP-227	28156	DGRP-819	28242
DGRP-324	25182	DGRP-228	28157	DGRP-821	28243
DGRP-335	25183	DGRP-239	28161	DGRP-822	28244
DGRP-357	25184	DGRP-256	28162	DGRP-832	28245
DGRP-358	25185	DGRP-280	28164	DGRP-837	28246
DGRP-360	25186	DGRP-287	28165	DGRP-843	28247
DGRP-362	25187	DGRP-309	28166	DGRP-849	28248
DGRP-375	25188	DGRP-317	28167	DGRP-850	28249
DGRP-379	25189	DGRP-318	28168	DGRP-855	28251
DGRP-380	25190	DGRP-332	28171	DGRP-857	28252
DGRP-391	25191	DGRP-336	28172	DGRP-861	28253
DGRP-399	25192	DGRP-338	28173	DGRP-879	28254
DGRP-427	25193	DGRP-340	28174	DGRP-882	28255
DGRP-437	25194	DGRP-350	28176	DGRP-884	28256
DGRP-486	25195	DGRP-356	28178	DGRP-890	28257
DGRP-517	25197	DGRP-359	28179	DGRP-892	28258
DGRP-555	25198	DGRP-361	28180	DGRP-897	28260
DGRP-639	25199	DGRP-370	28182	DGRP-900	28261
DGRP-707	25200	DGRP-371	28183	DGRP-907	28262
DGRP-712	25201	DGRP-373	28184	DGRP-908	28263
DGRP-730	25202	DGRP-374	28185	DGRP-911	28264
DGRP-732	25203	DGRP-377	28186	DGRP-913	28265
DGRP-765	25204	DGRP-381	28188	DGRP-85	28274
DGRP-774	25205	DGRP-382	28189	DGRP-235	28275
DGRP-786	25206	DGRP-383	28190	DGRP-310	28276
DGRP-799	25207	DGRP-385	28191	DGRP-409	28278
DGRP-820	25208	DGRP-386	28192	DGRP-40	29651
DGRP-852	25209	DGRP-392	28194	DGRP-57	29652
DGRP-859	25210	DGRP-426	28196	DGRP-229	29653
DGRP-365	25445	DGRP-440	28197	DGRP-320	29654
DGRP-705	25744	DGRP-441	28198	DGRP-321	29655

DGRP-714	25745	DGRP-443	28199	DGRP-405	29656
DGRP-21	28122	DGRP-461	28200	DGRP-406	29657
DGRP-26	28123	DGRP-491	28202	DGRP-513	29659
DGRP-28	28124	DGRP-492	28203	DGRP-306	37525
DGRP-38	28125	DGRP-502	28204	DGRP-31	55014
DGRP-41	28126	DGRP-508	28205	DGRP-32	55015
DGRP-42	28127	DGRP-509	28206	DGRP-48	55016
DGRP-45	28128	DGRP-531	28207	DGRP-100	55017
DGRP-59	28129	DGRP-535	28208	DGRP-319	55018
DGRP-69	28130	DGRP-563	28211	DGRP-348	55019
DGRP-73	28131	DGRP-584	28212	DGRP-354	55020
DGRP-75	28132	DGRP-589	28213	DGRP-390	55021
DGRP-83	28134	DGRP-595	28215	DGRP-395	55022
DGRP-88	28135	DGRP-703	28218	DGRP-397	55023
DGRP-91	28136	DGRP-716	28219	DGRP-505	55024
DGRP-93	28137	DGRP-721	28220	DGRP-528	55025
DGRP-101	28138	DGRP-738	28223	DGRP-551	55026
DGRP-105	28139	DGRP-748	28224	DGRP-559	55027
DGRP-109	28140	DGRP-757	28226	DGRP-566	55028
DGRP-129	28141	DGRP-761	28227	DGRP-596	55029
DGRP-136	28142	DGRP-776	28229	DGRP-627	55030
DGRP-138	28143	DGRP-783	28230	DGRP-630	55031
DGRP-142	28144	DGRP-790	28232	DGRP-634	55032
DGRP-149	28145	DGRP-796	28233	DGRP-355	55038
DGRP-153	28146	DGRP-801	28234	DGRP-352	83728
DGRP-161	28148	DGRP-802	28235	DGRP-737	83729

Appendix 2 List of primers

Gene	Forward primary sequence (5'-3')	Reverse primary sequence (5'-3')
RpL32	TCTTTTCGCTTCTGGTTTCCG	CTTGCGCCATTTGTGCGAC
CG7289	TGATGACAACAAGGCGGTGA	TTGTCGTCGGTTTTGCGTGA
Dlg5	GAGTGTGTTGGTGTTTCGCA	ACATACTCCGAGCTCTCTTCCT
fz2	TAACTTTGACAGACGCACGG	CAAACGGCGTGGTCTAACATT
Shab	GTTTCTGCACGACCAAGGACT	ATAGGCTCCTGCTTGACGAC
SPR	TCAGATTTACCAAGTGCAAGAATGT	TGGCGCTGCCTTAATTCTCA
Muc11A	CAGTGCGTTGATGACCTGAC	CTTGACCGGCACACAAATCTC

Appendix 3 Stone areas and tubule sizes of the DGRP lines

BDRC number	Stone area (mm^2)	Tubule size (mm^2)	BDRC number	Stone area (mm^2)	Tubule size (mm^2)
25745	0.00052	0.26550	28235	0.02350	0.35030
28129	0.00096	0.29879	25182	0.02374	0.27162
28145	0.00112	0.34470	28140	0.02385	0.31835
28130	0.00245	0.25006	28137	0.02389	0.27452
28126	0.00266	0.36000	29652	0.02400	0.30500
28149	0.00331	0.30268	55014	0.02400	0.26013
28146	0.00355	0.31329	29654	0.02402	0.29102
28134	0.00462	0.35931	28173	0.02450	0.32366
28207	0.00463	0.30450	25204	0.02454	0.30623
28260	0.00542	0.30865	28179	0.02540	0.28277
28174	0.00544	0.30848	25174	0.02559	0.27448
55038	0.00552	0.30517	28156	0.02606	0.28550
28178	0.00569	0.34344	28127	0.02607	0.34355
28131	0.00610	0.32908	28143	0.02608	0.26660
25195	0.00614	0.31071	25189	0.02620	0.24890
28212	0.00622	0.30352	25194	0.02670	0.30179
28232	0.00704	0.28467	28194	0.02677	0.29123
28239	0.00794	0.37856	25209	0.02683	0.23796
28196	0.00846	0.35067	28254	0.02683	0.28700
25198	0.00846	0.28792	25175	0.02685	0.44123
28172	0.00880	0.30500	28218	0.02687	0.25987
28242	0.00905	0.28236	28162	0.02733	0.43900
28245	0.00915	0.37485	28184	0.02742	0.31059
55021	0.00946	0.33895	28237	0.02761	0.28109
29659	0.00965	0.26238	28241	0.02782	0.32255
25180	0.00976	0.28608	28198	0.02818	0.29797
25181	0.00981	0.33286	37525	0.02852	0.34040
28255	0.01012	0.35600	25203	0.02882	0.30382
28276	0.01027	0.28088	25192	0.02936	0.27704
28226	0.01046	0.39567	29653	0.02937	0.28307
28171	0.01150	0.23037	28153	0.02947	0.32195
55024	0.01170	0.35026	83728	0.02958	0.32676
28157	0.01186	0.26893	28275	0.02972	0.33642
28240	0.01188	0.36088	55027	0.02973	0.37188
28192	0.01289	0.21200	28233	0.02978	0.30878
55020	0.01297	0.27650	83729	0.02983	0.32652
25208	0.01297	0.29738	28138	0.02996	0.27363
28164	0.01321	0.27525	55023	0.03008	0.28246
28148	0.01325	0.30592	28205	0.03020	0.32473

25188	0.01378	0.32719	28278	0.03038	0.25450
28136	0.01378	0.27113	28135	0.03050	0.39017
28256	0.01390	0.29177	55032	0.03057	0.30497
28188	0.01436	0.26317	55016	0.03058	0.30674
28128	0.01479	0.30221	28182	0.03107	0.29871
28274	0.01484	0.28888	28204	0.03118	0.26515
28122	0.01487	0.30640	55029	0.03119	0.32762
25190	0.01509	0.24239	28220	0.03127	0.26891
25193	0.01568	0.27792	25187	0.03149	0.26206
29651	0.01580	0.26635	25207	0.03167	0.30450
25210	0.01580	0.25184	25445	0.03167	0.37742
25199	0.01640	0.28710	28253	0.03235	0.37440
28200	0.01667	0.32400	28183	0.03250	0.27415
28186	0.01668	0.24977	28229	0.03255	0.28129
25744	0.01693	0.34257	55015	0.03275	0.32505
28165	0.01742	0.29055	28243	0.03339	0.33913
29655	0.01756	0.29278	28199	0.03391	0.35989
28211	0.01757	0.31540	28246	0.03471	0.43495
28125	0.01770	0.30760	55019	0.03512	0.27997
25206	0.01785	0.30623	28263	0.03521	0.26246
25200	0.01791	0.24831	28150	0.03529	0.35147
25205	0.01809	0.23645	28180	0.03557	0.28239
25191	0.01833	0.30413	28203	0.03596	0.34208
55031	0.01850	0.31343	55017	0.03668	0.32512
28132	0.01892	0.27765	25177	0.03700	0.32130
55026	0.01919	0.30187	28142	0.03750	0.27592
28215	0.01929	0.33971	28227	0.03763	0.30038
28151	0.01948	0.30596	28252	0.03808	0.32858
28123	0.01956	0.29938	28249	0.03838	0.30306
28152	0.01973	0.28940	28206	0.04037	0.26622
25183	0.01977	0.24191	25184	0.04165	0.26290
28202	0.02013	0.35656	28248	0.04329	0.41057
28168	0.02017	0.29517	28265	0.04406	0.27982
28213	0.02062	0.31138	55018	0.04435	0.27645
29656	0.02064	0.32904	28191	0.04479	0.28688
28144	0.02071	0.25954	28139	0.04594	0.28056
55025	0.02072	0.36294	28154	0.04612	0.37448
28264	0.02077	0.29100	28167	0.04681	0.35186
28247	0.02107	0.30104	28238	0.04731	0.31777
25201	0.02117	0.32823	28251	0.04750	0.34231
55030	0.02133	0.27267	28236	0.04900	0.34288
28234	0.02140	0.31373	28230	0.04953	0.33659
28257	0.02143	0.25917	28258	0.04960	0.38136
28185	0.02150	0.37204	25185	0.04975	0.31217
28224	0.02154	0.26392	28244	0.05125	0.32497
28261	0.02156	0.29867	28262	0.05206	0.27391

25176	0.02163	0.27163	55022	0.05244	0.29756
28197	0.02164	0.34476	28219	0.05365	0.31453
29657	0.02173	0.27718	28124	0.05409	0.26100
25197	0.02184	0.37025	28223	0.05518	0.33659
28141	0.02187	0.32117	55028	0.05548	0.31791
25179	0.02252	0.32803	25202	0.05600	0.33690
28190	0.02262	0.31688	25186	0.06008	0.30971
28208	0.02263	0.32266	28161	0.06378	0.35416

Appendix 4 Fluid secretion rates of the DGRP lines

BDRC number	Basal secretion rate (nl/min)	Capa-stimulated secretion rate (nl/min)	Capa&Kinin-stimulated secretion rate (nl/min)
28278	0.39623	0.92707	1.71497
29652	0.39872	0.78920	1.56715
25200	0.46265	0.83483	1.96852
25179	0.47368	0.66533	1.31519
28212	0.53862	0.62094	1.15573
55020	0.54123	1.34339	2.54753
28257	0.56380	1.07495	1.84565
28157	0.60210	1.19965	2.01705
25201	0.61124	0.93663	1.41560
28260	0.62187	1.01158	2.10812
28139	0.62284	0.99026	1.63880
29654	0.63042	0.74426	1.09204
28262	0.63985	1.11134	1.75092
28224	0.64152	1.00550	1.40320
28276	0.66191	1.15569	1.81229
25190	0.66472	1.43355	1.84494
28182	0.69081	1.25069	2.13551
37525	0.71484	0.73348	1.72004
28162	0.71768	1.15864	2.52928
25210	0.73267	1.07964	1.77789
28242	0.73291	1.34612	2.02653
25744	0.74372	1.14048	1.97005
28184	0.74999	1.04636	1.40683
28255	0.77074	1.24003	2.82741
28233	0.77586	0.85748	1.44511

28122	0.77650	1.34678	2.25946
28227	0.78081	1.13596	1.55003
28200	0.78139	1.15865	2.08133
29655	0.78486	1.48501	1.83105
28232	0.80379	1.05619	1.96847
25198	0.80856	1.39639	2.68311
28265	0.82278	1.32474	1.75058
28264	0.83301	1.46943	2.22787
28220	0.83793	1.45093	2.10035
28249	0.84072	1.34776	1.91824
28245	0.84331	1.42323	1.62656
28206	0.84439	1.03864	2.52231
28168	0.85646	1.32288	3.38068
25189	0.86787	1.11667	1.51168
83729	0.86806	1.31801	1.67148
28208	0.88637	1.01142	1.19385
28123	0.91632	1.32091	1.30646
28185	0.91667	1.38768	2.93814
55021	0.91670	1.39912	2.08771
25745	0.91758	1.26729	1.85493
28191	0.92220	1.33318	2.10696
25204	0.92936	1.15688	1.95429
28130	0.94004	1.76958	1.84136
25176	0.94198	1.31479	3.12886
28183	0.94441	1.61913	2.13039
28188	0.94523	1.43249	1.69130
28144	0.95328	1.48177	1.98649
28137	0.95349	1.69020	2.82086
55030	0.95371	1.40233	2.26070
55015	0.96025	1.49157	1.57732
55019	0.96091	1.91427	2.67026
28207	0.96512	1.34489	1.75182
28246	0.98008	1.47228	3.95574
25207	0.98129	1.52401	1.88657
25184	1.00634	1.72489	2.58504
25203	1.00726	1.90636	2.32864
55022	1.01341	1.23045	1.55364
28153	1.01521	1.56292	2.31512

28167	1.03415	1.80110	2.83284
28240	1.04113	1.43499	2.53077
28248	1.04147	1.61271	2.47771
25192	1.04269	1.63144	2.78375
28223	1.04401	1.91141	2.42228
55016	1.04457	1.92733	2.79624
55028	1.04626	1.85989	3.44416
28263	1.05167	1.94114	2.68165
28258	1.05799	1.56772	2.64349
55025	1.05929	1.23999	1.30504
28176	1.06212	1.57070	1.94767
25193	1.06757	1.51212	1.83101
28244	1.06904	1.42627	2.20956
28219	1.07116	1.54022	2.24312
28213	1.07160	1.37744	1.53446
28152	1.07270	1.90899	2.27844
28143	1.07783	1.54085	1.98257
25209	1.07839	1.44874	2.08982
28164	1.08145	1.73870	2.28561
28151	1.09419	1.36116	1.77105
25180	1.09590	1.42326	2.14846
29657	1.10424	1.37741	2.13390
55031	1.10646	1.62392	2.24279
28234	1.10748	1.43109	1.75161
25199	1.10782	1.49186	1.99783
28211	1.10917	1.73260	2.58640
25205	1.11137	1.42717	1.70068
28275	1.12390	1.81855	2.34389
28161	1.12949	1.89324	3.32484
28256	1.12994	1.51154	1.58063
25206	1.13188	1.67267	2.67553
28124	1.13549	2.15213	2.11597
28215	1.14410	1.87937	2.57218
25186	1.14720	1.92798	2.38676
28131	1.14809	1.39602	1.53394
28198	1.14952	1.81801	1.84842
28253	1.15651	2.22182	3.01843
55032	1.16171	1.79664	2.98143

28127	1.17241	1.54986	1.70593
28192	1.18696	2.09697	2.47292
28173	1.18746	1.73403	2.98823
28179	1.18784	1.05132	1.32911
28189	1.19130	2.16976	3.25820
28261	1.19310	2.04255	2.99877
28194	1.19478	2.17070	2.93270
28128	1.19596	1.29732	1.70839
55024	1.20422	1.82303	2.73972
29653	1.22577	1.85021	2.95840
28132	1.22599	1.66121	2.16757
25182	1.23561	1.48354	1.81512
28149	1.23952	2.46071	3.18613
28148	1.24068	1.90323	3.02725
28138	1.24511	1.67326	1.94367
28166	1.25321	1.55663	2.01552
28251	1.25815	1.65052	2.66485
28235	1.27500	1.49180	1.88361
25177	1.27780	1.84283	2.54811
25185	1.29282	2.07438	3.24773
28243	1.31668	1.94135	2.23084
28218	1.31984	2.15578	3.16964
28238	1.32535	2.38109	3.01481
25188	1.32952	1.61111	2.37218
28236	1.33546	2.00463	2.43726
28226	1.34447	2.82348	3.48722
28204	1.34563	2.06042	2.49719
28126	1.34813	1.96658	2.27667
28229	1.34894	1.42244	1.38647
28199	1.35494	2.19294	2.97046
28274	1.36124	2.07069	3.39173
28125	1.37275	1.88086	2.02469
25181	1.37864	2.74766	3.60732
28150	1.38215	2.09535	2.64142
28140	1.39019	1.50014	1.47676
28197	1.39699	1.95880	2.31636
28134	1.40128	1.71979	2.20090
83728	1.40554	2.04569	2.57750

28205	1.40585	1.55348	1.92815
25195	1.41724	1.89055	2.52606
28252	1.43407	2.02273	4.56210
28165	1.45389	2.25514	2.62713
55018	1.45766	1.86398	2.75893
28196	1.46304	2.30194	3.05433
25194	1.46440	1.52458	1.62403
28178	1.46446	2.45432	3.37475
25197	1.46797	2.40672	3.63504
55026	1.48004	2.52971	3.25165
28145	1.50436	2.99279	3.09363
28172	1.51244	1.76434	1.91024
28141	1.52486	1.68544	1.85082
28239	1.56241	2.40433	3.18452
28247	1.57157	2.09685	2.22600
55014	1.57778	2.16884	2.53607
25187	1.59110	2.03509	2.57540
28136	1.60024	2.10875	2.64826
55038	1.61474	2.07045	2.49824
28190	1.64908	2.10154	2.26676
28142	1.65917	2.38358	2.62677
25202	1.68677	2.02540	2.78480
28171	1.69611	2.43823	3.05336
25183	1.69985	2.33221	2.25386
28254	1.71086	2.17905	2.49984
28135	1.72229	2.06885	2.09421
25174	1.76084	2.22548	2.17191
28154	1.77596	2.42162	3.19533
55027	1.77771	2.13895	3.04546
25191	1.85049	2.84358	4.47152
28146	1.87330	2.52850	2.70795
55023	1.88110	2.34249	2.89774
25175	1.88688	2.44447	3.01045
25445	1.88795	2.44267	3.17998
28186	1.89889	2.70134	3.46940
28180	1.94058	2.36449	2.56956
28129	1.94303	2.00256	1.94846
28241	2.01815	2.30838	2.00410

28203	2.06236	3.08006	3.44190
28202	2.14034	3.12384	3.36948
55017	2.21575	3.08265	3.64095
28230	2.24209	2.85601	3.32816
29656	2.43777	2.87913	3.16991
25208	2.85299	3.22411	3.26859

Appendix 5 Top polymorphisms of analysis of stone area

Chr	SNP ID	Minor allele	Major allele	Allele frequency	p value
X	X_3542388_SNP	A	T	0.027	4.6812E-06
X	X_5001451_DEL	A	CAAAAT	0.079	9.77547E-06
X	X_5370595_SNP	A	G	0.022	5.15425E-06
X	X_5383133_SNP	T	C	0.022	1.66715E-06
X	X_17703972_SNP	G	A	0.033	9.89372E-06
X	X_20428796_INS	CC	C	0.023	9.16323E-07
2L	2L_285219_SNP	A	G	0.027	2.96022E-06
2L	2L_1120269_SNP	T	A	0.032	5.2667E-06
2L	2L_1249360_SNP	G	A	0.022	8.03724E-06
2L	2L_1486779_SNP	T	G	0.039	1.2503E-06
2L	2L_1950507_SNP	T	G	0.347	5.73572E-06
2L	2L_1982408_SNP	C	T	0.225	3.33527E-06
2L	2L_1982416_SNP	A	C	0.197	5.5099E-06
2L	2L_1982443_SNP	T	C	0.223	3.30143E-06
2L	2L_1982569_SNP	C	T	0.2	5.72173E-06
2L	2L_1982815_SNP	A	C	0.242	3.10787E-06
2L	2L_2426283_SNP	A	C	0.038	6.52344E-06
2L	2L_5396722_SNP	T	C	0.077	6.18927E-06
2L	2L_11509271_DEL	C	CTGTCC	0.091	6.31497E-06
2L	2L_15058974_SNP	C	T	0.253	5.77477E-06
2L	2L_20529315_SNP	T	C	0.253	1.32183E-06
2R	2R_800914_SNP	T	C	0.023	9.76187E-07
2R	2R_1142218_INS	AA	A	0.023	3.7E-06
2R	2R_5252821_SNP	C	T	0.229	7.26896E-06
2R	2R_5637813_SNP	G	C	0.022	5.68177E-06
2R	2R_6439647_SNP	T	G	0.284	2.39705E-06
2R	2R_16501261_SNP	T	A	0.086	5.07464E-06

2R	2R_18287816_SNP	G	A	0.354	6.21888E-06
2R	2R_19193174_DEL	T	TT	0.39	2.96642E-06
2R	2R_19193199_SNP	C	T	0.407	8.27508E-06
2R	2R_19350041_SNP	G	C	0.033	1.70596E-06
2R	2R_19350346_SNP	T	A	0.032	2.20746E-06
3L	3L_1680036_DEL	C	CC	0.032	7.74366E-06
3L	3L_1680045_SNP	C	G	0.032	7.74366E-06
3L	3L_1787565_SNP	T	C	0.022	9.1422E-06
3L	3L_2921152_SNP	G	C	0.238	9.73869E-06
3L	3L_2957059_SNP	A	C	0.351	6.07826E-06
3L	3L_2998114_SNP	T	A	0.098	2.90801E-07
3L	3L_5520198_SNP	A	G	0.038	9.93903E-06
3L	3L_7033608_INS	AA	A	0.029	7.83841E-06
3L	3L_7369366_SNP	T	G	0.022	6.55657E-06
3L	3L_7383180_SNP	C	G	0.022	7.08718E-06
3L	3L_15220891_SNP	A	G	0.088	6.2387E-06
3L	3L_15220917_SNP	G	A	0.083	4.38025E-07
3L	3L_15224069_DEL	C	CTC	0.055	3.62768E-06
3L	3L_15224108_DEL	G	GTTAGCTCG AGGGG	0.101	9.53118E-06
3L	3L_15225021_SNP	T	C	0.044	4.22195E-06
3L	3L_15505476_SNP	G	A	0.033	7.63607E-06
3L	3L_15505541_SNP	T	C	0.033	7.63607E-06
3L	3L_15506131_SNP	T	C	0.038	8.21403E-06
3L	3L_15507465_SNP	C	G	0.033	7.72593E-06
3L	3L_15526152_SNP	T	C	0.029	5.09083E-07
3L	3L_19185369_SNP	C	T	0.19	2.93061E-06
3L	3L_21922396_SNP	G	A	0.046	7.34651E-06
3R	3R_7880447_SNP	T	C	0.04	4.7705E-06
3R	3R_7891686_SNP	T	A	0.056	6.22966E-06
3R	3R_7894461_DEL	C	CTT	0.049	4.2061E-06
3R	3R_8977317_SNP	C	G	0.061	8.66496E-06
3R	3R_9002714_SNP	C	A	0.071	6.61372E-06
3R	3R_9003314_SNP	A	G	0.071	7.32803E-07
3R	3R_9004897_SNP	G	A	0.073	9.31953E-06
3R	3R_12016019_SNP	G	C	0.432	6.98192E-06
3R	3R_12704988_SNP	T	A	0.165	6.17035E-06
3R	3R_12705003_SNP	C	T	0.161	9.84109E-06

3R	3R_13097288_SNP	A	T	0.164	2.8028E-06
3R	3R_13346004_SNP	G	C	0.071	5.14531E-06
3R	3R_13491749_SNP	G	C	0.022	3.1594E-06
3R	3R_20593265_SNP	G	A	0.063	5.4661E-06

Appendix 6 Top polymorphisms of analysis of basal secretion rate

Chr	SNP ID	Minor allele	Major allele	Allele frequency	p value
X	X_2948798_SNP	G	C	0.022	6.68158E-06
X	X_4850767_SNP	T	A	0.105	4.40828E-06
X	X_4851226_INS	ACATA	A	0.105	3.69776E-06
X	X_4851239_SNP	C	T	0.094	9.83195E-06
X	X_6550831_SNP	T	G	0.028	1.62256E-06
X	X_6576223_SNP	G	T	0.033	2.14255E-07
X	X_8107539_DEL	A	AGAAA	0.033	1.13937E-06
X	X_8107551_SNP	A	G	0.039	9.55258E-07
X	X_8107612_SNP	G	T	0.034	7.60786E-07
X	X_8109749_SNP	A	G	0.055	1.85195E-06
X	X_8149631_SNP	C	G	0.108	7.87853E-06
X	X_8328135_SNP	C	G	0.101	4.6514E-06
X	X_8349363_SNP	G	A	0.475	6.56218E-06
X	X_10899677_SNP	C	A	0.056	3.33699E-07
X	X_12524917_SNP	G	A	0.027	8.62376E-08
X	X_12527726_SNP	T	A	0.022	5.42279E-06
X	X_13499163_INS	TTT	T	0.023	8.70141E-06
X	X_15032128_SNP	A	G	0.265	9.31469E-06
X	X_15896884_SNP	T	C	0.027	6.3929E-06
X	X_17584929_SNP	A	C	0.024	4.78155E-06
X	X_20472216_DEL	G	GAT	0.083	7.20456E-06
X	X_20472221_SNP	A	T	0.073	1.31216E-06
X	X_20472222_SNP	C	A	0.083	7.20456E-06
2L	2L_616482_SNP	G	A	0.022	2.68039E-06
2L	2L_2965218_SNP	G	A	0.056	8.56623E-06
2L	2L_3146240_SNP	T	C	0.022	3.58991E-06
2L	2L_3859676_SNP	A	G	0.129	2.86908E-06

2L	2L_4888223_SNP	A	G	0.022	9.15395E-07
2L	2L_5668587_SNP	A	T	0.08	8.63861E-06
2L	2L_7377435_SNP	A	G	0.022	1.50302E-06
2L	2L_7378867_SNP	T	C	0.027	4.39868E-06
2L	2L_7381870_SNP	A	G	0.038	2.10084E-06
2L	2L_7889317_SNP	A	T	0.033	3.45345E-06
2L	2L_7897614_SNP	A	T	0.022	1.21973E-06
2L	2L_10343636_SNP	T	A	0.022	1.67686E-06
2L	2L_10343637_SNP	A	G	0.022	1.65698E-06
2L	2L_10752737_SNP	T	C	0.022	5.55963E-06
2L	2L_11822426_SNP	A	T	0.045	2.66751E-08
2L	2L_12943802_SNP	G	C	0.103	6.44359E-06
2L	2L_12943931_SNP	G	A	0.092	5.73312E-06
2L	2L_14430388_SNP	T	C	0.154	7.05887E-06
2L	2L_17347799_SNP	T	C	0.04	8.80904E-06
2L	2L_17347801_INS	ATACTAAATG CACT	A	0.04	8.80904E-06
2L	2L_17347803_SNP	A	T	0.04	9.72596E-06
2L	2L_17439561_SNP	T	C	0.028	6.48649E-06
2L	2L_17514645_SNP	T	G	0.056	2.2525E-08
2R	2R_766549_SNP	A	T	0.023	5.06021E-08
2R	2R_774276_SNP	C	T	0.028	4.11947E-07
2R	2R_776690_SNP	T	A	0.022	6.02524E-08
2R	2R_782125_SNP	T	C	0.024	5.97624E-08
2R	2R_5085232_SNP	A	G	0.028	2.87606E-06
2R	2R_5088270_SNP	A	G	0.028	2.87606E-06
2R	2R_5088554_SNP	C	G	0.022	5.75919E-07
2R	2R_5089146_SNP	G	A	0.028	4.16943E-06
2R	2R_5089160_SNP	T	A	0.028	4.58532E-06
2R	2R_5093478_SNP	C	G	0.028	8.66146E-09
2R	2R_5100141_SNP	T	A	0.033	4.33097E-06
2R	2R_5403701_SNP	A	G	0.027	1.60681E-06
2R	2R_7324767_SNP	G	A	0.073	5.97307E-06
2R	2R_7917626_SNP	T	A	0.022	2.51298E-06
2R	2R_7921599_SNP	G	A	0.022	3.00928E-06
2R	2R_7931734_SNP	G	A	0.022	2.9399E-06
2R	2R_7931820_SNP	T	C	0.022	2.1706E-06
2R	2R_7931890_SNP	T	C	0.023	3.56814E-06

2R	2R_11085349_SNP	A	T	0.083	6.98304E-07
2R	2R_15289173_INS	ATAGATAG	A	0.023	1.54805E-07
2R	2R_15596206_DEL	A	ACCA	0.089	7.90106E-06
2R	2R_15596220_SNP	A	T	0.084	3.85966E-06
2R	2R_15596227_DEL	T	TTCT	0.09	6.09259E-06
2R	2R_16876197_SNP	C	G	0.028	7.75992E-06
2R	2R_17343770_DEL	G	GAAAA	0.103	4.37304E-06
2R	2R_17346153_SNP	A	C	0.033	6.70748E-07
2R	2R_17351631_INS	ACAGTATAATTCGCTTAGCTGCATCGATAGTTAGCTGCATCGGCAAGATATCTGCATTATTTTTCCATTTTTTTGTGTGAATAGAAAATAGAAAAATAGAAAAAAAAAATTAAGTTAGCTGCATTTTTAAGTTACCTGCATCGAGGCATTGTGCAAAGTACTCGAGGCAGCTAAGCGAATTATACTGTA	A	0.033	6.84591E-07
2R	2R_18063068_SNP	A	G	0.072	9.26109E-06
2R	2R_18746444_DEL	CATAC	G	0.098	2.34336E-06
2R	2R_18763827_DEL	A	AA	0.022	1.30789E-07
2R	2R_19717294_SNP	G	C	0.028	2.63369E-06
2R	2R_20347597_SNP	A	T	0.039	1.61227E-06
3L	3L_390542_SNP	T	A	0.177	9.4143E-06
3L	3L_1912554_SNP	T	C	0.039	4.60478E-06
3L	3L_2339887_SNP	A	T	0.022	3.99543E-06
3L	3L_5248433_SNP	C	T	0.071	2.93377E-07
3L	3L_5381338_SNP	T	C	0.022	6.24679E-06
3L	3L_5382509_SNP	C	G	0.033	8.37842E-06
3L	3L_7137933_SNP	T	C	0.027	2.79384E-06
3L	3L_8578661_SNP	A	T	0.027	5.77657E-06
3L	3L_9905387_SNP	A	G	0.022	1.82581E-06

3L	3L_10182483_DEL	T	AGGATC	0.033	2.84376E-06
3L	3L_10278242_SNP	T	C	0.033	6.7404E-06
3L	3L_10340992_SNP	A	T	0.125	8.24317E-06
3L	3L_11341035_DEL	T	GCCTG	0.029	5.55786E-07
3L	3L_11929553_SNP	T	G	0.169	1.60646E-06
3L	3L_11931870_SNP	G	A	0.169	4.9184E-07
3L	3L_11937847_SNP	A	T	0.144	1.9524E-07
3L	3L_12338118_SNP	G	A	0.022	3.25214E-06
3L	3L_12338138_SNP	A	C	0.023	2.95111E-06
3L	3L_12338139_SNP	G	A	0.023	2.95111E-06
3L	3L_12338143_SNP	C	A	0.023	3.02116E-06
3L	3L_12338982_SNP	A	G	0.022	3.25214E-06
3L	3L_12339917_SNP	C	T	0.027	4.12005E-06
3L	3L_12372745_SNP	A	C	0.039	2.15879E-07
3L	3L_12375122_SNP	C	T	0.044	3.02337E-06
3L	3L_12375243_SNP	C	T	0.044	3.02337E-06
3L	3L_12378504_SNP	A	T	0.044	3.60403E-06
3L	3L_12379877_SNP	A	G	0.044	3.60403E-06
3L	3L_12553964_SNP	T	G	0.089	2.39902E-06
3L	3L_12553969_SNP	G	C	0.089	3.2916E-06
3L	3L_12553970_SNP	A	C	0.089	2.2405E-06
3L	3L_12554022_SNP	T	C	0.238	1.78416E-06
3L	3L_12554039_SNP	T	A	0.235	3.6282E-06
3L	3L_12554052_SNP	T	A	0.275	2.86472E-07
3L	3L_12870339_SNP	G	A	0.056	6.42303E-06
3L	3L_13861190_SNP	T	C	0.122	7.31848E-06
3L	3L_14142892_SNP	C	A	0.022	6.46316E-07
3L	3L_15241449_SNP	G	A	0.022	2.07412E-06
3L	3L_15579674_SNP	A	G	0.056	1.21376E-07
3L	3L_15580957_SNP	A	G	0.045	5.11214E-06
3L	3L_15583146_SNP	A	G	0.034	6.77627E-06
3L	3L_15944542_SNP	A	G	0.056	1.89054E-06
3L	3L_16630268_SNP	C	T	0.022	6.04558E-06
3L	3L_16655050_SNP	A	G	0.027	3.99573E-07
3L	3L_16656679_SNP	T	A	0.028	3.28932E-07
3L	3L_16656682_SNP	G	T	0.028	2.99907E-07
3L	3L_16656683_SNP	C	T	0.028	3.37986E-07

3L	3L_16656696_SNP	G	A	0.028	3.37986E-07
3L	3L_16656747_SNP	T	C	0.028	4.90594E-07
3L	3L_16656857_DEL	G	GT	0.022	3.66894E-06
3L	3L_16664989_SNP	G	A	0.056	4.2488E-07
3L	3L_16665155_SNP	G	C	0.052	4.47807E-06
3L	3L_17420318_SNP	G	T	0.108	9.06959E-06
3L	3L_18404525_SNP	C	T	0.028	2.4693E-06
3L	3L_18839872_SNP	T	A	0.129	8.84631E-06
3L	3L_20037887_SNP	T	G	0.033	1.83894E-06
3R	3R_5687378_INS	TTTGGGT	G	0.022	9.2388E-06
3R	3R_5687733_SNP	T	G	0.022	9.98501E-06
3R	3R_5687741_DEL	A	ATCCA TTCCA TAAGT TTCGC CATGT CGATG ACAAA AAACA GACAC ACAAT TCGTA AGAA	0.022	9.98501E-06
3R	3R_5687804_SNP	A	T	0.022	9.98501E-06
3R	3R_5717021_SNP	G	A	0.028	5.14425E-06
3R	3R_5723598_DEL	C	AAAAA	0.04	1.90652E-08
3R	3R_5731260_SNP	G	A	0.069	5.8489E-06
3R	3R_6292892_SNP	T	G	0.023	8.34995E-06
3R	3R_6293461_SNP	A	G	0.028	4.70901E-07
3R	3R_6293570_SNP	T	C	0.028	3.55201E-07
3R	3R_9063148_SNP	T	G	0.04	4.56859E-06
3R	3R_10609369_SNP	G	T	0.056	5.56617E-08
3R	3R_11140205_SNP	C	T	0.022	2.88604E-06
3R	3R_12750151_SNP	C	T	0.028	2.30834E-07
3R	3R_13025063_DEL	T	TG	0.029	5.61902E-06
3R	3R_13065879_SNP	C	T	0.131	1.31205E-06
3R	3R_13065905_SNP	T	C	0.14	4.84496E-06
3R	3R_13332133_SNP	T	A	0.056	6.2002E-06
3R	3R_13768724_SNP	T	C	0.023	1.4572E-06
3R	3R_13793642_SNP	C	G	0.022	2.20213E-07
3R	3R_14295836_SNP	A	G	0.047	2.30546E-06

3R	3R_14298382_SNP	T	A	0.036	9.7445E-06

Appendix 7 Top polymorphisms of analysis of Capa-stimulated secretion index

Chr	SNP ID	Minor allele	Major allele	Allele frequency	p value
X	X_4312185_SNP	T	G	0.098	9.60099E-06
2L	2L_1740379_INS	T	TTAAAAGAACC	0.261	7.89012E-06
2L	2L_2261604_SNP	G	C	0.227	5.65855E-06
2L	2L_4444858_SNP	G	T	0.022	9.16203E-06
2L	2L_4445058_SNP	T	A	0.022	9.16203E-06
2L	2L_5400514_SNP	T	A	0.022	1.97209E-07
2L	2L_5400521_SNP	T	A	0.033	5.15208E-07
2L	2L_8330668_SNP	T	C	0.089	6.52345E-06
2L	2L_8331425_SNP	T	C	0.028	2.54873E-06
2L	2L_14205250_SNP	A	G	0.353	7.10769E-07
2L	2L_17744842_SNP	A	G	0.028	6.2422E-06
2L	2L_21999454_SNP	A	C	0.022	9.36694E-06
2L	2L_21999456_SNP	A	T	0.022	9.88299E-06
2L	2L_22044897_SNP	T	C	0.034	8.74912E-06
2R	2R_2442778_SNP	T	A	0.096	7.4068E-06
2R	2R_3915909_DEL	A	ACTCACTCA	0.036	7.78404E-06
2R	2R_5099937_SNP	T	C	0.133	7.41491E-06
2R	2R_6398725_SNP	T	A	0.028	1.25913E-06
2R	2R_8909813_SNP	C	G	0.088	1.82924E-06
2R	2R_9533588_SNP	A	C	0.177	8.06321E-06
2R	2R_14459725_SNP	C	T	0.033	9.87511E-06
2R	2R_14578826_SNP	A	G	0.027	5.87537E-07
2R	2R_14578891_SNP	T	G	0.033	3.64782E-06
2R	2R_14579055_SNP	A	C	0.033	2.72587E-06
2R	2R_14579532_SNP	A	T	0.079	6.54423E-06
2R	2R_16793754_SNP	A	T	0.05	5.7616E-06
2R	2R_16795068_SNP	T	C	0.028	8.29127E-09
2R	2R_17728162_DEL	G	GT	0.06	6.41848E-06
2R	2R_17764891_DEL	T	TTACAATAGT	0.121	2.22701E-06
2R	2R_18787991_SNP	A	G	0.044	1.03423E-07

3L	3L_1293743_SNP	T	C	0.022	4.97136E-07
3L	3L_1293772_SNP	T	A	0.033	3.99332E-06
3L	3L_6762790_SNP	T	A	0.061	9.461E-07
3L	3L_7470129_SNP	A	G	0.027	1.58054E-06
3L	3L_7820384_SNP	G	A	0.044	7.13535E-06
3L	3L_9943438_SNP	T	C	0.152	5.20672E-06
3L	3L_9943784_SNP	A	C	0.174	9.80092E-06
3L	3L_10118777_SNP	A	G	0.027	3.51456E-07
3L	3L_11580049_SNP	G	A	0.377	1.59647E-06
3L	3L_11646153_SNP	C	T	0.022	1.53314E-06
3L	3L_11646361_SNP	G	A	0.022	1.53314E-06
3L	3L_11646626_SNP	A	T	0.023	1.78962E-06
3L	3L_11646701_SNP	A	T	0.022	1.36183E-06
3L	3L_11689492_SNP	A	G	0.077	6.37864E-06
3L	3L_12081296_SNP	C	G	0.039	3.94516E-06
3L	3L_12264734_INS	AAA	A	0.045	7.32141E-06
3L	3L_13106613_SNP	A	T	0.027	3.34301E-08
3L	3L_14378597_SNP	C	T	0.067	8.81942E-06
3L	3L_19337111_SNP	G	C	0.022	3.08821E-07
3L	3L_19430774_INS	CAAATG	C	0.038	3.91186E-06
3L	3L_19479952_SNP	T	C	0.038	2.31639E-06
3L	3L_19484762_SNP	A	G	0.038	2.30214E-06
3L	3L_19491031_SNP	T	C	0.075	9.13292E-07
3R	3R_2720279_SNP	A	T	0.023	2.52208E-06
3R	3R_10571010_SNP	T	C	0.05	8.5239E-06
3R	3R_14219188_SNP	G	T	0.022	1.67435E-06
3R	3R_14222124_SNP	T	A	0.022	1.66608E-06
3R	3R_14563639_SNP	A	C	0.028	1.18343E-06
3R	3R_14766192_DEL	T	TTACGGAT	0.022	2.96923E-07

Appendix 8 Top polymorphisms of analysis of Kinin-stimulated secretion index

Chr	SNP ID	Minor allele	Major allele	Allele frequency	p value
X	X_3927111_DEL	A	AGAAAGC	0.027	5.42048E-08
X	X_6865782_SNP	A	G	0.087	7.83459E-06

X	X_7813471_SNP	T	G	0.277	2.62126E-06
X	X_7937882_SNP	T	A	0.071	5.33108E-06
X	X_7938159_SNP	G	C	0.066	1.0836E-08
X	X_7938168_SNP	T	C	0.066	1.12617E-08
X	X_7938169_SNP	G	A	0.066	1.0836E-08
X	X_12537154_DEL	C	CGAAATGC	0.029	7.44391E-06
X	X_20611365_INS	CC	C	0.109	6.88538E-06
2L	2L_2555233_SNP	G	T	0.022	6.0808E-06
2L	2L_4440375_INS	CAATT GTGTT GTGTT ACAAC	C	0.033	1.23297E-06
2L	2L_5583945_DEL	C	CC	0.022	6.70082E-06
2L	2L_6033627_SNP	A	G	0.028	5.7671E-06
2L	2L_6530562_SNP	A	G	0.074	6.02557E-06
2L	2L_10287264_SNP	C	G	0.022	2.18482E-07
2L	2L_16484658_SNP	C	T	0.022	1.9246E-07
2R	2R_4436098_INS	TCCTT	T	0.028	9.54585E-06
2R	2R_4438440_SNP	G	A	0.028	7.09304E-06
2R	2R_4567965_SNP	A	G	0.039	9.79954E-06
2R	2R_7150067_SNP	A	G	0.039	2.03019E-06
2R	2R_8523873_SNP	A	T	0.046	6.54684E-06
2R	2R_15286513_SNP	G	C	0.147	9.68439E-06
2R	2R_16492148_SNP	C	T	0.022	6.32819E-06
2R	2R_16948038_SNP	T	C	0.279	8.39763E-06
2R	2R_16948385_SNP	T	A	0.295	6.55332E-07
2R	2R_16948394_SNP	T	G	0.218	5.90945E-07
2R	2R_16948450_SNP	A	G	0.289	6.34349E-07
2R	2R_17847696_SNP	A	G	0.022	1.46848E-06
2R	2R_18374297_SNP	C	T	0.033	2.47342E-06
2R	2R_18387757_SNP	A	G	0.022	9.70767E-06
2R	2R_18387759_SNP	C	A	0.022	9.83609E-06
2R	2R_18944295_SNP	C	T	0.044	5.14777E-06
2R	2R_19552534_SNP	C	G	0.028	9.00542E-06
2R	2R_19680510_SNP	A	G	0.022	5.6711E-06
2R	2R_20083212_SNP	A	T	0.027	7.0156E-06
2R	2R_20123821_SNP	C	G	0.022	1.41625E-06
2R	2R_20152622_SNP	T	C	0.022	1.38887E-06
2R	2R_20152648_SNP	T	A	0.022	1.38887E-06

3L	3L_1534796_SNP	C	T	0.057	3.45187E-07
3L	3L_2217698_SNP	T	G	0.022	7.58163E-06
3L	3L_2538676_SNP	C	G	0.055	4.07602E-07
3L	3L_2539162_SNP	A	T	0.072	9.6213E-06
3L	3L_2539185_SNP	G	A	0.073	9.95152E-06
3L	3L_2539210_SNP	A	G	0.072	9.6213E-06
3L	3L_2539220_SNP	T	A	0.066	3.15825E-06
3L	3L_2539221_SNP	G	A	0.066	3.15825E-06
3L	3L_2539253_SNP	T	A	0.066	3.15825E-06
3L	3L_2539356_DEL	G	TT	0.067	2.17516E-06
3L	3L_2539433_SNP	A	C	0.061	7.65194E-07
3L	3L_2539438_SNP	A	C	0.066	4.32126E-06
3L	3L_2539491_DEL	A	ACAGACTTA	0.056	5.80386E-06
3L	3L_2539519_SNP	G	T	0.073	6.93806E-06
3L	3L_5121229_SNP	A	G	0.022	5.42692E-06
3L	3L_5699187_SNP	T	C	0.05	8.53607E-06
3L	3L_5918798_SNP	T	G	0.061	1.47633E-06
3L	3L_5924809_SNP	T	G	0.039	1.04894E-06
3L	3L_5932587_SNP	G	T	0.033	1.78892E-06
3L	3L_5932595_SNP	T	C	0.027	1.04274E-06
3L	3L_6211415_SNP	T	A	0.491	3.06073E-06
3L	3L_6211594_SNP	C	T	0.483	5.93019E-06
3L	3L_6669342_SNP	C	T	0.136	7.73255E-06
3L	3L_7410701_SNP	T	C	0.022	1.19196E-06
3L	3L_7512436_SNP	C	T	0.022	7.02641E-06
3L	3L_9769349_SNP	C	A	0.038	7.19676E-07
3L	3L_10388240_SNP	C	A	0.049	4.46064E-06
3L	3L_10403238_SNP	G	A	0.027	7.03718E-07
3L	3L_10415506_SNP	A	G	0.038	3.78017E-06
3L	3L_10419847_SNP	G	A	0.023	1.59092E-06
3L	3L_11025456_DEL	A	AA	0.171	3.52954E-06
3L	3L_11652795_SNP	A	C	0.024	3.48374E-06
3L	3L_12037022_SNP	A	T	0.124	8.22508E-06
3L	3L_12526105_SNP	C	T	0.027	9.7452E-06
3L	3L_12721898_SNP	T	C	0.033	2.58351E-06
3L	3L_12847777_SNP	C	A	0.022	8.1225E-08
3L	3L_12847786_SNP	A	C	0.022	8.10164E-08
3L	3L_12847790_SNP	C	T	0.022	8.1225E-08

3L	3L_12890843_SNP	T	C	0.039	6.99044E-07
3L	3L_12891205_SNP	T	C	0.124	1.07035E-06
3L	3L_14625180_SNP	C	A	0.033	4.71383E-06
3L	3L_14628828_INS	GG	G	0.033	3.04146E-06
3L	3L_14630490_SNP	A	G	0.033	3.28633E-06
3L	3L_14961171_SNP	T	A	0.055	9.09877E-07
3L	3L_15319298_SNP	G	C	0.179	2.58769E-06
3L	3L_15458819_SNP	T	A	0.022	2.65537E-06
3L	3L_15463243_SNP	C	T	0.022	2.65537E-06
3L	3L_15474051_SNP	C	A	0.023	2.67653E-06
3L	3L_15475140_SNP	T	A	0.028	9.20252E-06
3L	3L_15484378_SNP	T	A	0.022	2.61314E-06
3L	3L_15491963_SNP	T	G	0.028	9.14544E-08
3L	3L_15492841_SNP	T	C	0.028	6.8163E-08
3L	3L_15493950_SNP	T	C	0.027	8.98318E-08
3L	3L_15495039_SNP	C	T	0.033	6.32534E-07
3L	3L_15495102_SNP	A	G	0.033	6.55224E-07
3L	3L_15495176_SNP	T	A	0.028	6.92807E-08
3L	3L_15495226_SNP	G	T	0.028	6.92807E-08
3L	3L_15495244_SNP	C	G	0.034	8.48338E-07
3L	3L_15495658_SNP	T	A	0.028	9.70434E-08
3L	3L_15496397_SNP	G	T	0.027	8.98318E-08
3L	3L_15496935_SNP	G	A	0.022	4.59903E-06
3L	3L_15498337_SNP	A	T	0.023	6.96421E-06
3L	3L_15499193_SNP	T	A	0.022	4.59903E-06
3L	3L_15499258_SNP	T	A	0.022	4.59903E-06
3L	3L_15499489_SNP	G	C	0.028	9.74824E-08
3L	3L_15501752_SNP	T	C	0.033	4.51043E-07
3L	3L_15502634_SNP	T	C	0.027	8.98318E-08
3L	3L_15806539_SNP	A	G	0.039	3.68718E-07
3L	3L_16122585_SNP	A	T	0.022	2.61896E-06
3L	3L_16739976_DEL	G	ACCGGGGAA TCCAGGAACA CGACTACGC CAGGAATAT GGGA	0.067	2.9472E-06
3L	3L_17166836_SNP	T	A	0.082	3.39254E-06
3L	3L_17600630_SNP	C	T	0.022	8.75995E-09
3L	3L_17601782_SNP	A	G	0.022	8.97666E-09

3L	3L_17601812_SNP	T	G	0.022	8.97666E-09
3L	3L_18514035_SNP	A	C	0.028	2.10253E-07
3L	3L_18724704_SNP	C	T	0.027	1.23921E-06
3L	3L_18727456_INS	AA	A	0.023	1.46552E-06
3L	3L_18839003_SNP	A	C	0.124	1.37557E-07
3L	3L_18839543_DEL	T	TG	0.096	5.41764E-10
3L	3L_18926647_SNP	C	T	0.041	1.91022E-06
3L	3L_19293409_SNP	C	G	0.056	3.65422E-08
3L	3L_19306759_SNP	C	T	0.044	1.00821E-06
3L	3L_19316401_DEL	G	GA	0.044	1.09225E-06
3L	3L_19319502_SNP	C	G	0.033	6.06188E-07
3L	3L_19322466_SNP	A	G	0.038	5.93237E-06
3L	3L_19338433_SNP	G	A	0.027	4.20426E-07
3L	3L_19344423_SNP	G	A	0.027	4.20426E-07
3L	3L_19345686_SNP	C	G	0.028	4.2296E-07
3L	3L_19346806_SNP	A	G	0.033	3.76256E-07
3L	3L_19347926_INS	TTCA	C	0.038	3.05283E-07
3L	3L_19347931_INS	CA	C	0.028	5.67964E-07
3L	3L_19348264_SNP	T	G	0.028	3.38072E-07
3L	3L_19349146_SNP	C	T	0.033	3.62084E-07
3L	3L_19350399_SNP	T	G	0.028	1.4159E-06
3L	3L_19354987_SNP	T	A	0.028	1.4159E-06
3L	3L_19355423_SNP	T	A	0.033	3.62084E-07
3L	3L_19355697_SNP	C	T	0.027	4.15927E-07
3L	3L_19355915_SNP	A	G	0.033	4.52449E-07
3L	3L_19355916_SNP	T	A	0.033	4.52449E-07
3L	3L_19356885_SNP	A	T	0.033	3.62084E-07
3L	3L_19356897_SNP	A	T	0.033	3.62084E-07
3L	3L_19359143_SNP	T	C	0.039	8.29104E-06
3L	3L_19359201_SNP	A	T	0.033	3.62084E-07
3L	3L_19360339_SNP	T	C	0.033	3.4856E-07
3L	3L_19360816_SNP	T	G	0.033	3.62084E-07
3L	3L_19361982_SNP	A	C	0.038	2.9677E-07
3L	3L_19362864_SNP	A	C	0.034	4.13152E-07
3L	3L_19363032_SNP	T	A	0.033	3.91729E-07
3L	3L_19363719_SNP	T	A	0.033	3.62084E-07
3L	3L_19364123_SNP	G	A	0.033	3.62084E-07
3L	3L_19364692_SNP	G	A	0.035	6.22327E-07

3L	3L_19365502_SNP	C	T	0.027	1.62103E-06
3L	3L_19367970_SNP	G	A	0.027	4.20426E-07
3L	3L_19369164_SNP	A	G	0.022	1.31728E-06
3L	3L_19915457_SNP	G	T	0.039	1.5026E-06
3L	3L_19991848_SNP	A	C	0.022	8.38358E-08
3L	3L_20236754_DEL	A	ATACCCCATCAC	0.023	6.69039E-07
3L	3L_21729799_SNP	A	C	0.023	3.79765E-06
3L	3L_21729823_SNP	C	G	0.023	3.94771E-06
3L	3L_21729967_SNP	C	A	0.023	4.27664E-06
3R	3R_427896_SNP	T	A	0.034	9.73656E-06
3R	3R_1065696_SNP	T	C	0.022	5.80668E-06
3R	3R_3364516_SNP	G	A	0.08	3.29498E-06
3R	3R_4719116_SNP	A	C	0.094	2.235E-06
3R	3R_4722057_SNP	T	C	0.105	4.1061E-06
3R	3R_5818976_SNP	C	T	0.244	2.34911E-06
3R	3R_5819202_SNP	A	C	0.068	5.56356E-06
3R	3R_5819596_SNP	A	C	0.167	7.42623E-07
3R	3R_9497562_SNP	G	A	0.491	9.33934E-07
3R	3R_9869997_SNP	T	A	0.052	8.92921E-07
3R	3R_9944597_SNP	C	G	0.029	2.90873E-06
3R	3R_10353498_SNP	C	G	0.027	1.25237E-08
3R	3R_10353890_SNP	T	C	0.028	8.31733E-09
3R	3R_10366690_SNP	G	T	0.022	2.01514E-06
3R	3R_10580216_SNP	T	A	0.062	8.21626E-06
3R	3R_10584029_SNP	T	G	0.022	2.69915E-07
3R	3R_10587405_INS	TGTCAACGTTATGT	T	0.028	9.68704E-07
3R	3R_10587406_DEL	C	CAAGGAAATTGTTCAGA	0.028	7.807E-07
3R	3R_10589593_SNP	T	G	0.079	5.71977E-06
3R	3R_10592229_SNP	G	T	0.039	4.06761E-07
3R	3R_10824792_SNP	T	C	0.044	9.66124E-07
3R	3R_11622639_SNP	A	C	0.04	2.18129E-09
3R	3R_12501411_SNP	T	C	0.04	1.51903E-07
3R	3R_13197346_SNP	G	C	0.091	7.85518E-06
3R	3R_13255194_SNP	A	T	0.078	3.7837E-07
3R	3R_13256111_SNP	T	C	0.072	2.20731E-07
3R	3R_13291264_SNP	T	G	0.062	6.84051E-06

3R	3R_13326339_SNP	A	G	0.079	2.72459E-06
3R	3R_15468785_DEL	A	AT	0.027	2.13623E-06
3R	3R_17298320_SNP	G	A	0.029	5.41231E-06
3R	3R_21489997_SNP	G	T	0.022	2.25108E-06
3R	3R_21494507_SNP	A	C	0.022	2.35831E-06
3R	3R_24192062_SNP	C	A	0.056	3.31747E-06
3R	3R_24639356_SNP	A	G	0.257	5.16282E-06
3R	3R_24639452_SNP	T	C	0.292	5.22236E-06
3R	3R_24722478_SNP	A	G	0.029	4.04441E-06
3R	3R_25908175_SNP	A	T	0.182	3.41295E-06
3R	3R_26174730_SNP	A	C	0.084	5.9538E-06
3R	3R_26991864_SNP	C	T	0.044	4.04851E-06

Appendix 9 RNAi lines and corresponding isogenic control lines

Gene symbol	Stock number	*Gal4* driver line	Targeted tissues	Control line
CG7289	BDSC#60460	*da-Gal4*	Whole fly	BDSC#36304
Dlg5	BDSC#61334	*ctB-Gal4*	MTs	BDSC#36304
Shab	BDSC#55682	*ctB-Gal4*	MTs	BDSC#36303
MsrA	BDSC#42877	*ctB-Gal4*	MTs	BDSC#36304
ATP8B	BDSC#63037	*ctB-Gal4*	MTs	BDSC#36304
timeout	BDSC#36863	*ctB-Gal4*	MTs	BDSC#36303
fz2	VDRC#108998	*c724-Gal4; CapaR-Gal4*	MTs	VDRC#60100
SPR	VDRC#106804	*ctB-Gal4*	MTs	VDRC#60100
sdt	BDSC#37510	*c724-Gal4; CapaR-Gal4*	MTs	BDSC#36304
RunxA	BDSC#33353	*da-Gal4*	Whole fly	BDSC#36303
Pde1c	BDSC#55925	*c724-Gal4*	MTs	BDSC#36304
Ncc69	BDSC#28682	*c724-Gal4*	MTs	BDSC#36303
sowah	BDSC#65930	*ctB-Gal4*	MTs	BDSC#36303
RhoGAP71E	BDSC#32417	*ctB-Gal4*	MTs	BDSC#36303
Baldspot	BDSC#44101	*ctB-Gal4*	MTs	BDSC#36304
Gaf	BDSC#43201	*c724-Gal4; CapaR-Gal4*	MTs	BDSC#36304
Glut4EF	BDSC#57461	*c724-Gal4; CapaR-Gal4*	MTs	BDSC#36304
CG8027	VDRC#109400	*da-Gal4*	Whole fly	VDRC#60100
CG7656	VDRC#100791	*c724-Gal4; CapaR-Gal4*	MTs	VDRC#60100

Indy	VDRC#9981	*CapaR-Gal4*	MTs	w^{1118}
jvl	BDSC#67897	*c724-Gal4; CapaR-Gal4*	MTs	BDSC#36304
bi	BDSC#28341	*ctB-Gal4*	MTs	BDSC#36303
Pdp1	BDSC#40863	*c724-Gal4; CapaR-Gal4*	MTs	BDSC#36304
Sik3	BDSC#57302	*c724-Gal4; CapaR-Gal4*	MTs	BDSC#36304
smp-30	VDRC#103377	*ctB-Gal4*	MTs	VDRC#60100
CG32206	BDSC#66946	*da-Gal4*	Whole fly	BDSC#36304
Eip74EF	BDSC#29353	*ctB-Gal4*	MTs	BDSC#36303
Ent3	VDRC#47537	*ctB-Gal4*	MTs	w^{1118}
fs(1)h	BDSC#41693	*ctB-Gal4; Gal80^{TS}*	MTs	BDSC#36304
Pde6	BDSC#25828	*ctB-Gal4*	MTs	BDSC#36303
Pde8	BDSC#51892	*c724-Gal4; CapaR-Gal4*	MTs	BDSC#36304
pip	BDSC#34613	*da-Gal4*	Whole fly	BDSC#36303

References

ADAMS, M. D., CELNIKER, S. E., HOLT, R. A., EVANS, C. A., GOCAYNE, J. D., AMANATIDES, P. G., SCHERER, S. E., LI, P. W., HOSKINS, R. A., GALLE, R. F., GEORGE, R. A., LEWIS, S. E., RICHARDS, S., ASHBURNER, M., HENDERSON, S. N., SUTTON, G. G., WORTMAN, J. R., YANDELL, M. D., ZHANG, Q., CHEN, L. X., BRANDON, R. C., ROGERS, Y. H., BLAZEJ, R. G., CHAMPE, M., PFEIFFER, B. D., WAN, K. H., DOYLE, C., BAXTER, E. G., HELT, G., NELSON, C. R., GABOR, G. L., ABRIL, J. F., AGBAYANI, A., AN, H. J., ANDREWS-PFANNKOCH, C., BALDWIN, D., BALLEW, R. M., BASU, A., BAXENDALE, J., BAYRAKTAROGLU, L., BEASLEY, E. M., BEESON, K. Y., BENOS, P. V., BERMAN, B. P., BHANDARI, D., BOLSHAKOV, S., BORKOVA, D., BOTCHAN, M. R., BOUCK, J., BROKSTEIN, P., BROTTIER, P., BURTIS, K. C., BUSAM, D. A., BUTLER, H., CADIEU, E., CENTER, A., CHANDRA, I., CHERRY, J. M., CAWLEY, S., DAHLKE, C., DAVENPORT, L. B., DAVIES, P., DE PABLOS, B., DELCHER, A., DENG, Z., MAYS, A. D., DEW, I., DIETZ, S. M., DODSON, K., DOUP, L. E., DOWNES, M., DUGAN-ROCHA, S., DUNKOV, B. C., DUNN, P., DURBIN, K. J., EVANGELISTA, C. C., FERRAZ, C., FERRIERA, S., FLEISCHMANN, W., FOSLER, C., GABRIELIAN, A. E., GARG, N. S., GELBART, W. M., GLASSER, K., GLODEK, A., GONG, F., GORRELL, J. H., GU, Z., GUAN, P., HARRIS, M., HARRIS, N. L., HARVEY, D., HEIMAN, T. J., HERNANDEZ, J. R., HOUCK, J., HOSTIN, D., HOUSTON, K. A., HOWLAND, T. J., WEI, M. H., IBEGWAM, C., et al. 2000. The genome sequence of *Drosophila melanogaster*. *Science,* 287**,** 2185-2195.

AGGARWAL, K. P., NARULA, S., KAKKAR, M. & TANDON, C. 2013. Nephrolithiasis: molecular mechanism of renal stone formation and the critical role played by modulators. *Biomed Res. Int.*, 2013**,** 292953.

AHMED, S., HASAN, M. M. & MAHMOOD, Z. A. 2016. In vitro urolithiasis models: an evaluation of prophylactic management against kidney stones. *J. Pharmacogn. Phytochem.,* 5**,** 28-35.

ALELIGN, T. & PETROS, B. 2018. Kidney stone disease: an update on current concepts. *Adv. Urol.,* 2018**,** 3068365.

ALEXANDER, R. T., DIMKE, H. & CORDAT, E. 2013. Proximal tubular NHEs: sodium, protons and calcium? *Am. J. Physiol. Renal Physiol.,* 305**,** F229-F236.

ALEXANDER, R. T., HEMMELGARN, B. R., WIEBE, N., BELLO, A., MORGAN, C., SAMUEL, S., KLARENBACH, S. W., CURHAN, G. C. & TONELLI, M. 2012. Kidney stones and kidney function loss: a cohort study. *Br. Med. J.,* 345**,** e5287.

ALI, S. N., DAYARATHNA, T. K., ALI, A. N., OSUMAH, T., AHMED, M., COOPER, T. T., POWER, N. E., ZHANG, D., KIM, D., KIM, R., ST. AMANT, A., HOU, J., TAILLY, T., YANG, J., LUYT, L., SPAGNUOLO, P. A., BURTON, J. P., RAZVI, H. & LEONG, H. S. 2018. *Drosophila melanogaster* as a function-based high-throughput screening model for antinephrolithiasis agents in kidney stone patients. *Dis. Models Mech.,* 11**,** dmm035873.

ALLAN, A. K., DU, J., DAVIES, S. A. & DOW, J. A. T. 2005. Genome-wide survey of V-ATPase genes in *Drosophila* reveals a conserved renal phenotype for lethal alleles. *Physiol. Genomics,* 22**,** 128-138.

ALLEN, G. E. 1975. The introduction of *Drosophila* into the study of heredity and evolution: 1900-1910. *Isis,* 66**,** 322-333.

ALPER, S., NATALE, J., GLUCK, S., LODISH, H. & BROWN, D. 1989. Subtypes of intercalated cells in rat kidney collecting duct defined by antibodies against erythroid band 3 and renal vacuolar H^+-ATPase. *Proc. Natl. Acad. Sci. U.S.A.,* 86**,** 5429-5433.

AMIRLAK, I. & DAWSON, K. 2000. Bartter syndrome: an overview. *QJM,* 93**,** 207-215.

ANDERSEN, M. K., MACMILLAN, H. A., DONINI, A. & OVERGAARD, J. 2017. Cold tolerance of *Drosophila* species is tightly linked to the epithelial K^+ transport capacity of the Malpighian tubules and rectal pads. *J. Exp. Biol.,* 220**,** 4261-4269.

ANDOLFATTO, P., WALL, J. D. & KREITMAN, M. 1999. Unusual haplotype structure at the proximal breakpoint of In (2L) t in a natural population of *Drosophila melanogaster*. *Genetics,* 153**,** 1297-1311.

ANGLANI, F., GIANESELLO, L., BEARA – LASIC, L. & LIESKE, J. 2019. Dent disease: A window into calcium and phosphate transport. *J. Cell. Mol. Med.,* 23**,** 7132-7142.

ANHOLT, R. R. H. & MACKAY, T. F. C. 2018. The road less traveled: from genotype to phenotype in flies and humans. *Mamm. Genome,* 29**,** 5-23.

ANTONELLI, J. A., MAALOUF, N. M., PEARLE, M. S. & LOTAN, Y. 2014. Use of the national health and nutrition examination survey to calculate the impact of obesity and diabetes on cost and prevalence of urolithiasis in 2030. *Eur. Urol.,* 66**,** 724-729.

ANZAI, N., ICHIDA, K., JUTABHA, P., KIMURA, T., BABU, E., JIN, C. J., SRIVASTAVA, S., KITAMURA, K., HISATOME, I. & ENDOU, H. 2008. Plasma urate level is directly regulated by a voltage-driven urate efflux

transporter URATv1 (SLC2A9) in humans. *J. Biol. Chem.,* 283, 26834-26838.

ANZAI, N., JUTABHA, P., AMONPATUMRAT-TAKAHASHI, S. & SAKURAI, H. 2012. Recent advances in renal urate transport: characterization of candidate transporters indicated by genome-wide association studies. *Clin. Exp. Nephrol.,* 16, 89-95.

ASHBURNER, M. & DRYSDALE, R. 1994. FlyBase-the *Drosophila* genetic database. *Development,* 120, 2077-2079.

AUERBACH, C. 1949. Chemical mutagenesis. *Biol. Rev.,* 24, 355-391.

AUGUSTIN, R., CARAYANNOPOULOS, M. O., DOWD, L. O., PHAY, J. E., MOLEY, J. F. & MOLEY, K. H. 2004. Identification and characterization of human glucose transporter-like protein-9 (GLUT9): alternative splicing alters trafficking. *J. Biol. Chem.,* 279, 16229-16236.

AYALA, F. J., RZHETSKY, A. & AYALA, F. J. 1998. Origin of the metazoan phyla: molecular clocks confirm paleontological estimates. *Proc. Natl. Acad. Sci. U.S.A.,* 95, 606-611.

BACHMANN, A., SCHNEIDER, M., THEILENBERG, E., GRAWE, F. & KNUST, E. 2001. *Drosophila* Stardust is a partner of Crumbs in the control of epithelial cell polarity. *Nature,* 414, 638-643.

BAMSHAD, M., WOODING, S., SALISBURY, B. A. & STEPHENS, J. C. 2004. Deconstructing the relationship between genetics and race. *Nat. Rev. Genet.,* 5, 598-609.

BANSIL, R. & TURNER, B. S. 2006. Mucin structure, aggregation, physiological functions and biomedical applications. *Curr. Opin. Colloid Interface Sci.,* 11, 164-170.

BARGIELLO, T. A., JACKSON, F. R. & YOUNG, M. W. 1984. Restoration of circadian behavioural rhythms by gene transfer in *Drosophila*. *Nature,* 312, 752-754.

BARKER, T., BOON, M. & JONES, F. 2020. The role of zinc ions in calcium oxalate monohydrate crystallization. *J. Cryst. Growth,* 546, 125777.

BASAVARAJ, D. R., BIYANI, C. S., BROWNING, A. J. & CARTLEDGE, J. J. 2007. The role of urinary kidney stone inhibitors and promoters in the pathogenesis of calcium containing renal stones. *EAU-EBU Update Ser.,* 5, 126-136.

BASSETT, A. R., TIBBIT, C., PONTING, C. P. & LIU, J. L. 2013. Highly efficient targeted mutagenesis of *Drosophila* with the CRISPR/Cas9 system. *Cell Rep.,* 4**,** 220-228.

BATES, D., MäCHLER, M., BOLKER, B. M. & WALKER, S. C. 2015. Fitting linear mixed-effects models using lme4. *J. Stat. Softw.,* 67**,** 1-48.

BECKER, G. 2007. Uric acid stones. *Nephrology,* 12**,** 21-25.

BELLEN, H. J., LEVIS, R. W., LIAO, G., HE, Y., CARLSON, J. W., TSANG, G., EVANS-HOLM, M., HIESINGER, P. R., SCHULZE, K. L., RUBIN, G. M., HOSKINS, R. A. & SPRADLING, A. C. 2004. The BDGP gene disruption project: single transposon insertions associated with 40% of *Drosophila* genes. *Genetics,* 167**,** 761-781.

BELLEN, H. J., TONG, C. & TSUDA, H. 2010. 100 years of *Drosophila* research and its impact on vertebrate neuroscience: a history lesson for the future. *Nat. Rev. Neurosci.,* 11**,** 514-522.

BENSATAL, A. & OUAHRANI, M. 2008. Inhibition of crystallization of calcium oxalate by the extraction of *Tamarix gallica* L. *Urol. Res.,* 36**,** 283-287.

BERGHAUS, C., GROH, A.-C., BRELJAK, D., CIARIMBOLI, G., SABOLIĆ, I., PAVENSTäDT, H. & WEIDE, T. 2022. Impact of Pals1 on expression and localization of transporters belonging to the solute carrier family. *Front. Mol. Biosci.,* 9**,** 792829.

BERGMANN, C., GUAY-WOODFORD, L. M., HARRIS, P. C., HORIE, S., PETERS, D. J. & TORRES, V. E. 2018. Polycystic kidney disease. *Nat. Rev. Dis. Primers,* 4**,** 50.

BERGMANN, C., MOUSAEI, K., RIZZOLI, S. O. & TCHUMATCHENKO, T. 2025. How energy determines spatial localisation and copy number of molecules in neurons. *Nat. Commun.,* 16**,** 1424.

BEYENBACH, K. W. 2003. Transport mechanisms of diuresis in Malpighian tubules of insects. *J. Exp. Biol.,* 206**,** 3845-3856.

BEYENBACH, K. W., SKAER, H. & DOW, J. A. T. 2010. The developmental, molecular, and transport biology of Malpighian tubules. *Annu. Rev. Entomol.,* 55**,** 351-374.

BIE, P. 2018. Mechanisms of sodium balance: total body sodium, surrogate variables, and renal sodium excretion. *Am. J. Physiol. Regul. Integr. Comp. Physiol.,* 315**,** R945-R962.

BIYANI, C. S. & CARTLEDGE, J. J. 2006. Cystinuria-diagnosis and management. *EAU-EBU Update Ser.,* 4**,** 175-183.

BLAINE, J., CHONCHOL, M. & LEVI, M. 2015. Renal control of calcium, phosphate, and magnesium homeostasis. *Clin. J. Am. Soc. Nephrol.,* 10**,** 1257-1272.

BLANCHARD, A., CURIS, E., GUYON-ROGER, T., KAHILA, D., TREARD, C., BAUDOUIN, V., BéRARD, E., CHAMPION, G., COCHAT, P. & DUBOURG, J. 2016. Observations of a large Dent disease cohort. *Kidney Int.,* 90**,** 430-439.

BOBULESCU, I. A. & MOE, O. W. 2012. Renal transport of uric acid: evolving concepts and uncertainties. *Adv. Chronic Kidney Dis.,* 19**,** 358-371.

BOCKENHAUER, D., BOKENKAMP, A., VAN'T HOFF, W., LEVTCHENKO, E., KIST-VAN HOLTHE, J. E., TASIC, V. & LUDWIG, M. 2008. Renal phenotype in Lowe syndrome: a selective proximal tubular dysfunction. *Clin. J. Am. Soc. Nephrol.,* 3**,** 1430-1436.

BOROS, S., BINDELS, R. J. & HOENDEROP, J. G. 2009. Active Ca^{2+} reabsorption in the connecting tubule. *Pflug. Arch. Eur. J. Physiol.,* 458**,** 99-109.

BOSE, M. & MUKHERJEE, P. 2020. Microbe-MUC1 crosstalk in cancer-associated infections. *Trends Mol. Med.,* 26**,** 324-336.

BOURSOT, P., AUFFRAY, J.-C., BRITTON-DAVIDIAN, J. & BONHOMME, F. 1993. The evolution of house mice. *Annu. Rev. Ecol. Syst.,* 119-152.

BRAND, A. H. & PERRIMON, N. 1993. Targeted gene expression as a means of altering cell fates and generating dominant phenotypes. *Development,* 118**,** 401-415.

BRAUN, D. A., LAWSON, J. A., GEE, H. Y., HALBRITTER, J., SHRIL, S., TAN, W., STEIN, D., WASSNER, A. J., FERGUSON, M. A. & GUCEV, Z. 2016. Prevalence of monogenic causes in pediatric patients with nephrolithiasis or nephrocalcinosis. *Clin. J. Am. Soc. Nephrol.,* 11**,** 664-672.

BRETON, S. & BROWN, D. 2013. Regulation of luminal acidification by the V-ATPase. *Physiology (Bethesda),* 28**,** 318-329.

BROMAN, K. W. & SEN, S. 2009. *A guide to QTL mapping with R/qtl*, Springer.

BROWN, D. & STOW, J. L. 1996. Protein trafficking and polarity in kidney epithelium: from cell biology to physiology. *Physiol. Rev.,* 76**,** 245-297.

BROWN, T. R. 1901. On the relation between the variety of microorganisms and the composition of stone in calculous pyelone. *J. Am. Med. Assoc.,* 36**,** 1395-1397.

BROWNE, A. & O'DONNELL, M. J. 2016. Segment-specific Ca^{2+} transport by isolated Malpighian tubules of *Drosophila melanogaster* : a comparison of larval and adult stages. *J. Insect Physiol.,* 87**,** 1-11.

BRUNATI, M., PERUCCA, S., HAN, L., CATTANEO, A., CONSOLATO, F., ANDOLFO, A., SCHAEFFER, C., OLINGER, E., PENG, J. & SANTAMBROGIO, S. 2015. The serine protease hepsin mediates urinary secretion and polymerisation of Zona Pellucida domain protein uromodulin. *Elife,* 4**,** e08887.

CABRERO, P., TERHZAZ, S., DORNAN, A. J., GHIMIRE, S., HOLMES, H. L., TURIN, D. R., ROMERO, M. F., DAVIES, S. A. & DOW, J. A. T. 2020. Specialized stellate cells offer a privileged route for rapid water flux in *Drosophila* renal tubule. *Proc. Natl. Acad. Sci. U.S.A.,* 117**,** 1779-1787.

CABRERO, P., TERHZAZ, S., ROMERO, M. F., DAVIES, S. A., BLUMENTHAL, E. M. & DOW, J. A. T. 2014. Chloride channels in stellate cells are essential for uniquely high secretion rates in neuropeptide-stimulated *Drosophila* diuresis. *Proc. Natl. Acad. Sci. U.S.A.,* 111**,** 14301-14306.

CANELA, V. H., BOWEN, W. S., FERREIRA, R. M., SYED, F., LINGEMAN, J. E., SABO, A. R., BARWINSKA, D., WINFREE, S., LAKE, B. B., CHENG, Y. H., GAUT, J. P., FERKOWICZ, M., LAFAVERS, K. A., ZHANG, K., COE, F. L., WORCESTER, E., KIDNEY PRECISION MEDICINE, P., JAIN, S., EADON, M. T., WILLIAMS, J. C., JR. & EL-ACHKAR, T. M. 2023. A spatially anchored transcriptomic atlas of the human kidney papilla identifies significant immune injury in patients with stone disease. *Nat. Commun.,* 14**,** 4140.

CANO, A., MILLER, R. T., ALPERN, R. J. & PREISIG, P. A. 1994. Angiotensin II stimulation of Na-H antiporter activity is cAMP independent in OKP cells. *Am. J. Physiol. Cell Physiol.,* 266**,** C1603-C1608.

CARMOSINO, M., GERBINO, A., HENDY, G. N., TORRETTA, S., RIZZO, F., DEBELLIS, L., PROCINO, G. & SVELTO, M. 2015. NKCC2 activity is inhibited by the Bartter's syndrome type 5 gain-of-function CaR-A843E mutant in renal cells. *Biol. Cell,* 107**,** 98-110.

CARPENTER, F. W. 1905. The reactions of the pomace fly (*Drosophila ampelophila* Loew) to light, gravity, and mechanical stimulation. *Am. Nat.,* 39**,** 157-171.

CASSO, D., RAMIREZ-WEBER, F. A. & KORNBERG, T. B. 1999. GFP-tagged balancer chromosomes for *Drosophila melanogaster*. *Mech. Dev.,* 88**,** 229-232.

CASTLE, W. E., CARPENTER, F. W., CLARK, A. H., MAST, S. O. & BARROWS, W. M. 1906. The effects of inbreeding, cross-breeding, and selection upon the fertility and variability of *Drosophila*. *Proc. Am. Acad. Arts Sci.,* 41, 731-786.

CERINI, C., GEIDER, S., DUSSOL, B., HENNEQUIN, C., DAUDON, M., VEESLER, S., NITSCHE, S., BOISTELLE, R., BERTHéZèNE, P. & DUPUY, P. 1999. Nucleation of calcium oxalate crystals by albumin: involvement in the prevention of stone formation. *Kidney Int.,* 55, 1776-1786.

CHAUSOVSKY, A., BERSHADSKY, A. D. & BORISY, G. G. 2000. Cadherin-mediated regulation of microtubule dynamics. *Nat. Cell Biol.,* 2, 797-804.

CHEN, Y., ZELNICK, L. R., WANG, K., HOOFNAGLE, A. N., BECKER, J. O., HSU, C.-Y., FELDMAN, H. I., MEHTA, R. C., LASH, J. P. & WAIKAR, S. S. 2020. Kidney clearance of secretory solutes is associated with progression of CKD: the CRIC study. *J. Am. Soc. Nephrol.,* 31, 817-827.

CHEN, Y. H., LIU, H. P., CHEN, H. Y., TSAI, F. J., CHANG, C. H., LEE, Y. J., LIN, W. Y. & CHEN, W. C. 2011. Ethylene glycol induces calcium oxalate crystal deposition in Malpighian tubules: a *Drosophila* model for nephrolithiasis/urolithiasis. *Kidney Int.,* 80, 369-377.

CHI, T., KIM, M. S., LANG, S., BOSE, N., KAHN, A., FLECHNER, L., BLASCHKO, S. D., ZEE, T., MUTELIEFU, G., BOND, N., KOLIPINSKI, M., FAKRA, S. C., MANDEL, N., MILLER, J., RAMANATHAN, A., KILLILEA, D. W., BRüCKNER, K., KAPAHI, P. & STOLLER, M. L. 2015. A model identifies a critical role for zinc in mineralization for kidney stone disease. *PLoS One,* 10, e0124150.

CHINTAPALLI, V. R., TERHZAZ, S., WANG, J., AL BRATTY, M., WATSON, D. G., HERZYK, P., DAVIES, S. A. & DOW, J. A. T. 2012. Functional correlates of positional and gender-specific renal asymmetry in *Drosophila*. *PLoS One,* 7, e32577.

CHINTAPALLI, V. R., WANG, J. & DOW, J. A. T. 2007. Using FlyAtlas to identify better *Drosophila melanogaster* models of human disease. *Nat. Genet.,* 39, 715-720.

CHO, E. A. & DRESSLER, G. R. 2003. Formation and development of nephrons. *The Kidney*. San Diego: Academic Press.

CHO, S., KIM, K., KIM, Y. J., LEE, J. K., CHO, Y. S., LEE, J. Y., HAN, B. G., KIM, H., OTT, J. & PARK, T. 2010. Joint identification of multiple genetic variants via elastic-net variable selection in a genome-wide association analysis. *Ann. Hum. Genet.,* 74, 416-428.

CHRISTENSEN, E. L., BIRN, H., VERROUST, P. & MOESTRUP, S. K. 1998. Membrane receptors for endocytosis in the renal proximal tubule. *Int. Rev. Cytol,* 180**,** 237-284.

CHUANG, T. F., HUNG, H. C., LI, S. F., LEE, M. W., PAI, J. Y. & HUNG, C. T. 2020. Risk of chronic kidney disease in patients with kidney stones-a nationwide cohort study. *BMC Nephrol.,* 21**,** 292.

CLAYTON, D. L. & PAIETTA, J. V. 1972. Selection for circadian eclosion time in *Drosophila melanogaster*. *Science,* 178**,** 994-995.

COAST, G. M., WEBSTER, S. G., SCHEGG, K. M., TOBE, S. S. & SCHOOLEY, D. A. 2001. The *Drosophila melanogaster* homologue of an insect calcitonin-like diuretic peptide stimulates V-ATPase activity in fruit fly Malpighian tubules. *J. Exp. Biol.,* 204**,** 1795-1804.

COCHAT, P., LIUTKUS, A., FARGUE, S., BASMAISON, O., RANCHIN, B. & ROLLAND, M.-O. 2006. Primary hyperoxaluria type 1: still challenging! *Pediatr. Nephrol.,* 21**,** 1075-1081.

COCHAT, P. & RUMSBY, G. 2013. Primary hyperoxaluria. *N. Engl. J. Med.,* 369**,** 649-658.

COE, F. L., EVAN, A. & WORCESTER, E. 2005. Kidney stone disease. *J. Clin. Investig.,* 115**,** 2598-2608.

COE, F. L., EVAN, A. P., WORCESTER, E. M. & LINGEMAN, J. E. 2010. Three pathways for human kidney stone formation. *Urol. Res.,* 38**,** 147-160.

COLINET, H., FAI LEE, S. & HOFFMANN, A. 2010. Functional characterization of the *Frost* gene in *Drosophila melanogaster*: importance for recovery from chill coma. *PLoS One,* 5**,** e10925.

COLUZZI, M., PETRARCA, V. & DI DECO, M. A. 1985. Chromosomal inversion intergradation and incipient speciation in *Anopheles gambiae*. *Ital. J. Zool.,* 52**,** 45-63.

CONSORTIUM, C. T. 2003. The nature and identification of quantitative trait loci: a community's view. *Nat. Rev. Genet.,* 4**,** 911-916.

COOLEY, L., KELLEY, R. & SPRADLING, A. 1988. Insertional mutagenesis of the *Drosophila* genome with single P elements. *Science,* 239**,** 1121-1128.

COURBEBAISSE, M., PROT-BERTOYE, C., BERTOCCHIO, J., BARON, S., MARUANI, G., BRIAND, S., DAUDON, M. & HOUILLIER, P. 2016. Nephrolithiasis of

adult: from mechanisms to preventive medical treatment. *Rev. Med. Interne.,* 38**,** 44-52.

CSARDI, G. & NEPUSZ, T. 2006. The Igraph software package for complex network research. *Inter. Journal.,* Complex Systems**,** 1695.

CURRY, J. N., SAURETTE, M., ASKARI, M., PEI, L., FILLA, M. B., BEGGS, M. R., ROWE, P. S., FIELDS, T., SOMMER, A. J. & TANIKAWA, C. 2020. Claudin-2 deficiency associates with hypercalciuria in mice and human kidney stone disease. *J. Clin. Invest.,* 130**,** 1948-1960.

DAL MORO, F., MANCINI, M., TAVOLINI, I. M., DE MARCO, V. & BASSI, P. 2005. Cellular and molecular gateways to urolithiasis: a new insight. *Urol. Int.,* 74**,** 193-197.

DARROW, D. C. & YANNET, H. 1935. The changes in the distribution of body water accompanying increase and decrease in extracellular electrolyte. *J. Clin. Invest.,* 14**,** 266-275.

DAUDON, M., DORé, J.-C., JUNGERS, P. & LACOUR, B. 2004. Changes in stone composition according to age and gender of patients: a multivariate epidemiological approach. *Urol. Res.,* 32**,** 241-247.

DAUDON, M., TRAXER, O., CONORT, P., LACOUR, B. & JUNGERS, P. 2006. Type 2 diabetes increases the risk for uric acid stones. *J. Am. Soc. Nephrol.,* 17**,** 2026-2033.

DAVIES, S. A., CABRERO, P., MARLEY, R., CORRALES, G. M., GHIMIRE, S., DORNAN, A. J. & DOW, J. A. T. 2019. Epithelial function in the *Drosophila* Malpighian tubule: an in vivo renal model. *Methods Mol. Biol.,* 1926**,** 203-221.

DAY, J. P., HOUSLAY, M. D. & DAVIES, S. A. 2006. A novel role for a *Drosophila* homologue of cGMP-specific phosphodiesterase in the active transport of cGMP. *Biochem. J.,* 393**,** 481-488.

DEFRANCO, P. E., HARAGSIM, L., SCHMITZ, P. G. & BASTANI, B. 1995. Absence of vacuolar H^+-ATPase pump in the collecting duct of a patient with hypokalemic distal renal tubular acidosis and Sjögren's syndrome. *J. Am. Soc. Nephrol.,* 6**,** 295-301.

DELPIRE, E. & GAGNON, K. B. 2018. Water homeostasis and cell volume maintenance and regulation. *Curr. Top. Membr.,* 81**,** 3-52.

DENG, D., HAN, X., DIAO, Z. & LIU, W. 2021. Secreted frizzled-related protein 5 ameliorates vascular calcification in a rat model of chronic kidney disease

through the Wnt/ß-catenin pathway. *Kidney Blood Press. Res.,* 46**,** 758-767.

DENHOLM, B. 2013. Shaping up for action: the path to physiological maturation in the renal tubules of *Drosophila*. *Organogenesis,* 9**,** 40-54.

DENHOLM, B., SUDARSAN, V., PASALODOS-SANCHEZ, S., ARTERO, R., LAWRENCE, P., MADDRELL, S., BAYLIES, M. & SKAER, H. 2003. Dual origin of the renal tubules in *Drosophila*: Mesodermal cells integrate and polarize to establish secretory function. *Curr. Biol.,* 13**,** 1052-1057.

DEVUYST, O., OLINGER, E. & RAMPOLDI, L. 2017. Uromodulin: from physiology to rare and complex kidney disorders. *Nat. Rev. Nephrol.,* 13**,** 525-544.

DHAYAT, N. A., SCHALLER, A., ALBANO, G., POINDEXTER, J., GRIFFITH, C., PASCH, A., GALLATI, S., VOGT, B., MOE, O. W. & FUSTER, D. G. 2016. The vacuolar H^+-ATPase B1 subunit polymorphism p.E161K associates with impaired urinary acidification in recurrent stone formers. *J. Am. Soc. Nephrol.,* 27**,** 1544-1554.

DJ, P. 1992. Genetic heterogeneity of polycystic kidney disease in Europe. *Contrib. Nephrol.,* 97**,** 128-139.

DOBSON, A. J., CHASTON, J. M., NEWELL, P. D., DONAHUE, L., HERMANN, S. L., SANNINO, D. R., WESTMILLER, S., WONG, A. C.-N., CLARK, A. G., LAZZARO, B. P. & DOUGLAS, A. E. 2015. Host genetic determinants of microbiota-dependent nutrition revealed by genome-wide analysis of *Drosophila melanogaster*. *Nat. Commun.,* 6**,** 6312.

DONCHEVA, N. T., MORRIS, J. H., GORODKIN, J. & JENSEN, L. J. 2019. Cytoscape StringApp: network analysis and visualization of proteomics data. *J. Proteome Res.,* 18**,** 623-632.

DORNAN, A. J., HALBERG, K. V., BEUTER, L. K., DAVIES, S. A. & DOW, J. A. T. 2023. Compromised junctional integrity phenocopies age-dependent renal dysfunction in *Drosophila Snakeskin* mutants. *J. Cell Sci.,* 136**,** jcs261118.

DOW, J. A. T. 2009. Insights into the Malpighian tubule from functional genomics. *J. Exp. Biol.,* 212**,** 435-445.

DOW, J. A. T. & DAVIES, S. A. 2001. *The Drosophila melanogaster malpighian tubule*, Academic Press, London.

DOW, J. A. T., KRAUSE, S. A. & HERZYK, P. 2021. Updates on ion and water transport by the Malpighian tubule. *Curr. Opin. Insect Sci.,* 47**,** 31-37.

DOW, J. A. T., MADDRELL, S. H., GORTZ, A., SKAER, N. J., BROGAN, S. & KAISER, K. 1994. The malpighian tubules of *Drosophila melanogaster*: a novel phenotype for studies of fluid secretion and its control. *J. Exp. Biol.,* 197**,** 421-428.

DOW, J. A. T. & ROMERO, M. F. 2010. *Drosophila* provides rapid modeling of renal development, function, and disease. *Am. J. Physiol. Renal Physiol.,* 299**,** F1237-F1244.

DOW, J. A. T., SIMONS, M. & ROMERO, M. F. 2022. *Drosophila melanogaster*: a simple genetic model of kidney structure, function and disease. *Nat. Rev. Nephrol.,* 417-434.

DOWNIE, M. L. & ALEXANDER, R. T. 2022. Molecular mechanisms altering tubular calcium reabsorption. *Pediatr. Nephrol.,* 1-12.

DOWNIE, M. L., GARCIA, S. C. L., KLETA, R. & BOCKENHAUER, D. 2021. Inherited tubulopathies of the kidney: insights from genetics. *Clin. J. Am. Soc. Nephrol.,* 16**,** 620-630.

DUBE, K., MCDONALD, D. G. & O'DONNELL, M. J. 2000a. Calcium transport by isolated anterior and posterior Malpighian tubules of *Drosophila melanogaster*: roles of sequestration and secretion. *J. Insect Physiol.,* 46**,** 1449-1460.

DUBE, K. A., MCDONALD, D. G. & O'DONNELL, M. J. 2000b. Calcium homeostasis in larval and adult *Drosophila melanogaster*. *Arch. Insect Biochem. Physiol.,* 44**,** 27-39.

DURANTON, F., COHEN, G., DE SMET, R., RODRIGUEZ, M., JANKOWSKI, J., VANHOLDER, R., ARGILES, A. & GROUP, E. U. T. W. 2012. Normal and pathologic concentrations of uremic toxins. *J. Am. Soc. Nephrol.,* 23**,** 1258-1270.

EDWARDS, A. & BONNY, O. 2018. A model of calcium transport and regulation in the proximal tubule. *Am. J. Physiol. Renal Physiol.,* 315**,** F942-F953.

EGLI, D., HAFEN, E. & SCHAFFNER, W. 2004. An efficient method to generate chromosomal rearrangements by targeted DNA double-strand breaks in *Drosophila melanogaster*. *Genome Res.,* 14**,** 1382-1393.

EHLAYEL, A. M. & COPELOVITCH, L. 2019. Update on Dent disease. *Pediatr. Clin.,* 66**,** 169-178.

EKERUO, W. O., TAN, Y. H., YOUNG, M. D., DAHM, P., MALONEY, M. E., MATHIAS, B. J., ALBALA, D. M. & PREMINGER, G. M. 2004. Metabolic risk

factors and the impact of medical therapy on the management of nephrolithiasis in obese patients. *J. Urol.,* 172**,** 159-163.

EWEN-CAMPEN, B., LUAN, H., XU, J., SINGH, R., JOSHI, N., THAKKAR, T., BERGER, B., WHITE, B. H. & PERRIMON, N. 2023. Split-intein Gal4 provides intersectional genetic labeling that is repressible by Gal80. *Proc. Natl. Acad. Sci. U.S.A.,* 120**,** e2304730120.

FAGERBERG, L., HALLSTRöM, B. M., OKSVOLD, P., KAMPF, C., DJUREINOVIC, D., ODEBERG, J., HABUKA, M., TAHMASEBPOOR, S., DANIELSSON, A. & EDLUND, K. 2014. Analysis of the human tissue-specific expression by genome-wide integration of transcriptomics and antibody-based proteomics. *Mol. Cell. Proteom.,* 13**,** 397-406.

FAN, Q. X., GONG, S. Q., HONG, X. Z., FENG, X. M. & ZHANG, F. J. 2020. Clinical-grade *Garcinia cambogia* extract dissolves calcium oxalate crystals in *Drosophila* kidney stone models. *Eur. Rev. Med. Pharmacol. Sci.,* 24**,** 6434-6445.

FATTAH, H., HAMBAROUSH, Y. & GOLDFARB, D. S. 2014. Cystine nephrolithiasis. *Transl. Androl. Urol.,* 3**,** 228.

FEINGOLD, D., KNOGLER, L., STARC, T., DRAPEAU, P., O'DONNELL, M. J., NILSON, L. A. & DENT, J. A. 2019. *secCl* is a cys-loop ion channel necessary for the chloride conductance that mediates hormone-induced fluid secretion in *Drosophila*. *Sci. Rep.,* 9**,** 7464.

FELLSTRöM, B., DANIELSON, B., KARLSTRöM, B., LITHELL, H., LJUNGHALL, S. & VESSBY, B. 1983. The influence of a high dietary intake of purine-rich animal protein on urinary urate excretion and supersaturation in renal stone disease. *Clin. Sci.,* 64**,** 399-405.

FINCO, D. R. 1997. Kidney function. *Clinical biochemistry of domestic animals.* Elsevier.

FINLAYSON, B. & REID, F. 1978. The expectation of free and fixed particles in urinary stone disease. *Invest. Urol.,* 15**,** 442-448.

FISCHER, J. A., GINIGER, E., MANIATIS, T. & PTASHNE, M. 1988. GAL4 activates transcription in *Drosophila*. *Nature,* 332**,** 853-856.

FISHER, R. A. 1918. The correlation between relatives on the supposition of Mendelian inheritance. *Trans. R. Soc. Edinb.,* 52**,** 399-433.

FOUET, C., GRAY, E., BESANSKY, N. J. & COSTANTINI, C. 2012. Adaptation to aridity in the malaria mosquito *Anopheles gambiae*: chromosomal

inversion polymorphism and body size influence resistance to desiccation. *PLoS One,* 7**,** e34841.

FRANTZ, C., STEWART, K. M. & WEAVER, V. M. 2010. The extracellular matrix at a glance. *J. Cell Sci.,* 123**,** 4195-4200.

GALLAGHER, M. D. & CHEN-PLOTKIN, A. S. 2018. The post-GWAS era: from association to function. *Am. J. Hum. Genet.,* 102**,** 717-730.

GAMBERI, C., HIPFNER, D. R., TRUDEL, M. & LUBELL, W. D. 2017. *Bicaudal C* mutation causes *myc* and TOR pathway up-regulation and polycystic kidney disease-like phenotypes in *Drosophila*. *PLoS Genet.,* 13**,** e1006694.

GARCIA, M. A., NELSON, W. J. & CHAVEZ, N. 2018. Cell-cell junctions organize structural and signaling networks. *Cold Spring Harb. Perspect. Biol.,* 10**,** a029181.

GARIMELLA, P. S., KATZ, R., WAIKAR, S. S., SRIVASTAVA, A., SCHMIDT, I., HOOFNAGLE, A., PALSSON, R., RENNKE, H. G., STILLMAN, I. E., WANG, K., KESTENBAUM, B. R. & IX, J. H. 2022. Kidney tubulointerstitial fibrosis and tubular secretion. *Am. J. Kidney Dis.,* 79**,** 709-716.

GARLAPOW, M. E., EVERETT, L. J., ZHOU, S., GEARHART, A. W., FAY, K. A., HUANG, W., MOROZOVA, T. V., ARYA, G. H., TURLAPATI, L. & ST. ARMOUR, G. 2017. Genetic and genomic response to selection for food consumption in *Drosophila melanogaster*. *Behav. Genet.,* 47**,** 227-243.

GARRELFS, S. F., RUMSBY, G., PETERS-SENGERS, H., ERGER, F., GROOTHOFF, J. W., BECK, B. B., OOSTERVELD, M. J., PELLE, A., NEUHAUS, T. & ADAMS, B. 2019. Patients with primary hyperoxaluria type 2 have significant morbidity and require careful follow-up. *Kidney Int.,* 96**,** 1389-1399.

GEORGE, B., YOU, D., JOY, M. S. & ALEKSUNES, L. M. 2017. Xenobiotic transporters and kidney injury. *Adv. Drug Deliv. Rev.,* 116**,** 73-91.

GERKE, P., SELLIN, L., KRETZ, O., PETRASCHKA, D., ZENTGRAF, H., BENZING, T. & WALZ, G. 2005. NEPH2 is located at the glomerular slit diaphragm, interacts with nephrin and is cleaved from podocytes by metalloproteinases. *J. Am. Soc. Nephrol.,* 16**,** 1693-1702.

GHIMIRE, S. 2019. *Identifying genetic loci for metabolic disorders affecting the renal tract*. University of Glasgow.

GILLEN, D. L., WORCESTER, E. M. & COE, F. L. 2005. Decreased renal function among adults with a history of nephrolithiasis: a study of NHANES III. *Kidney Int.,* 67**,** 685-690.

GOLDFARB, D. S., AVERY, A. R., BEARA-LASIC, L., DUNCAN, G. E. & GOLDBERG, J. 2019. A twin study of genetic influences on nephrolithiasis in women and men. *Kidney Int. Rep.,* 4**,** 535-540.

GOLDFARB, D. S., FISCHER, M. E., KEICH, Y. & GOLDBERG, J. 2005. A twin study of genetic and dietary influences on nephrolithiasis: a report from the Vietnam Era Twin (VET) Registry. *Kidney Int.,* 67**,** 1053-1061.

GOLDSTEIN, D. B. 2009. Common genetic variation and human traits. *N. Engl. J. Med.,* 360**,** 1696-1698.

GRATZ, S. J., CUMMINGS, A. M., NGUYEN, J. N., HAMM, D. C., DONOHUE, L. K., HARRISON, M. M., WILDONGER, J. & O'CONNOR-GILES, K. M. 2013. Genome engineering of *Drosophila* with the CRISPR RNA-guided Cas9 nuclease. *Genetics,* 194**,** 1029-1035.

GRAY, E. M., ROCCA, K. A., COSTANTINI, C. & BESANSKY, N. J. 2009. Inversion 2La is associated with enhanced desiccation resistance in *Anopheles gambiae*. *Malar. J.,* 8**,** 1-12.

GREENBERG, A. & VERBALIS, J. 2006. Vasopressin receptor antagonists. *Kidney Int.,* 69**,** 2124-2130.

GRIFFING, B. 1956. Concept of general and specific combining ability in relation to diallel crossing systems. *Aust. J. Biol. Sci.,* 9**,** 463-493.

GRIFFITH, D. P. 1978. Struvite stones. *Kidney Int.,* 13**,** 372-382.

GRILLO, A., SALVI, L., CORUZZI, P., SALVI, P. & PARATI, G. 2019. Sodium intake and hypertension. *Nutrients,* 11**,** 1970.

GUBINA, N., NAUDI, A., STEFANATOS, R., JOVE, M., SCIALO, F., FERNANDEZ-AYALA, D. J., RANTAPERO, T., YURKEVYCH, I., PORTERO-OTIN, M., NYKTER, M., LUSHCHAK, O., NAVAS, P., PAMPLONA, R. & SANZ, A. 2019. Essential physiological differences characterize short- and long-lived strains of *Drosophila melanogaster*. *J. Gerontol. A Biol. Sci. Med. Sci.,* 74**,** 1835-1843.

GUDBJARTSSON, D. F., HOLM, H., INDRIDASON, O. S., THORLEIFSSON, G., EDVARDSSON, V., SULEM, P., DE VEGT, F., D'ANCONA, F. C., DEN HEIJER, M. & FRANZSON, L. 2010. Association of variants at *UMOD* with chronic kidney disease and kidney stones-role of age and comorbid diseases. *PLoS Genet.,* 6**,** e1001039.

GURUHARSHA, K., RUAL, J.-F., ZHAI, B., MINTSERIS, J., VAIDYA, P., VAIDYA, N., BEEKMAN, C., WONG, C., RHEE, D. Y. & CENAJ, O. 2011. A protein complex network of *Drosophila melanogaster*. *Cell,* 147**,** 690-703.

HALBERG, K. A., TERHZAZ, S., CABRERO, P., DAVIES, S. A. & DOW, J. A. T. 2015. Tracing the evolutionary origins of insect renal function. *Nat. Commun.,* 6**,** 6800.

HALBRITTER, J., BAUM, M., HYNES, A. M., RICE, S. J., THWAITES, D. T., GUCEV, Z. S., FISHER, B., SPANEAS, L., PORATH, J. D., BRAUN, D. A., WASSNER, A. J., NELSON, C. P., TASIC, V., SAYER, J. A. & HILDEBRANDT, F. 2015. Fourteen monogenic genes account for 15% of nephrolithiasis/nephrocalcinosis. *J. Am. Soc. Nephrol.,* 26**,** 543-551.

HALEY, W. E., ENDERS, F. T., VAUGHAN, L. E., MEHTA, R. A., THOMAN, M. E., VRTISKA, T. J., KRAMBECK, A. E., LIESKE, J. C. & RULE, A. D. 2016. Kidney function after the first kidney stone event. *Mayo Clin. Proc.,* 91**,** 1744-1752.

HALL, A. M., UNWIN, R. J., PARKER, N. & DUCHEN, M. R. 2009. Multiphoton imaging reveals differences in mitochondrial function between nephron segments. *J. Am. Soc. Nephrol.,* 20**,** 1293-1302.

HAN, H., SEGAL, A. M., SEIFTER, J. L. & DWYER, J. T. 2015. Nutritional management of kidney stones (nephrolithiasis). *Clin. Nutr. Res.,* 4**,** 137-152.

HANSEN, J., SEALFON, R., MENON, R., EADON, M. T., LAKE, B. B., STECK, B., ANJANI, K., PARIKH, S., SIGDEL, T. K., ZHANG, G., VELICKOVIC, D., BARWINSKA, D., ALEXANDROV, T., DOBI, D., RASHMI, P., OTTO, E. A., RIVERA, M., ROSE, M. P., ANDERTON, C. R., SHAPIRO, J. P., PAMREDDY, A., WINFREE, S., XIONG, Y., HE, Y., DE BOER, I. H., HODGIN, J. B., BARISONI, L., NAIK, A. S., SHARMA, K., SARWAL, M. M., ZHANG, K., HIMMELFARB, J., ROVIN, B., EL-ACHKAR, T. M., LASZIK, Z., HE, J. C., DAGHER, P. C., VALERIUS, M. T., JAIN, S., SATLIN, L. M., TROYANSKAYA, O. G., KRETZLER, M., IYENGAR, R., AZELOGLU, E. U. & KIDNEY PRECISION MEDICINE, P. 2022. A reference tissue atlas for the human kidney. *Sci. Adv.,* 8**,** eabn4965.

HAO, X. J., SHAO, Z. H., ZHANG, N., JIANG, M. H., CAO, X., LI, S., GUAN, Y. L. & WANG, C. L. 2023. Integrative genome-wide analyses identify novel loci associated with kidney stones and provide insights into its genetic architecture. *Nat. Commun.,* 14**,** 7498.

HARDIN, P. E., HALL, J. C. & ROSBASH, M. 1990. Feedback of the *Drosophila* period gene product on circadian cycling of its messenger RNA levels. *Nature,* 343**,** 536-540.

HARNISH, J. M., DEAL, S. L., NETWORK, U. D., CHAO, H.-T., WANGLER, M. F. & YAMAMOTO, S. 2019. In vivo functional study of disease-associated rare human variants using *Drosophila*. *J. Vis. Exp.*, 10.3791/59658.

HATTON-ELLIS, E., AINSWORTH, C., SUSHAMA, Y., WAN, S., VIJAYRAGHAVAN, K. & SKAER, H. 2007. Genetic regulation of patterned tubular branching in *Drosophila*. *Proc. Natl. Acad. Sci. U.S.A.,* 104**,** 169-174.

HAYMAN, B. 1954. The theory and analysis of diallel crosses. *Genetics,* 39**,** 789.

HE, B. Z., LUDWIG, M. Z., DICKERSON, D. A., BARSE, L., ARUN, B., VILHJALMSSON, B. J., JIANG, P., PARK, S. Y., TAMARINA, N. A., SELLECK, S. B., WITTKOPP, P. J., BELL, G. I. & KREITMAN, M. 2014. Effect of genetic variation in a *Drosophila* model of diabetes-associated misfolded human proinsulin. *Genetics,* 196**,** 557-567.

HENTGES, K. E. & JUSTICE, M. J. 2004. Checks and balancers: balancer chromosomes to facilitate genome annotation. *TiG,* 20**,** 252-259.

HILL, N. R., FATOBA, S. T., OKE, J. L., HIRST, J. A., O'CALLAGHAN, C. A., LASSERSON, D. S. & HOBBS, F. D. 2016. Global prevalence of chronic kidney disease-a systematic review and meta-analysis. *PLoS One,* 11**,** e0158765.

HIRATA, T., CABRERO, P., BERKHOLZ, D. S., BONDESON, D. P., RITMAN, E. L., THOMPSON, J. R., DOW, J. A. T. & ROMERO, M. F. 2012. In vivo genetic model for calcium oxalate nephrolithiasis. *Am. J. Physiol. Renal Physiol.,* 303**,** F1555-F1562.

HODEIFY, R., KREYDIYYEH, S. & ZAID, L. M. J. 2024. Identified and potential internalization signals involved in trafficking and regulation of Na^+/K^+ ATPase activity. *Mol. Cell. Biochem.,* 479**,** 1583-1598.

HOPPE, B. 2012. An update on primary hyperoxaluria. *Nat. Rev. Nephrol.,* 8**,** 467-475.

HOWLES, S. A. & THAKKER, R. V. 2020. Genetics of kidney stone disease. *Nat. Rev. Urol.,* 17**,** 407-421.

HSI, R. S., KABAGAMBE, E. K., SHU, X., HAN, X., MILLER, N. L. & LIPWORTH, L. 2018. Race-and sex-related differences in nephrolithiasis risk among blacks and whites in the southern community cohort study. *Urology,* 118**,** 36-42.

HU, Y., COMJEAN, A., RODIGER, J., LIU, Y., GAO, Y., CHUNG, V., ZIRIN, J., PERRIMON, N. & MOHR, S. E. 2021. FlyRNAi.org-the database of the

Drosophila RNAi screening center and transgenic RNAi project: 2021 update. *Nucleic Acids Res.,* 49**,** D908-D915.

HU, Y., FLOCKHART, I., VINAYAGAM, A., BERGWITZ, C., BERGER, B., PERRIMON, N. & MOHR, S. E. 2011. An integrative approach to ortholog prediction for disease-focused and other functional studies. *BMC Bioinformatics,* 12**,** 357.

HUANG, W., CAMPBELL, T., CARBONE, M. A., JONES, W. E., UNSELT, D., ANHOLT, R. R. H. & MACKAY, T. F. C. 2020. Context-dependent genetic architecture of *Drosophila* life span. *PLoS Biol.,* 18**,** e3000645.

HUANG, W., MASSOURAS, A., INOUE, Y., PEIFFER, J., RAMIA, M., TARONE, A. M., TURLAPATI, L., ZICHNER, T., ZHU, D. H., LYMAN, R. F., MAGWIRE, M. M., BLANKENBURG, K., CARBONE, M. A., CHANG, K., ELLIS, L. L., FERNANDEZ, S., HAN, Y., HIGHNAM, G., HJELMEN, C. E., JACK, J. R., JAVAID, M., JAYASEELAN, J., KALRA, D., LEE, S., LEWIS, L., MUNIDASA, M., ONGERI, F., PATEL, S., PERALES, L., PEREZ, A., PU, L. L., ROLLMANN, S. M., RUTH, R., SAADA, N., WARNER, C., WILLIAMS, A., WU, Y. Q., YAMAMOTO, A., ZHANG, Y. Q., ZHU, Y. M., ANHOLT, R. R. H., KORBEL, J. O., MITTELMAN, D., MUZNY, D. M., GIBBS, R. A., BARBADILLA, A., JOHNSTON, J. S., STONE, E. A., RICHARDS, S., DEPLANCKE, B. & MACKAY, T. F. C. 2014. Natural variation in genome architecture among 205 *Drosophila melanogaster* Genetic Reference Panel lines. *Genome Res.,* 24**,** 1193-1208.

HUANG, W., RICHARDS, S., CARBONE, M. A., ZHU, D., ANHOLT, R. R., AYROLES, J. F., DUNCAN, L., JORDAN, K. W., LAWRENCE, F. & MAGWIRE, M. M. 2012. Epistasis dominates the genetic architecture of *Drosophila* quantitative traits. *Proc. Natl. Acad. Sci. U.S.A.,* 109**,** 15553-15559.

HYDE, R. R. A high fecundity record for *Drosophila melanogaster*. Proc. Indiana Acad. Sci., 1921. 259-260.

ICHIDA, K., MATSUMURA, T., SAKUMA, R., HOSOYA, T. & NISHINO, T. 2001. Mutation of human molybdenum cofactor sulfurase gene is responsible for classical xanthinuria type II. *Biochem. Biophys. Res. Commun.,* 282**,** 1194-1200.

IOANNIDIS, J. P. 2008. Why most discovered true associations are inflated. *Epidemiol.,* 19**,** 640-648.

IVANOV, D. K., ESCOTT-PRICE, V., ZIEHM, M., MAGWIRE, M. M., MACKAY, T. F. C., PARTRIDGE, L. & THOMTON, J. M. 2015. Longevity GWAS using the genetic reference panel. *J. Gerontol. A. Biol. Sci. Med. Sci.,* 70**,** 1470-1478.

JACK, J. & MYETTE, G. 1999. Mutations that alter the morphology of the malpighian tubules in *Drosophila*. *Dev. Genes Evol.,* 209**,** 546-554.

JACOBSSON, J. A., SCHIOTH, H. B. & FREDRIKSSON, R. 2012. The impact of intronic single nucleotide polymorphisms and ethnic diversity for studies on the obesity gene *FTO*. *Obes. Rev.,* 13**,** 1096-109.

JANNING, W., LUTZ, A. & WISSEN, D. 1986. Clonal analysis of the blastoderm anlage of the Malpighian tubules in *Drosophila melanogaster*. *Roux's Arch. Dev. Biol.,* 195**,** 22-32.

JOSEPH, C. B., MARINIELLO, M., YOSHIFUJI, A., SCHIANO, G., LAKE, J., MARTEN, J., RICHMOND, A., HUFFMAN, J. E., CAMPBELL, A., HARRIS, S. E., TROYANOV, S., COCCA, M., ROBINO, A., THéRIAULT, S., ECKARDT, K.-U., WUTTKE, M., CHENG, Y., CORRE, T., KOLCIC, I., BLACK, C., BRUAT, V., CONCAS, M. P., SALA, C., AESCHBACHER, S., SCHAEFER, F., BERGMANN, S., CAMPBELL, H., OLDEN, M., POLASEK, O., PORTEOUS, D. J., DEARY, I. J., MADORE, F., AWADALLA, P., GIROTTO, G., ULIVI, S., CONEN, D., WUEHL, E., OLINGER, E., WILSON, J. F., BOCHUD, M., KöTTGEN, A., HAYWARD, C. & DEVUYST, O. 2022. Meta-GWAS reveals novel genetic variants associated with urinary excretion of uromodulin. *J. Am. Soc. Nephrol. ,* 33**,** 511-529.

JOU, Y.-C., TSAI, Y.-S., HSIEH, H.-Y., SHEN, C.-H., FANG, C.-Y., CHEN, S.-Y., LIN, M.-F., CHEN, F.-H. & HSU, C.-D. 2014. Age-dependent association between Dickkopf-1 and calcium-containing urolithiasis. *Urology,* 83**,** 1006-1010.

KAKIDANI, H. & PTASHNE, M. 1988. GAL4 activates gene expression in mammalian cells. *Cell,* 52**,** 161-167.

KARET, F. E., FINBERG, K. E., NELSON, R. D., NAYIR, A., MOCAN, H., SANJAD, S. A., RODRIGUEZ-SORIANO, J., SANTOS, F., CREMERS, C. W. & PIETRO, A. D. 1999. Mutations in the gene encoding B1 subunit of H^+-ATPase cause renal tubular acidosis with sensorineural deafness. *Nat. Genet.,* 21**,** 84-90.

KEAN, L., CAZENAVE, W., COSTES, L., BRODERICK, K. E., GRAHAM, S., POLLOCK, V. P., DAVIES, S. A., VEENSTRA, J. A. & DOW, J. A. T. 2002. Two nitridergic peptides are encoded by the gene capability in *Drosophila melanogaster*. *Am. J. Physiol. Regul. Integr. Comp. Physiol.,* 282**,** R1297-R1307.

KEARSEY, M. & POONI, H. 2020. *Genetical analysis of quantitative traits*, Garland Science.

KELLER, A. 2007. *Drosophila melanogaster*'s history as a human commensal. *Curr. Biol.,* 17**,** R77-R81.

KHAN, S., GLENTON, P. & BYER, K. 2006. Modeling of hyperoxaluric calcium oxalate nephrolithiasis: experimental induction of hyperoxaluria by hydroxy-L-proline. *Kidney Int.,* 70**,** 914-923.

KHAN, S. R. 2006. Renal tubular damage/dysfunction: key to the formation of kidney stones. *Urol. Res.,* 34**,** 86-91.

KHAN, S. R., BYER, K. J., THAMILSELVAN, S., HACKETT, R. L., MCCORMACK, W. T., BENSON, N. A., VAUGHN, K. L. & ERDOS, G. W. 1999. Crystal-cell interaction and apoptosis in oxalate-associated injury of renal epithelial cells. *J. Am. Soc. Nephrol.,* 10**,** S457-S463.

KHAN, S. R. & CANALES, B. K. 2015. Unified theory on the pathogenesis of Randall's plaques and plugs. *Urolithiasis,* 43**,** 109-123.

KHAN, S. R., GLENTON, P. A., BACKOV, R. & TALHAM, D. R. 2002. Presence of lipids in urine, crystals and stones: implications for the formation of kidney stones. *Kidney Int.,* 62**,** 2062-2072.

KHAN, S. R. & HACKETT, R. L. 1987. Urolithogenesis of mixed foreign body stones. *J. Urol.,* 138**,** 1321-1328.

KHAN, S. R., PEARLE, M. S., ROBERTSON, W. G., GAMBARO, G., CANALES, B. K., DOIZI, S., TRAXER, O. & TISELIUS, H.-G. 2016. Kidney stones. *Nat. Rev. Dis. Primers,* 2**,** 1-23.

KIDWELL, M. G., KIDWELL, J. F. & SVED, J. A. 1977. Hybrid dysgenesis in *Drosophila melanogaster*: a syndrome of aberrant traits including mutation, sterility and male recombination. *Genetics,* 86**,** 813-833.

KIM, J., KOO, B.-K. & KNOBLICH, J. A. 2020. Human organoids: model systems for human biology and medicine. *Nat. Rev. Mol. Cell Biol.,* 21**,** 571-584.

KLEIN, R. J., ZEISS, C., CHEW, E. Y., TSAI, J.-Y., SACKLER, R. S., HAYNES, C., HENNING, A. K., SANGIOVANNI, J. P., MANE, S. M. & MAYNE, S. T. 2005. Complement factor H polymorphism in age-related macular degeneration. *Science,* 308**,** 385-389.

KLEINMAN, H. K., PHILP, D. & HOFFMAN, M. P. 2003. Role of the extracellular matrix in morphogenesis. *Curr. Opin. Biotechnol.,* 14**,** 526-532.

KNEPPER, M. A. 1997. Molecular physiology of urinary concentrating mechanism: regulation of aquaporin water channels by vasopressin. *Am. J. Physiol. Renal Physiol.,* 272**,** F3-F12.

KOK, D. J. & KHAN, S. R. 1994. Calcium oxalate nephrolithiasis, a free or fixed particle disease. *Kidney Int.,* 46**,** 847-854.

KONOPKA, R. J. & BENZER, S. 1971. Clock mutants of *Drosophila melanogaster*. *Proc. Natl. Acad. Sci. U.S.A.,* 68**,** 2112-2116.

KUBLI, E. 1992. My favorite molecule. the sex-peptide. *Bioessays,* 14**,** 779-784.

KULMS, D., DüSSMANN, H., PöPPELMANN, B., STäNDER, S., SCHWARZ, A. & SCHWARZ, T. 2002. Apoptosis induced by disruption of the actin cytoskeleton is mediated via activation of CD95 (Fas/APO-1). *Cell Death Differ.,* 9**,** 598-608.

KUZNETSOVA, A., BROCKHOFF, P. B. & CHRISTENSEN, R. H. B. 2017. lmerTest Package: tests in linear mixed effects models. *J. Stat. Softw.,* 82**,** 1-26.

LAKE, B. B., MENON, R., WINFREE, S., HU, Q., MELO FERREIRA, R., KALHOR, K., BARWINSKA, D., OTTO, E. A., FERKOWICZ, M. & DIEP, D. 2023. An atlas of healthy and injured cell states and niches in the human kidney. *Nature,* 619**,** 585-594.

LEABMAN, M. K. & GIACOMINI, K. M. 2003. Estimating the contribution of genes and environment to variation in renal drug clearance. *Pharmacogenetics,* 13**,** 581-584.

LEADER, D. P., KRAUSE, S. A., PANDIT, A., DAVIES, S. A. & DOW, J. A. T. 2018. FlyAtlas 2: a new version of the expression atlas with RNA-Seq, miRNA-Seq and sex-specific data. *Nucleic Acids Res.,* 46**,** D809-D815.

LEE, H. W., HANDLOGTEN, M. E., OSIS, G., CLAPP, W. L., WAKEFIELD, D. N., VERLANDER, J. W. & WEINER, I. D. 2017. Expression of sodium-dependent dicarboxylate transporter 1 (NaDC1/SLC13A2) in normal and neoplastic human kidney. *Am. J. Physiol. Renal Physiol.,* 312**,** F427-F435.

LEMAITRE, B., NICOLAS, E., MICHAUT, L., REICHHART, J. M. & HOFFMANN, J. A. 1996. The dorsoventral regulatory gene cassette *spatzle/Toll/cactus* controls the potent antifungal response in *Drosophila* adults. *Cell,* 86**,** 973-983.

LI, H. J., JANSSENS, J., DE WAEGENEER, M., KOLLURU, S. S., DAVIE, K., GARDEUX, V., SAELENS, W., DAVID, F., BRBIC, M., LESKOVEC, J., MCLAUGHLIN, C. N., XIE, Q. J., JONES, R. C., BRUECKNER, K., SHIM, J., TATTIKOTA, S. G., SCHNORRER, F., RUST, K., NYSTUL, T. G., CARVALHO-SANTOS, Z., RIBEIRO, C., PAL, S., MAHADEVARAJU, S., PRZYTYCKA, T. M., ALLEN, A. M., GOODWIN, S. F., BERRY, C. W., FULLER, M. T., WHITE-COOPER, H., MATUNIS, E. L., DINARDO, S., GALENZA, A., O'BRIEN, L. E.,

DOW, J. A. T., JASPER, H., OLIVER, B., PERRIMON, N., DEPLANCKE, B., QUAKE, S. R., LUO, L. Q., AERTS, S. & CONSORTIUM, F. 2022. Fly Cell Atlas: a single-nucleus transcriptomic atlas of the adult fruit fly. *Science,* 375**,** eabk2432.

LI, S., SANNA, S., MASCHIO, A., BUSONERO, F., USALA, G., MULAS, A., LAI, S., DEI, M., ORRù, M. & ALBAI, G. 2007. The *GLUT9* gene is associated with serum uric acid levels in Sardinia and Chianti cohorts. *PLoS Genet.,* 3**,** e194.

LI, X., DANG, X., CHENG, Y., ZHANG, D., ZHANG, X., ZOU, T. & XING, J. 2018. Common variants in *ALPL* gene contribute to the risk of kidney stones in the Han Chinese population. *Genet. Test. Mol. Biomark.,* 22**,** 187-192.

LIESKE, J. C., SPARGO, B. H. & TOBACK, F. G. 1992. Endocytosis of calcium oxalate crystals and proliferation of renal tubular epithelial cells in a patient with type 1 primary hyperoxaluria. *J. Urol.,* 148**,** 1517-1519.

LIN, Y., CHEN, Z.-X., OLIVER, B. & HARBISON, S. T. 2016. Microenvironmental gene expression plasticity among individual *Drosophila melanogaster*. *G3 (Bethesda),* 6**,** 4197-4210.

LIN, Z., JIN, S., DUAN, X., WANG, T., MARTINI, S., HULAMM, P., CHA, B., HUBBARD, A., DONOWITZ, M. & GUGGINO, S. E. 2011. Chloride channel (Clc)-5 is necessary for exocytic trafficking of Na^+/H^+ exchanger 3 (NHE3). *J. Biol. Chem.,* 286**,** 22833-22845.

LINNES, M. P., KRAMBECK, A. E., CORNELL, L., WILLIAMS JR, J. C., KORINEK, M., BERGSTRALH, E. J., LI, X., RULE, A. D., MCCOLLOUGH, C. M. & VRTISKA, T. J. 2013. Phenotypic characterization of kidney stone formers by endoscopic and histological quantification of intrarenal calcification. *Kidney Int.,* 84**,** 818-825.

LOGANATHAN, R., LITTLE, C. D. & RONGISH, B. J. 2020. Extracellular matrix dynamics in tubulogenesis. *Cell Signal.,* 72**,** 109619.

LOPEZ-NOVOA, J. M., MARTINEZ-SALGADO, C., RODRIGUEZ-PENA, A. B. & LOPEZ-HERNANDEZ, F. J. 2010. Common pathophysiological mechanisms of chronic kidney disease: therapeutic perspectives. *Pharmacol. Ther.,* 128**,** 61-81.

LORD, S. J., VELLE, K. B., MULLINS, R. D. & FRITZ-LAYLIN, L. K. 2020. SuperPlots: Communicating reproducibility and variability in cell biology. *J. Cell Biol.,* 219**,** e202001064.

LUAN, H., PEABODY, N. C., VINSON, C. R. & WHITE, B. H. 2006. Refined spatial manipulation of neuronal function by combinatorial restriction of transgene expression. *Neuron,* 52**,** 425-436.

MA, Y., CREANGA, A., LUM, L. & BEACHY, P. A. 2006. Prevalence of off-target effects in *Drosophila* RNA interference screens. *Nature,* 443**,** 359-363.

MACKAY, T. F. 2001. The genetic architecture of quantitative traits. *Annu. Rev. Genet.,* 35**,** 303-339.

MACKAY, T. F., STONE, E. A. & AYROLES, J. F. 2009. The genetics of quantitative traits: challenges and prospects. *Nat. Rev. Genet.,* 10**,** 565-577.

MACKAY, T. F. C. & HUANG, W. 2018. Charting the genotype-phenotype map: lessons from the *Drosophila melanogaste*r Genetic Reference Panel. *Wiley Interdiscip. Rev. Dev. Biol.,* 7**,** e289.

MACKAY, T. F. C., RICHARDS, S., STONE, E. A., BARBADILLA, A., AYROLES, J. F., ZHU, D. H., CASILLAS, S., HAN, Y., MAGWIRE, M. M., CRIDLAND, J. M., RICHARDSON, M. F., ANHOLT, R. R. H., BARRON, M., BESS, C., BLANKENBURG, K. P., CARBONE, M. A., CASTELLANO, D., CHABOUB, L., DUNCAN, L., HARRIS, Z., JAVAID, M., JAYASEELAN, J. C., JHANGIANI, S. N., JORDAN, K. W., LARA, F., LAWRENCE, F., LEE, S. L., LIBRADO, P., LINHEIRO, R. S., LYMAN, R. F., MACKEY, A. J., MUNIDASA, M., MUZNY, D. M., NAZARETH, L., NEWSHAM, I., PERALES, L., PU, L. L., QU, C., RAMIA, M., REID, J. G., ROLLMANN, S. M., ROZAS, J., SAADA, N., TURLAPATI, L., WORLEY, K. C., WU, Y. Q., YAMAMOTO, A., ZHU, Y. M., BERGMAN, C. M., THORNTON, K. R., MITTELMAN, D. & GIBBS, R. A. 2012. The *Drosophila melanogaster* Genetic Reference Panel. *Nature,* 482**,** 173-178.

MACMILLAN, H. A., ANDERSEN, J. L., DAVIES, S. A. & OVERGAARD, J. 2015. The capacity to maintain ion and water homeostasis underlies interspecific variation in *Drosophila* cold tolerance. *Sci. Rep.,* 5**,** 18607.

MACMILLAN, H. A. & SINCLAIR, B. J. 2011. Mechanisms underlying insect chill-coma. *J. Insect Physiol.,* 57**,** 12-20.

MADDRELL, S. H. 1991. The fastest fluid-secreting cell known: the upper Malpighian tubule of *Rhodnius*. *BioEssays,* 13**,** 357-362.

MANOLIO, T. A., COLLINS, F. S., COX, N. J., GOLDSTEIN, D. B., HINDORFF, L. A., HUNTER, D. J., MCCARTHY, M. I., RAMOS, E. M., CARDON, L. R. & CHAKRAVARTI, A. 2009. Finding the missing heritability of complex diseases. *Nature,* 461**,** 747-753.

MANRIQUE-CABALLERO, C. L., BARASCH, J., ZAIDI, S. K., BATES, C. M., RAY, E. C., KLEYMAN, T. R. & AL-BATAINEH, M. M. 2025. Expression and distribution of MUC1 in the developing and adult kidney. *Am. J. Physiol. Renal Physiol.,* 328**,** F107-F120.

MARCHINI, J., CARDON, L. R., PHILLIPS, M. S. & DONNELLY, P. 2004. The effects of human population structure on large genetic association studies. *Nat. Genet.,* 36**,** 512-517.

MARIGORTA, U. M., RODRíGUEZ, J. A., GIBSON, G. & NAVARRO, A. 2018. Replicability and prediction: lessons and challenges from GWAS. *Trends Genet.,* 34**,** 504-517.

MARKOW, T. A. 2015. The secret lives of *Drosophila* flies. *Elife,* 4**,** e06793.

MARTINEZ, S. A., KAREL, I. Z., SILVAROLI, J. A., AHMED, E., KIM, J. Y., STAYTON, A., PATEL, P. S., AFJAL, M. A., HORTON, T. & BOHMER, M. 2025. Resazurin dye is an in vivo sensor of kidney tubular function. *Kidney Int.,* 107**,** 508-520.

MAZEROLLE, M. J. 2020. AICcmodavg: Model selection and multimodel inference based on (Q)AIC(c). *R package version 2.3-1.*

MCARDLE, P. F., PARSA, A., CHANG, Y. P. C., WEIR, M. R., O'CONNELL, J. R., MITCHELL, B. D. & SHULDINER, A. R. 2008. Association of a common nonsynonymous variant in GLUT9 with serum uric acid levels in old order amish. *Arthritis Rheum.,* 58**,** 2874-2881.

MCAULEY, J. L., LINDEN, S. K., PNG, C. W., KING, R. M., PENNINGTON, H. L., GENDLER, S. J., FLORIN, T. H., HILL, G. R., KOROLIK, V. & MCGUCKIN, M. A. 2007. MUC1 cell surface mucin is a critical element of the mucosal barrier to infection. *J. Clin. Invest.,* 117**,** 2313-2324.

MCCLELLAN, J. & KING, M.-C. 2010. Genetic heterogeneity in human disease. *Cell,* 141**,** 210-217.

MCCLINTOCK, B. Controlling elements and the gene. Cold Spring Harbor symposia on quantitative biology, 1956. Cold Spr. Harb. Symp. Quant. Biol., 197-216.

MCGEOWN, M. 1960. Heredity in renal stone disease. *Clin. Sci.,* 19**,** 465-471.

MCGONIGLE, P. & RUGGERI, B. 2014. Animal models of human disease: challenges in enabling translation. *Biochem. Pharmacol.,* 87**,** 162-171.

MCKEE, M., YADAV, M., FOSTER, B., SOMERMAN, M., FARQUHARSON, C. & MILLáN, J. 2013. Compounded PHOSPHO1/ALPL deficiencies reduce dentin mineralization. *J. Dent. Res.,* 92**,** 721-727.

MICCHELLI, C. A. & PERRIMON, N. 2006. Evidence that stem cells reside in the adult *Drosophila* midgut epithelium. *Nature,* 439**,** 475-479.

MILLER, D. E., COOK, K. R. & HAWLEY, R. S. 2019. The joy of balancers. *PLoS Genet.,* 15**,** e1008421.

MILLER, J., CHI, T., KAPAHI, P., KAHN, A. J., KIM, M. S., HIRATA, T., ROMERO, M. F., DOW, J. A. T. & STOLLER, M. L. 2013. *Drosophila melanogaster* as an emerging translational model of human nephrolithiasis. *J. Urol.,* 190**,** 1648-1656.

MITCHELL, H. K. & GLASSMAN, E. 1959. Hypoxanthine in rosy and maroon-like mutants of *Drosophila melanogaster*. *Science,* 129**,** 268.

MOE, O. W. 2006. Kidney stones: pathophysiology and medical management. *The lancet,* 367**,** 333-344.

MOHAN, S., TIWARI, M. N., BIALA, Y. & YAARI, Y. 2019. Regulation of neuronal Na^+/K^+-ATPase by specific protein kinases and protein phosphatases. *J. Neurosci.,* 39**,** 5440-5451.

MORGAN, T. H. 1910. Sex limited inheritance in *Drosophila*. *Science,* 32**,** 120-122.

MORGANTE, F., SøRENSEN, P., SORENSEN, D. A., MALTECCA, C. & MACKAY, T. F. 2015. Genetic architecture of micro-environmental plasticity in *Drosophila melanogaster*. *Sci. Rep.,* 5**,** 9785.

MORNET, E., STURA, E., LIA-BALDINI, A.-S., STIGBRAND, T., MéNEZ, A. & LE DU, M.-H. L. N. 2001. Structural evidence for a functional role of human tissue nonspecific alkaline phosphatase in bone mineralization. *J. Biol. Chem.,* 276**,** 31171-31178.

MULLER, H. J. 1918. Genetic variability, twin hybrids and constant hybrids, in a case of balanced lethal factors. *Genetics,* 3**,** 422.

MULLER, H. J. 1927. Artificial transmutation of the gene. *Science,* 66**,** 84-87.

NARULA, S., TANDON, S., KUMAR, D., VARSHNEY, S., ADLAKHA, K., SENGUPTA, S., SINGH, S. K. & TANDON, C. 2020. Human kidney stone matrix proteins alleviate hyperoxaluria induced renal stress by targeting cell-crystal interactions. *Life Sci.,* 262**,** 118498.

NEUMANN-HAEFELIN, E., KRAMER-ZUCKER, A., SLANCHEV, K., HARTLEBEN, B., NOUTSOU, F., MARTIN, K., WANNER, N., RITTER, A., GöDEL, M. & PAGEL, P. 2010. A model organism approach: defining the role of Neph proteins as regulators of neuron and kidney morphogenesis. *Hum. Mol. Genet.,* 19**,** 2347-2359.

NIE, M., BAL, M. S., YANG, Z., LIU, J., RIVERA, C., WENZEL, A., BECK, B. B., SAKHAEE, K., MARCIANO, D. K. & WOLF, M. T. 2016. Mucin-1 increases renal TRPV5 activity in vitro, and urinary level associates with calcium nephrolithiasis in patients. *J. Am. Soc. Nephrol.,* 27**,** 3447-3458.

NIELSEN, R., CHRISTENSEN, E. I. & BIRN, H. 2016. Megalin and cubilin in proximal tubule protein reabsorption: from experimental models to human disease. *Kidney Int.,* 89**,** 58-67.

O'DONNELL, M. J. & MADDRELL, S. H. 1995. Fluid reabsorption and ion transport by the lower Malpighian tubules of adult female *Drosophila*. *J. Exp. Biol.,* 198**,** 1647-1653.

O'KANE, C. J. & GEHRING, W. J. 1987. Detection in situ of genomic regulatory elements in *Drosophila*. *Proc. Natl. Acad. Sci. U.S.A.,* 84**,** 9123-9127.

O'DONNELL, M. J. 2022. A perspective on insect water balance. *J. Exp. Biol.,* 225**,** jeb242358.

ODDSSON, A., SULEM, P., HELGASON, H., EDVARDSSON, V. O., THORLEIFSSON, G., SVEINBJöRNSSON, G., HARALDSDOTTIR, E., EYJOLFSSON, G. I., SIGURDARDOTTIR, O. & OLAFSSON, I. 2015. Common and rare variants associated with kidney stones and biochemical traits. *Nat. Commun.,* 6**,** 7975.

OLBY, R. 1989. The dimensions of scientific controversy: the biometric-Mendelian debate. *Br. J. Hist. Sci.,* 22**,** 299-320.

OLIET, S. H. & BOURQUE, C. 1993. Mechanosensitive channels transduce osmosensitivity in supraoptic neurons. *Nature,* 364**,** 341-343.

OZAKI, K., OHNISHI, Y., IIDA, A., SEKINE, A., YAMADA, R., TSUNODA, T., SATO, H., SATO, H., HORI, M. & NAKAMURA, Y. 2002. Functional SNPs in the lymphotoxin-α gene that are associated with susceptibility to myocardial infarction. *Nat. Genet.,* 32**,** 650-654.

OZIEH, M. N., BISHU, K. G., DISMUKE, C. E. & EGEDE, L. E. 2017. Trends in healthcare expenditure in United States adults with chronic kidney disease: 2002-2011. *BMC Health Serv. Res.,* 17**,** 368.

PAK, C. Y. & PETERSON, R. 1986. Successful treatment of hyperuricosuric calcium oxalate nephrolithiasis with potassium citrate. *Arch. Intern. Med.,* 146**,** 863-867.

PAK, C. Y., SAKHAEE, K. & FULLER, C. 1986. Successful management of uric acid nephrolithiasis with potassium citrate. *Kidney Int.,* 30**,** 422-428.

PAUL, M., POYAN MEHR, A. & KREUTZ, R. 2006. Physiology of local renin-angiotensin systems. *Physiol. Rev.,* 86**,** 747-803.

PERKINS, L. A., HOLDERBAUM, L., TAO, R., HU, Y., SOPKO, R., MCCALL, K., YANG-ZHOU, D., FLOCKHART, I., BINARI, R. & SHIM, H.-S. 2015. The transgenic RNAi project at Harvard medical school: resources and validation. *Genetics,* 201**,** 843-852.

PLOMIN, R., HAWORTH, C. M. & DAVIS, O. S. 2009. Common disorders are quantitative traits. *Nat. Rev. Genet.,* 10**,** 872-878.

POLICASTRO, L. J., SAGGI, S. J., GOLDFARB, D. S. & WEISS, J. P. 2018. Personalized intervention in monogenic stone formers. *J. Urol.,* 199**,** 623-632.

POLLOCK, V. P., MCGETTIGAN, J., CABRERO, P., MAUDLIN, I. M., DOW, J. A. T. & DAVIES, S. A. 2004. Conservation of capa peptide-induced nitric oxide signalling in Diptera. *J. Exp. Biol.,* 207**,** 4135-4145.

POLTORAK, A., HE, X., SMIRNOVA, I., LIU, M. Y., VAN HUFFEL, C., DU, X., BIRDWELL, D., ALEJOS, E., SILVA, M., GALANOS, C., FREUDENBERG, M., RICCIARDI-CASTAGNOLI, P., LAYTON, B. & BEUTLER, B. 1998. Defective LPS signaling in C3H/HeJ and C57BL/10ScCr mice: mutations in *Tlr4* gene. *Science,* 282**,** 2085-2088.

POTTER, C. J. & LUO, L. 2011. Using the Q system in *Drosophila melanogaster*. *Nat. Protoc.,* 6**,** 1105-1120.

PRICE, A. L., ZAITLEN, N. A., REICH, D. & PATTERSON, N. 2010. New approaches to population stratification in genome-wide association studies. *Nat. Rev. Genet.,* 11**,** 459-463.

PROKOP, A. & ROOT, J. 2013. A rough guide to *Drosophila* mating schemes. *Figshare*.

PRUYNE, D. & BRETSCHER, A. 2000. Polarization of cell growth in yeast. *J. Cell Sci.,* 113 (Pt 4)**,** 571-585.

PTASHNE, M. 1988. How eukaryotic transcriptional activators work. *Nature,* 335**,** 683-689.

PUIJK, K. & DE JONG, G. 1972. Alpha-amylases in a population of *D. melanogaster* from Dahomey. *Drosoph. Inf. Serv.,* 49**,** 61.

PURCELL, S., NEALE, B., TODD-BROWN, K., THOMAS, L., FERREIRA, M. A. R., BENDER, D., MALLER, J., SKLAR, P., DE BAKKER, P. I. W., DALY, M. J. & SHAM, P. C. 2007. PLINK: a tool set for whole-genome association and population-based linkage analyses. *Am. J. Hum. Genet.,* 81**,** 559-575.

PUSCH, M. & ZIFARELLI, G. 2015. ClC-5: physiological role and biophysical mechanisms. *Cell Calcium,* 58**,** 57-66.

R CORE TEAM, R. 2013. R: A language and environment for statistical computing. R foundation for statistical computing Vienna, Austria.

RADFORD, J. C., DAVIES, S. A. & DOW, J. A. T. 2002. Systematic G-protein-coupled receptor analysis in *Drosophila melanogaster* identifies a leucokinin receptor with novel roles. *J. Biol. Chem.,* 277**,** 38810-38817.

REITER, L. T., POTOCKI, L., CHIEN, S., GRIBSKOV, M. & BIER, E. 2001. A systematic analysis of human disease-associated gene sequences in *Drosophila melanogaster*. *Genome Res.,* 11**,** 1114-1125.

REN, J., ZHOU, Y., ZHANG, G., ZHOU, L., ZHAO, J., WEI, Y. & WU, X. A. 2015. Role of age-related decrease of renal organic cation transporter 2 in the effect of atenolol on renal excretion of metformin in rats. *Eur. J. Drug Metab. Pharmacokinet.,* 40**,** 349-354.

RESNICK, M., PRIDGEN, D. B. & GOODMAN, H. O. 1968. Genetic predisposition to formation of calcium oxalate renal calculi. *N. Engl. J. Med.,* 278**,** 1313-1318.

RIVARA, M. B., ZELNICK, L. R., HOOFNAGLE, A. N., NEWITT, R., TRACY, R. P., KRATZ, M., WEIGLE, D. S. & KESTENBAUM, B. R. 2017. Diurnal and long-term variation in plasma concentrations and renal clearances of circulating markers of kidney proximal tubular secretion. *Clin. Chem.,* 63**,** 915-923.

ROBERSON, D., SPERLING, C., SHAH, A. & ZIEMBA, J. 2020. Economic considerations in the management of nephrolithiasis. *Curr. Urol. Rep.,* 21**,** 18.

ROBERTS, P. A. 1970. Screening for x-ray-induced crossover suppressors in *Drosophila melanogaster*: prevalence and effectiveness of translocations. *Genetics,* 65**,** 429.

ROBERTSON, W. 1969. Measurement of ionized calcium in biological fluids. *Clin. Chim. Acta,* 24**,** 149-157.

ROBINSON-COHEN, C., BARTZ, T. M., LAI, D., IKIZLER, T. A., PEACOCK, M., IMEL, E. A., MICHOS, E. D., FOROUD, T. M., AKESSON, K. & TAYLOR, K. D. 2018. Genetic variants associated with circulating fibroblast growth factor 23. *J. Am. Soc. Nephrol.,* 29**,** 2583-2592.

ROCHE, S. E., SCHIFF, M. & RIO, D. C. 1995. P-element repressor autoregulation involves germ-line transcriptional repression and reduction of third intron splicing. *Genes Dev.,* 9**,** 1278-1288.

RODAN, A. R., BAUM, M. & HUANG, C.-L. 2012. The *Drosophila* NKCC Ncc69 is required for normal renal tubule function. *Am. J. Physiol. Cell Physiol.,* 303**,** C883-C894.

RODERICK, T. H. & HAWES, N. L. 1970. Two radiation-induced chromosomal inversions in mice (*Mus musculus*). *Proc. Natl. Acad. Sci. U.S.A.,* 67**,** 961-967.

RODMAN, J. 1998. Struvite stones. *Nephron,* 81**,** 50-59.

ROMERO, V., AKPINAR, H. & ASSIMOS, D. G. 2010. Kidney stones: a global picture of prevalence, incidence, and associated risk factors. *Rev. Urol.,* 12**,** e86-96.

ROSE, E., LEE, D., XIAO, E., ZHAO, W. Z., WEE, M., COHEN, J. & BERGWITZ, C. 2019. Endocrine regulation of MFS2 by branchless controls phosphate excretion and stone formation in *Drosophila* renal tubules. *Sci. Rep.,* 9**,** 8798.

ROSSETTI, S., CONSUGAR, M. B., CHAPMAN, A. B., TORRES, V. E., GUAY-WOODFORD, L. M., GRANTHAM, J. J., BENNETT, W. M., MEYERS, C. M., WALKER, D. L. & BAE, K. 2007. Comprehensive molecular diagnostics in autosomal dominant polycystic kidney disease. *J. Am. Soc. Nephrol.,* 18**,** 2143-2160.

RUBIN, G. M. & SPRADLING, A. C. 1982. Genetic transformation of *Drosophila* with transposable element vectors. *Science,* 218**,** 348-353.

RUKA, K. A., MILLER, A. P. & BLUMENTHAL, E. M. 2013. Inhibition of diuretic stimulation of an insect secretory epithelium by a cGMP-dependent protein kinase. *Am. J. Physiol. Renal Physiol.,* 304**,** F1210-F1216.

RULE, A. D., BERGSTRALH, E. J., MELTON, L. J., LI, X. J., WEAVER, A. L. & LIESKE, J. C. 2009. Kidney stones and the risk for chronic kidney disease. *Clin. J. Am. Soc. Nephrol.,* 4**,** 804-811.

SACHIDANANDAM, R., WEISSMAN, D., SCHMIDT, S. C., KAKOL, J. M., STEIN, L. D., MARTH, G., SHERRY, S., MULLIKIN, J. C., MORTIMORE, B. J., WILLEY, D. L., HUNT, S. E., COLE, C. G., COGGILL, P. C., RICE, C. M., NING, Z., ROGERS, J., BENTLEY, D. R., KWOK, P.-Y., MARDIS, E. R., YEH, R. T., SCHULTZ, B., COOK, L., DAVENPORT, R., DANTE, M., FULTON, L., HILLIER, L., WATERSTON, R. H., MCPHERSON, J. D., GILMAN, B., SCHAFFNER, S., VAN ETTEN, W. J., REICH, D., HIGGINS, J., DALY, M. J., BLUMENSTIEL, B., BALDWIN, J., STANGE-THOMANN, N., ZODY, M. C., LINTON, L., LANDER, E. S., ALTSHULER, D., THE INTERNATIONAL, S. N. P. M. W. G., COLD SPRING HARBOR, L., NATIONAL CENTER FOR BIOTECHNOLOGY, I., THE SANGER, C., WASHINGTON UNIVERSITY IN ST, L. & WHITEHEAD, M. I. T. C. F. G. R. 2001. A map of human genome sequence variation containing 1.42 million single nucleotide polymorphisms. *Nature,* 409**,** 928-933.

SAKHAEE, K., ADAMS-HUET, B., MOE, O. W. & PAK, C. Y. 2002. Pathophysiologic basis for normouricosuric uric acid nephrolithiasis. *Kidney Int.,* 62**,** 971-979.

SAKISAKA, T. & TAKAI, Y. 2004. Biology and pathology of nectins and nectin-like molecules. *Curr. Opin. Cell Biol.,* 16**,** 513-521.

SALBREUX, G., CHARRAS, G. & PALUCH, E. 2012. Actin cortex mechanics and cellular morphogenesis. *Trends Cell Biol.,* 22**,** 536-545.

SANTAMARIA, R., DIAZ-TOCADOS, J. M., PENDON-RUIZ DE MIER, M. V., ROBLES, A., SALMERON-RODRIGUEZ, M. D., RUIZ, E., VERGARA, N., AGUILERA-TEJERO, E., RAYA, A., ORTEGA, R., FELSENFELD, A., MUNOZ-CASTANEDA, J. R., MARTIN-MALO, A., ALJAMA, P. & RODRIGUEZ, M. 2018. Increased phosphaturia accelerates the decline in renal function: a search for mechanisms. *Sci. Rep.,* 8**,** 13701.

SANZ, A., FERNáNDEZ-AYALA, D. J., STEFANATOS, R. K. & JACOBS, H. T. 2010. Mitochondrial ROS production correlates with, but does not directly regulate lifespan in *Drosophila*. *Aging (Albany NY),* 2**,** 200.

SAX, K. 1923. The association of size differences with seed-coat pattern and pigmentation in *Phaseolus vulgaris*. *Genetics,* 8**,** 552.

SCHELLINGER, J. N. & RODAN, A. R. 2015. Use of the Ramsay assay to measure fluid secretion and ion flux rates in the *Drosophila melanogaster* malpighian tubule. *JoVE*, e53144.

SCHINDELIN, J., ARGANDA-CARRERAS, I., FRISE, E., KAYNIG, V., LONGAIR, M., PIETZSCH, T., PREIBISCH, S., RUEDEN, C., SAALFELD, S., SCHMID, B., TINEVEZ, J. Y., WHITE, D. J., HARTENSTEIN, V., ELICEIRI, K., TOMANCAK, P. & CARDONA, A. 2012. Fiji: an open-source platform for biological-image analysis. *Nat. Methods,* 9, 676-682.

SCHRIER, R. W. 2006. Water and sodium retention in edematous disorders: role of vasopressin and aldosterone. *Am. J. Med.,* 119, S47-S53.

SEIFARTH, J. E., MCGOWAN, C. L. & MILNE, K. J. 2012. Sex and life expectancy. *Gend. Med.,* 9, 390-401.

SELKURT, E. E. 1954. Sodium excretion by the mammalian kidney. *Physiol. Rev.,* 34, 287-333.

SEYBERTH, H. W. 2008. An improved terminology and classification of Bartter-like syndromes. *Nat. Clin. Pract. Nephrol.,* 4, 560-567.

SEYBERTH, H. W. & SCHLINGMANN, K. P. 2011. Bartter-and Gitelman-like syndromes: salt-losing tubulopathies with loop or DCT defects. *Pediatr. Nephrol.,* 26, 1789-1802.

SHEKARRIZ, B. & STOLLER, M. L. 2002. Uric acid nephrolithiasis: current concepts and controversies. *J. Urol.,* 168, 1307-1314.

SHEN, Z., XU, L., WU, T., WANG, H., WANG, Q., GE, X., KONG, F., HUANG, G. & PAN, X. 2024. Structural basis for urate recognition and apigenin inhibition of human GLUT9. *Nat. Commun.,* 15, 5039.

SHORTER, J., COUCH, C., HUANG, W., CARBONE, M. A., PEIFFER, J., ANHOLT, R. R. H. & MACKAY, T. F. C. 2015. Genetic architecture of natural variation in aggressive behavior. *Proc. Natl. Acad. Sci. U.S.A.,* 112, E3555-E3563.

SHUKLA, A. & TAPADIA, M. G. 2011. Differential localization and processing of apoptotic proteins in Malpighian tubules of *Drosophila* during metamorphosis. *Eur. J. Cell Biol.,* 90, 72-80.

SIENER, R., NETZER, L. & HESSE, A. 2013. Determinants of brushite stone formation: a case-control study. *PloS one,* 8, e78996.

SIKIRIĆ, M., BABIĆ-IVANČIĆ, V. & TONKOVIĆ, M. 1997. Precipitation of calcium oxalate and calcium phosphate in the presence of uric acid. *Colloids Surf. A Physicochem. Eng. Asp.,* 121**,** 145-150.

SIMEONE, A., GULISANO, M., ACAMPORA, D., STORNAIUOLO, A., RAMBALDI, M. & BONCINELLI, E. 1992. Two vertebrate homeobox genes related to the *Drosophila empty spiracles* gene are expressed in the embryonic cerebral cortex. *EMBO J.,* 11**,** 2541-2550.

SIMON, D. B., KARET, F. E., HAMDAN, J. M., PIETRO, A. D., SANJAD, S. A. & LIFTON, R. P. 1996a. Bartter's syndrome, hypokalaemic alkalosis with hypercalciuria, is caused by mutations in the Na-K-2CI cotransporter NKCC2. *Nat. Genet.,* 13**,** 183-188.

SIMON, D. B., KARET, F. E., RODRIGUEZ-SORIANO, J., HAMDAN, J. H., DIPIETRO, A., TRACHTMAN, H., SANJAD, S. A. & LIFTON, R. P. 1996b. Genetic heterogeneity of Barter's syndrome revealed by mutations in the K^+ channel, ROMK. *Nat. Genet.,* 14**,** 152-156.

SINGH, P., ENDERS, F. T., VAUGHAN, L. E., BERGSTRALH, E. J., KNOEDLER, J. J., KRAMBECK, A. E., LIESKE, J. C. & RULE, A. D. 2015. Stone composition among first-time symptomatic kidney stone formers in the community. *Mayo Clin. Proc.,* 90**,** 1356-1365.

SINGH, P., HARRIS, P. C., SAS, D. J. & LIESKE, J. C. 2022a. The genetics of kidney stone disease and nephrocalcinosis. *Nat. Rev. Nephrol.,* 18**,** 224-240.

SINGH, P., VIEHMAN, J. K., MEHTA, R. A., COGAL, A. G., HASADSRI, L., OGLESBEE, D., OLSON, J. B., SEIDE, B. M., SAS, D. J. & HARRIS, P. C. 2022b. Clinical characterization of primary hyperoxaluria type 3 in comparison with types 1 and 2. *Nephrol. Dial. Transplant.,* 37**,** 869-875.

SINGH, S. R., LIU, W. & HOU, S. X. 2007. The adult *Drosophila* malpighian tubules are maintained by multipotent stem cells. *Cell Stem Cell,* 1**,** 191-203.

SKAER, H. & ARIAS, A. M. 1992. The wingless product is required for cell proliferation in the Malpighian tubule anlage of *Drosophila melanogaster*. *Development,* 116**,** 745-754.

SLEIMAN, M. S. B., OSMAN, D., MASSOURAS, A., HOFFMANN, A. A., LEMAITRE, B. & DEPLANCKE, B. 2015. Genetic, molecular and physiological basis of variation in gut immunocompetence. *Nat. Commun.,* 6**,** 7829.

SNOW, P. M., BIEBER, A. J. & GOODMAN, C. S. 1989. Fasciclin III: a novel homophilic adhesion molecule in *Drosophila*. *Cell,* 59**,** 313-323.

SOUCIE, J. M., THUN, M. J., COATES, R. J., MCCLELLAN, W. & AUSTIN, H. 1994. Demographic and geographic variability of kidney stones in the United States. *Kidney Int.,* 46**,** 893-899.

SOZEN, M. A., ARMSTRONG, J. D., YANG, M., KAISER, K. & DOW, J. A. T. 1997. Functional domains are specified to single-cell resolution in a *Drosophila* epithelium. *Proc. Natl. Acad. Sci. U.S.A.,* 94**,** 5207-5212.

SPIERER, A. N., MOSSMAN, J. A., SMITH, S. P., CRAWFORD, L., RAMACHANDRAN, S. & RAND, D. M. 2021. Natural variation in the regulation of neurodevelopmental genes modifies flight performance in *Drosophila*. *PLoS Genet.,* 17**,** e1008887.

SPRADLING, A. C. & RUBIN, G. M. 1982. Transposition of cloned P elements into *Drosophila* germ line chromosomes. *Science,* 218**,** 341-347.

SPRADLING, A. C., STERN, D., BEATON, A., RHEM, E. J., LAVERTY, T., MOZDEN, N., MISRA, S. & RUBIN, G. M. 1999. The Berkeley *Drosophila* genome project gene disruption project: single P-element insertions mutating 25% of vital *Drosophila* genes. *Genetics,* 153**,** 135-177.

STARK, C., BREITKREUTZ, B. J., REGULY, T., BOUCHER, L., BREITKREUTZ, A. & TYERS, M. 2006. BioGRID: a general repository for interaction datasets. *Nucleic Acids Res.,* 34**,** D535-D539.

STERN, C. & SCHAEFFER, E. W. 1943. On primary attributes of alleles in *Drosophila melanogaster*. *Proc. Natl. Acad. Sci. U.S.A.,* 29**,** 351-61.

STOVER, E., BORTHWICK, K., BAVALIA, C., EADY, N., FRITZ, D., RUNGROJ, N., GIERSCH, A., MORTON, C., AXON, P. & AKIL, I. 2002. Novel *ATP6V1B1* and *ATP6V0A4* mutations in autosomal recessive distal renal tubular acidosis with new evidence for hearing loss. *J. Med. Genet.,* 39**,** 796-803.

STRICKER, J., FALZONE, T. & GARDEL, M. L. 2010. Mechanics of the F-actin cytoskeleton. *J. Biomech.,* 43**,** 9-14.

SUCHY-DICEY, A. M., LAHA, T., HOOFNAGLE, A., NEWITT, R., SIRICH, T. L., MEYER, T. W., THUMMEL, K. E., YANEZ, N. D., HIMMELFARB, J., WEISS, N. S. & KESTENBAUM, B. R. 2016. Tubular secretion in CKD. *J. Am. Soc. Nephrol.,* 27**,** 2148-2155.

SUDARSAN, V., PASALODOS-SANCHEZ, S., WAN, S., GAMPEL, A. & SKAER, H. 2002. A genetic hierarchy establishes mitogenic signalling and mitotic

competence in the renal tubules of *Drosophila*. *Development,* 129**,** 935-944.

SUGAWARA, Y., HIRAKAWA, Y., NAGASU, H., NARITA, A., KATAYAMA, A., WADA, J., SHIMIZU, M., WADA, T., KITAMURA, H., NAKANO, T., YOKOI, H., YANAGITA, M., GOTO, S., NARITA, I., KOSHIBA, S., TAMIYA, G., NANGAKU, M., YAMAMOTO, M. & KASHIHARA, N. 2023. Genome-wide association study of the risk of chronic kidney disease and kidney-related traits in the Japanese population: J-Kidney-Biobank. *J. Hum. Genet.,* 68**,** 55-64.

SVED, J. 1979. The "hybrid dysgenesis" syndrome in *Drosophila melanogaster*. *Bioscience,* 29**,** 659-664.

SWARUP, S., HUANG, W., MACKAY, T. F. & ANHOLT, R. R. 2013. Analysis of natural variation reveals neurogenetic networks for *Drosophila* olfactory behavior. *Proc. Natl. Acad. Sci. U.S.A.,* 110**,** 1017-1022.

SYED, Z. A., HäRD, T., UV, A. & VAN DIJK-HäRD, I. F. 2008. A potential role for *Drosophila* mucins in development and physiology. *PLoS One,* 3**,** e3041.

TALSNESS, D. M., OWINGS, K. G., COELHO, E., MERCENNE, G., PLEINIS, J. M., PARTHA, R., HOPE, K. A., ZUBERI, A. R., CLARK, N. L., LUTZ, C. M., RODAN, A. R. & CHOW, C. Y. 2020. A *Drosophila* screen identifies NKCC1 as a modifier of NGLY1 deficiency. *Elife,* 9**,** e57831.

TAM, V., PATEL, N., TURCOTTE, M., BOSSé, Y., PARé, G. & MEYRE, D. 2019. Benefits and limitations of genome-wide association studies. *Nat. Rev. Genet.,* 20**,** 467-484.

TAPADIA, M. G. & GAUTAM, N. K. 2011. Non-apoptotic function of apoptotic proteins in the development of Malpighian tubules of *Drosophila melanogaster*. *J. Biosci.,* 36**,** 531-544.

TEPASS, U., TANENTZAPF, G., WARD, R. & FEHON, R. 2001. Epithelial cell polarity and cell junctions in *Drosophila*. *Annu. Rev. Genet.,* 35**,** 747-784.

TERHZAZ, S., ALFORD, L., YEOH, J. G., MARLEY, R., DORNAN, A. J., DOW, J. A. T. & DAVIES, S. A. 2018. Renal neuroendocrine control of desiccation and cold tolerance by *Drosophila suzukii*. *Pest Manag. Sci.,* 74**,** 800-810.

TERHZAZ, S., CABRERO, P., ROBBEN, J. H., RADFORD, J. C., HUDSON, B. D., MILLIGAN, G., DOW, J. A. T. & DAVIES, S. A. 2012. Mechanism and function of *Drosophila* capa GPCR: a desiccation stress-responsive receptor with functional homology to human neuromedinU receptor. *PLoS One,* 7**,** e29897.

TERHZAZ, S., SOUTHALL, T. D., LILLEY, K. S., KEAN, L., ALLAN, A. K., DAVIES, S. A. & DOW, J. A. T. 2006. Differential gel electrophoresis and transgenic mitochondrial calcium reporters demonstrate spatiotemporal filtering in calcium control of mitochondria. *J. Biol. Chem.,* 281**,** 18849-18858.

TERHZAZ, S., TEETS, N. M., CABRERO, P., HENDERSON, L., RITCHIE, M. G., NACHMAN, R. J., DOW, J. A. T., DENLINGER, D. L. & DAVIES, S. A. 2015. Insect capa neuropeptides impact desiccation and cold tolerance. *Proc. Natl. Acad. Sci. U.S.A.,* 112**,** 2882-2887.

THORLEIFSSON, G., HOLM, H., EDVARDSSON, V., WALTERS, G. B., STYRKARSDOTTIR, U., GUDBJARTSSON, D. F., SULEM, P., HALLDORSSON, B. V., DE VEGT, F., D'ANCONA, F. C. H., DEN HEIJER, M., FRANZSON, L., CHRISTIANSEN, C., ALEXANDERSEN, P., RAFNAR, T., KRISTJANSSON, K., SIGURDSSON, G., KIEMENEY, L. A., BODVARSSON, M., INDRIDASON, O. S., PALSSON, R., KONG, A., THORSTEINSDOTTIR, U. & STEFANSSON, K. 2009. Sequence variants in the gene associate with kidney stones and bone mineral density. *Nat. Genet.,* 41**,** 926-930.

TOKA, H. R., AL-ROMAIH, K., KOSHY, J. M., DIBARTOLO III, S., KOS, C. H., QUINN, S. J., CURHAN, G. C., MOUNT, D. B., BROWN, E. M. & POLLAK, M. R. 2012. Deficiency of the calcium-sensing receptor in the kidney causes parathyroid hormone–independent hypocalciuria. *J. Am. Soc. Nephrol.,* 23**,** 1879-1890.

TORRIE, L. S., RADFORD, J. C., SOUTHALL, T. D., KEAN, L., DINSMORE, A. J., DAVIES, S. A. & DOW, J. A. T. 2004. Resolution of the insect ouabain paradox. *Proc. Natl. Acad. Sci. U.S.A.,* 101**,** 13689-13693.

TRAN, U., ZAKIN, L., SCHWEICKERT, A., AGRAWAL, R., DöGER, R., BLUM, M., DE ROBERTIS, E. & WESSELY, O. 2010. The RNA-binding protein bicaudal C regulates polycystin 2 in the kidney by antagonizing *miR-17* activity. *Development,* 137**,** 1107-1116.

UCHIZONO, S. & TANIMURA, T. 2017. Genetic variation in taste sensitivity to sugars in *Drosophila melanogaster*. *Chem. Senses,* 42**,** 287-294.

URABE, Y., TANIKAWA, C., TAKAHASHI, A., OKADA, Y., MORIZONO, T., TSUNODA, T., KAMATANI, N., KOHRI, K., CHAYAMA, K. & KUBO, M. 2012. A genome-wide association study of nephrolithiasis in the Japanese population identifies novel susceptible loci at 5q35.3, 7p14.3, and 13q14.1. *PLoS Genet.,* 8**,** e1002541.

URE, M. E., HEYDARI, E., PAN, W., RAMESH, A., REHMAN, S., MORGAN, C., PINSK, M., ERICKSON, R., HERRMANN, J. M. & DIMKE, H. 2017. A variant in a *cis*-regulatory element enhances claudin-14 expression and is associated with

pediatric – onset hypercalciuria and kidney stones. *Hum. Mutat.,* 38**,** 649-657.

VAIKAKKARA CHITHRAN, A., ALLAN, D. W. & O'CONNOR, T. P. 2024. Adult expression of the cell adhesion protein Fasciclin 3 is required for the maintenance of adult olfactory interneurons. *J. Cell Sci.,* 137**,** jcs261759.

VENTER, J. C., ADAMS, M. D., MYERS, E. W., LI, P. W., MURAL, R. J., SUTTON, G. G., SMITH, H. O., YANDELL, M., EVANS, C. A. & HOLT, R. A. 2001. The sequence of the human genome. *Science,* 291**,** 1304-1351.

VERBALIS, J. G. 2003. Disorders of body water homeostasis. *Best Pract. Res. Clin. Endocrinol. Metab.,* 17**,** 471-503.

VERNEY, E. B. 1947. Croonian lecture-the antidiuretic hormone and the factors which determine its release. *Proc. R. Soc. London Ser. B,* 135**,** 25-106.

VOSSHALL, L. B., PRICE, J. L., SEHGAL, A., SAEZ, L. & YOUNG, M. W. 1994. Block in nuclear localization of period protein by a second clock mutation, *timeless. Science,* 263**,** 1606-1609.

WAGNER, A. 2005. Energy constraints on the evolution of gene expression. *Mol. Biol. Evol.,* 22**,** 1365-1374.

WAGNER, C. A. 2008. When proton pumps go sour: urinary acidification and kidney stones. *Kidney Int.,* 73**,** 1103-1105.

WAGNER, C. A., FINBERG, K. E., BRETON, S., MARSHANSKY, V., BROWN, D. & GEIBEL, J. P. 2004. Renal vacuolar H^+-ATPase. *Physiol. Rev.,* 84**,** 1263-1314.

WAGNER, C. A., UNWIN, R., LOPEZ-GARCIA, S. C., KLETA, R., BOCKENHAUER, D. & WALSH, S. 2023. The pathophysiology of distal renal tubular acidosis. *Nat. Rev. Nephrol.,* 19**,** 384-400.

WALL, S. M., KNEPPER, M. A., HASSELL, K. A., FISCHER, M. P., SHODEINDE, A., SHIN, W., PHAM, T. D., MEYER, J. W., LORENZ, J. N., BEIERWALTES, W. H., DIETZ, J. R., SHULL, G. E. & KIM, Y. H. 2006. Hypotension in *NKCC1* null mice: role of the kidneys. *Am. J. Physiol. Renal Physiol.,* 290**,** F409-F416.

WALLACE, M. A. 1998. Anatomy and physiology of the kidney. *AORN J.,* 68**,** 799-820.

WANG, C. & SPRADLING, A. C. 2020. An abundant quiescent stem cell population in *Drosophila* Malpighian tubules protects principal cells from kidney stones. *Elife,* 9**,** e54096.

WANG, C. & SPRADLING, A. C. 2022. *Drosophila* renal stem cells enhance fitness by delayed remodeling of adult Malpighian tubules. *Sci. Adv.,* 8**,** eabn7436.

WANG, J., KEAN, L., YANG, J., ALLAN, A. K., DAVIES, S. A., HERZYK, P. & DOW, J. A. T. 2004. Function-informed transcriptome analysis of *Drosophila* renal tubule. *Genome Biol.,* 5**,** 1-21.

WANG, K. & KESTENBAUM, B. 2018. Proximal tubular secretory clearance: a neglected partner of kidney function. *Clin. J. Am. Soc. Nephrol.,* 13**,** 1291-1296.

WANG, S. S., DEVUYST, O., COURTOY, P. J., WANG, X.-T., WANG, H., WANG, Y., THAKKER, R. V., GUGGINO, S. & GUGGINO, W. B. 2000. Mice lacking renal chloride channel, CLC-5, are a model for Dent's disease, a nephrolithiasis disorder associated with defective receptor-mediated endocytosis. *Hum. Mol. Genet.,* 9**,** 2937-2945.

WARE, E. B., SMITH, J. A., ZHAO, W., GANESVOORT, R. T., CURHAN, G. C., POLLAK, M., MOUNT, D. B., TURNER, S. T., CHEN, G. & SHAH, R. J. 2019. Genome-wide association study of 24-hour urinary excretion of calcium, magnesium, and uric acid. *Mayo Clin. Proc. Innov. Qual. Outcomes.,* 3**,** 448-460.

WATANABE, T. 2018. Improving outcomes for patients with distal renal tubular acidosis: recent advances and challenges ahead. *Pediatr. Health Med. Ther.***,** 181-190.

WAYLAND, M. T., DEFAYE, A., ROCHA, J., JAYARAM, S. A., ROYET, J., MIGUEL-ALIAGA, I., LEULIER, F. & COGNIGNI, P. 2014. Spotting the differences: probing host/microbiota interactions with a dedicated software tool for the analysis of faecal outputs in *Drosophila*. *J. Insect Physiol.,* 69**,** 126-135.

WEBER, S., SCHNEIDER, L., PETERS, M., MISSELWITZ, J., RöNNEFARTH, G., BöSWALD, M., BONZEL, K. E., SEEMAN, T., SULáKOVá, T. & KUWERTZ-BRöKING, E. 2001. Novel paracellin-1 mutations in 25 families with familial hypomagnesemia with hypercalciuria and nephrocalcinosis. *J. Am. Soc. Nephrol.,* 12**,** 1872-1881.

WEBSTER, A. C., NAGLER, E. V., MORTON, R. L. & MASSON, P. 2017. Chronic kidney disease. *The lancet,* 389**,** 1238-1252.

WEBSTER, N., JIN, J. R., GREEN, S., HOLLIS, M. & CHAMBON, P. 1988. The yeast UAS_G is a transcriptional enhancer in human HeLa cells in the presence of the GAL4 *trans*-activator. *Cell,* 52**,** 169-178.

WEEDON, M. N., LANGO, H., LINDGREN, C. M., WALLACE, C., EVANS, D. M., MANGINO, M., FREATHY, R. M., PERRY, J. R., STEVENS, S. & HALL, A. S. 2008. Genome-wide association analysis identifies 20 loci that influence adult height. *Nat. Genet.,* 40**,** 575-583.

WEIDE, T., VOLLENBROKER, B., SCHULZE, U., DJURIC, I., EDELING, M., BONSE, J., HOCHAPFEL, F., PANICHKINA, O., WENNMANN, D. O., GEORGE, B., KIM, S., DANIEL, C., SEGGEWISS, J., AMANN, K., KRIZ, W., KRAHN, M. P. & PAVENSTADT, H. 2017. *Pals1* haploinsufficiency results in proteinuria and cyst formation. *J. Am. Soc. Nephrol.,* 28**,** 2093-2107.

WESSING, A. & EICHELBERG, D. 1978. The genetics and biology of *Drosophila*. Academic Press, London.

WESSING, A. & ZIEROLD, K. 1992. Metal-salt feeding causes alterations in concretions in *Drosophila* larval Malpighian tubules as revealed by X-ray microanalysis. *J. Insect Physiol.,* 38**,** 623-632.

WIKOFF, W. R., NAGLE, M. A., KOUZNETSOVA, V. L., TSIGELNY, I. F. & NIGAM, S. K. 2011. Untargeted metabolomics identifies enterobiome metabolites and putative uremic toxins as substrates of organic anion transporter 1 (Oat1). *J. Proteome Res.,* 10**,** 2842-2851.

WILSON, K. A., BECK, J. N., NELSON, C. S., HILSABECK, T. A., PROMISLOW, D., BREM, R. B. & KAPAHI, P. 2020. GWAS for lifespan and decline in climbing ability in flies upon dietary restriction reveal decima as a mediator of insulin-like peptide production. *Curr. Biol.,* 30**,** 2749-2760.e3.

WILSON, S. B., SANTOS, I. P., WILDFANG, L., IMSA, K. & LITTLE, M. H. 2025. Generation of multi-lineage kidney assembloids with integration between nephrons and a single exiting collecting duct. *bioRxiv***,** 640561.

WOODLING, N. 2024. Sex- and strain-dependent effects of ageing on sleep and activity patterns in *Drosophila*. *PLoS One,* 19**,** e0308652.

WOODS, D. F., HOUGH, C., PEEL, D., CALLAINI, G. & BRYANT, P. J. 1996. Dlg protein is required for junction structure, cell polarity, and proliferation control in *Drosophila* epithelia. *J. Cell Biol.,* 134**,** 1469-1482.

WU, Q., YU, G. X., PARK, S. J., GAO, Y., JA, W. W. & YANG, M. Y. 2020. Excreta Quantification (EX-Q) for longitudinal measurements of food intake in *Drosophila*. *Iscience,* 23**,** 100776.

WU, S., LI, C., LI, Y., LIU, J., RONG, C., PEI, H., LI, X., ZENG, X. & MAO, W. 2024. SLC2A9 rs16890979 reduces uric acid absorption by kidney organoids. *Front. Cell Dev. Biol.,* 11**,** 1268226.

XING, G., LIN, C. Y., WOODING, S. P. & XING, C. 2012. Blindly using Wald's test can miss rare disease-causal variants in case-control association studies. *Ann. Hum. Genet.,* 76**,** 168-177.

XU, C., ZHANG, W., LU, P., CHEN, J.-C., ZHOU, Y.-Q., SHEN, G., WANG, Z.-F., MA, Z., JIANG, M.-J. & SONG, R.-J. 2021. Mutation of *Klotho* rs3752472 protect the kidney from the renal epithelial cell injury caused by CaOx crystals through the Wnt/ß-catenin signaling pathway. *Urolithiasis,* 49**,** 543-550.

XU, J., LIU, Y., LI, H., TARASHANSKY, A. J., KALICKI, C. H., HUNG, R. J., HU, Y., COMJEAN, A., KOLLURU, S. S., WANG, B., QUAKE, S. R., LUO, L., MCMAHON, A. P., DOW, J. A. T. & PERRIMON, N. 2022. Transcriptional and functional motifs defining renal function revealed by single-nucleus RNA sequencing. *Proc. Natl. Acad. Sci. U.S.A.,* 119**,** e2203179119.

YAMAMOTO, S., JAISWAL, M., CHARNG, W. L., GAMBIN, T., KARACA, E., MIRZAA, G., WISZNIEWSKI, W., SANDOVAL, H., HAELTERMAN, N. A., XIONG, B., ZHANG, K., BAYAT, V., DAVID, G., LI, T., CHEN, K., GALA, U., HAREL, T., PEHLIVAN, D., PENNEY, S., VISSERS, L., DE LIGT, J., JHANGIANI, S. N., XIE, Y., TSANG, S. H., PARMAN, Y., SIVACI, M., BATTALOGLU, E., MUZNY, D., WAN, Y. W., LIU, Z., LIN-MOORE, A. T., CLARK, R. D., CURRY, C. J., LINK, N., SCHULZE, K. L., BOERWINKLE, E., DOBYNS, W. B., ALLIKMETS, R., GIBBS, R. A., CHEN, R., LUPSKI, J. R., WANGLER, M. F. & BELLEN, H. J. 2014. A *Drosophila* genetic resource of mutants to study mechanisms underlying human genetic diseases. *Cell,* 159**,** 200-214.

YANG, H., MALE, M., LI, Y., WANG, N., ZHAO, C., JIN, S., HU, J., CHEN, Z., YE, Z. & XU, H. 2018. Efficacy of Hydroxy-L-proline (HYP) analogs in the treatment of primary hyperoxaluria in *Drosophila melanogaster*. *BMC Nephrol.,* 19**,** 1-12.

YANG, Z., ZHOU, T., SUN, B., WANG, Q., DONG, X., HU, X., ZHONG, J., SONG, B. & LI, L. 2017. *PDE1A* polymorphism contributes to the susceptibility of nephrolithiasis. *BMC Genomics,* 18**,** 982.

YE, J., COULOURIS, G., ZARETSKAYA, I., CUTCUTACHE, I., ROZEN, S. & MADDEN, T. L. 2012. Primer-BLAST: a tool to design target-specific primers for polymerase chain reaction. *BMC Bioinformatics,* 13**,** 134.

YIN, O. Q., TOMLINSON, B. & CHOW, M. S. 2006. Variability in renal clearance of substrates for renal transporters in chinese subjects. *J. Clin. Pharmacol.,* 46**,** 157-163.

YOON, J., SINGH, N. K., JANG, J. & CHO, D.-W. 2022. 3D bioprinted in vitro secondary hyperoxaluria model by mimicking intestinal-oxalate-malabsorption-related kidney stone disease. *Appl. Phys. Rev.,* 9**,** 041408.

YOSHIDA, T., KATO, K., FUJIMAKI, T., YOKOI, K., OGURI, M., WATANABE, S., METOKI, N., YOSHIDA, H., SATOH, K., AOYAGI, Y., NISHIGAKI, Y., TANAKA, M., NOZAWA, Y. & YAMADA, Y. 2009. Association of a polymorphism of the apolipoprotein E gene with chronic kidney disease in Japanese individuals with metabolic syndrome. *Genomics,* 93**,** 221-226.

YOUNG, M. D., MITCHELL, T. J., VIEIRA BRAGA, F. A., TRAN, M. G., STEWART, B. J., FERDINAND, J. R., COLLORD, G., BOTTING, R. A., POPESCU, D.-M. & LOUDON, K. W. 2018. Single-cell transcriptomes from human kidneys reveal the cellular identity of renal tumors. *Science,* 361**,** 594-599.

YOUNG, M. W. & KAY, S. A. 2001. Time zones: a comparative genetics of circadian clocks. *Nat. Rev. Genet.,* 2**,** 702-715.

YU, L.-G., ANDREWS, N., ZHAO, Q., MCKEAN, D., WILLIAMS, J. F., CONNOR, L. J., GERASIMENKO, O. V., HILKENS, J., HIRABAYASHI, J. & KASAI, K. 2007. Galectin-3 interaction with Thomsen-Friedenreich disaccharide on cancer-associated MUC1 causes increased cancer cell endothelial adhesion. *J. Biol. Chem.,* 282**,** 773-781.

ZEHRING, W. A., WHEELER, D. A., REDDY, P., KONOPKA, R. J., KYRIACOU, C. P., ROSBASH, M. & HALL, J. C. 1984. P-element transformation with period locus DNA restores rhythmicity to mutant, arrhythmic *Drosophila melanogaster*. *Cell,* 39**,** 369-376.

ZHANG, S., AMOURDA, C., GARFIELD, D. & SAUNDERS, T. E. 2018. Selective filopodia adhesion ensures robust cell matching in the *Drosophila* heart. *Dev. Cell,* 46**,** 189-203. e4.

ZHOU, X. & STEPHENS, M. 2012. Genome-wide efficient mixed-model analysis for association studies. *Nat. Genet.,* 44**,** 821-824.

ZHU, W., QIONG, D., YANLI, G., MIN, L., YING, Z., QIYI, H., SHENPING, Z., XISHENG, W. & HUI, L. 2023. Proteomics and transcriptomics profiling reveals distinct aspects of kidney stone related genes in calculi rats. *BMC Genomics,* 24**,** 127.

ZHU, Z., CUI, Y., HUANG, F., ZENG, H., XIA, W., ZENG, F., HE, C., CHEN, J., CHEN, Z. & CHEN, H. 2020. Long non-coding RNA H19 promotes osteogenic differentiation of renal interstitial fibroblasts through Wnt-β-catenin pathway. *Mol. Cell. Biochem.,* 470**,** 145-155.